CRANFIELD UNIVERSITY

ZORAN JELIĆ

OPTIMISATION OF DESIGN PARAMETERS FOR MODULAR RANGE ENHANCED PROJECTILE

CRANFIELD DEFENCE AND SECURITY

PhD Thesis
Academic Year: 2014 - 2015

Supervisor: Prof. Amer Hameed
February 2015

CRANFIELD UNIVERSITY

CRANFIELD DEFENCE AND SECURITY

Academic Year 2014 - 2015

ZORAN JELIĆ

Optimisation of Design Parameters for Modular Range Enhanced Projectile

Supervisor: Prof. Amer Hameed

February 2015

PhD Thesis

ABSTRACT

There is an underpinning requirement for artillery systems to achieve longer range, better precision, and an adequate lethal effect. The main objective of this research is to investigate various methods of range increase and propose optimal solution for range extension of existing artillery systems. The proposed solution is novel, modular projectile design. Several methodologies for projectile range increment (such as improved aerodynamics and ballistic profile) were combined to achieve the "goal", but mainly work was concentrated on projectile's "assisted" propulsion with Base Bleed (BB) and Solid Rocket Motor (SRM). The gun's interior ballistics, i.e. ordnance parameters (propelling charge, volume of combustion chamber, length of the barrel and muzzle velocity) remains unchanged. The novel concept of modular design of an artillery projectile includes separate modules for propulsion, drag reduction, and payload. Various payload module configurations should allow diverse lethal effects, and four different propulsion configurations allow engagement of various targets. Among all "possible" projectile configurations, the focus was on arrangement that will fly longest from given ordnance, with fragmentation effect on target. To achieve projectile's "aims," it required development of new chemical composition for BB and SRM propellant. In addition, new type of BB propellant grain geometry was developed, for efficient base drag reduction (by injecting sufficient amount of gaseous products in the downstream wake zone of the projectile base), and new SRM module was designed for projectile range enhancement. Both propellant compositions and grain shapes were optimised to produce required "thrust" and to withstand severe gun launching conditions - high acceleration and pressure in gun barrel. The research work also includes investigation and optimisation of complex flight mechanics of a gun launched - solid rocket motor propelled - base bleed projectile, as well aerodynamic shape optimisation, and overall modular projectile design optimisation in order to improve payload efficiency. The research work covers theoretical calculations, numerical simulations and their validation through experiments, with results confirming the feasibility of the concept.

Keywords: Aerodynamics, Rocekt Propulsion, Base-Bleed, Solid Rocket Propellant, Flight Mechanics, Structural Reliabilty.

DEDICATION

This work is dedicated to my children Helena and Mihailo.

ACKNOWLEDGEMENTS

I would like to thank my wife Marija for all her love and kindness, especially for tolerating my long hours at work. Without her support and encouragement, this work would be immensely difficult. A special thanks for my family for their support.

I would like to thank Prof. Amer Hameed for giving me opportunity to undertake this project and for supervision, help and advice he gave me throughout this work.

The author is grateful to Cranfield Defence and Security for enabling this research.

TABLE OF CONTENTS

LIST OF FIGURES

LIST OF TABLES

GLOSSARY

List of symbols

a	- constant in propellant burning rate law (burning rate in vacuum)
$A_{1,2,3,4,5}$	- polynomial coefficients (drag reduction coefficient relation)
A_E	- nozzle's exit area
A_j	- area of Base Bleed Unit orifice
A_T	- nozzle's throat area
b	- constant in propellant burning rate law
$B_{1,2,3}$	- polynomial coefficients (drag reduction coefficient relation)
$\bar{c}$	- fins cord length relative to projectile reference diameter
C_D	- drag coefficient
C_{D0}	- total drag coefficient
C_{Db}	- base drag coefficient
C_{Db0}	- base drag coefficient without Base-Bleed influence
C_{DbBB}	- base drag coefficient with Base-Bleed influence
C_{Df}	- skin friction drag coefficient
$C_{D\alpha}{}^2$	- induced drag coefficient
$C_{L\alpha}$	- lift force coefficient
$C_{m\alpha}$	- coefficient of overturning moment
C_P	- specific heat at constant pressure of mixture
C_{pb}	- base pressure coefficient
$C_{pb\ cyl}$	- base pressure coefficient of the projectile's cylindrical base
C^*	- characteristic velocity (chemical equilibrium)
d	- reference diameter – projectile's calibre
d_b	- diameter of the projectile's base
d_{BND}	- rotating band diameter
d_n	- meplat diameter
$\vec{D}$	- drag force
D_f	- skin friction drag force
e	- burn-out propellant web
F	- force

$\vec{g}$, g - gravity acceleration 9.80665 m/s^2

H - enthalpy

I - injection parameter

I_{high} - higher limit for injection parameter

I_{low} - lower limit for injection parameter

I_{opt} - optimal injection parameter

K_1 - correction factor in base pressure equation

K_b - correction factor for base pressure relative to projectile's rear cone angle

$\vec{L}$ - lift force

L - length of the projectile

L_1 - length of the projectile's nose (ogive)

L_2 - theoretical length of the projectile's nose

L_k - length of the projectile's rear cone

Ln - length of the projectile's ogive

m (m_P) - projectile's mass

$\dot{m}_b$ - mass flux through projectile base (reference flux –"virtual")

$\dot{m}_j$ - Base – Bleed mass flux at the orifice

$\dot{m}_P$ - mass flux of propellant combustion products

M - Mach number

M - molecular weight of the combustion products

n - exponent in propellant burning rate law

p - pressure

p_b - base pressure

$-\overline{p}_b$ - base pressure coefficient

p_0 - combustion pressure inside the Base-Bleed Unit/Total pressure

p_∞ - static pressure of the free stream

p - angular velocity of the projectile (as derivative)

P - projectile's wetted surface without base area

$\overline{P}_{b0}$ - relative base pressure (relative to pressure of the free stream)

$\overline{P}_{bBB}$	- relative base pressure with influence of Base-Bleed effect
$\Delta\overline{P}_{bBB}$	- relative contribution to the base pressure by Base-Bleed effect
Pc	- combustion pressure
q_{∞}	- dynamic pressure of the free stream = $\frac{1}{2}\rho_{\infty}\cdot V^{2}{}_{\infty}$
r	- burning rate
$\vec{r}$	- radius vector
r_b	- radius of the projectile's base
R	- universal gas constant 8314.15 J/(kg-mol·K)
R	- specific gas constant
R	- radius of the projectile's secant ogive
Re	- Reynolds number
R_T	- radius of equivalent tangent ogive of the projectile
S	- entropy
S	- area (surface) – reference area (calibre)
S	- propellant burning surface
S_b	- area of the projectile's base
$S_{b\ ekv}$	- equivalent area of the projectile's base
$\overline{S}_b$	- relative base area S_b/S
S_j	- nozzle's area
S_P	- propellant actual burning surface (area)
t	- time
t_b	- ballistic temperature
t_{BB}	- active time of the Base-Bleed
$\vec{T}$	- thrust (force)
T	- temperature
T_0	- combustion temperature inside Base-Bleed Unit/Total temperature
T_j	- temperature at the Base-Bleed orifice
$\vec{T}_L$	- thrust moment
T_{∞}	- air temperature of the free stream
U	- internal energy of the mixture

$\vec{v}$ - velocity (vector)

V - velocity

V_0 - muzzle velocity of the projectile

$V_{x,y,z}$ - velocity (components)

V_r - resulting velocity

V_∞ - velocity of the free stream (air)

w_j - velocity of the combustion products at the Base-Bleed orifice

W, $W_{x,y,z}$ - wind velocity components

X, Y, Z - projectile coordinates (trajectory)

$\vec{i}, \vec{j}, \vec{k}$ - unit vectors (trajectory)

α - angle of attack

α_d - yaw of repose (angel of attack of the dynamic equilibrium)

α_T - total angle of attack

β - correction factor – Base-Bleed effect

γ - adiabatic exponent (air)

κ - isentropic exponent – combustion products

λ, λ_f - projectile aspect ratio L/d

π - math. constant = 3.141592653589

θ - rear cone angle (double value)

θ_0 - gun elevation angle

ρ - density

ρ_0 - density of the combustion products

ρ_j - density of the combustion products at Base-Bleed orifice

ρ_∞ - air density – free stream

τ_m - average tangential potential on surface P (wetted surface)

ω - projectile angular velocity

Abbreviations

AP	- ammonium perchlorate
BB	- Base – Bleed
BT	- Boat -Tail
CFD	- Computational Fluid Dynamics
ER-BB	- Extended Range – Base Bleed
ERFB	- Extended Range Full Bore
FEA	- Finite Element Analysis
HE-ER	- High Explosive – Extended Range
HTPB	- Hydroxyl-terminated Polybutadiene
IB	- Interior Ballistics
INS	- Inertial Navigation Systems
IMU	- Inertial Measurement Unit
MEMS	- Microelectromechanical Systems
M-REP	- Modular Range Enhanced Projectile
MPMT	- Modified Point Mass Trajectory
SAL	-Semi Active Laser (guidance)
SRM	- Solid Rocket Motor

1 AN OVERVIEW OF THE WORK

1.1 Statement of Objective

The “Design Process” of missiles or complex projectiles, can be regarded as an elaborate process, a process that can be “pictured” as a path that brings together many engineering disciplines and activities. On that path, work is conducted in parallel “streams” of different engineering specialities such as aerodynamics, exterior ballistics, guidance and control, materials engineering, chemistry of propellants and explosives, interior ballistics, structural analysis, terminal effect analysis, physical testing. Optimisation of projectile design is reached through iterations (“closed-loop” process), by comparing each iteration against projectile’s technical requirements defined at beginning of a process, i.e. “experts” converge on the “solution” only at the end of each optimization cycle. Technical requirements represent projectile’s “performance” list, with most important feature, i.e. feature that requires most improvement at the top of the list. For large calibre gun-howitzer projectiles, main improvement aims (in order of significance) are range (primary), accuracy (secondary), and lethality (tertiary) [1-3]. Therefore, design of classical artillery shells did not change much in the last century, and propulsion and “guidance and control” were “reserved” for various types of missiles, but not for “standard” gun projectiles. With recent advancement in electronics, the leap in design of artillery ammunition has been made [3], but with increased complexity and costing, contrary to intended use of artillery [4].

1.1.1 Motivation

The motivation for this research work is to propose future artillery projectile with significant increase in range, low cost and with modularity required to engage different targets, i.e. to have different mission profiles. In order to overcome the complexity of guided missiles, thus cost of a projectile, this work explores techniques related to improvement of artillery shell aerodynamics, propulsion, and flight mechanics.

1.1.2 Aims and Objectives

The aims of this thesis are to (i) design the new Modular Range Enhanced Projectile (M-REP) and to (ii) present detailed modelling and optimisation process of innovative M-REP design, as “pattern” for future large calibre ammunition development. The M-REP offers significant enhancement in range for selected launch platforms (i.e. 155 mm ordnances, with 39 and 52 calibre barrel length), while maintaining similar lethality and accuracy in comparison to existing pallet of 155mm projectiles.

To achieve the above set aims, proposed M-REP design requires in-depth understanding of interior and exterior ballistics, rocket science, chemistry of propellant and explosives, structural mechanics of various materials under high strain and stress rates uncommon to general engineering practice, terminal ballistics and various experimental and testing procedures. Following is the “inventory” of objectives required to achieve desired goals:

- Review of the “previous art” and work published by the peer researchers in relevant scientific and engineering fields;
- Investigation of new range of solid rocket propellant compositions with high specific impulse, validation of new propellant energetic and mechanical properties through simulations and experiments;
- Research on base drag and design of a Base Bleed (BB) unit, new design of multi-propellant base bleed grain for efficient reduction of projectile’s drag from muzzle to trajectory apogee; development of suitable mathematical model for “base bleed” phenomenon, and validation through comparison with experimental data;
- Research and design of Solid Rocket Motor for gun launched projectile, investigation of novel methods in design of SRM’s interior ballistics and burning surface development with multitude of embedded heat conductors, burning surface modelling and interior ballistics calculations;

- Investigation and modelling of novel exterior ballistics profiling methods for gun launched projectiles using rocket propulsion, in order to increase range and decrease projectile dispersion on target;
- Investigation and designing of aerodynamically optimized projectile body to reduce profile drag;
- Investigation and designing of modular payload to improve the projectile lethality, i.e. investigation and optimisation of "metal jacket to explosive" ratio for projectiles with reduced "payload" volume, and design validation through lethality modelling and simulations;
- Validating the compatibility of new design with standard 39-calibre ordnance with 19 litres combustion chamber volume against aim to reach +40 km in range at sea level. Validating new design against 52-calibre gun systems with 23 litres combustion chamber volume to reach +50 km, when fired form the howitzer at sea level.

The overall objective is to establish the "template" for artillery shell design for all types of large calibre guns using methodology presented in M-REP engineering design process. Proposed design optimisation also aims to provide a solution for low cost range enhancement that still can be upgraded with "trajectory correction" module for enhanced precision on target.

1.2 Structure of the Work

This document is arranged in nine chapters. The current chapter covers the introduction, overview of the project, and briefly point out thesis aims and objectives.

Second Chapter: Literature review on various methods to enhance the projectile range has been undertaken in the second chapter, i.e. discussion related on improvement of projectile dimensions and aerodynamic shape, base drag reduction, flight profile alteration and possible use of propulsion.

Third Chapter: The design methodology of a base bleed unit, its performance calculation, and optimisation are presented in this chapter.

Concept of base drag is introduced. Mathematical model for base drag reduction is developed, as well as method for design of an appropriate base bleed propellant grain. The optimal propellant formulation is investigated and solution is given. Series of simulations and experiments are conducted, and compared with experimental results from static and firing test. The results confirm validity of proposed model and design.

Fourth Chapter: The design methodology for a gun launched solid rocket motor (SRM) is presented in fourth chapter. A generalised mathematical model is developed for solid rocket motor thrust, using the governing equations. Model is amended to describe increase in propellant burning surface area using embedded “hot wire” mechanism, in order to enhance local burning rate thus resulting in higher rocket motor thrust. Thermo-chemical and interior ballistics parameters of a novel thermoplastics poly-plastisol composite propellant used in SRM “design” are also investigated and elaborated in this chapter. Series of experiments and simulations are conducted, with results confirming the postulated model and methodology.

Fifth Chapter: Calculation of flight parameters of range enhanced projectile is presented in this chapter. Aerodynamic coefficients for M-REP are calculated using analytical and numerical methods. The trajectories and trajectory’s parameters are calculated using 4DOF and 6DOF (degrees-of-freedom) equations of motion, modified to include the effects of base bleed unit and rocket propulsion on a trajectory. The optimal trajectory for maximum range and minimum dispersion due to solid rocket motor ignition delay and de-spin is investigated. Feasibility study includes simulations in different software tools, confirming viability of M-REP’s design goals. Simulation results are tabulated and presented on appropriate diagrams.

Sixth Chapter: Structural integrity assessment of M-REP is presented in this chapter. The research is focused on simulation of solid rocket propellant grains for BB and SRM under severe pressure and inertial loads during firing sequence. The mechanical model for visco-elastic propellant derived from experiments is incorporated into the investigation of structural integrity of M-

REP modules. The projectile structural response under dynamic loading is presented.

Seventh Chapter: A review of interior ballistics of gun –projectile - system is presented in this chapter. The modelling of projectile inside the gun tube is undertaken in order to check the compatibility of projectile with corresponding ordnance. Results are presented in the form of tables and diagrams.

Eighth Chapter: An investigation of payload's lethality is conducted. The assessment of payload module (naturally fragmenting warhead with standard energetic materials COPMB B (RDX/TNT) or TNT with aluminium powder) through simulations has yielded satisfactory result.

Ninth Chapter: The thesis concludes with "Conclusions and Recommendation" which gives the overview of the project. The research results are summarised, conclusions derived with reference to the aims and objectives set in First Chapter, and recommendation and guidance for future work are given, based on thesis outcomes.

1.3 Outcomes and Contribution to Knowledge

The direct outcomes of investigations made in this work are as follows:

- New inventive design of Modular Range Enhanced Projectile (M-REP) in 155mm calibre, with one of the longest range among contemporary 155mm ammunition, with diverse effect on targets;

- Innovative design of base bleed module commutable with all existing 155mm ER-BB projectiles, which contributes to range increase and reliability of BB ammunition;

- Novel design of SRM for gun-launched projectiles that can withstand the severe acceleration loads in gun barrel.

- Novel class of thermoplastic "Poly-Plastisol" solid rocket propellants with energetic plasticizer;

The contribution to knowledge made in this thesis is as follows:

- Methodology for calculation and optimisation of base drag reduction using “base bleed” effect; methodology for design of BB propellant grain, BB chemical composition, size, and shape;

- Methodology for computation of SRM interior ballistics with propellant grain using multitude of imbedded heat conductors for burning rate augmentation, in order to decrease active time of end-burning propellant grains;

- Methodology for ballistic trajectory optimisation of spin stabilized artillery projectile using propulsion module with ignition delay and de-spinning effect;

- A model of modular artillery projectile with reduced payload volume capable to engage different targets, without reduction in terminal effect, for naturally fragmenting warhead, in particular;

2 LITERATURE REVIEW

2.1 Introduction

The ultimate design requirement for weapons systems including artillery is to enable engagement of enemy forces at distances longer then enemy could fire back at your own firing position [3-6]. In addition, the level of precision and payload lethality must be sufficient to defeat enemy targets efficiently. The goal of this work is to enhance the effectiveness of current systems within the constraints of contemporary requirements defined in strategic development plans for defence sector (e.g. developing defence capabilities across Defence Lines of Development - DLoDs, as defined in UK defence “doctrine”), or similar international defence framework that describes strategic development intentions Therefore, one of the aim of this study is to use existing platform and charge system to propel a new artillery round with enhanced range while conforming to guidelines described in strategic documents, such as Joint Ballistic Memorandum of Understanding (JBMOU) [1]. According to JBMoU new developments of artillery projectiles should be 100% compatible with existing weapon systems [5]. Therefore, the mass and overall geometry of a new projectile should comply with existing weapons system (e.g. 155mm howitzer), i.e. the new projectile when it is fired from the current ordnance, it must not exceed designed chamber pressure [5, 6]. Moreover, lethality of new projectile should be comparable to the existing rounds [3, 7], i.e. the lethality should not be lower than target defeating capability of standard M107 HE projectile in 155mm calibre.

Number of solutions are available to ammunition designers to extend range of an artillery projectile. In the following paragraphs, we will review and discuss those methods, and we will evaluate the most efficient technique for enhancing the effectiveness of a new proposed solution.

2.2 Overview of the range increasing methods

As previously suggested, range, accuracy and lethality represent “only true” R&D goals for any new design or improvement of artillery system. Therefore, referring to postulated problems, different algorithms can be used to solve it, or different methods can be combined to find the proper solution.

One of the methods that is proposed in this thesis, is to implement “hybrid concept” [8, 9] with base bleed and solid rocket motor incorporated in artillery shell, which will provide longest effective range from given ordnance, as BB will act as drag reduction device and SRM as additional propulsion to the projectile. Another solution which appeared with advancement of sensor technology (INS, IMU, MEMS) - technology that can withstand severe launching conditions in gun barrel [10-12], is “gliding concept”. An additional “gliding” surface (an aerodynamic-lift surface such as tail fins and canards) can be introduced on a projectile, in order to achieve long ranges by maintaining high lift-to-drag ratio during projectile flight, by guidance system. Gliding projectile can be more accurate, but with significant increase in cost of a projectile [4, 12-14], which becomes a guided missile. Hence, proposed platform of “Modular Range Enhanced Projectile” M-REP, do not aim for “guidance and control”, but tries to adopt the best of “mechanical” solutions for achieving longer ranges and better accuracy, which are:

I) Changing the Interior Ballistic [5, 6, 15] of a gun, i.e. increase in muzzle velocity will enhance range of artillery shell. That can be solved with:

1) Longer barrel, [5, 6]
2) Higher working pressures inside “barrel chamber” [5, 6, 15],
3) Liquid or solid high-energetic propellant charges [5, 6, 15], that burn in a way which maintain high pressure behind traveling shot.

However, Interior Ballistics solutions, at least solutions 1) and 2) cannot be implemented as we have to utilise existing howitzers, and solution 3) requires many changes in how howitzer operates.

II) Exterior ballistics [5, 16-31] methods for range increasing:

1) Drag reduction:

a) Pressure-Wave Drag reduction by changing the shape of the ogive [16-21, 24, 25, 27-29, 31],

b) Base Drag reduction,

- Changing the bottom shape of the shell [32],
- Lifting base pressure using the gas generator – "base bleed" unit [6, 33-47], and/or,

2) Designing the sabot ammunition, stabilised by rotation and/or with tail fins [6, 21, 27, 29],

III) Rocket Assisted Projectiles (RAP) – projectile with solid rocket motor [9, 48-54]

IV) Ramjet projectiles – particularly solid fuel ramjet projectiles (SFRJ) [55-59]

The 155mm calibre ordnances will be used as platform for comparison, as they are still No. 1 artillery weapons systems in majority of armed forces around the world.

The maximum range, with preserving the same ratio of explosive filling vs. metal jacket, as in standard projectile (e.g.155 mm M107 HE), can be achieved by utilising projectile drag reduction (pressure-wave drag reduction by changing ogive's shape and base drag reduction with base bleed unit). All other techniques including rocket assisted and ramjet projectiles, as well as guided gliding ammunition, have significant influence on warhead volume. However, the lethality of the payload can be kept on the same level as standard projectile using some advanced design solutions for payload. Existing Rocket Assisted Projectiles (such as 155mm M549A1) have similar maximum range with ER/BB projectiles when fired from 39 calibre guns and utilising max. gun propelling powder charge, but they cannot be fired from 52 calibre howitzers with corresponding max. propellant charge for 52 calibre gun, due to structural problems. The lethality of rocket assisted projectile is reduced in comparison to standard 155 mm M107 HE ammunition, i.e. approximately 45% of the projectile's volume is occupied with SRM. Gun Launched Solid Fuel Ramjet

(SFRJ) projectile can achieve very long range (theoretically), however the ratio of specific impulse per unit mass is less than SRM. In addition, the volume for projectile's explosive charge is compromised by relatively large annular cavity required for airflow. Yet, gun launched SFRJ projectile due to significantly complex operating conditions [55-59], in comparison to SRM, did not found application as howitzer projectiles. The feasible solution for maximum range is "modular" projectile with rocket engine and base bleed combined together with optimised ogive and base shape [8]. Modular projectile has much longer range comparing to BB projectile or RAP with same "body" shape, and fired with same muzzle velocity. Proposed design of 155mm M-REP, although mass of explosive filling is 70% of ERFB-BB's HE, has similar level of target defeating capability. The equivalent lethality can be achieved using modern HE compositions and optimised fragmentation of payload's metal jacket [7, 60, 61]. The "operation" of proposed "modular" projectile is simple: fired form the gun, streamlined ogive in combination with novel BB and new type of "thruster" propels projectile to ranges beyond reach of contemporary artillery systems.

Recently, the emphasis of development in ammunition technology is on "glide" ammunition [4, 12-14]. The glide control-guiding system of gun launched projectile takes over in descending part of the trajectory, using movable canards and tail lifting surfaces. Projectile glides toward target, simultaneously guiding itself for precision strike – CEP (circular error probability) less than 20m. However, even "glide" technology cannot provide extended ranges without assistance of base bleed and/or solid rocket motor. Further, cost of guided ammunition [9] is 20-30 times more expensive then proposed "modular" projectile. Max. ranges of contemporary guided ammunition [4] are less than lover values of "modular" projectile max. range fired from 39 calibre howitzer. In addition, precision of "modular" projectile can be significantly increased if COTS (commercially-of-the-shelf) components for trajectory correction (1D or 2D correction – range/lateral dispersion) [9] are added to the projectile. The recent advancement in production of GPS (Global Positioning System) receivers and IMU (inertial measurement unit) sensors contributed to new types of navigational devices that can withstand high acceleration during gun launch.

Those devices, combined with trajectory correction techniques, such as aerodynamic brakes or spoilers, can provide to “modular” projectile increased precision for some type of potential targets [2, 10, 11, 30, 62, 63].

2.3 Recent developments overview

One of the most dynamic areas in artillery research and development is field of long range ammunition, especially in 155 mm calibre. Not so long ago, several large projects were introduced, with aim to provide extended range and enhanced precision using contemporary 155mm ordnance systems. One of those programs, is XM982 Excalibur projectile [4,9]. The “Excalibur block 1a” has been successfully tested and deployed using base-bleed and gliding technology, but without any significant increase in range, i.e. the operational range achieved is “only” 24 km. The “Excalibur block 1b” recently completed proof trials suggest that range of 35km and 40km can be reached from selected ordnances - also using base bleed and gliding technology (program lead by Raytheon - BAE-Bofors); USA Army recently rejects concept developed by ”ATK Systems” with SRM and gliding technology. Similar projects like BTREM, LRLAP and ER(G)M – extender range munitions for naval guns using SRM and gliding technology (although the projects have the potential to reach beyond 70km, all of them have been halted or going through reviewing process). European program VULCANO using sabot projectile with fins and canards and gliding technology has not yet achieved low rate production. [9, 64]. Further, there is extensive academic research in field of related technologies, that are studied separately, especially in the field of trajectory correction and projectile guidance [2, 4, 10-14, 30, 62, 63]

If large and reliable increase in range is primary objective, it cannot not be achieved with base bleed, rocket assistance or gliding technology exclusively. The most effective way to increase range and keeping projectile simple, with small production costs, is combination of optimised base bleed and rocket propulsion. The BB and SRM should be utilised at most effective part of projectile’s ballistic path – ascending trajectory. Optimal combination can be

updated with increased precision devices such as PGK (Precision Guidance Kit) [TCF (Trajectory Correction Fuze) or Top Gun Fuze [9], or it can be build-up with “gliding” technology [14]. However, gliding guiding concept (with inertial navigation system and GPS, and sometimes semi-active laser homing) will increase price and complexity of system to a high level, that is not in “scope” how to utilise artillery (artillery should be cheap and to deliver large quantities of relatively inexpensive payloads, from a safe distance).

One of the projects that are in line with these requirements is 155mm VLAP (velocity enhanced long range artillery projectile) form Denel-South Africa [9, 66]. It is utilising both base bleed and solid rocket motor with ERFB (extended range full bore) projectile shape. The significant increase in range is achieved, ranges between 39km-51km at sea level has been reached, using 39-52 calibre 155mm howitzers respectively. The design has its own “ conceptual delays” due to fact that solid rocket motor is in line with base-bleed unit, ejecting combustion products through base bleed cavity. This has negative influence toward base bleed “active” time [33-47, 65]. The rocket ignition time-delay is approximately 11s for V-LAP projectile, so rocket engine interferes very early with base bleed to allow BB to have optimum effect on the trajectory. The ignition of rocket motor will produce higher pressure in a base bleed unit that will shorten active time of base bleed, i.e. it will consume the large portion of base bleed propellant very quickly. Secondly, solid rocket propellant grain is influenced by combustion gases from the gun powder propellant charge that can have impact on structural integrity of SRM propellant grain (propellant grain with the central port) [67] and reliability of the projectile. The main setback of the design is the significantly reduced lethality of the projectile, as the explosive charge is 4.5 kg i.e. 50% of the standard ERFB-BB projectile, and it is situated in the nose, most unfavourable for use with point detonating fuzes. Although it is advertised [9] for several years as completed round, no army adopted projectile as part of their arsenal.

2.4 The Concept of Modular Range Enhanced Projectile

The M-REP projectile is devised as reliable concept of separated base bleed unit with optimised propellant grain to reduce drag during the significant part of the trajectory, as well as separated SRM with mono-block propellant grain that can withstand high in-barrel acceleration, with ignition at most adequate time of the trajectory to produce max. range and minimum dispersion. The calculated range is 41km from 39 and 52 km from 52 calibre howitzers respectively. The projectile reliability should be high -99.99% at 80% lower bound confidence, during the storage life of M-REP, having the base bleed and solid rocket working independently. The target defeating capability will be the at least the same as with conventional projectile, exploiting the new energetic materials and with higher terminal velocities [15,68].

The M-REP solid rocket motor design rely on the novel thermoplastic propellant, with “exotic” solution for burning surface development – using approx. 50 heat conductors-copper wires to augment the propellant burning rate [8, 69-75]. The working pressure of the solid rocket motor is above 150 bars allowing the relatively slow burning rate propellant due to higher content of binder to burn with higher burning rate. The higher content of binder is required with reference to structural integrity of the propellant grain, i.e. to withstand high accelerations load during launch. Solid propellant is monolithic block confined in combustion chamber, only having technological gaps between the walls of combustion chamber and outer diameter of the propellant grain, it should withstand the as high as 18000g acceleration in the gun barrel. The nozzles (6 pcs.) are deployed radial, with inclination angle to the projectile axis of 30^0. This configuration allows thrust to be divided onto 6 parts, so the any misalignment of the thrust is reduced by 1/6. The cant angle of approx. 8 deg to the nozzles can be introduced to de-spin the projectile. The nozzle throats are made of refractory metal that can withstand the high temperature and fluxes without ablation.

Aerodynamic shape [16-21, 24, 25, 27-29, 31, 32] of the projectile exploits the optimised ogive with aspect ratio 4:1 and projectile boat-tail optimised for the base bleed configuration. The shape, overall length and mass of the projectile corresponds to the existing pallet of ammunition for the 155mm ordnance (in-service), as well as with NATO JBMoU. Payload (explosive mass) is kept on the level 85% of the standard 155mm M107 projectile, however the terminal effect is better than standard HE projectile using new type of energetic material and exploiting the higher impact velocities (both axial and angular) of the M-REP.

2.5 Summary

The proposed M-REP design represents contribution to the methodology for development of artillery ammunition, especially long-range artillery shells. The applied new design methods which will be presented in detail in next chapters, implementing new design techniques, new propellants and propellant configurations, allows at least 80% longer ranges comparing to the standard ammunition. In combination with modules that replace the SRM and base bleed with additional payload module or boat tail module, the M-REP can become “only” projectile in the inventory, capable to replace the entire pallet of ammunition. The modular projectiles can be upgraded with trajectory correction fuze in order to achieve enhanced precision, or it can be a used as platform with gliding capabilities if module with lift generating fins is added.

3 METHODOLOGY FOR M-REP'S BASE BLEED PERFORMANCE CALCULATION AND OPTIMISATION

3.1 Introduction

Methodology for base bleed performance calculation and optimisation represents the algorithm for trajectory calculation of artillery projectiles with base bleed unit in conjunction with calculation of the in-flight combustion process of base bleed propellant grain. The methodology presented in this chapter enabled development and optimisation of innovative base bleed unit design. New design includes new BB propellant, novel pyrotechnic compounds for sustaining the flame in BB unit at muzzle, new shape of propellant grain for optimized injection of combustion gases in the wake zone of the projectile, and design of the BB casing. The novel propellant formulation is based on newly developed type of "Poly-Plastisol" composite solid rocket propellant. New Base-Bleed propellant grain shape is evaluated against the existing BB grain design. The simulations and comparison with experiments confirm optimization of base bleed injection along projectile ballistics trajectory and increase in range due to base drag reduction.

Therefore, the aim to improve design and formulation of BB propellant and burning surface shape, so that the overall design of the M-REP can optimally exploit the effect of base-drag reduction, is achieved by investigation of the following aspects of base bleed unit design:

a) critically review literature on base bleed and evaluate up-to date development in Base-Bleed technology as well as to review existing modelling of base-drag phenomenon,
b) to investigate the mechanism of base-drag reduction, both through simulations and experimentally,
c) to study the formulation of a novel Base-Bleed propellant and grain design validation through simulations and experiments, and
d) to model the influence of "base bleed" on projectile's flight.

3.1.1 The BB concept

The general concept [3] behind BB is to alter (increase) the base pressure, i.e. to decrease base pressure drag of a supersonic projectile by injecting small amount of hot gas (i.e. combustion products) into the flow field (wake) behind base of a projectile. By injecting the hot gases, negative pressure at the base is raised to lower negative magnitude. For the same muzzle velocity that corresponds to the maximum range from a given ordnance, the Base-Bleed projectile should fly at least 30% more compared to same long-range projectile fired without BB (e.g. ERFB-BT or ER-BT).

Physical phenomena: the large turbulent (recirculation) zone at the projectile base during the supersonic (trans-sub-sonic) flight is generally divided into two regions; first is a recirculation region which remains at the projectile's axis of symmetry, and the second is situated right behind the projectile's base edge as shown on fig. 3-1.

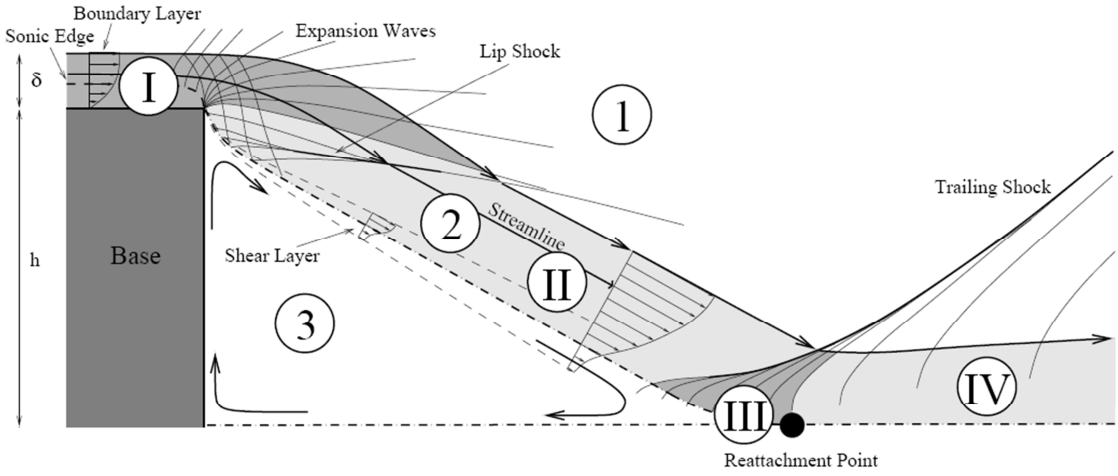

I – Fully developed turbulent boundary layer
II – Supersonic stream that converges to the projectile axis of symmetry
III – Compressible Shock Waves Zone
IV – Wake
1 – Free stream conditions
2 – Streamlines
3 – Recirculation Zone

Figure 3-1 Flow behind projectile in supersonic flight [47]

As the mass flow rate is increased by injecting the Base-Bleed combustion products, the recirculation region at the axis is expelled further out, while the region at the base edge becomes larger. The main flow separates from the base edge and the wake turns with the expanding flow, and eventually compresses back to be aligned with the axis of symmetry – Figure 3-2. If the mass flow rate is further increased, the recirculation region near the axis disappears, and the Base-Bleed flow follows a straight path. In that way significant reduction in base drag is achieved – low pressure zone that is inducing the base drag is altered. The problem to solve is how much of the hot (burning) gases must be injected in the base region to reduce the base drag.

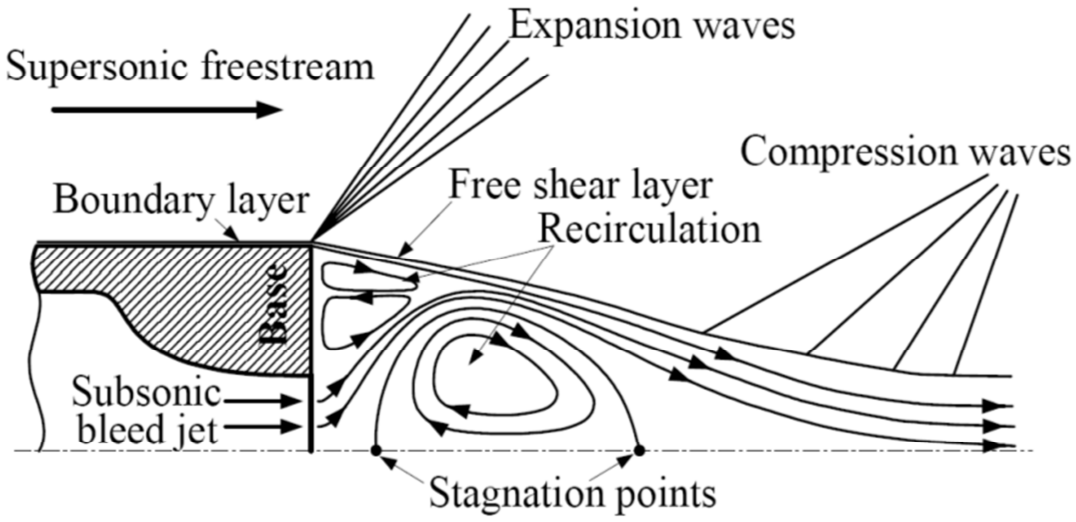

Figure 3-2 Representation of the flow behind the supersonic projectile with Base-Bleed injection [46]

On a conceptual level, the complexity of the real physical model and problem solving paths (analytical or numerical including CFD) directs that solution should be balance between the complexity of the model and the important physical details included in the computation. The investigation methods emphasise the interactive model for trajectory calculation and “dimensioning” the projectile’s Base-Bleed units and solid rocket motor. With semi-empirical correlations between main parameters of drag reduction, developed algorithm for trajectory calculation of the in-flight combustion process of Base-Bleed propellant grain, particularly takes into account combustion of the

novel type of fuel rich “Poly-Plastisol” propellant – as the main subject of interest and contribution to the M-REP design and development.

3.2 Review of base drag and base bleed mathematical models

There has been constant overlapping between two parallel processes in base drag research: first, understanding the base drag phenomenon, and attempt to model (mathematically describe) the flow in the wake of the projectile. Second process, to find a practical solution for base drag reduction using available engineering methods:

- Streamlining the projectile - changing the bottom shape of the shell [6],
- Reducing the base drag by injecting the gases into the wake zone of a projectile, e.g. Base-Bleed unit [2-5, 11, 12, 17-19, 32, 34-36, 62, 69-71].

Background: The existence of base drag reduction phenomenon due to “gas-generator” at the bottom of a projectile was noticed before and during WWII. The anti-aircraft gun projectiles with tracers (tracer ammunition) have velocity reduction on the trajectory slower than without tracer, thus more flat trajectory and greater ranges. Yet, this incidence was not investigated in details until mid-1960’s when real testing of the effect started in USA, UK and Sweden. At the beginning, air at room temperature is used as base bleed gas. Later, as research progresses, positive effects of using the gases with smaller molecular weight at high temperature were observed and significant experimental results on base drag reduction – (base pressure increase) were achieved. Experiments in wind tunnel with Hydrogen (H_2), burning in the wake of the projectile (projectile base) produced the best results in drag reduction.

As research evolved, scientists and engineers were discussing practical solutions [39]. If compressed gas is used (gaseous hydrogen or liquid hydrogen) as bleeding gas that burns in the wake behind a projectile, combustion of hydrogen is very efficient from aspect of base drag reduction, but gas amount confined in projectile was very small. Furthermore, major setback is the way of storing the compressed gas and shelf-life of such projectile.

Researchers returned to solutions that exploit gas generated by combustion of tracer mixtures. However, effects on base pressure were significantly smaller comparing to the combustion of hydrogen. At that time, solution with solid rocket composite propellant imposes itself as source of gases with appropriate molecular weight and combustion temperature.

Beside the combustion characteristics and gas volume production, significant parameters that influence Base-Bleed design are mechanical properties of solid rocket propellant used for Base-Bleed grain manufacturing. The Base-Bleed grain must withstand high acceleration and pressures inside gun chamber and barrel during firing. Appropriate mass flow of combustion products is achieved with adequate geometry of propellant grain (burning surface vs. web) and adequate propellant burning rate at projectile's trajectory. With few approximations, results showed that combustion products of Base-Bleed unit must have drag reducing effect, at least during the first 1/3 of projectile's trajectory, in order to achieve significant increase in range.

Testing of the given concepts, gave general approach to the desirable characteristics of "base-bleed" unit design [39]:

a) Most important is to minimise or even eliminate the interim time of gas-generator reigniting after leaving the barrel muzzle, and to equalise difference in reigniting time after each consecutive firing, if the interim exists. Hence, design of BB Unit features "sustainer-igniter", a small pyrotechnic subassembly (pyrotechnic mixture insensitive to pressure disturbances) with characteristic that helps keeping the combustion of main Base-Bleed propellant after leaving the gun muzzle – figure 3.3.
b) Solid Composite Propellant that contains less oxidiser then usual solid propellant mixtures produces better results for increase of base pressure, owing to effect of afterburning of combustion products in the wake of a projectile. However, lower content of oxidiser then optimal in propellant mixture, reduces Base-Bleed performance due to lower combustion temperature, also affecting the stability of ignition of the BB propellant grain at the muzzle.

c) Adding solid particles (powder metals, such as aluminium or magnesium) in propellant mixture to gain higher combustion temperature would have negative influence. It is due to higher burning rate of solid propellant (with same content of oxidiser), that will produce shorter effective combustion time of BB on projectile's trajectory, thus resulting with shorter range. Beside augmenting the burning rate, solid particles have higher kinetic energy, therefore it is difficult to absorb solid particles in recirculation zone at the bottom of a projectile, resulting in even more reduced base bleed effect.

Figure 3-3 Testing of HE-ER/BB 105mm [38], observe burning of the BB just after the muzzle exit (no interim in burning)

3.2.1 Principles of Base Drag

Base drag represents significant contribution to the total drag of an artillery projectile, especially with artillery shells that have optimised shape of ogive (reduced pressure-wave drag). For ER projectiles, base drag represents more than 50% of the total drag. It is evident, that reduction of base drag is essential in order to increase the range of the projectile.

Base drag, otherwise drag of the projectile bottom, occurs due to low pressure at the projectile bottom (base), as an effect of recirculation and de-attached airflow behind the basis of flying projectile – figure 3.1.

Flow (wake zone) behind flying projectile represents complex phenomenon, and if we take in account all influences that are involved in the phenomenon, problem solving become even more complex. There is no mathematical model that produces an analytical solution of the base pressure (drag) coefficient, nor correlate base pressure with parameters that characterise wake- flow phenomenon. As a “expository” solution, base pressure coefficient is introduced and described by the relation 3-1 [21]:

$$-Cp_b = \frac{p_b - p_\infty}{q_\infty} \qquad \textbf{(3-1)}$$

Where p_∞ (static pressure) and q_∞ (dynamic pressure) are conditions of a free air stream.

To reach a solution of the base drag problem, either experimental approach with hypothetical empirical equations for the wake flow, or CFD (computational fluid dynamics) methods with semi-empirical relations [42-44], can be utilised.

Two essential states of base flow can be distinguished – subsonic and supersonic flow. Common hypothetical postulates (preconditions) for both flow cases are:

a) Base pressure p_b is equal at each and every point of base surface S_b – i.e. base pressure is not function of a radius r_b (r_b -radius measured form projectile axis of symmetry);

b) Base pressure p_b is same for the flow cases where a projectile is in the axis-symmetric air stream or it is under the angle of attack (AoA), so-called total AoA - α_T (with premise that total AoA- α_T is relatively small).

3.2.2 Subsonic flow

Subsonic flow behind a projectile produces an extended boundary layer in shape of a cylindrical surface, with “accelerated” increase in layer thickness. In central part of the cylinder in vicinity of the base we can observe relatively “motionless”- static volume of air contrary to the air close to boundary layer, that is flowing air stream. These differences between velocities in layers induce occurrence of sub-pressure p_b in vicinity of the base. The sub-pressure decreases with distance from the base, while thickness of the turbulent boundary layer increases. The sub-pressure influence streamlines to converge toward the axis of symmetry. Hence, “value” of the base pressure is directly coupled with the thickness of the boundary layer. Furthermore, using boundary layer theory, shear (tangential) potential is inversely proportional to the thickness of boundary layer. Therewithal, tests were conducted for obtaining the correlation between shear potential and sub-pressure at the base of the projectile. The acquired results[16, 21, 25], can be described with next equations:

$$Cp_b = -\frac{0.029}{\sqrt{\frac{\tau_m}{q_\infty}\cdot\frac{P}{S_b}}} \qquad \textbf{(3-2)}$$

where τ_m is average tangential potential at surface P (projectile wetted surface without base). Since,

$$\tau_m = \frac{D_f}{P} = \frac{C_{Df}\cdot q_\infty \cdot S}{P} \qquad \textbf{(3-3)}$$

and

$$C_{Db} = -Cp_b \cdot \frac{S_b}{S} \quad \textbf{(3-4)}$$

The base pressure coefficient for subsonic flow is:

$$C_{Db} = \frac{0.029}{\sqrt{C_{Df}}} \cdot \overline{S}_b^{\,1.5} \quad \textbf{(3-5)}$$

Where $\overline{S}_b$ is ratio between S_b/S. In case of a rocket, during the "active" phase of flight, base drag reduction is calculated by subtracting the nozzle exit areas ΣS_j from base area S_b, in case of multi-nozzle design of a rocket engine. Thus, equation becomes:

$$C_{Db} = \frac{0.029}{\sqrt{C_{Df}}} \cdot \frac{d_b}{d} \cdot \frac{S_b - \sum S_j}{S} \quad \textbf{(3-6)}$$

Similar semi-empirical equation is used for estimating the subsonic base drag coefficient, which yields similar results:

$$C_{Db} = \frac{0.0155}{\sqrt{\lambda_f \cdot C_{Df}}} \cdot \frac{d_b}{d} \cdot \frac{S_{b\,ekv}}{S} \quad \textbf{(3-7)}$$

where λ_f is projectile aspect ratio L/d.

3.2.3 Supersonic flow

Supersonic flow behind projectile produces sub-pressure at the base of a projectile, very similar to subsonic flow. Sub-pressure causes the same effect pushing the streamlines to converge toward the axis of symmetry (behind the projectile). Near the axis of symmetry, stream "bends" once more to be parallel with the axis. That "straightening" of air stream is followed with shock waves that feature as main flow characteristics for the projectile in supersonic flight regime. Shock waves are accompanied with turbulent wake, which can be regarded as "solid body" for the airflow (Figure 3-1). At the point where streamlines are confronted (inflow), pressure rises and start to push the airflow toward the base of the projectile. Supersonic flow in conjunction with boundary (bended, prolonged part of boundary layer) layer, absorbs the air from the base and produce recirculation flow at the bottom of the projectile. These

experimental observations induced theoretical work, which had a goal to describe supersonic base drag pressure and base drag coefficients as empirical relations [25]. Figure 3-3, figure 3-4, and figure 3-5 describe relations between base drag pressure (base drag coefficient), and Reynolds number – Re, Mach number – M, $\frac{L}{d \cdot \sqrt{\mathrm{Re}}}$ (non-dimensional ratio) for laminar boundary layer, $\frac{L}{d \cdot \sqrt[5]{\mathrm{Re}}}$ (non- dimensional ratio) for turbulent boundary layer, and non-dimensional ratio of $tg\theta / \bar{S}_b$, in case that projectile poses rear cone.

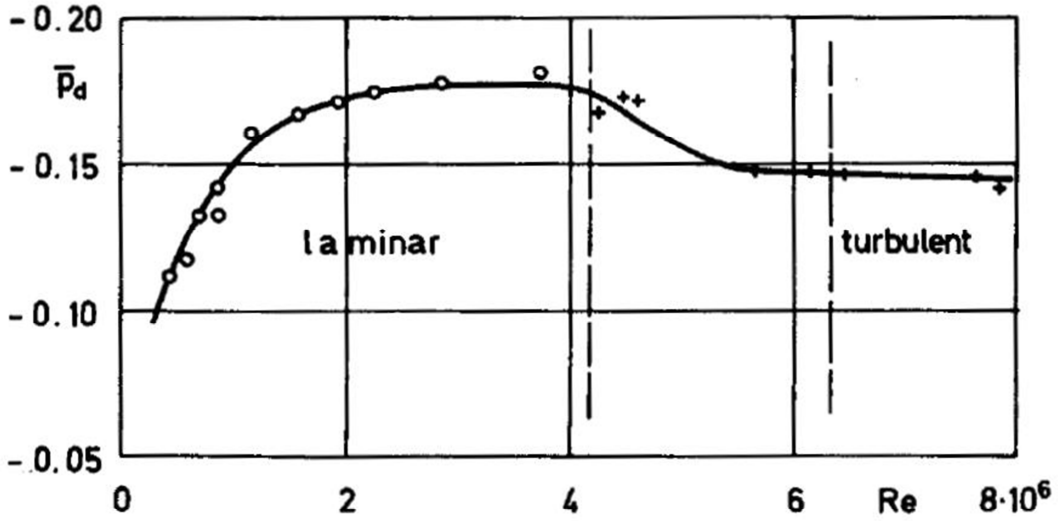

Figure 3-4 Base pressure coefficient vs. Reynolds number [21]

In case when Re is greater than $6 \cdot 10^6$, i.e. in case of turbulent flow, C_{Pb} becomes function of the Mach number only, i.e. irrespective of the Re. That dependency is presented in figure 3-4 [21] and equation 3-8 ($C_{Db} = -Cp_b$ for cylindrical "end" of the projectile). If case of a projectile with fins, (M-REP has no fins), Cp_b is augmented due to presence of wings in vicinity of the projectile base (again with cylindrical "end") for transonic speeds and supersonic speeds up to Mach 3 (figure 3-4).

$$C_{Db} = -Cp_b = \left(1 - \frac{p_b}{p_\infty}\right) \cdot \frac{1}{0.7 \cdot M^2} \qquad \textbf{(3-8)}$$

In case of vacuum at the base of the projectile, Cp_b value becomes:

$$-Cp_b = \frac{1.43}{M^2} \quad \textbf{(3-9)}$$

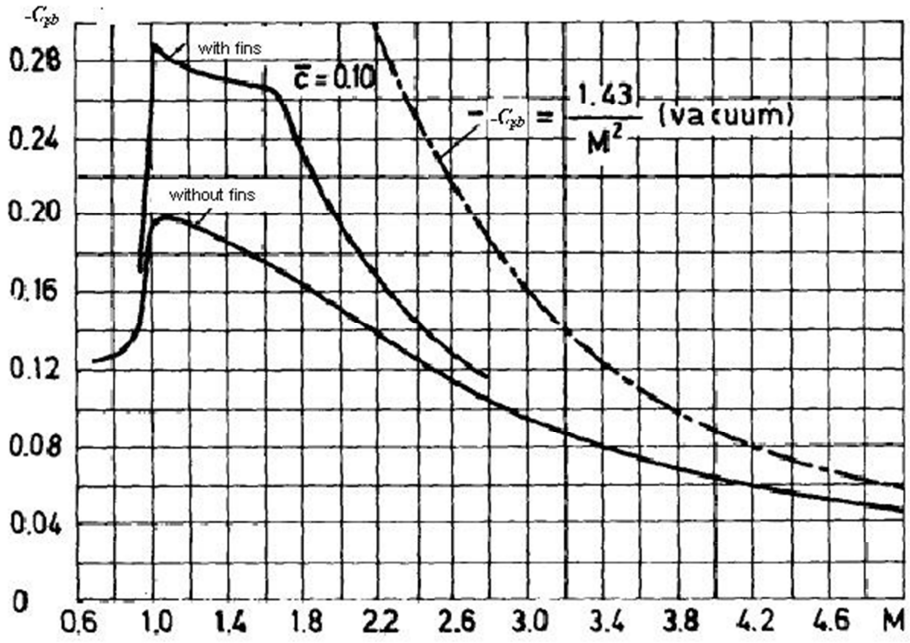

Figure 3-5 Base pressure coefficient vs. Mach number [21]
(for cylindrical "end" of the projectile, and with fins with relative cord thickness of 0.1)

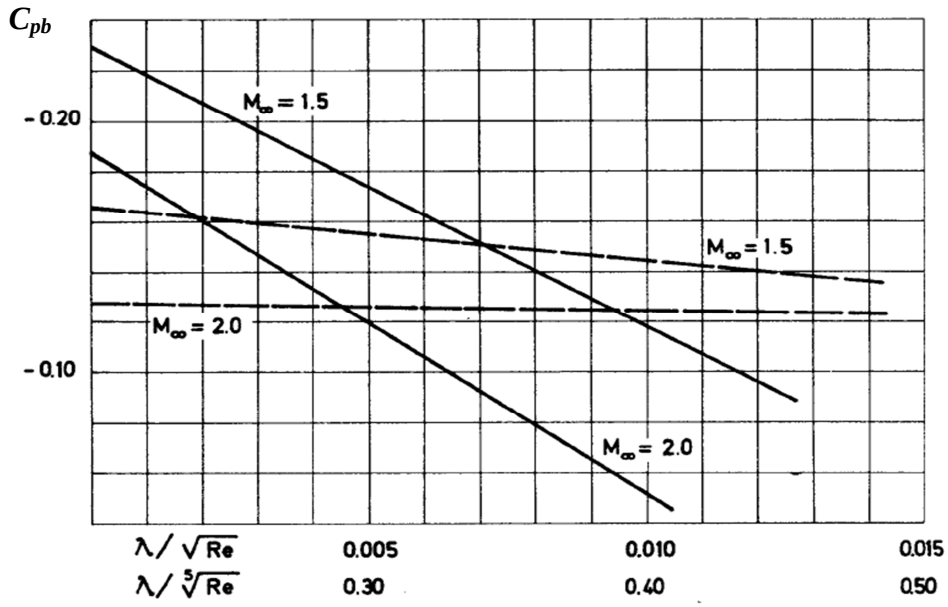

Figure 3-6 Base pressure coefficient vs. Mach and Reynolds numbers [21]

In case of laminar flow, base drag is function of Mach number and parameter $\frac{L}{d \cdot \sqrt{\mathrm{Re}}}$. For Mach number values between 1 and 1.5 and turbulent flow, Re number has less influence, i.e. "weighting" parameter is $\frac{L}{d \cdot \sqrt[5]{\mathrm{Re}}}$.

Rear cone geometry $tg\theta / \overline{S}_b$ is taken in account through empirical multiplying factor *Kb* (the multiplier to the base pressure coefficient with cylindrical end of a projectile). With high values of Mach number, influence of rear cone on total drag decreases. In those cases, the large rear cone even decreases base pressure - p_b.

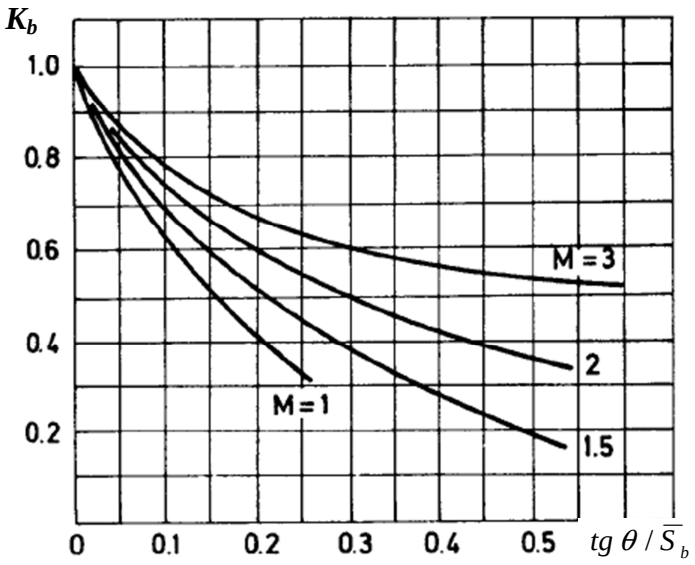

Figure 3-7 Rear cone geometry vs. base pressure factor K_b [21]

Rear cone effect can be approximated with relation 3-10 [27]:

$$C_{Db} = -Cp_{b\,cyl} \cdot \left(\frac{d_b}{d} \right)^3 \qquad \textbf{(3-10)}$$

where $Cp_{b\,cyl}$ base pressure coefficient for cylindrical body, d_b is base diameter, d – reference diameter (i.e. projectile calibre).

In order to numerically solve aerodynamics of a projectile, the base drag coefficient is represented with approximate equations that include presence of

rear cone and its influence on base pressure. Equation 3-13, indicates that influence of rear cone can be correlated using base diameter d_b [39].

$$\left(\frac{p_b}{p_\infty}\right)_{cyl} = 1 - 0.214 \cdot M^2 \cdot e^{-0.353 \cdot M} \quad \text{for } M > 1 \qquad \textbf{(3-11)}$$

$$\left(\frac{p_b}{p_\infty}\right)_{cyl} = 1 - 0.84 \cdot M^2 \quad \text{for } M \le 1 \qquad \textbf{(3-12)}$$

$$\left(\frac{p_b}{p_\infty}\right)_{BT} = \left(\frac{p_b}{p_\infty}\right)_{cyl} + \frac{1}{2} \cdot \gamma \cdot \left(\frac{d}{d_b}\right)^2 \cdot \left(1 - \frac{d_b}{d}\right) \cdot (0.608 - 0.148 \cdot M) \qquad \textbf{(3-13)}$$

Base drag coefficient with rear cone influence (without nozzles), for all range of Mach number, can be represented by the equations [25]:

$$\overline{p}_b = \left(\frac{p_b}{p_\infty}\right) = \left[1 + 0.09 \cdot M^2 \cdot \left(1 - e^{L_1 - L}\right)\right] \cdot \left[1 + 0.25 \cdot M^2 \cdot \left(1 - \frac{d_b}{d}\right)\right] \qquad \textbf{(3-14)}$$

where L is projectile length, and L_1 nose length.

Correction factors for subsonic and supersonic flow [25] are:

$$K_1 = \frac{1}{1 + 0.1875 \cdot M^2 + 0.0531 \cdot M^4} \quad \text{for M} < 1 \qquad \textbf{(3-15)}$$

$$K_1 = \frac{1}{1 + 0.2477 \cdot M^2 + 0.0345 \cdot M^4} \quad \text{for M} \ge 1 \qquad \textbf{(3-16)}$$

In that case, reduced base pressure is:

$$\overline{P}_b = K_1 \cdot \overline{p}_b \qquad \textbf{(3-17)}$$

and base drag coefficient is:

$$C_{Db} = \frac{1.4286 \cdot \left(1 - \overline{P}_b\right) \cdot \overline{d}_b^{\,2}}{M^2} \qquad \textbf{(3-18)}$$

In general, for same “free stream” conditions, rear cone reduces base area of a projectile (lower absolute base drag), but increases base pressure in comparison to projectile with cylindrical end. However, for supersonic flow, there is contribution to wave-pressure drag due to rear cone, which results in optimal rear cone length and angle (6^0-7^0), that provides maximum possible

base drag reduction without BB. Optimal angles and lengths of rear cone for supersonic flow conditions exist [21, 39], and values varies for artillery shells without BB unit ("classic" bottom or boat tail) from 0.6D to 0.8D for length, and 6^0 to 7^0 for rear cone angle. For projectiles with BB-unit, values are 0.7D to 0.8D and 3^0 for angle. For gyro-stabilised projectile, an additional problem is reduction of static stability due to presence of a rear cone, and expanding flow around it. Therefore, the solution for maximum base drag reduction is "base pressure increase" method utilising the base bleed effect. If appropriate mass flow is injected into the wake zone of a projectile, flow pattern will be changed in a way that the base pressure will increase, thus base drag will decrease. The BB should reduce base drag during ascending part of projectiles' ballistic trajectory, when the action of BB is most effective. Due to presence of BB gas-generator, rear shape of a projectile must be carefully designed, taking in account specific aerodynamics of base bleed phenomenon.

The conclusions derived from experiments [39] indicate that injecting the gas with low molecular weight and high temperature, will have the best effect on base drag reduction. The ideal gas will be hydrogen, which burns at high temperature, but hydrogen useful application is limited to wind tunnel tests. If the mass flow injection is combined with releasing of heat, i.e. additional combustion (afterburning) of combustion products in the wake, effect of base drag reduction is increased, and base pressure is significantly elevated. Various authors [39] have published their work on hydrogen combustion at projectile's base, which resulted in almost 100% base drag reduction. In case when they used solid rocket propellant for testing in wind tunnels, results indicated that afterburning effect performs better in riding the base pressure than injection of inert gas of the same temperature. Therefore, the main task is to find proper propellant mixture that will provide the afterburning of combustion products in the wake recirculation zone.

Injection of subsonic combustion products with afterburning effect (base bleed) in projectiles' wake is very different to combustion of solid rocket motor and SRM's supersonic jet. Combustion of a propellant in a solid rocket motor propels projectile in very short time (few seconds) with high acceleration, to very

high velocity. In case of rocket propulsion, during “active time” of rocket motor, base drag exists only on projectiles’ base surface not covered with exit area of the nozzle(s) eq. 3-20 [27]:

$$C_{Db} = -Cp_b = \left(1 - \frac{p_b}{p_\infty}\right) \cdot \frac{1}{0.7 \cdot M^2} \cdot \left(\frac{S_b - S_j}{S}\right) \quad \textbf{(3-19)}$$

In contrast, “propelling force” (thrust) of a BB gas-generator is negligible, but effect of base drag reduction spreads on entire base surface, and it can last for a several tens of seconds. In order to exploit effect of base drag reduction in best possible way, mass flow rate of BB combustion products should be appropriate and active time of gas generator should be adequate, i.e. the BB should burn at least 30% to 50% (up to apogee) of projectile flight time at maximum range. In addition, lower total drag of a projectile contributes to lesser influence of atmospheric disturbances [21, 27, 39] on projectile trajectory, thus higher precision.

We can represent the effect of base bleed on base pressure, for the purpose of base drag reduction with mathematical expression 3-20:

$$\lim_{I \to I_{opt}} \overline{P}_b \to 1 \quad \textbf{(3-20)}$$

where *I* represents non-dimensional ratio of combustion products mass flow vs. virtual mass flow of free air stream throughout base area of diameter d_b. The optimal base injection will be achieved when base pressure $\overline{P}_b$ is equal to 1.

3.2.4 Modelling the “effect” of base bleed combustion products mass injection on the projectiles’ base pressure

There are two different methods to approach the problem of raising the base pressure by injecting solid propellant combustion products in the wake. In both cases, base-pressure “increase” is function related to parameter *I*.

Parameter *I* (non-dimensional ratio between mass flow of combustion products in kg/s and “virtual” mass flow of air with free stream conditions through the projectile base area, in kg/s), can be mathematically described as:

$$I = \frac{\dot{m}_P}{\dot{m}_b} \qquad \dot{m}_P = I \cdot \dot{m}_b \qquad \dot{m}_b = V_\infty \cdot S_b \cdot \rho_\infty \tag{3-21}$$

For projectiles with BB gas-generator, this parameter determines propellant burning rate law and grain geometry, i.e. burning surface vs. burned web.

First mode, or method, is to utilise wind tunnel experimental results to establish correlation between $\left(\frac{p_b}{p_\infty}\right)_{BB}$ vs. *I*. Test results show, that low speed (subsonic) mass injection (appropriate low velocity mass injection), has “linear” influence on base pressure increase (eq. 3-22 to 3-24).

$$\left(\frac{p_b}{p_\infty}\right)_{BB} = \left(\frac{p_b}{p_\infty}\right)_0 + \Delta\left(\frac{p_b}{p_\infty}\right)_{BB} \tag{3-22}$$

$$\overline{P}_{bBB} = \overline{P}_{b0} + \Delta\overline{P}_{bBB} \tag{3-23}$$

$$\overline{P}_{bBB} = \overline{P}_{b0} + \left(\frac{\Delta\overline{P}_b}{\Delta I}\right)_{BB} \cdot I \tag{3-24}$$

The multiplying factor of parameter *I* according to some authors [35, 39], depends only on combustion temperature of solid propellant products, or the temperature of pure hot gases, when they are injected. Other researchers [42-47] conclude that second influencing parameter is Mach number of free stream. Those dependencies are:

$$\left(\frac{\Delta\overline{P}_b}{\Delta I}\right)_{BB} = 12.25 + 0.005 \cdot (T_0 - T_\infty) \tag{3-25}$$

$$\left(\frac{\Delta\overline{P}_b}{\Delta I}\right)_{BB} = 12.25 + 0.002778 \cdot (T_0 - T_\infty) \tag{3-26}$$

$$\left(\frac{\Delta\overline{P}_b}{\Delta I}\right)_{BB} = (-5.3953 + 0.01723 \cdot T_0) \cdot M + (4.6101 - 0.01463 \cdot T_0) \cdot M^2 + (-0.5660 + 0.00446 \cdot T_0) \cdot M^3 \tag{3-27}$$

Further, variation of the equation 3-24 gives:

$$\overline{P}_{bBB} = \overline{P}_{b0} + \frac{\left(\frac{\Delta \overline{P}_b}{\Delta I}\right)_{BB} \cdot I}{1 + \beta \cdot \left(\frac{\Delta \overline{P}_b}{\Delta I}\right)_{BB} \cdot I} \quad \textbf{(3-28)}$$

using the equation 3-26 and correction factor:

$$\beta = 15.1 - 46.3(M - 0.71) \quad \textbf{(3-29)}$$

But if the β is less than 2.6 then it should be fixed to value of 2.6.

These dependencies should correlate all types of injection products, however results are satisfactory and appropriate only to the tested cases of base injection, so for other formulations the correction factor have to be introduced.

Second method addresses the most common types of BB composite solid rocket propellant, which contain 65% to 75% of oxidiser (ammonium-perchlorate), and base bleed model is obtained directly from firing tests. Observed firing data provide relation between base drag reduction (base pressure increase) and injection of combustion products and its afterburning in the wake, i.e. $\left(\frac{p_b}{p_\infty}\right)_{BB}$ vs. I .

Total drag coefficient of projectile with Base-Bleed differ to the total drag coefficient of projectile without Base-Bleed for the value of ΔC_D [38]:

$$C_D = C_{D0} - \Delta C_D \quad \textbf{(3-30)}$$

Difference between projectile's total drag coefficients is the difference between base drag coefficients with and without Base-Bleed:

$$\Delta C_D = C_{Db_0} - C_{Db_{BB}} \quad \textbf{(3-31)}$$

Further, we can represent base drag coefficient reduction with new coefficient of reduction:

$$\Delta C_D = C_{Db_0} \cdot C_{RED} \quad \textbf{(3-32)}$$

If we replace in base drag equation (ratio of base pressure and free stream static pressure) this mathematical expression (3-32), following equations can be obtained:

Base drag coefficient is [16, 25]:

$$C_{Db_0} = \frac{1.4286 \cdot \left(1 - \overline{P}_{b0}\right) \cdot \overline{d}_b^{\,2}}{M^2} \quad \textbf{(3-33)}$$

Difference is equal to:

$$\Delta C_D = \frac{1.4286 \cdot \left(1 - \overline{P}_{b0}\right) \cdot \overline{d}_b^{\,2}}{M^2} \cdot C_{RED} \quad \textbf{(3-34)}$$

Replacing previous expressions in (3-32), we obtain:

$$\left(1 - \overline{P}_{b0}\right) - \left(1 - \overline{P}_{bBB}\right) = \left(1 - \overline{P}_{b0}\right) \cdot C_{RED} \quad \textbf{(3-35)}$$

$$-\left(\overline{P}_{b0} - \overline{P}_{bBB}\right) = \left(1 - \overline{P}_{b0}\right) \cdot C_{RED} \quad \textbf{(3-36)}$$

Relation between coefficient of reduction and base pressure increase is:

$$\Delta \overline{P}_{bBB} = \left(1 - \overline{P}_{b0}\right) \cdot C_{RED} \quad \textbf{(3-37)}$$

$$C_{RED} = \frac{\Delta \overline{P}_{bBB}}{\left(1 - \overline{P}_{b0}\right)} \quad \textbf{(3-38)}$$

Relations between coefficient of reduction C_{RED} and parameter *I*, is approximated with experimental functions usually given as polynomial and exponential relations between weighting parameters, i.e. reduction factor C_{RED} is a function of the free stream Mach number and injection parameter I combined together in one relation 3-39.

$$C_{RED} = C_{RED_M}(M) \cdot C_{RED_I}(I) \quad \textbf{(3-39)}$$

Data reduction from experiments [8, 38] showed that the dependences between parameters can be presented through fitting functions:

$$C_{RED_M}(M) = K_1 + K_2 \cdot M + K_3 \cdot M^2 + K_4 \cdot M^3 + K_5 \cdot M^4 \quad \textbf{(3-40)}$$

Second expression represents relation between injection parameter *I* and base drag reduction coefficient – figure 3-8 :

for $I_{low} < I \leq I_{opt}$

$$C_{RED_I}(I) = C_1 \cdot (1 - e^{(-C_2 \cdot I)}) \quad \textbf{(3-41)}$$

for $I_{opt} < I \leq I_{high}$

$$C_{RED_I} = C_{RED_I}(I_{opt}) \quad \textbf{(3-42)}$$

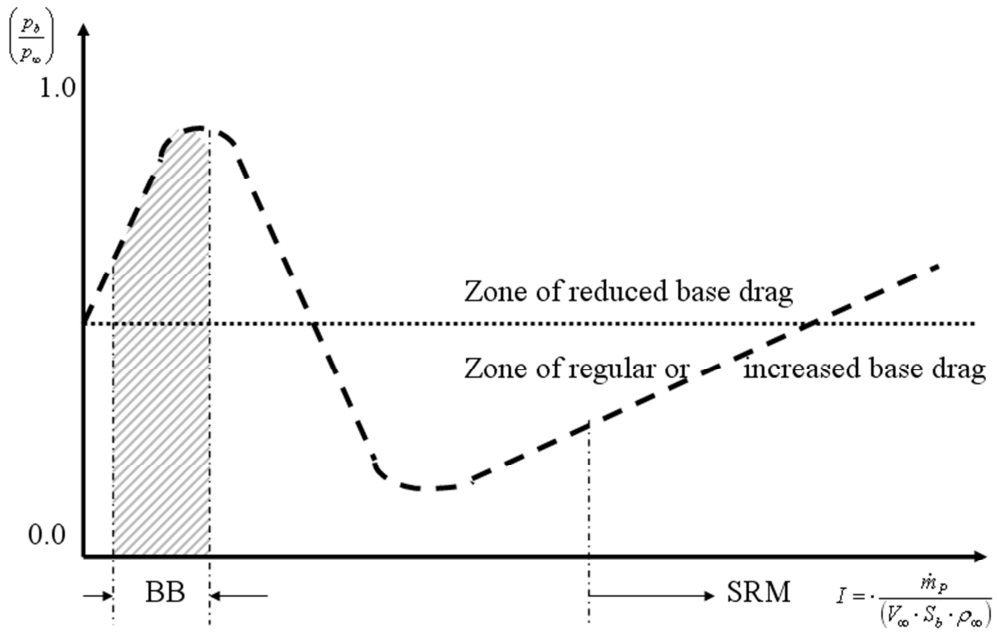

Figure 3-8 Mass injection vs. base pressure increase [6, 58]

Limits (border values) $I_{low,}$ I_{opt} and I_{high} are determined empirically, i.e. injection below I_{low} do not contribute to the base bleed effect, or the contribution is negligible. The optimal injection parameter I_{opt} is related to the propellant composition and its combustion properties, i.e. coefficient K_i and $C_{i,}$ derived from aerodynamic calculations and experimental data reduction. The K_i, $C_{i,}$ are functions of combustion temperature of the Base Bleed propellant, molecular

weight and composition of combustion products (after-burning effect), spin of the projectile, quadrant elevation as well as the function of the disposition of base bleed orifice and shape of the base bleed bottom("base cavity"). Beyond I_{opt} up to I_{high} , there is no further contribution of injection to base drag reduction. Any injection larger than I_{high} start to produce a negative effect, injection is more like a jet (if flow conditions are achieved - even supersonic jet), reducing the drag only at the exit cross-section of the BB orifice, but not over the entire base area. With injection parameter I> I_{high}, injected particles have more kinetic energy, i.e. combustion products are not able to re-circulate in the wake.

In a similar way, the NATO's "Modified point mass and five degrees of freedom trajectory models", correlate the base bleed effect, although fitting factors have been much more divided, i.e. there are fitting factors for quadrant elevation, burning rate, base bleed fuel temperature, local atmospheric pressure, axial spin of a projectile. The method developed and used in this thesis calculates influence of those parameters trough of computation of BB unit interior ballistics, making method simpler and more accurate.

As a rule, mass flow of BB combustion products during ascending part of flight should be regressive. Regressive mass flow is obtained through appropriate shape of propellant grain, i.e. by calculation of regressive burning surface of the propellant grain. Mass flow of combustion products through exit area (BB orifice) at the BB bottom element is low and subsonic. The pressure inside BB unit is negligibly higher than base pressure altered by BB. Practically, base bleed propellant burns under sub-atmospheric conditions, from start, at the gun muzzle, all along "burning" time of base bleed at projectile's trajectory. Since atmospheric pressure drops with altitude, then burning rate also decreases with altitude (i.e. the burning rate corresponds to gun elevation). Furthermore, burning time is increased and effect of base drag reduction is prolonged, at higher elevations. Since burning time of base bleed propellant grain depends on gun elevation, yet, it is another parameter that significantly complicates production of firing tables for given base bleed projectile. The influence of quadrant elevation (QE) is solved, as mentioned in previous

paragraph, by calculating interior ballistics of the BB unit along the trajectory, not by fitting factors.

The base bleed propellant grain undergoes great stress and strain due to exceptionally high acceleration, pressures, temperatures, and spin in gun barrel. Therefore, it is essential to choose appropriate propellant type, shape of grain and grain arrangement (installation) in BB unit, to withstand those severe loads during firing. The mechanical characteristics of base bleed propellant must be obtained prior to ballistics tests in order to have information regarding the propellant grain behaviour under loading conditions.

3.2.5 Base-Bleed Flow Equations

Combustion of Base-Bleed propellant grain on trajectory is sub-atmospheric, thus flow is subsonic. For sub-atmospheric combustion, the hypothesis is made that the burning rate *r* is a function of pressure inside BB unit *p,* and for very small values of absolute pressure (i.e. vacuum) the propellant burning rate is function of exothermic chemical reactions below the burning surface – proportional to the coefficient of convective heat transfer, eq. 3-43 [39] parameter a.

$$r = r(p) = a + b \cdot p^n \qquad \textbf{(3-43)}$$

Further, combustion model is based on the hypothesis that the combustion pressure is equal in every point of burning surface and burning rate law is unique for entire observed pressure interval.

To describe the Base-Bleed flow [38], some hypothesis must be given:

- Flow gas is ideal and equation of ideal gas is valid,
- There is no change of static pressure inside Base-Bleed unit
- Flow is non-dimensional (or unidirectional),

Effect of base drag reduction is related to increase of base pressure, and optimal reduction is related to subsonic flow (regarded as incompressible flow). Then, with combustion hypothesis, we can simplify system of equation for problem solving [19, 38, 39].

One of Saint-Venant's Equations(energy conservation) in integral form is:

$$\frac{1}{2}\cdot w^2+\frac{\kappa}{\kappa-1}\cdot\frac{p}{\rho}=const \qquad \textbf{(3-44)}$$

If we replace assumed base pressure and pressure inside Base-Bleed unit, equation 3-44 becomes:

$$\frac{1}{2}\cdot w_j^{\,2}+\frac{\kappa}{\kappa-1}\cdot\frac{p_b}{\rho_j}=\frac{\kappa}{\kappa-1}\cdot\frac{p_0}{\rho_0} \qquad \textbf{(3-45)}$$

Then, inserting the total (combustion) temperature and gas constant of products in equation, the equation transforms to:

$$\frac{1}{2}\cdot w_j^{\,2}+\frac{\kappa}{\kappa-1}\cdot\frac{p_b}{\rho_j}=\frac{\kappa}{\kappa-1}\cdot R\cdot T_0 \qquad \textbf{(3-46)}$$

Bernoulli equation for Base-Bleed model show that mass flow of combustion products from burning surface is equal to mass flow through exit area of Base-Bleed bottom element:

$$\dot{m}_P=r\cdot S_P\cdot\rho_P;\quad \dot{m}_j=w_j\cdot A_j\cdot\rho_j;\quad \dot{m}_P=\dot{m}_j \qquad \textbf{(3-47)}$$

Function of base pressure increase due to mass injection is related to parameter *I*. Relationship between p_b/p_∞ vs. *I* is shown in figure 3-8. For projectiles with Base-Bleed, this is most significant parameter that determines necessary characteristics of solid rocket propellant and for burning surface vs. web optimisation (geometry of Base-Bleed grain). Input data are obtained from live firing tests on proving grounds [38].

$$I=\frac{\dot{m}_P}{\dot{m}_b} \qquad \textbf{(3-48)}$$

$$\dot{m}_P = I \cdot \dot{m}_b$$

$$\dot{m}_b = V_\infty \cdot S_b \cdot \rho_\infty$$

Combining these equations, relation between the parameter *I* and combustion products mass flow can be obtained:

$$\dot{m}_P = I \cdot \left(V_\infty \cdot S_b \cdot \rho_\infty\right) \quad \textbf{(3-49)}$$

Inserting the equation 3-47 into equation 3-46, a second order polynomial is received, with only one unknown parameter – density of combustion products at BB orifice exit area.

$$\frac{1}{\rho_j} = \frac{(-1)\cdot\frac{\kappa}{\kappa-1}\cdot\left(\overline{P}_{bBB}\cdot p_\infty\right)+\sqrt{\left[\frac{\kappa}{\kappa-1}\cdot\left(\overline{P}_{bBB}\cdot p_\infty\right)\right]^2+4\cdot\left(\frac{1}{2}\cdot\frac{\dot{m}_P{}^2}{A_j{}^2}\right)\cdot\frac{\kappa}{\kappa-1}\cdot\left(R\cdot T_0\right)}}{2\cdot\left(\frac{1}{2}\cdot\frac{\dot{m}_P{}^2}{A_j{}^2}\right)} \quad \textbf{(3-50)}$$

With density determined, we can calculate other parameters of flow inside Base-Bleed unit:

$$T_j = \frac{\left(\overline{P}_{bBB}\cdot p_\infty\right)}{\rho_j \cdot R} \quad \textbf{(3-51)}$$

$$p_0 = \frac{\overline{P}_{bBB}\cdot p_\infty}{\left(\frac{T_j}{T_0}\right)^{\frac{\kappa}{\kappa-1}}} \quad \textbf{(3-52)}$$

By calculating the pressure inside BB unit, we can compute burning rate *r*, burnt web *e* and burning surface *S*.

$$r = r(p_0) \qquad e = e(r) \qquad S = S(e) \quad \textbf{(3-53)}$$

In each iteration step, critical flow conditions should be checked. If the flow is supersonic, base drag reduction is less than in case of subsonic flow.

During the optimisation process, supercritical flow conditions must be avoided, by proper design of burning surface development or by appropriate formulation of Base-Bleed propellant burning rate.

3.3 The M-REP's Base-Bleed Modelling and Simulation

The Modelling and Simulation of the M-REP's BB unit, calculation of its performance, represent solving of complex physical and chemical combustion phenomenon intertwined with BB unit design task. The prime task in design of BB unit is to define mass flow and thermodynamic characteristics of combustion products required for efficient drag reduction during the ascend part of the trajectory. However, other aspects of base bleed design significantly affect the performance of the BB unit, such as aerodynamic shape of the projectile's base, structural integrity of the BB propellant grain and BB casing, and reliability of ignition.

Therefore, in next paragraphs, novel approach to the Base-Bleed modelling process will be presented. Taking in consideration, different hypothesis concerning a gun (muzzle velocity and elevation), projectile (mass, aerodynamic shape, dimensions, structural integrity, solid rocket motor), base bleed propellant (density, molecular weight of combustion products, specific heat ratio of combustion products, temperature of combustion, burning rate, burning surface development, structural integrity) solutions should converge to optimal design of a BB unit, with primary goal set as range increase of the given artillery system. The solution of the optimisation process is primarily concerned with:

- Base-Bleed trajectory calculation for projectile with additional thrusters (solid rocket motor) and solving base pressure increment by injecting the hot gases and afterburning of the combustion products in the wake zone;
- Structural integrity of the base bleed casing and base bleed propellant grain under gun launching conditions.

3.3.1 Fuel-binder system formulation for M-REP's base bleed grain composite propellant

Background: Solid Rocket Propulsion technology is under constant development. The rapid growth of polymer science and plastics has contributed to the development of new types of polymers that can find application in solid rocket propellant formulation and manufacturing. One of the most vibrant fields of propellant composition research is the field of thermoplastics elastomers, energetic binders and plasticisers, which allowed development of new types of thermoplastic composite rocket propellants .

The solid rocket composite propellants are constantly improving, and contemporary focus is on "performance" improvements, such as high specific impulse, "environment" friendly propellants, safety – insensitive munitions compatibility, and long life storage abilities. Solid rocket composite propellants are able to provide the thrust either to minute delivery systems such as model rockets, up to large launch vehicles used in Space programs. The modern day composite propellants that take "greatest load" in production of solid rocket motors are based on hydroxyl-terminated polybutadiene (HTPB) as fuel and ammonium perchlorate (AP) as oxidiser. Improvements of existing rockets and new designs in rocket propulsion, requires upgrade in qualitative properties of composite propellants especially with regards to propellant performance and productivity. The work conducted in this research project is focused on investigation of solid composite propellants with novel thermoplastic/elastomeric binder system (fuel), which is based on modified technology for Vinyl-compounds. The effect of the novel thermoplastic/elastomeric binder system on propellant combustion properties required for base bleed application has been examined. Further, the compatible energetic plasticisers such as Low Molecular Weight Glycidyl Azide Polymer (GAP) were simulated as additives to the thermoplastic binder system, and their influence on combustion properties of base bleed propellant has been studied. These propellants revealed to have better performance required for the BB application than HTPB/AP compositions, as well as better processing and aging characteristics.

The first composite propellant for solid rocket motors, has been developed as mixture of $KClO_4$ (Potassium Perchlorate) and asphalt. When the mixture of those two components is formed, it goes in to the process of pressing and heating to become a propellant grain of desired shape and weight. Similar process can be applied to the present day composite propellant based on thermoplastic/elastomeric binder systems, including binders that utilise polyvinyl chloride as base matrix. The range of plasticisers, either non-energetic (improving flexibility) and/or energetic (improving flexibility and combustion properties) can be added to the mixture. The novel BB propellant composition utilises Ammonium Perchlorate as oxidiser, however other types of oxidiser can be used, such as Potassium Perchlorate or Lithium Perchlorate. Ingredients for binder system are commercially available, except in case of energetic plasticisers. Utilisation of novel binders enables performance improvements both for gas generators for base bleed units as well as of rocket motors, but also significantly improves processing of composite propellant. Several compositions of novel poly-plastisol binder system have been surveyed with focus on their energetic and mechanical properties.

The composite propellants with binder consisting of polyesters, acrylates, epoxies, polyurethanes, or hydroxyl-terminated polybutadiene significantly differ in manufacturing process comparing to thermoplastic-elastomeric composite propellants. Non-thermoplastic – thermoset composite propellants types usually contain 60%-85% by weight of solid filler – oxidiser (NH_4ClO_4, in most cases) blended with metal particles (in most cases fine Aluminium powder), uniformly dispersed in a matrix of thermoset-elastomeric binder. Powdered metals have been used to enhance energetic characteristics of the compound. The process of manufacturing of the cast propellant grains starts by blending solid and liquid ingredients into the viscous compound (mixture), which makes a fuel-binder. Second stage is degassing of blend in order to remove air bubbles entrapped during the mixing process. Further, process of moulding of degassed mixture into the molds is conducted, usually with mandrel that forms central port of the propellant grain. The last stage is solidifying of the propellant – curing process. Thermoset composite propellants usually represent non-volatile liquid

compounds composed of monomers/low molecular weight pre-polymers, and curing process, i.e. hardening, is achieved through polymerisation reactions. The critical path in propellant production is slow polymerisation that follows, i.e. the critical stage of production is control of the physical properties of the mixture - “post-cure”. The cured thermoset becomes infusible/insoluble material, and the curing process represents permanent, irreversible polymerisation. Curing process starts as formation of a polymer with linear chains, the next stage of polymerisation results in final cross-linked structure, with oxidiser particle embedded in the matrix. Depending on the formulation, propellant can be made rigid or flexible.

Furthermore, with thermoplastic-elastomeric poly-plastisol composite propellants all polymerisation reactions are happening during the specific process of propellant mixing. Solidification is obtained by blending – solvation of the polymer particles in non-volatile liquid – plasticiser, with addition of solid filler - oxidiser. Solvation or “curing - process” is achieved by heat addition, i.e. the mixture is heated to a temperature at which the polymer particles dissolve rapidly in the plasticiser to form a gel that after returning to a room temperature becomes solid similar to rubber. Technological process of manufacturing and aging of thermoplastic propellants has more advantages compared to other types of composite propellants, i.e. the thermoplastic propellant can go under repeated cycle of “solvation”, i.e. it can be recycled.

Thermoplastic/elastomeric poly plastisol composite propellant is particularly suited for base bleed application. Modified poly plastisol propellant is easy to process into complex shapes, by moulding and machining in order to get desired development of the burning surface. Thermoplastic poly-plastisol composite propellant allows high productivity rate for small size propellant grains and reliable manufacturing. The viscosity of the thermoplastic/energetic binder system decreases with temperature increase. Therefore, the production of propellant compositions based on the thermoplastic/elastomeric “poly-plastisol” binder system is possible using different processing technique such as extruding, injection moulding, two-roll milling, or pressing. Temperature of

processing can be between 135^{o}C - 160^{o}C, depending on the manufacturing process method. As polymerisation reactions are completed in entirety, before propellant manufacture begins, post process curing is eliminated. Propellant compositions using the novel formulation binder system can accept up to 90% of filler, which depends on the type of process used. The main advantage is production of free standing grains, as the inhibitor uses the same type of binder, except that the filler is inert, but if design requires, polyurethane/epoxy bonding system can be applied to achieve case bonded propellant grains. Thermoplastic poly plastisol propellant production process allows minimum quality check procedures as curing cycle does not exist. After processing in “extruder-homogeniser” under pressure and temperature, no bubbles or cracks can be found in the propellant, nor sedimentation of the oxidiser. Propellant compositions can be tailored to have mechanical properties appropriate for base bleed application:

- low glass transition temperature below negative temperature required by MIL standards [91] ;
- mechanical strength to withstand firing in the gun barrel;
- grain ”inhibitor” can be made of similar composition as binder, filled with the inert non-combustible material, such as calcium carbonate or silica-glass powder; if propellant and shares the same type of “binder” (inhibitor will not have energetic plasticiser in its composition) it will allow strong cohesive bonds between the propellant and the inhibitor, preventing the separation and peeling- off the inhibitor;
- Propellant burning rate at low pressures can be easily adjusted using burning rate catalysts and size of the oxidiser particles. At low pressures, burning rate is not significantly affected with the spin, in comparison to HTPB/AP propellant ;

The basic formulation of novel thermoplastic/elastomeric poly-plastisol binder system represents mixture/matrix of polyvinylchloride resin with copolymer (crystalline and amorphous phase) with addition of non-energetic plasticiser, and additives (lubricants, stabilisers, coupling agent, anti-oxidant, etc) [98]. The PVC $(C_2\ H_3\ Cl)_x$ used in formulation is suspension type with

viscosity number 116-132 and K-value in range of 68-72. To improve the "intake" of oxidiser filler, and to "bond" the inorganic salt particles into the binder matrix, the copolymer and "coupling agent" compounds like Chloroethylene-vinyl acetate copolymer $(C_4\ H_6\ O_2\ C_2\ H_3\ Cl)x$ and titanium IV 2,2(bis 2-propenolatomethyl) butanolato, tris(dioctyl) pryophosphate-O on hydrated amorphous silica or neoalkoxy titanate and gamma-Aminopropyltriethoxysilane coupling agents have been investigated [98]. Further the range of non-energetic plasctisers are tested in order to find the solution for required mechanical properties especially at low temperatures: di-(2-ethylhexyl) phthalate (DOP), di(2-propylheptyl) phthalate, dibutyl phtalate, didecyl phtalate, di-(2-ethylhexyl) adipate (DOA), dihexyl adipate, diisodecyl adipate, dihexyl azelate, acetyltributyl citrate, diethylene glycol dibenzoate, isodecyl benzoate, di-(2-ethylhexyl) sebacate (DOS), di-(2-ethylhexyl) trimellitate, and polymer plasiticisers like ethylene-vinyl acetate-carbon monoxide terpolymer, nitrile rubber and other polymers blended with PVC. As compatible energetic plasticiser, Low Molecular Weight Glycidyl Azide Polymer (GAP) [98] was studied. The processing additives (stearic acid, calcium stearate, paraffin wax, carbon black, etc…), and thermal stabilisers (sodium perchlorate, Dioctyltin di(isooctyl thioglycolate), barium/zinc carboxylates, calcium/zinc carboxylates, magnesium/zinc carboxylate, potassium/zinc carboxylates, etc. [98]) were consider, too. Additives and stabilisers constitutes less than 2% of the compound, providing the binder system required processing and functional properties, but their influence on the combustion properties are minimal.

Formulation: The equivalent formula of the basic thermoplastic/elastomeric binder system with non-energetic binder is $C_{5.68}H_{9.78}O_{0.93}Cl_{0.20}$, and weight ratios of the elements in a compound are:

- C 68.25 %
- H 9.85 %
- O 14.95 %
- Cl 6.95 %

The basic properties of the thermoplastic/elastomeric binder system with non-energetic plasticisers (at 20 ^{o}C and crosshead speed of tensile testing machine 50mm/s) are given in Table 3-1.

Table 3-1 Characteristic parameters of new "non-energetic" thermoplastic "poly-plastisol" system

Property	Unit	Value
Density, ρ	kg/m^3	1116
Enthalpy of formation ΔH_f^0	kJ/mol	-2399.29
"Glass" transition temperature, T_g	^{o}C	-65
Softening temperature, T_s	^{o}C	82
Melting temperature, T_m	^{o}C	135
Tensile strength, σ_m	MPa	16.8
Elongation at break	%	358

The equivalent formula of the thermoplastic/elastomeric binder system with energetic plasticiser (Low Molecular Weight GAP) is $C_{4.94}H_{9.06}O_{0.88}Cl_{0.29}N_{0.51}$, and weight ratios of the elements in a compound are:

- C 59.32 %
- H 9.13 %
- O 14.02 %
- Cl 10.44 %
- N 7.08 %

The basic properties of the thermoplastic/elastomeric binder system with energetic plasticisers are given in Table 3-2 (tensile test were conducted at 20^{o}C and crosshead speed of tensile testing machine 50mm/s).

Table 3-2 Characteristic parameters of new "energetic" thermoplastic "poly-plastisol" system

Property	Unit	Value
Density, ρ	kg/m^3	1200
Enthalpy of formation ΔH_f^0	kJ/mol	-1372.55
"Glass" transition temperature, T_g	^{o}C	-59
Softening temperature, T_s	^{o}C	85
Melting temperature, T_m	^{o}C	140
Tensile strength, σ_m	MPa	14.8
Elongation at break	%	330

3.3.2 Novel base bleed thermoplastic/elastomeric poly plastisol propellant formulation and testing

The propellant composition considered for base bleed application has the ammonium perchlorate (AP) as oxidiser in amount of 670 phr, relative to the PVC content in the binder (PVC = 100 phr) as reference compound, both for binder with energetic, and binder without energetic plasticiser. The equivalent formula of the basic compound of thermoplastic/elastomeric composite propellant for base bleed with 70% of AP is $C_{2.56}H_{6.26}O_{2.29}Cl_{0.56}\ N_{0.47}$, and weight ratios of the elements in formulation are:

- C 30.70 %
- H 6.31 %
- O 36.61 %
- Cl 19.84 %
- N 6.54 %

The equivalent formula of the basic compound of base bleed propellant with energetic plasticiser for base bleed with 70% of AP is $C_{1.75}H_{5.39}O_{2.51}Cl_{0.66}N_{0.73}$, and weight ratios of the elements in a compound are:

- C 20.96 %
- H 5.44 %
- O 40.10 %
- Cl 23.32 %
- N 10.18 %

Base bleed propellant composition has to provide low molecular weight, and high combustion temperature gaseous combustion products, combustible at sub-atmosphere pressures, in order to efficiently reduce base drag of supersonic projectile. For selection of propellant mixture (ratio of oxidiser /fuel) beside combustion properties, mechanical properties represent the main factor for selection of base bleed propellant, as BB propellant grains should withstand high acceleration and pressure loads in the gun barrel. The trade-off between mechanical and combustion properties of the propellant has to be made. The theoretical performances of base bleed propellant compositions are investigated along with influence of energetic plasticisers on base bleed propellant combustion properties. The ratios of the non-energetic/energetic components have been preserved, as presented in equivalent formulas for binder system,

but the amount of filler – ammonium perchlorate has been varied. The results are shown on Figure 3-9.

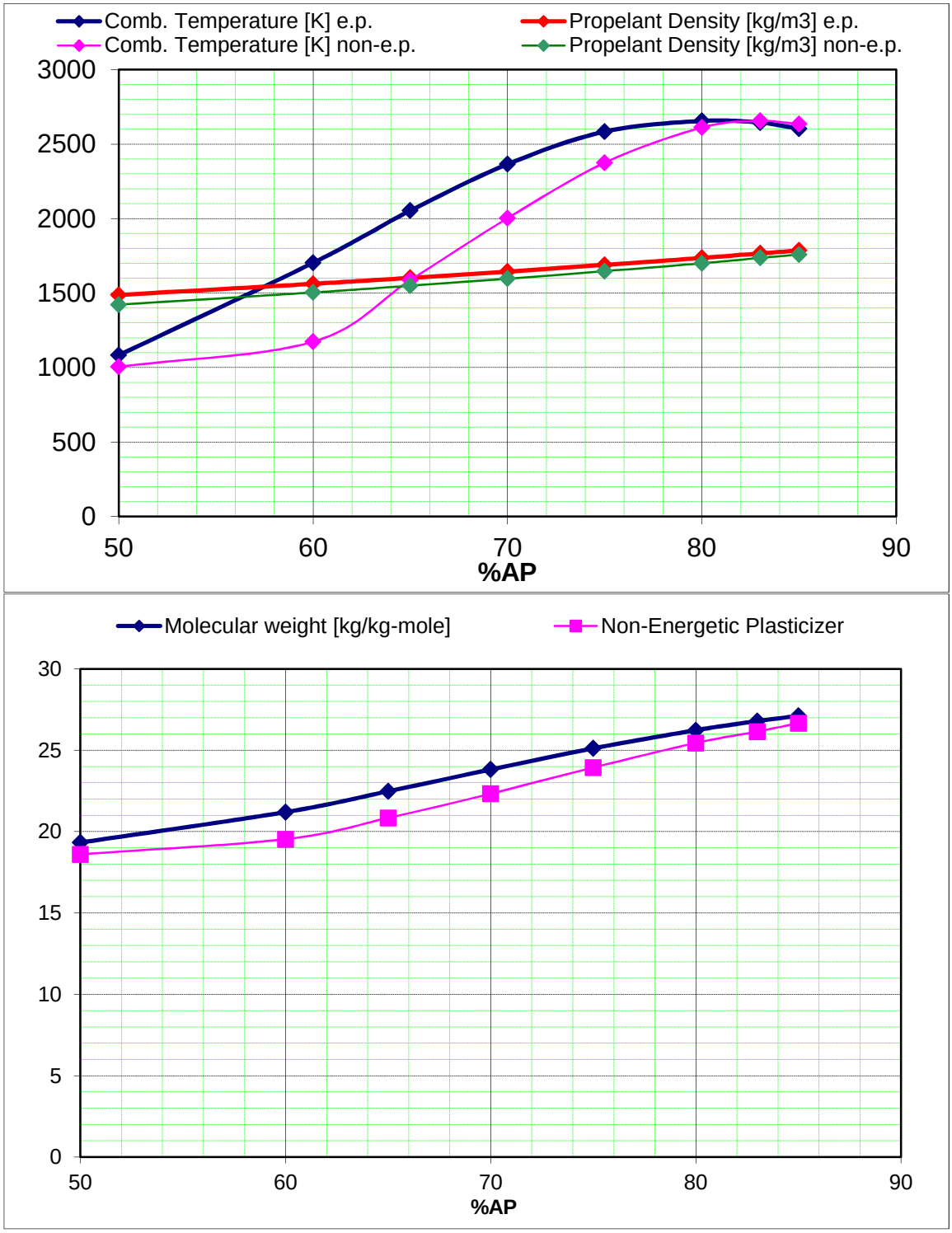

Figure 3-9 Theoretical combustion properties of the Base Bleed propellant with energetic/non-energetic plasticiser with reference to AP% content

Theoretical performances of all propellants compositions have been obtained from modified Computer Program for Calculation of Complex Chemical Equilibrium Compositions and Applications – CEA and ICT-Code [76, 99]. CEA software allows complex calculation of theoretical thermodynamic properties of the system by knowing the chemical equilibrium compositions of a chemical system. Further it can calculate ideal - theoretical rocket performances, for finite or infinite area combustion chambers, as well as detonation and shock tube parameters. The combustion temperature and molecular weight of the base bleed propellant combustion products in Figure 3-9, has been calculated for adiabatic combustion at pressure of 0.1 MPa (1 bar), followed by isentropic expansion to 0.01 MPa pressure (simulation of Base Bleed combustion). Chemical composition of the combustion process is changing during expansion, equilibrium performances are based on assumption of instantaneous chemical equilibrium during expansion of base bleed combustion products in to the “vacuum” behind the supersonic projectile (the Infinitive Area Combustor model for theoretical rocket performance has been assumed).

The results of base bleed propellant combustion calculations shows that due to high content of AP in propellant compositions the benefits of use of energetic-plasticisers to combustion process are reflecting on improvement of volumetric density of the propellant up to 2% comparing to use of non-energetic plasticiser, and the combustion temperature is higher (for the AP mass portion of 70%) comparing to the non-energetic plasticiser for the same content of AP. Again, the molecular weight of the combustion product of propellant with non-energetic plasticiser is 7% lower, than to equivalent propellant with energetic plasticiser. The non-energetic propellant is further elaborated, as it is more “cost effective” then the propellant with energetic plasticiser. The combustion analysis is performed and results are presented in Tables 3-3 and 3-4. The pressure ratio is 2 for expansion from 2 bars to the atmospheric pressure in order to obtain combustion parameters such as combustion temperature and molar mass of gaseous products, in a different way than “CEA rocket analysis” is used, i.e. not to obtain sonic conditions in the throat

Table 3-3 Theoretical combustion performance assuming equilibrium composition during expansion – new thermoplastic non-energetic plasticiser "poly-plastisol" propellant 70% AP

MIXTURE THEORETICAL DENSITY 1623.9 kg/m3

	CHAMBER	THROAT	EXIT
P_C/P	1.0000	1.8017	2.0000
P, bar	2.0000	1.1101	1.0000
T, K	2124.1	1895.1	1856.1
ρ, kg/m3	0.2590	0.1613	0.1483
H, KJ/kg	-2461.85	-2891.51	-2962.65
U, KJ/kg	-3234.12	-3579.90	-3636.86
G, KJ/kg	-26196.2	-24066.0	-23702.4
S, KJ/kgK	11.1736	11.1736	11.1736
M, MOL WT	22.869	22.888	22.890
C_P, KJ/kgK	1.9569	1.8433	1.8309
κ	1.2359	1.2483	1.2498
SONIC VEL,m/s	977.0	927.0	918.0
MACH NUMBER	0.000	1.000	1.090
A_E/A_T		1.0000	1.0070
C*, m/s		1338	1338

Table 3-4 Theoretical combustion performance assuming frozen composition during expansion – new thermoplastic non-energetic plasticiser "poly-plastisol" propellant 70% AP

MIXTURE THEORETICAL DENSITY 1623.9 kg/m3

	CHAMBER	THROAT	EXIT
P_c/P	1.0000	1.8093	2.0000
P, bar	2.0000	1.1054	1.0000
T, K	2124.1	1881.0	1842.3
ρ, kg/m^3	0.2590	0.1616	0.1493
H, KJ/kg	-2461.85	-2893.10	-2960.93
U, KJ/kg	-3234.12	-3576.97	-3630.72
G, KJ/kg	-26196.2	-23910.6	-23545.8
S, KJ/kgK	11.1736	11.1736	11.1736
M, MOL WT	22.869	22.869	22.869
C_P, KJ/kgK	1.7909	1.7552	1.7488
κ	1.2547	1.2613	1.2625
SONC VEL,m/s	984.4	928.7	919.6
MACH NUMBER	0.000	1.000	1.086
A_E/A_T		1.0000	1.0064
C*, m/s		1332	1332

To round up all information required to characterise base bleed propellant, the mechanical properties of new formulation have been investigated. Due to high inertial loads (axial and angular acceleration, and spin) and pressure from gun-charge combustion gases, stresses are induced in the propellant grain. In order to withstand firing from the gun, propellant has to maintain good mechanical properties and flexibility at all operating temperatures (from -40^{o}C to +60^{o}C). In addition, appropriate grain geometry and appropriate arrangement inside base bleed combustion chamber, should be able to secure the mechanical reliability of base bleed during firing sequence. The mechanical properties of the base bleed thermoplastic "poly-plastisol" propellant have been tested by Universal Testing Machine with constant strain rate (cross-head speed) and environmental chamber. Uniaxial/Isothermal tensile tests were performed using JANNAF dog bone specimens "C" (fig. 3-10) and appropriate procedure according to STANAG 4506 [103] at ambient temperature +20^{o}C with strain rate of 50 mm/min, as well as on -40^{o}C, -30^{o}C and +50^{o}C with same strain rate. Tension force and elongation were measured with load cell and extensometer in temperature controlled chamber. Acquired data has been analysed, and maximum stress (tensile strength)- σ_m, strain at maximum stress- ε_m, and initial tangent modulus- E_o, were calculated as average values from several measurements. The results of tensile tests are presented on Figures 3-11 to 3-14.

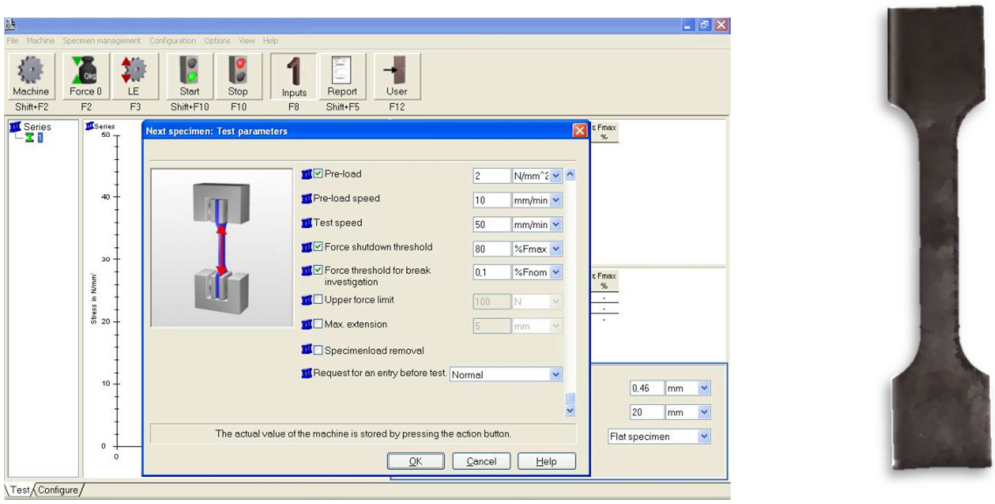

Figure 3-10 Setup of tensile test (left), standard JANNAF specimen for propellant mechanical characterization (right)

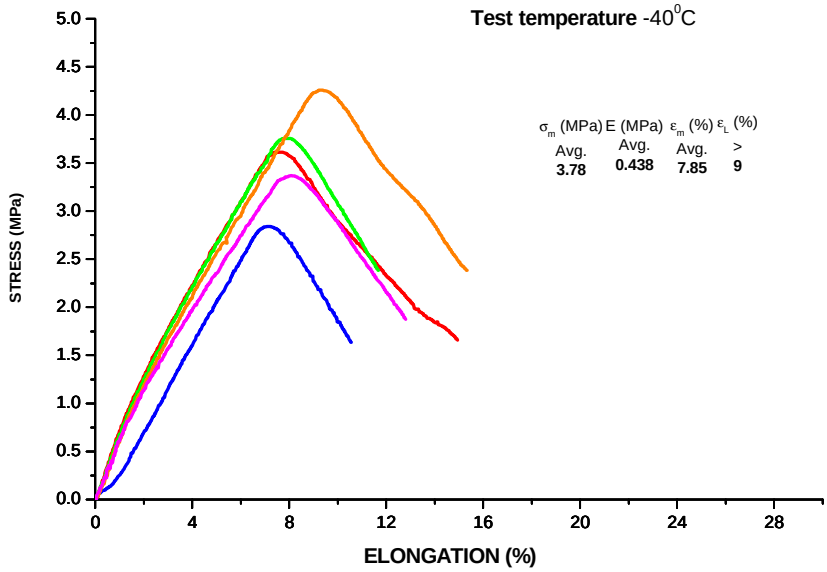

Figure 3-11: **The thermoplastic/elastomeric base bleed propellant, 70 AP% content, Tensile properties test -40°C, 5 tensile specimens**

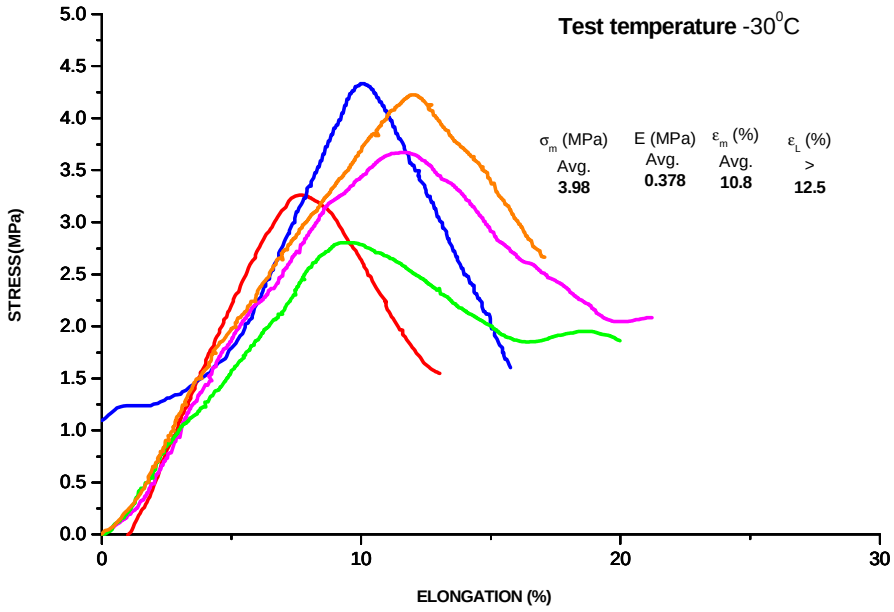

Figure 3-12: Thermoplastic/elastomeric base bleed propellant, 70 AP% content, Tensile properties test -30°C, 5 tensile specimens

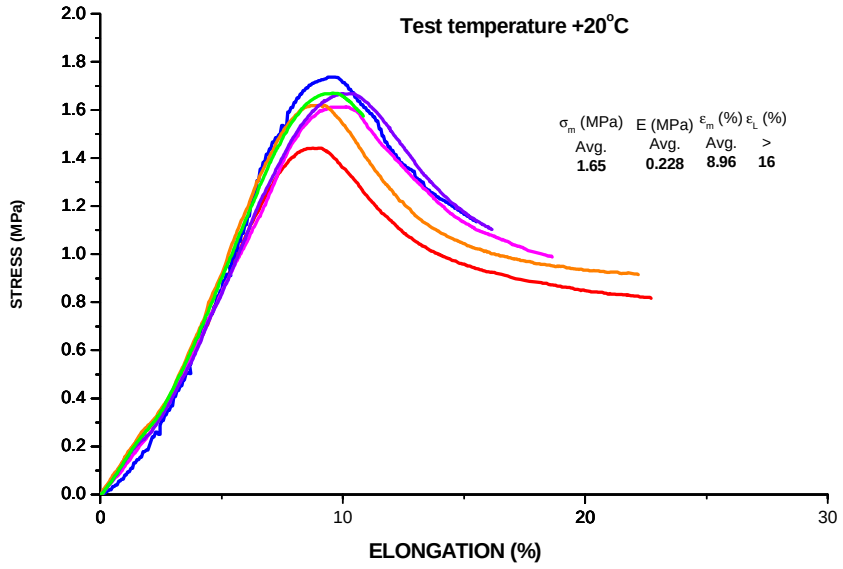

Figure 3-13: Thermoplastic/elastomeric base bleed propellant, 70 AP% content, Tensile properties test +20 °C, 5 tensile specimens

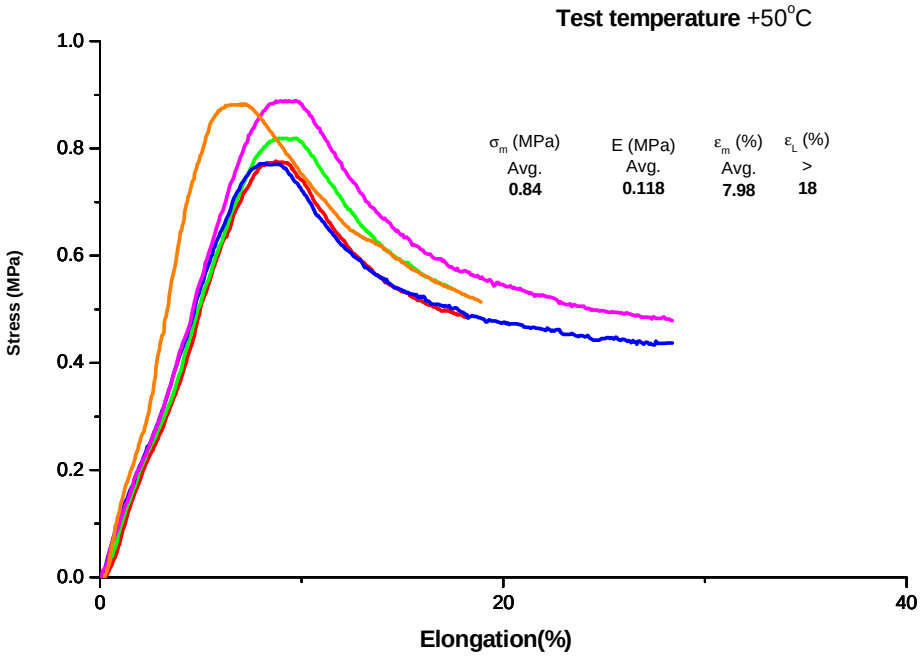

Figure 3-14: Thermoplastic/elastomeric base bleed propellant, 70 AP% content, Tensile properties test +50°C, 5 tensile specimens

In order to establish glass transition temperature (T_g) and visco-elastic properties of thermoplastic/elastomeric propellant for base bleed propellant grain, required for structural analysis , the DMA (dynamic material analysis)

tests have been performed. The temperature scans and frequency scans has been conducted in order to establish parameters for William-Landel-Ferry WLF equation [77] that describes time-temperature-superposition (TTS) phenomenon of visco-elastic material. Tests have been carried out on specimens with same composition as propellant (same binder and ratio of binder/oxidizer) but with inert filler- $CaCO_3$.instead of AP Components, polymer resin, copolymer, liquid and solid plasticisers, coupling agents and processing additives, have been mixed, then pressed in temperature controlled hydraulic press to form thick plastic sheet (foil). Results of the DMA tests are presented on Figures 3-17, and 3-18, and Table 3-5. The T_g (transition temperature from "glassy" to visco-elastic material behaviour) has been established for BB propellant, and it is within temperature region of -58°C to -65°C,.

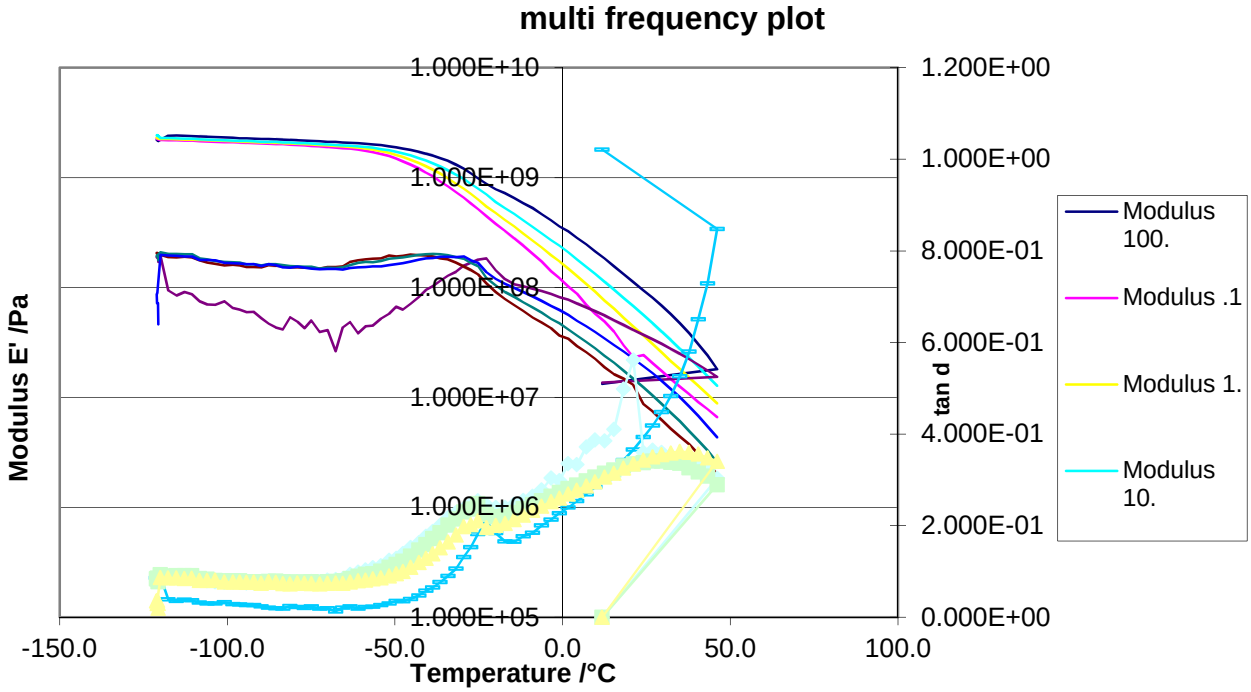

Figure 3-15: Temperature scan for thermoplastic/elastomeric BB propellant, without energetic plasticiser, multiple frequencies, "glass" transition temperature to be found in region of -58°C to -65°C

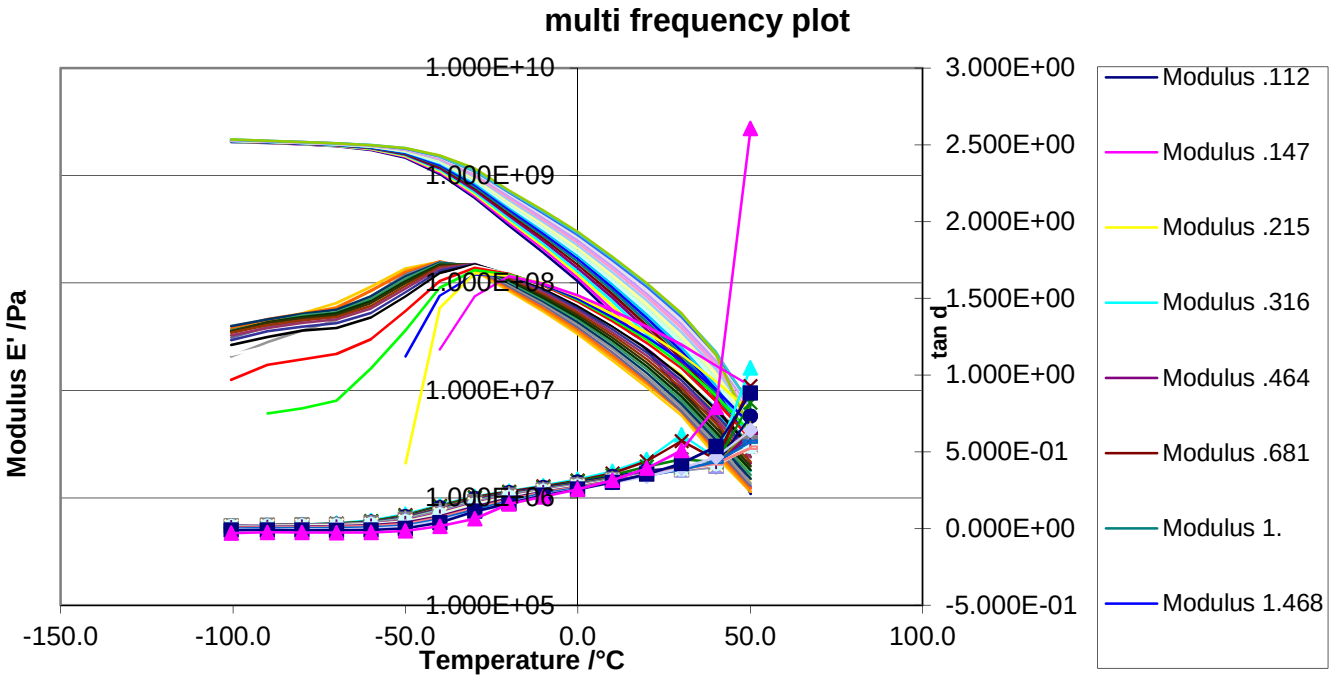

Figure 3-16: Frequency scan for thermoplastic/elastomeric BB propellant, without energetic plasticiser

Time - Temperature dependences of rheological parameters is associated with a concept of free volume and described by Williams-Landel-Ferry (WLF) equation [77-78], which defines shift factor, a_T, for change in temperature:

$$\log a_T = \log \frac{E'}{E'_0} = \frac{-C_1(T-T_0)}{C_2+T-T_0}; \qquad \textbf{(3-54)}$$

where are:

T – test temperature, T_0 – reference temperature, E' - storage modulus at test temperature T, E_0' - loss modulus at reference temperature T_0, C_1, C_2 – WLF equation coefficients.

The results of TTS analysis have been analysed and the correlation between tensile test at different temperatures and TTS analysis has been establish. Coefficients in WLF equation are calculated for BB propellant. The WLF coefficient has been appended to the material model and used for the structural integrity analysis of BB propellant grain during the launch sequence.

Table 3-5 WLF Shift factor a_T for BB propellant.

Temperature	Log At
-100	35.81548
-90	27.02321
-80	20.35926
-70	15.13429
-60	10.92761
-50	7.467986
-40	4.572638
-30	2.113924
-20	0
-10	-1.83691
0	-3.4479
10	-4.87225
20	-6.14061
30	-7.27727
40	-8.30173

Coefficient of WLF equations are found as : C_1= 28 C_2=142

3.3.3 Calculation of base drag reduction by M-REP's base bleed unit

For the calculation of base-drag reduction with coupled impact of solid rocket motor on the projectile's range, the modified point mass trajectory model is used [5, 22, 26], with calculation of interior ballistics of the base bleed on the trajectory is used. The flight mechanics the MREP's is described in detail in Chapter Five. The modified point mass trajectory model is chosen due to complexity of problem; Modified Point Mass (MPM) Trajectory Code with Combustion Model of base bleed is programmed in FORTRAN programming language. The model is also incorporated in the six degrees-of-freedom trajectory program which will be discussed in Chapter 5. The MPM Equations of Motion are used to determine trajectory's mathematical model, incorporates only essential aerodynamic coefficients, and they yield accurate trajectory prediction of base bleed influence on projectile's flight. Also, profile of the rocket motor thrust, as well as SRM total impulse and ignition delay, were combined to "test" range of projectile. The base reduction algorithm incorporates

experimental data from firing range tests (Chapter 3.4) as described in Chapter 3.2.4, equations 3-39 to 3-42

Based only on projectile body geometry, firing conditions and base bleed parameters (propellant combustion characteristic defined by CAE Code [76] and date derived from experiments [38]), program itself calculate drag coefficients necessary for trajectory calculation. Drag coefficients calculations, including the BB base drag, require exact position of the projectile in space (i.e.. altitude and related atmospheric parameters – density, temperature, pressure, and velocity-Mach number).

Total drag coefficient C_D (without Base-Bleed) is function of Mach number only - $C_D = f(M)$, unlike base drag coefficient with base bleed C_{Db}, which represents function of two parameters - Mach number and Injection parameter, $C_{Db} = f(M, I)$. Injection parameter depends on both interior ballistics of base bleed and exterior ballistics of the projectile.

During the Base-Bleed active phase (time t_{BB}), assumption is made, that the total drag represents difference between the total drag without Base-Bleed and the product of base drag reduction coefficient multiplied by the base drag coefficient without Base-Bleed (equations 3-30 to 3-38).

The empirical model defined in Chapter 3.2 is utilised to determine the coefficients of base drag reduction. Required geometry parameters for the defining the aerodynamically model of the projectile is given on figure 3-16.

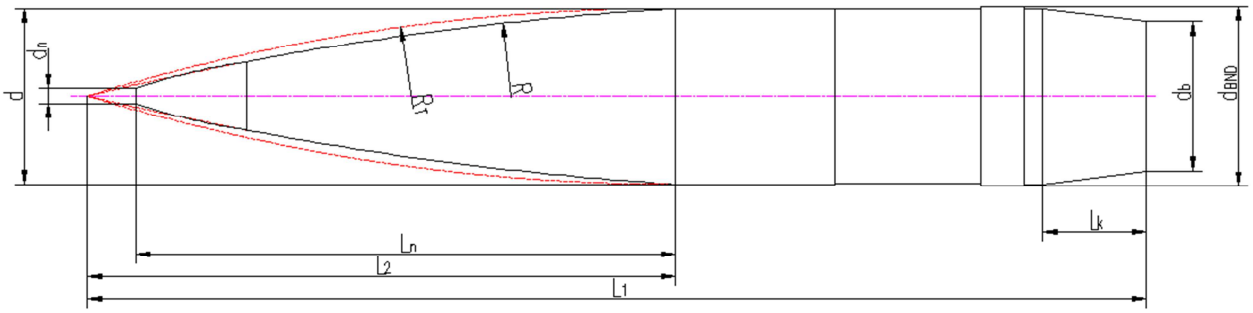

Figure 3-17 Characteristic dimensions of the projectile

Algorithm (calculation steps) for base bleed performance computation and optimisation of base bleed propellant grain design, as follows:

1. Step one: ratio $\frac{p_b}{p_\infty}$ without base bleed influence is calculated; Ratio of base pressure with base bleed is computed (initial value of base bleed pressure ratio for computation is assumed to be 0.95)

2. Step two: Difference between those two ratios is calculated;
3. Step three: For calculated difference injection parameter *I* is determined*;*
4. Step four: Mass flow rate $\dot{m}$ is calculated based on parameter *I;*
5. Step five: Computed mass flow rate, coupled with equations of perfect gas for combustion products, mass and energy conservation and subsonic flow conditions, yields combustion pressure in base bleed unit
6. Step six: burning rate is computed;
7. Step seven: burnt web is calculated;
8. Step eight: burning surface is calculated;
9. Step nine: the result for burning surface is compared with input burning surface vs. web function. If difference is within pre-set error value, then algorithm proceeds to next iteration, otherwise assumed pressure ratio on the projectile base is changed, in order to calculate a new value of the burning surface that will satisfy algorithm accuracy (repeating iterations).
10. Step ten: If request is to optimise size and shape of Base-Bleed propellant grain, assumed base pressure ratio with base bleed is determined to correspond to I_{opt} derived from experiments. Thus, computed burning surface represents optimal burning surface development for given projectile-base bleed–muzzle velocity- quadrant elevation combination, i.e. shape of base bleed propellant grain is determined. Each subsequent algorithm's step is step in integration of projectile's trajectory for a given drag coefficient, incorporating "burning" conditions of the base bleed along the trajectory.

Block diagram of the method is given in figure 3-17.

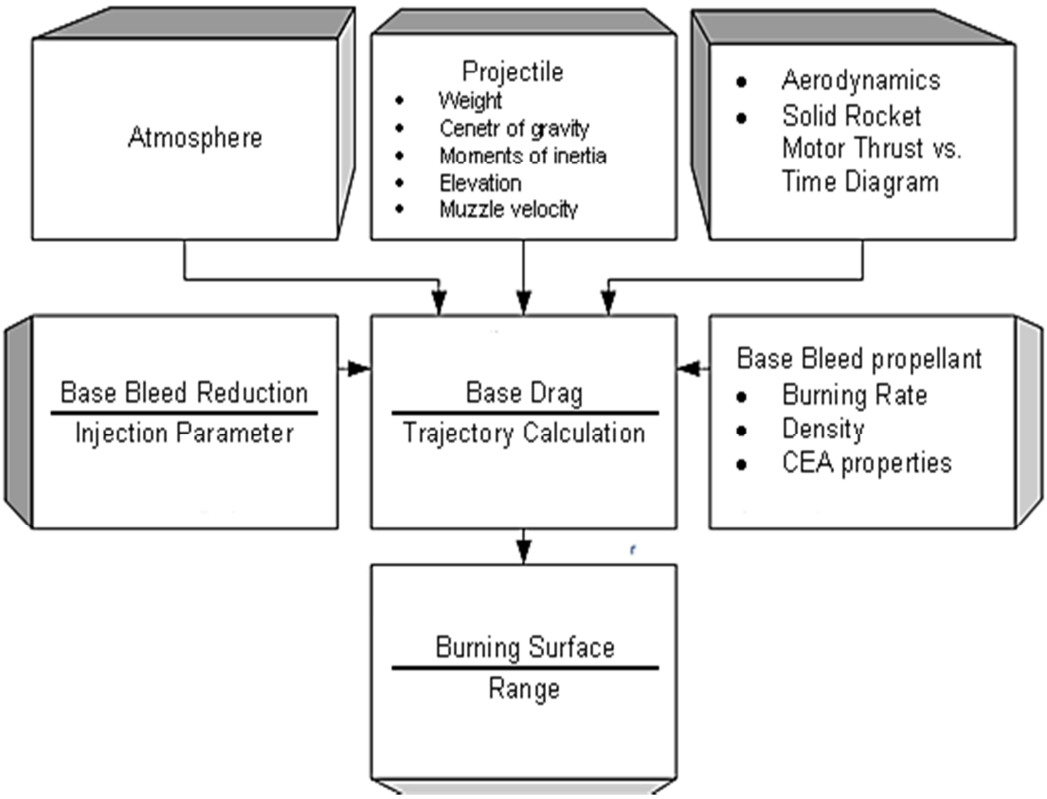

Figure 3-18 Block diagram of Algorithm for trajectory calculation for projectile with base bleed unit and solid rocket motor

Aerodynamic coefficients required for trajectory calculation can be obtain from experimental and semi-empirical methods and equations [5,22,36,38]. Aerodynamic coefficients should be computed entire range of projectile's Mach numbers.

The diagram of total drag coefficient C_{D0} (without induced drag) for M-REP shell is presented on figure 3-18. The C_{D0} is computed using self-developed FORTRAN code and compared with PRODAS [79] results. The curves of total drag vs. Mach number are aligned.

The model developed for base bleed computations, yields all substantial parameters of projectile flight, including interior ballistics parameters of base burn on the trajectory. Numerical method for calculation (Runge-Kutta, 4-th order) is chosen, so that fast and accurate computations can be obtained.

Figure 3-19 shows $\Delta C_{Db,}$ i.e. computed optimal ΔC_{Db} for M-REP, for muzzle velocities of 821m/s and 930m/s, that correspond to maximum gun charge in 39 calibres and 52 calibres howitzers and optimal quadrant elevation for maximum range at sea level.

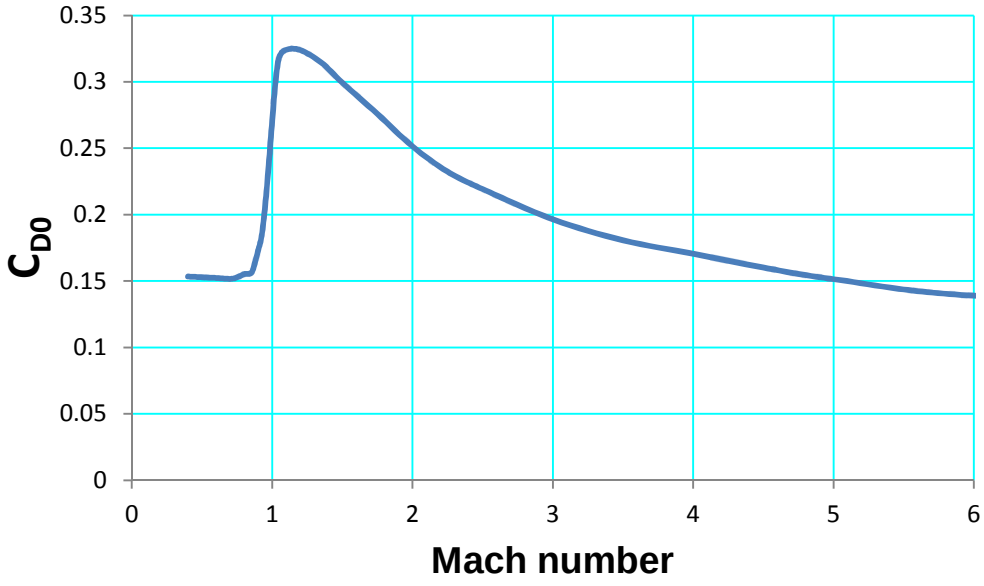

Figure 3-19 Diagram Zero Yaw Drag vs. Mach number

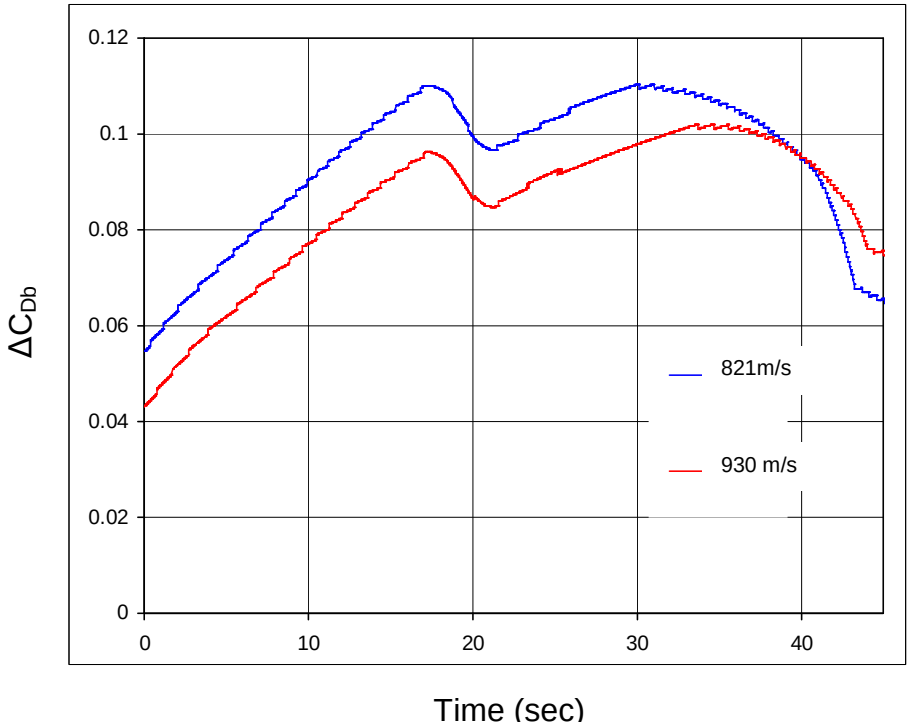

Figure 3-20 ΔC_{Db} vs. time (sec)

After computing optimal burning surface, next step in base bleed modelling is to design a feasible solution for base bleed propellant grain shape that should provide appropriate mass injection into wake zone. The design of propellant shape includes analysis of available “free” volume for BB unit, design of BB unit casing (aerodynamic shape and structural design), and analysis of design’s “ease of manufacture”.

The calculations presented in diagram fig. 3-19 (required mass injection of combustion products) have led to improved design of base bleed propellant grain (Figures 3-20, 3-21 and 3-22). Regarding shape and composition of the propellant grain, novel approach is investigated, with combination of base bleed propellant and pyrotechnic compound merged in one propellant grain. First ingredient is propellant is based on novel binder (fuel) system described in Chapter 3.3.1, and propellant composition elaborated in Chapter 3.3.2. Second ingredient is pyrotechnic compound based on the same binder system but with high content of metal powder (~30%), mixture of aluminium powder (pyrotechnic grade – “Dark Pyro”) or magnesium powder. For pyrotechnic ingredient portion of ammonium perchlorate is supplemented by mix of metal powder with strontium sulphate. The function of pyro-compound is to secure reliable ignition of primary propellant. Thin layer of pyrotechnic mixture is arranged in zone of the “sustainer.”. Pyrotechnics stays ignited at muzzle, it is not sensitive to high-pressure drop when projectile exits the muzzle, due to high content of solid metal fuel particles. Bonding between base bleed propellant and pyrotechnic mixture is enabled by technological process of thermoplastic poly-plastisol rocket propellant manufacturing, as both compounds share same type of binder. Figure 3-22 represent the arrangement of propellant, pyrotechnics layer, and inhibitor in the BB grain. The overall

- Propellant grain mass: 1.32 kg.
- Base-Bleed propellant density: 1624 kg/m^3
- Inhibitor density: 1760 kg/m^3

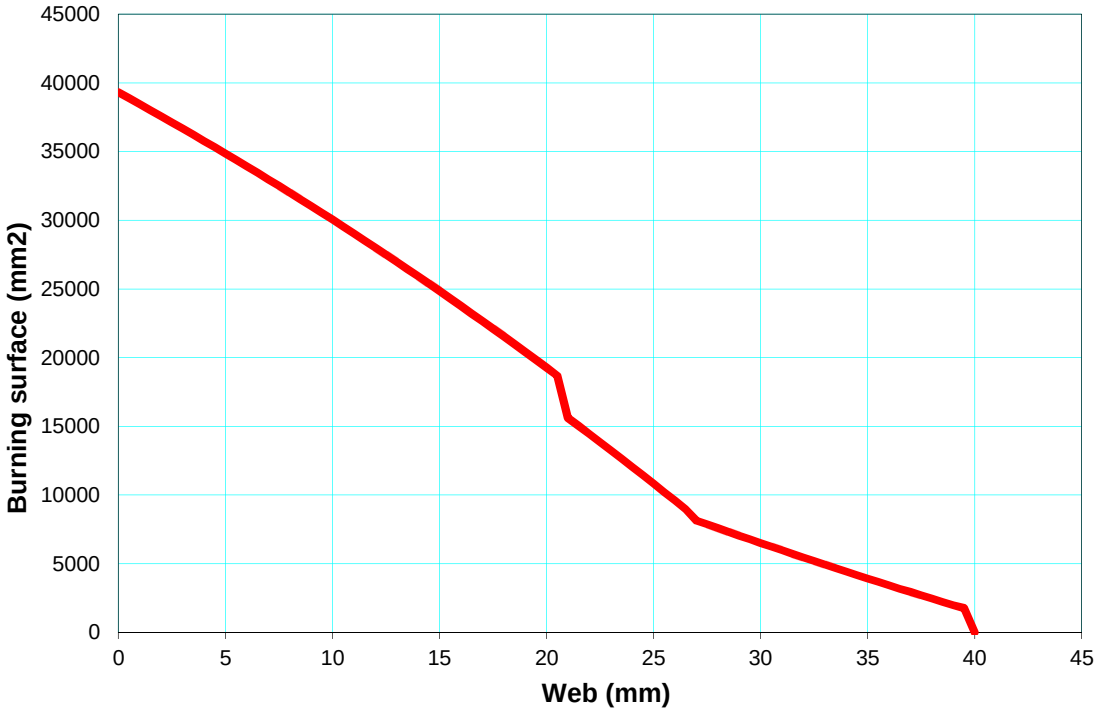

Figure 3-21 Burning surface development vs. web, for M-REP Base-Bleed Propellant Grain Configuration

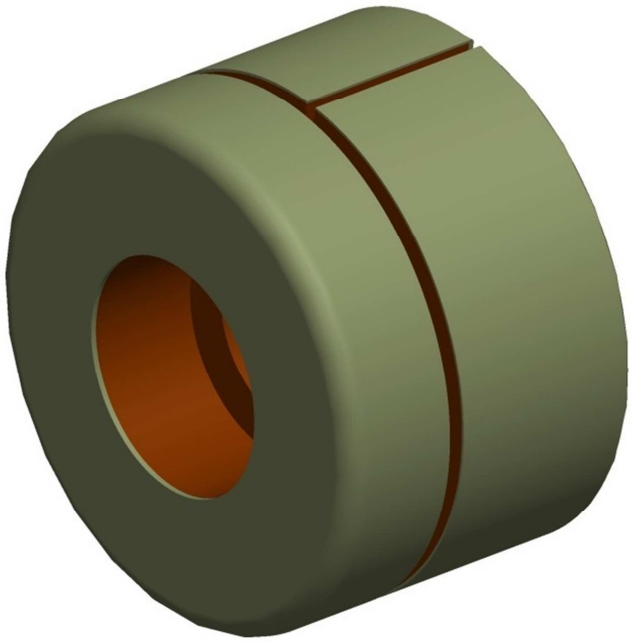

Figure 3-22 3D model of M-REP Base-Bleed Propellant Grain

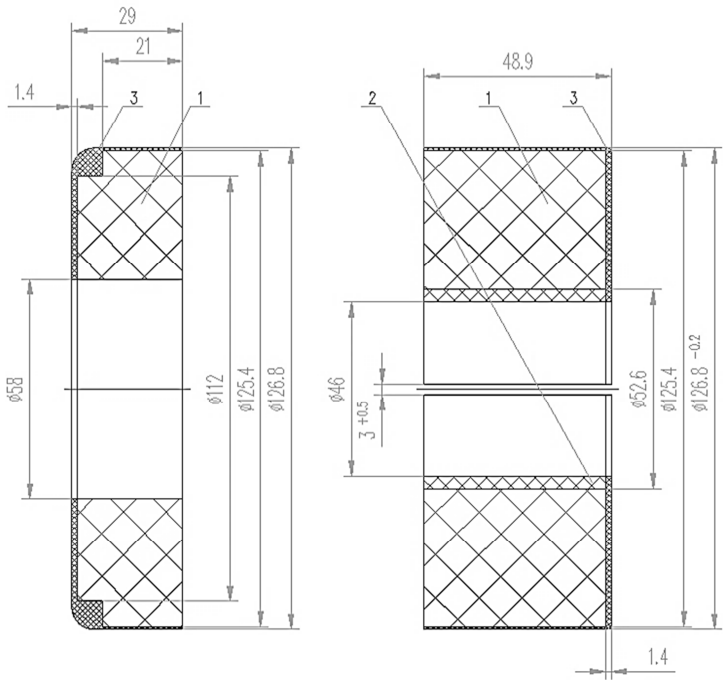

1- Primary BB Propellant;
2- Layer of Pyrotechnic compound (re-ignition mixture)
3- Inhibitor

Figure 3-23 ERP's Base-Bleed Propellant grain cross section

Using the burning surface development (fig. 3-20), and computing the mass injection of base bleed combustion products and its effect on base drag decrease, M-REP's trajectories are simulated (detailed description of trajectory modelling is presented in Chapter 5. For optimal elevation angle (i.e. quadrant elevation for max. range) for given ordnance and initial conditions (firing ground altitude, muzzle velocity - gun propellant charge, solid rocket motor total impulse and thrust profile), simulation results are:

- 39 calibre gun, muzzle velocity 821m/s, standard atmosphere conditions, H=0m - sea level: range 40,748 m, figures 3-23
- 52 calibre gun, muzzle velocity 930 m/s, standard atmosphere conditions, H=0m - sea level: range 51,581 m, figures 3-24

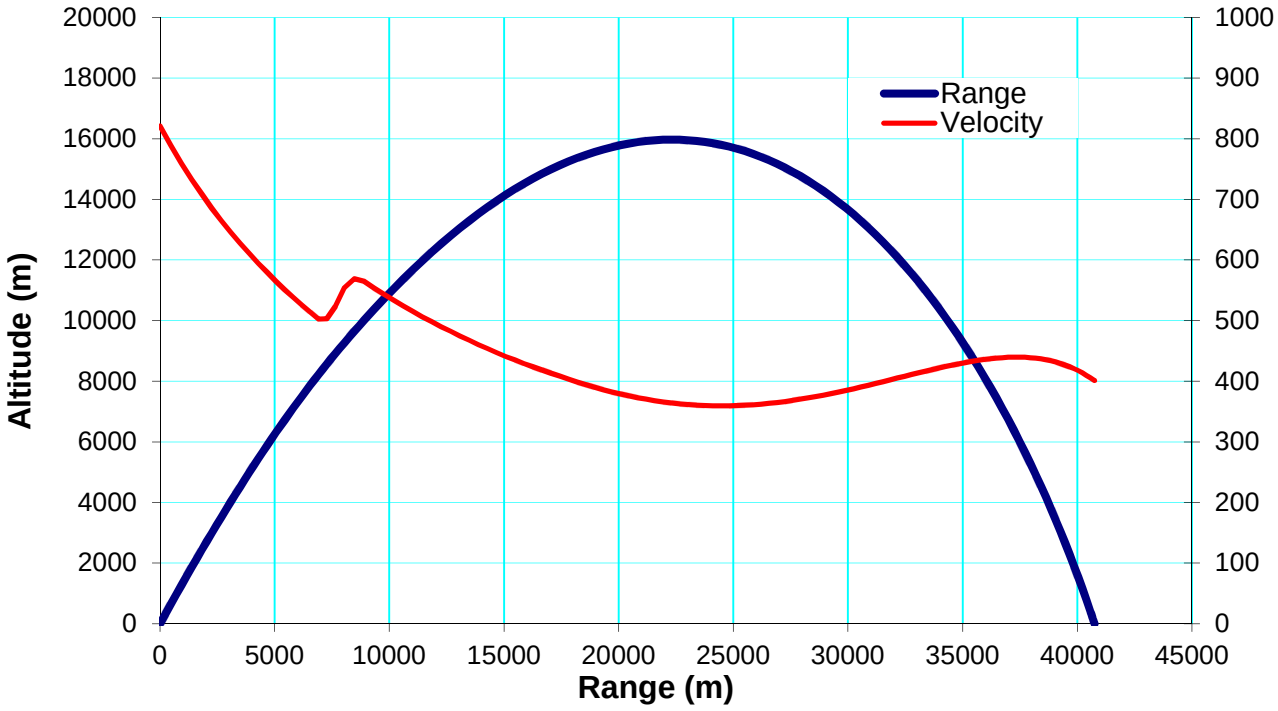

Figure 3-24 Trajectory and velocity profile, 39 calibre gun, max. range

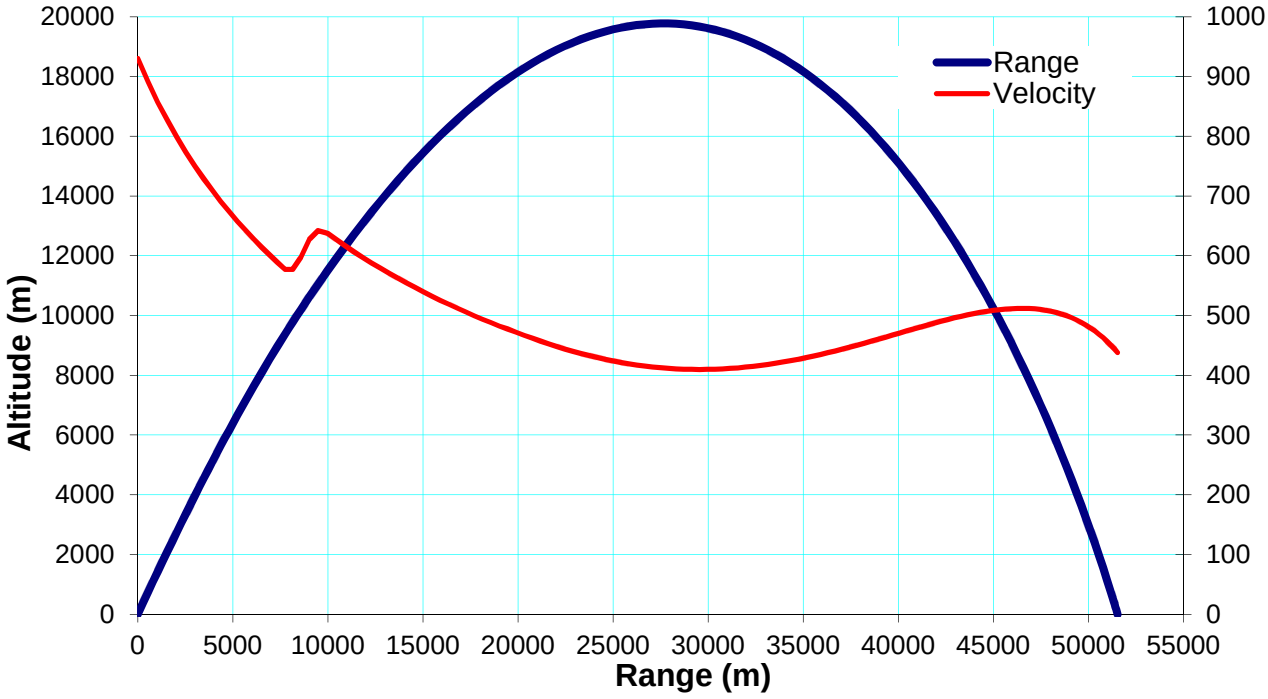

Figure 3-25 Trajectory and velocity profile, 52 calibre gun, max. range

3.4 Validation of the base bleed model through comparison with experiments

To validate methodology for BB effect computation, base bleed model defined in Chapters 3.2.4, 3.2.5 and 3.3.1 will be compared with existing experimental results [38]. The experimental projectile is shown in figure 3-25. The experimental base bleed unit is connected to the projectile's metal jacket at the bottom of the projectile.

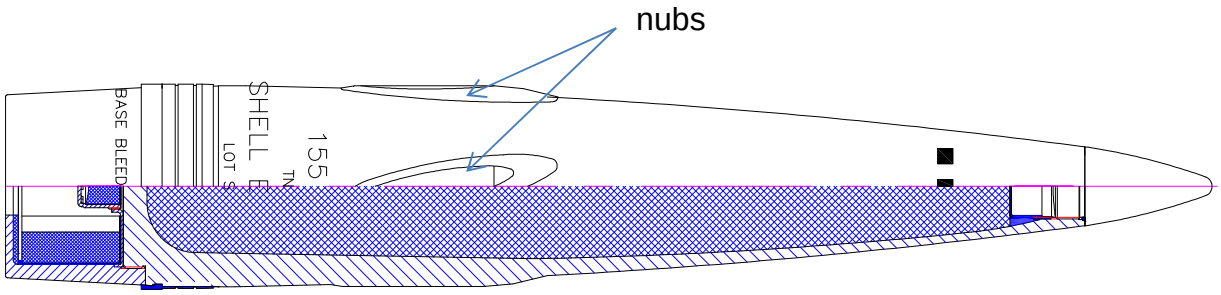

Figure 3-26 Projectile with Base-Bleed unit [38]

The type of experimental projectile shown on figure 3-25, is 155mm calibre Extended Range Full Bore (ERFB), with nubs and optimized ogive profile. Ogive (metal jacket) has aspect ratio 6:1 and R_T/R ratio is 0.95. At the bottom of the projectile, the BB unit comprises propellant grain, placed inside unit against rear wall of the projectile – figure 3-26. Due to high aspect ratio of its ogive, instead of front driving band, projectile has four "nubs" distributed around the outer perimeter of the projectile's ogive, giving the projectile necessary stability inside the gun barrel and at the muzzle.

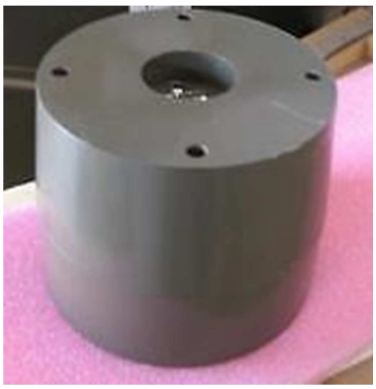

Figure 3-27 Base-Bleed unit for 155mm ERFB-BB projectile [38]

Besides propellant grain, the experimental base bleed unit contains “igniter”, and bottom element with exit orifice - BB “nozzle”. BB unit is connected to the metal jacket with a thread, behind the driving (rotating) band and nylon obturator.

During gun firing, propellant grain and “igniter” are ignited by combustion of main gun propellant charge hot gases. High pressure drop Δp at the muzzle, tends to extinguish base bleed propellant. Therefore, base bleed unit has “igniter” which ignites base bleed propellant after the projectile leaves the muzzle. It is most important for “igniter” to have a high reliability (99,99%) of igniting in gun barrel, i.e. it must ensure that production of base bleed combustion gases and afterburning in the wake begins immediately as projectile leaves the muzzle. To start combustion process at muzzle is the most important requirement for BB, as this is the stage where absolute values of drag are “highest”.

Base bleed propellant utilised for experimental evaluation was composite propellant based on a polyvinylchloride resin [38, 93] as fuel-binder and ammonium perchlorate (NH_4ClO_4) as oxidiser.

The experiments were conducted with the propellant grain shape presented on figure 3-27 and figure 3-28. The propellant formulation was prepared to correspond to the described propellant composition (HTPB/AP) from reference [6, 58], chosen for the modelling of the base drag reduction coefficient. The shape of the propellant is legacy shape, existing in several BB projectiles currently in inventory with several armies around the world.

The experimental propellant grain parameters are:

- Propellant grain mass: 1.09 kg.
- Base-Bleed propellant density: 1619 kg/m^3
- Inhibitor density: 1750 kg/m^3

Figure 3-28 155mm experimental base bleed propellant grain [38]

Projectile assembly, metal jacket with explosive filling and base bleed unit is shown in figure 3-29. The BB unit is behind the rotating band, which seal off gun combustion chamber from barrel, so BB unit is completely immersed in the gun's combustion chamber. When fired, charge combustion pressure is uniformly, inside-out distributed over the BB unit elements. Entire projectile assembly has nominal mass of 47.5 kg, muzzle velocity from 52-calibre gun-howitzer is varies form 925 m/s to 930m/s

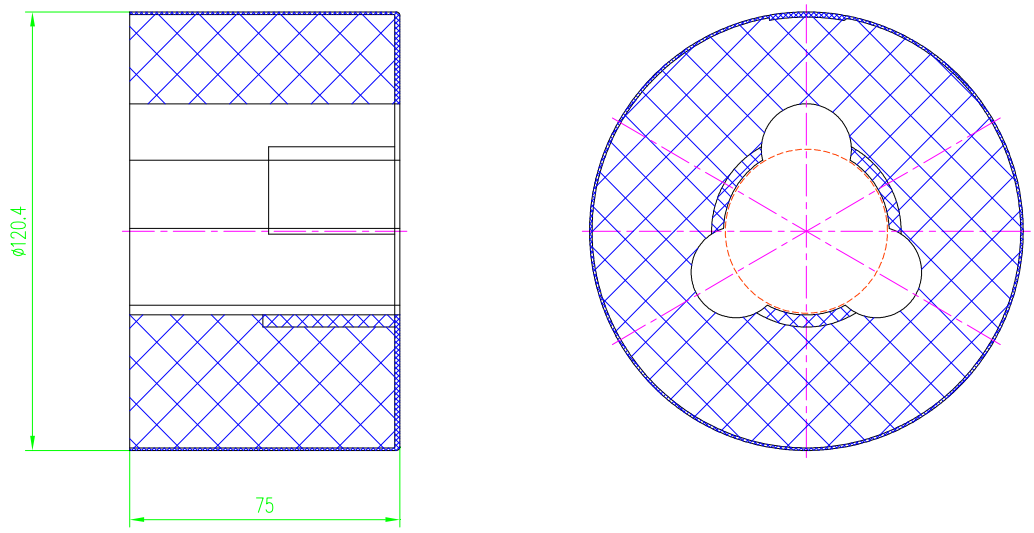

Figure 3-29 Shape and dimensions of reference propellant grain [38]

Figure 3-30 Projectile 155mm ERFB with base bleed unit [38]

One of the parameter that should be empirically determined is burning rate of the propellant. In order to establish the burning rate law, raw data from interior ballistics tests of propellant specimens [38] (figures 3-30 and 3-31), has been processed to find coefficients in experimental propellant burning rate law for pressures in range 20 bars to 100 bars and ambient temperature -20^{o}C and +20 ^{o}C (initial temperatures of propellant). The raw data from two different temperatures are required to establish the temperature sensitivity factor for the burning rate. For lower pressures, burning rate has been extracted from experimental raw data [38] at ambient pressure (figure 3-32), and for sub-atmospheric values of pressure, burning rate was obtained by extrapolation of processed raw data and using heterogonous combustion model of AP based composite propellant burning rate at low pressure/ vacuum [54,74, 80-83], which is, in essence, simple pyrolysis.

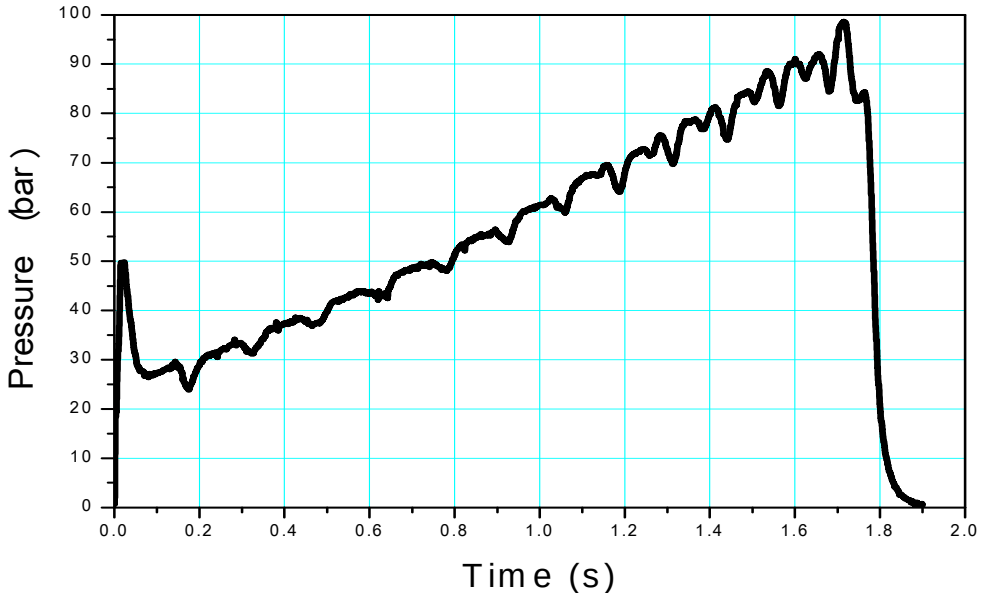

Figure 3-31 Experimental diagram [38] of interior ballistic specimen with 70% of AP content, pressures in range between 2 MPa and 10 MPa, ambient temperature 20^{o}C

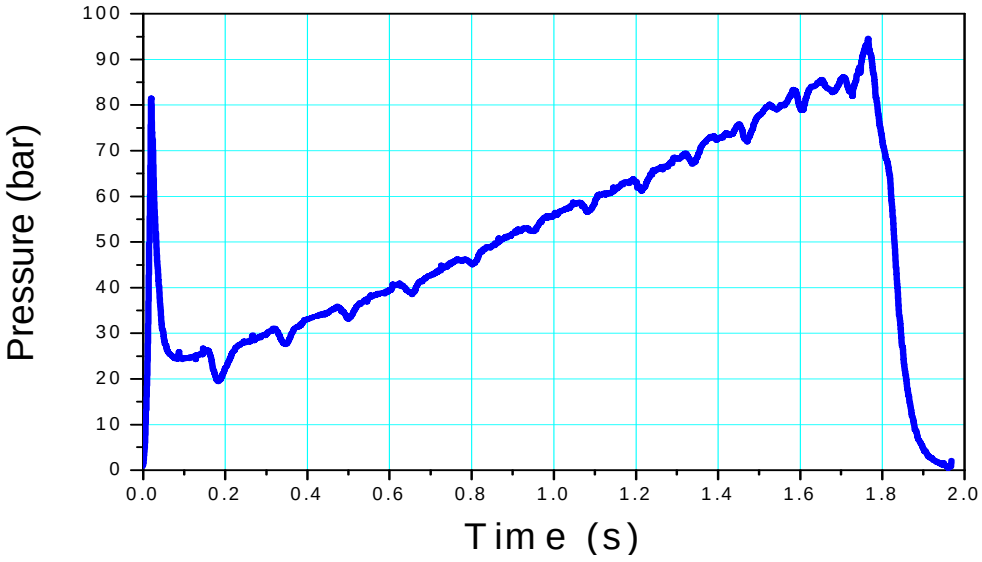

Figure 3-32 Experimental diagram [38] of interior ballistic specimen with 70% of AP content, pressures in range between 2 MPa and 10 MPa, ambient temperature -20^{o}C

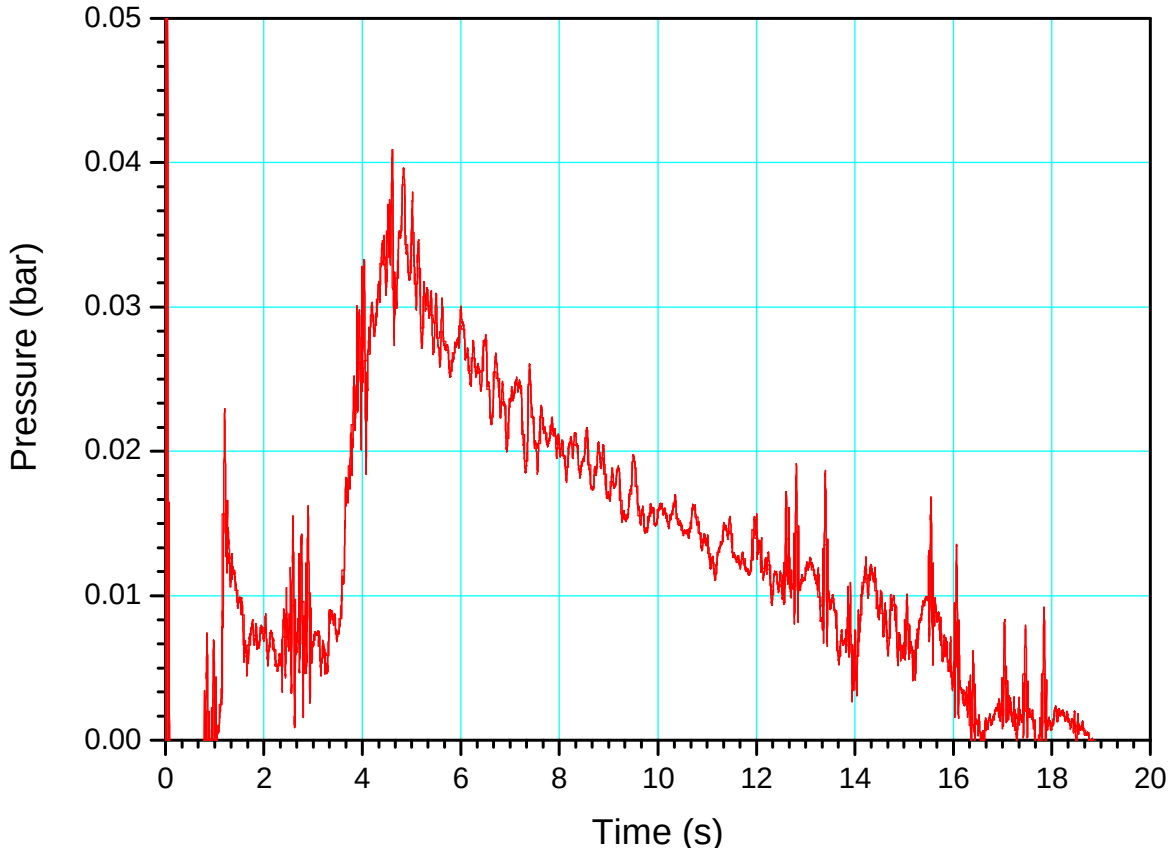

Figure 3-33: Experimental diagram [38] of interior ballistic specimen with 70% of AP content, ambient pressure 1 atm (overpressure measured), ambient temperature 20^{o}C

Tests [38] conducted to establish burning rate law for experimental composition in pressure domain from 20 to 100 bars has been performed with nozzles enabling critical conditions in nozzle throat and supersonic flow in divergent part of the nozzle. However, the burning rate law at ambient pressure (1 atm), has been tested without nozzle. Burning rate has been computed from geometry and measurement of total burning time of specimen grain (fig. 3-32).

The experimental propellant specimens were hollow cylinders, outer diameter 50mm, inner diameter 14mm or 22mm, length 100 mm, inhibited at entire outer surface. When ignited, specimen burns only from inside, i.e. through central port. The burning surface progresses in radial direction, in parallel/offset layers. To test specimens in specific range of burning pressures,

initial size of grain central “hole” and nozzle throat diameter should be selected. After the test, once raw data is collected and pressure vs. time diagram obtained, then for known geometry of specimen propellant grain and nozzle dimensions (nozzle represents a flow meter), we can compute instantaneous burning rate at different pressures. To find burning rate at atmospheric and sub-atmospheric pressures, test without nozzle and with forehead burning specimens should be used. Combining results from different ballistics tests, burning rate can be calculated for entire pressure range, including the sub-atmospheric pressures by interpolation of test results, and by extrapolation of calculated burning rate to be aligned with theoretical value of burning rate in vacuum. Burning rate in vacuum can be estimated using Arrhenius equation, i.e. calculated rate of chemical reactions for heterogeneous system (AP and binder) should corresponds to the burning rate of the propellant in vacuum . The instantaneous burning rate, based on empirical Saint Robert's equation, will be:

$$\mathrm{r} = a + \mathrm{b}\cdot \mathrm{P_c}^{n} \qquad \textbf{(3-55)}$$

where r is burning rate, P_c is combustion pressure in rocket motor chamber, a is “basic” burning rate – or burning rate in “vacuum”, b is the pressure coefficient, and n is pressure exponent.

The measured and computed burning rate equations are given in eq. system 3-56., and shown on figures 3-33 and 3-34.

$$\begin{aligned} &r[\mathrm{m}] = a + b\cdot P_c[\mathrm{Pa}]^n,\ a=0.00074,\ b = 1.37\cdot 10^{-7},\ n = 0.685, \text{ for } P_c < 120000 \text{ Pa} \\ &r[\mathrm{m}] = b\cdot P_c[\mathrm{Pa}]^n, \qquad b = 3.76\cdot 10^{-7},\ n = 0.72 \text{ for } 110000 < P_c < 800000 \text{ Pa} \\ &r[\mathrm{m}] = b\cdot P_c[\mathrm{Pa}]^n, \qquad b = 1.12\cdot 10^{-4},\ n = 0.28, \text{ for } P_c > 800000 \text{ Pa} \end{aligned} \qquad \textbf{(3-56)}$$

The properties of experimental propellant’s combustion gases [38] necessary for base drag reduction model were obtained from Chemical Equilibrium Analysis Code and ICT-Code [76, 99]: burning temperature of the prime propellant T_0 = 2119.3 K, molecular weight of combustion products: M = 22.385, specific heat ratio: κ = 1.255.

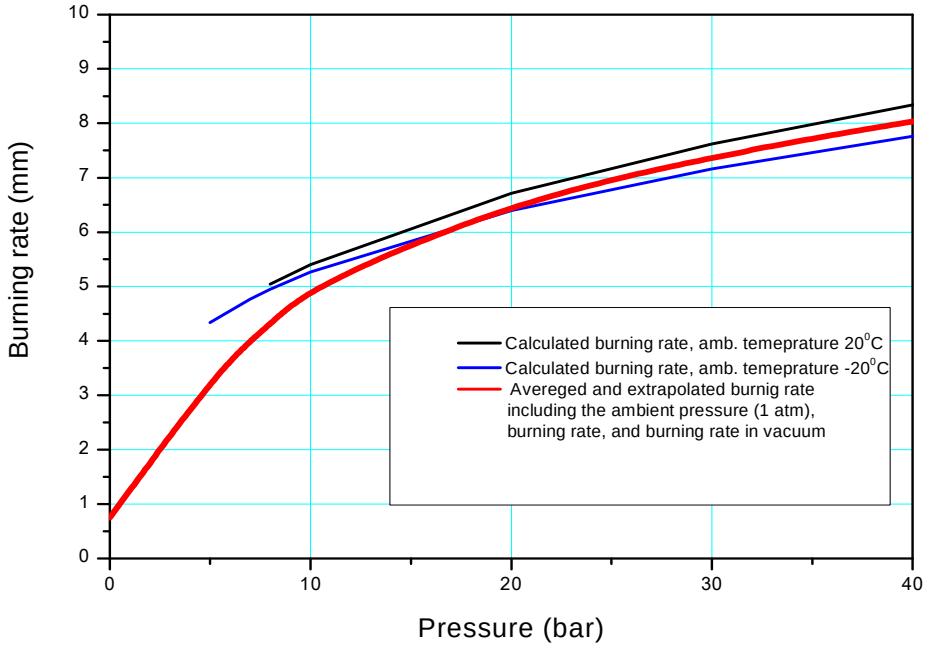

Figure 3-34 Burning Rate diagram for experimental base bleed propellant, for all ranges of pressures

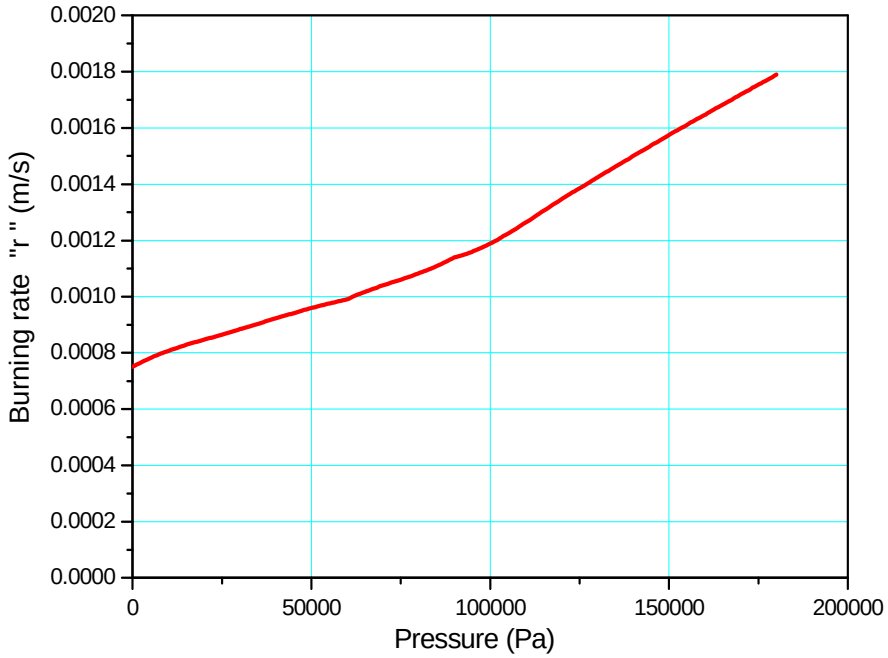

Figure 3-35 Burning rate of experimental propellant, “zoom-in” into zone of base bleed combustion

The diagram of burning surface vs. web development (experimental base bleed propellant grain) [38] (fig. 3-35), and diagram of BB burning in static conditions (figure 3-37), have been used as model burning surface, “active time” and “overpressure” in BB unit for calculation of base bleed effect during BB projectile flight. The fig. 3-37 is produced from raw data gathered during static test of experimental base bleed unit (fig. 3-36).

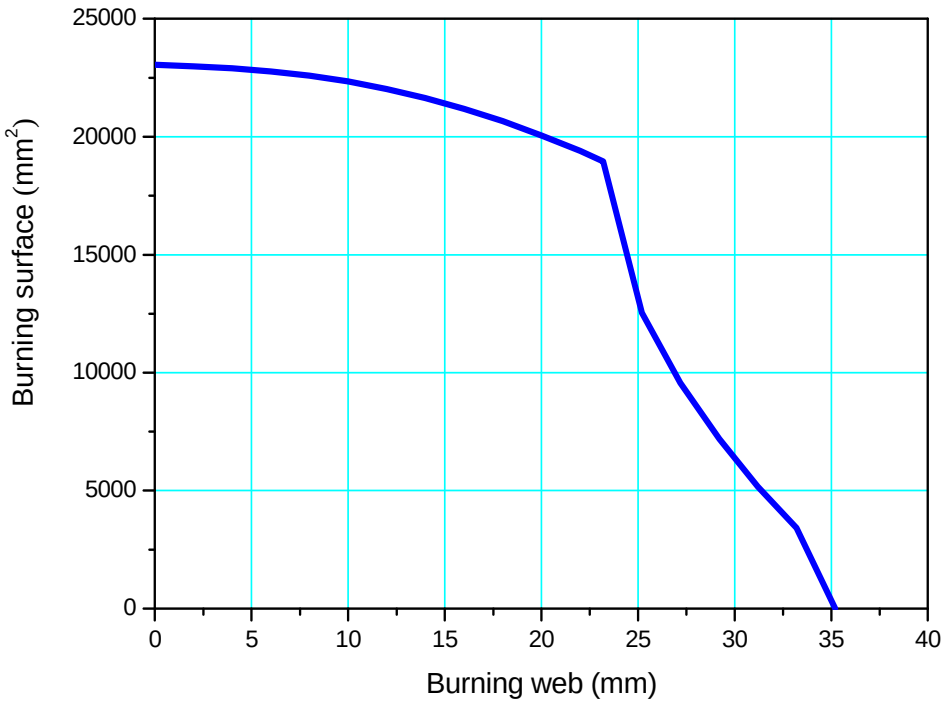

Figure 3-36 Burning surface development vs. web, for experimental configuration of 155 mm BB unit [38]

Figure 3-37 Static trial of exp. 155mm BB unit [38]

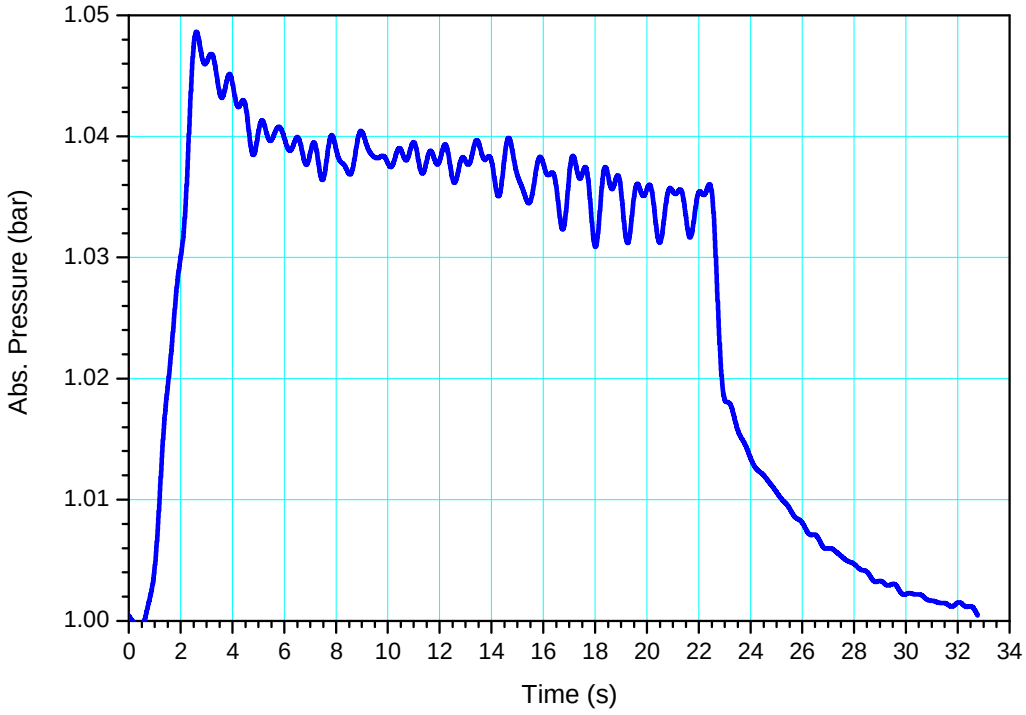

Figure 3-38 Pressure inside experimental 155 mm BB unit during static test (ambient conditions) [38]

To validate the BB drag reduction model, exterior ballistics simulations have been made and compared against raw firing data [38] of experimental BB unit with 155mm ERFB projectiles. Trials were conducted with 155mm 45 calibre ordnance, gun-propellant charge M11C (zone 10), and flight trajectories were measured with Ranging Doppler Radar System. Firing test results (representative group) are presented in table 3-6 and figures 3-38 to 3-42.

Table 3-6 Exterior ballistics trials – experimental 155mm BB projectile [38]

		Measured values					
		Zone	**t_b [°C]**	**θ_0 1/6400**	**V_0 [m/s]**	**X [m]**	**Z [m]**
1	47.197	10	+21	320	896.4	23647	-58
2	47.542	10	+21	320	897.2	23489	-78
3	47.653	10	+21	320	893.7	23578	-98
4	47.613	10	+21	320	898.7	23740	-59
5*	47.679	10	+21	320	890.8	23591	-100
Mean values				**320**	**895.4**	**23609**	**-79**
Remark: * projectile No. 5 had not been tracked by radar							

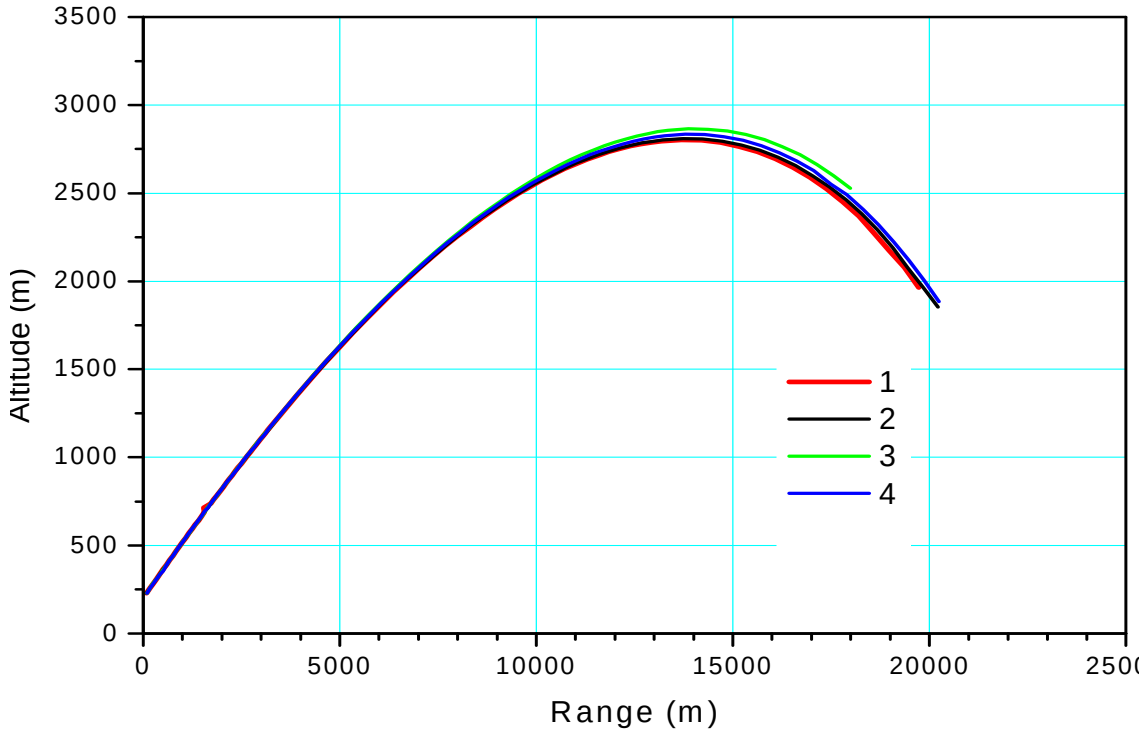

Figure 3-39 Trajectories (radar data) of exp. 155mm BB projectiles – ref. Table 3-6, projectiles 1-4

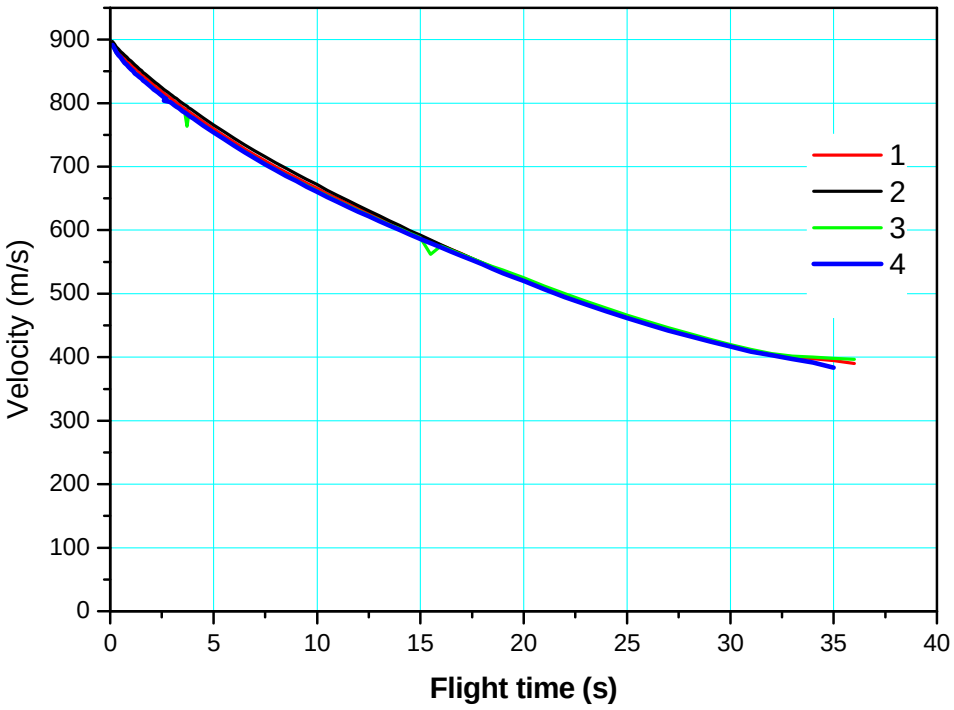

Figure 3-40 Radar data for Velocity vs. Time – ref. Table 3-6

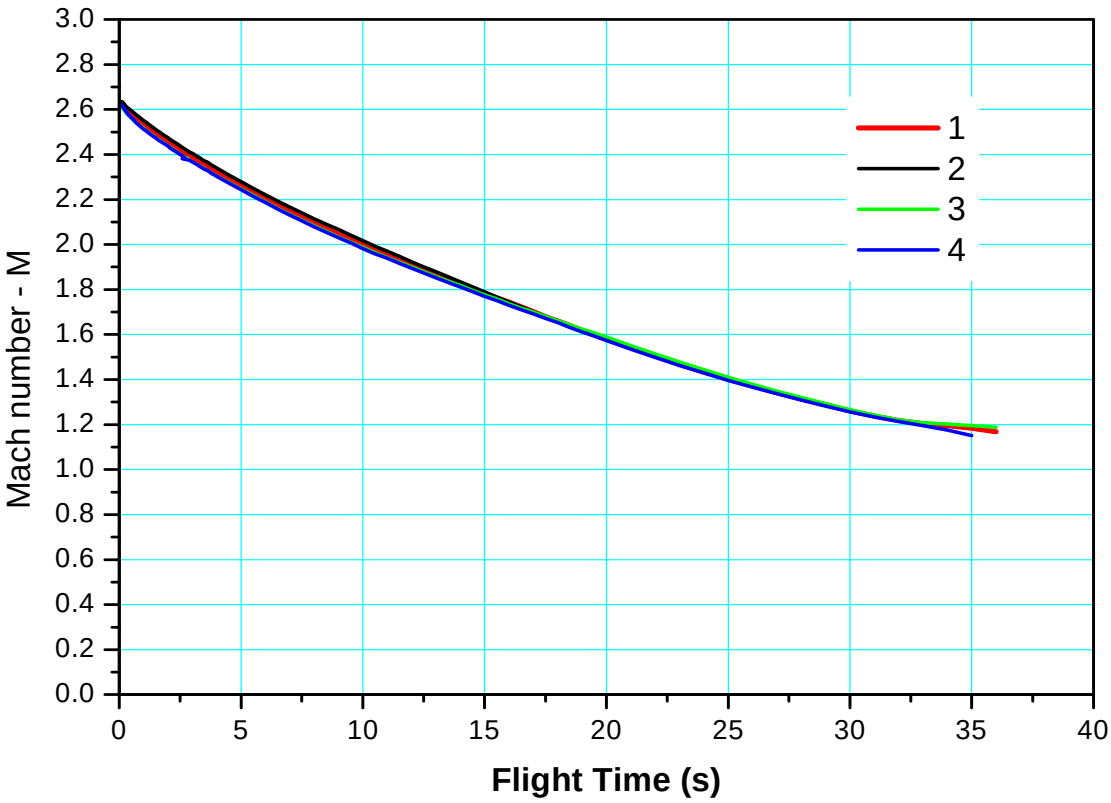

Figure 3-41 Mach number vs. Time – ref. Table 3-6

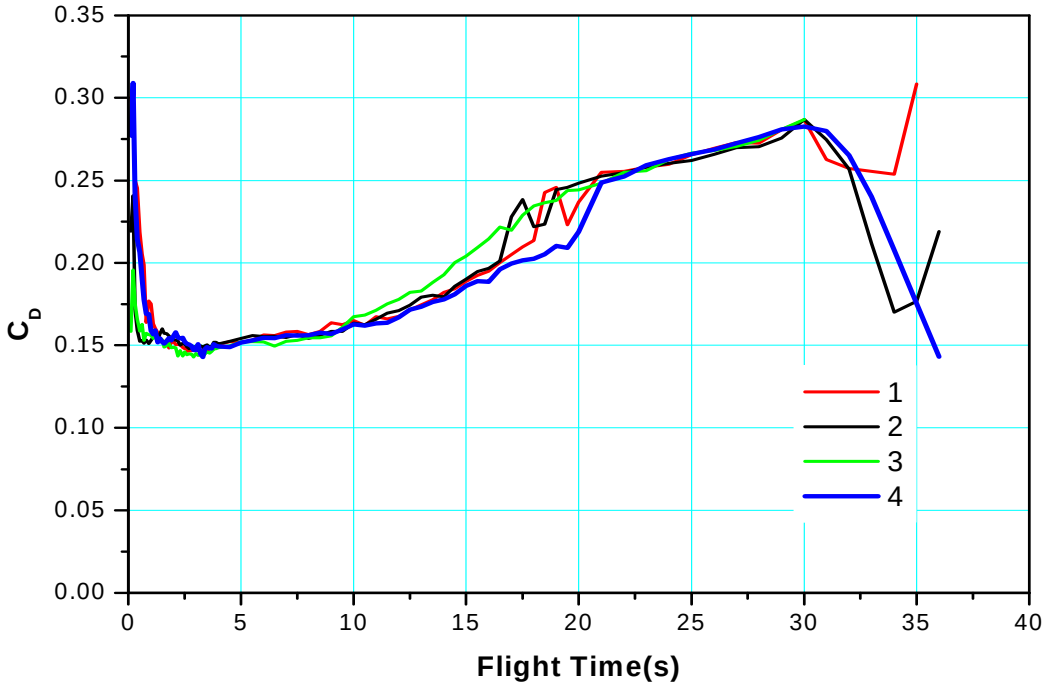

Figure 3-42 Total drag coefficient vs. Time – ref. Table 3-6

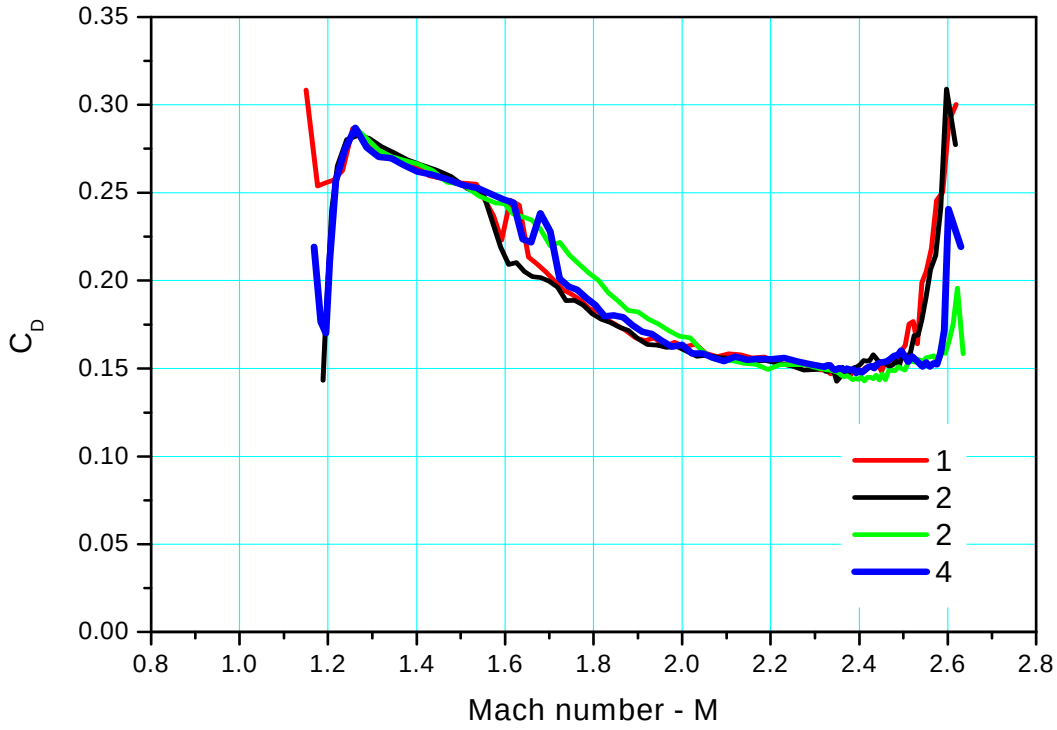

Figure 3-43 **Total drag coefficient vs. Mach number – ref. Table 3-6**

Analysing experimental results, supplementing initial conditions (firing data: altitude of firing place, atmospheric data, azimuth, and elevation) and inserting experimental base bleed propellant grain parameters into BB computational model, drag reduction results have been obtained and compared with actual trials. Highly accurate predictions of trajectory with base bleed were achieved. Calculated range is 23625m (figure 3-43). Comparison between experiments and computations for trajectory profile and total drag is shown on figures 3-43 and 3-44. Minor differences between calculated and measured values that can be observed on total drag diagram, represent data acquisition errors, and input errors in algorithm of Doppler radar. Difference between drag computations and experimentally measured/calculated drag is augmented in zone of transonic flight (Mach numbers between 0.9 Mach and 1.4 Mach) where base bleed effect is significantly reduced. The difference, again, can be attributed to the less sophisticated Doppler Radar software, that calculate in linear manner, projectile mass reduction due to BB grain consumption, over predetermined period of time. Further, very good matching between calculated

and measured C_{DBB} in region of high Mach numbers is evident. The spikes of drag values at highest Mach numbers correspond to the projectile exit at muzzle, before Doppler Radar measurements are stabilized.

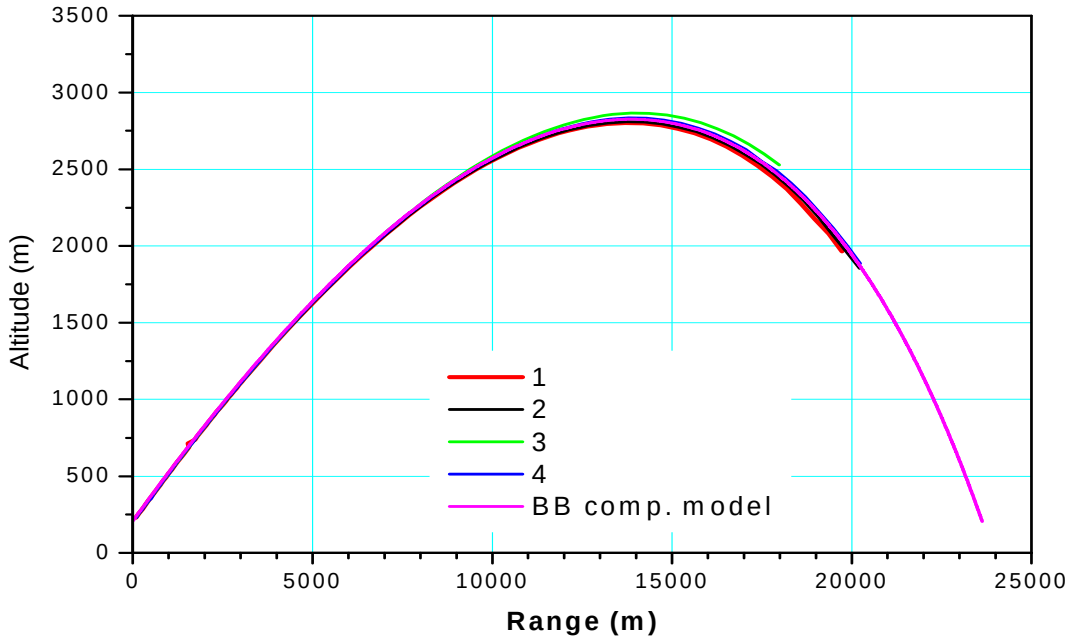

Figure 3-44 **Comparison between experimental and computational trajectory for 155mm BB projectile**

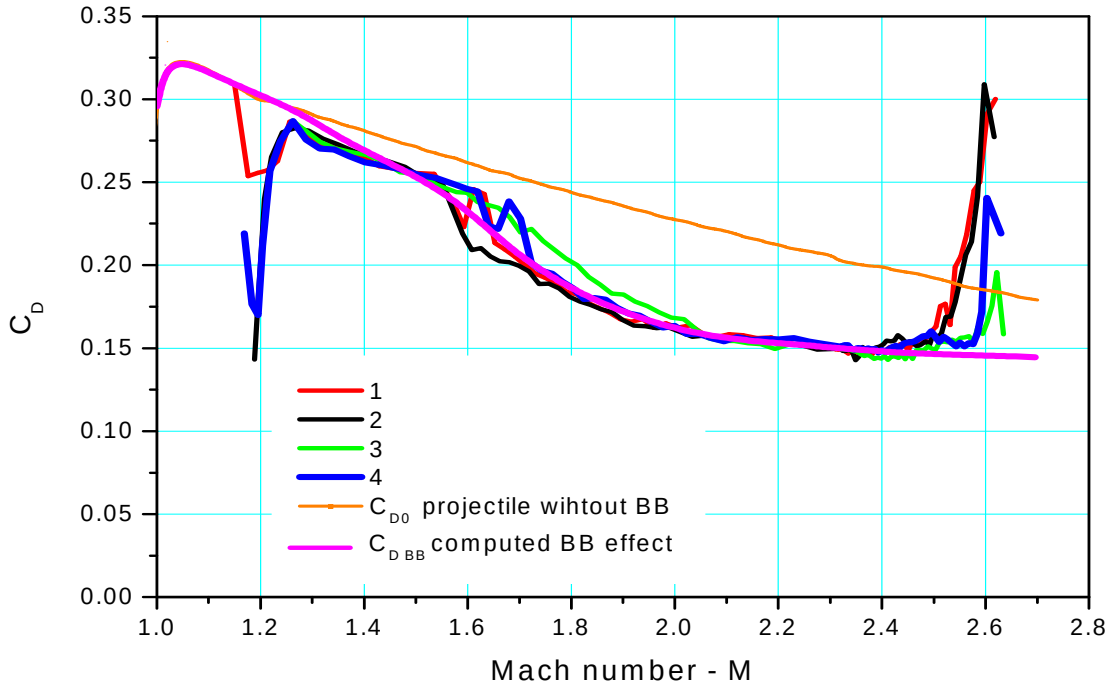

Figure 3-45 Comparison between experiment and calculation of the total drag coefficients vs. Mach number – 155mm BB projectile

The BB modelling has been further tested by comparing the simulation results with firings at max. range (Table 3-7) [38]. Table shows representative group of 4 projectile with experimental BB grain, the average muzzle velocity was 930 m/s. For the same QE of 52^0, at sea level conditions calculated range is 42475 m. Median "range" is 41858m, which means that the calculated range is within 1.4‰, i.e. the error it is less than standard dispersion in range for contemporary 155 mm ERFB-BB ammunition [9]. The sample is not representative (not enough firings), the results has been studies used for comparison with established BB model

Table 3-7 Exterior ballistics trials with experimental 155mm ERFB-BB projectile [30] ("S" - standard BB propellant grain)

No.	Shell Designation Mark	Propellant charge zone	Weight (kg)	Elevation QE (1/6400) $^0/_{00}$	Range (m)
1.	ERFB-BB-S 64	Zone 10	48.105	926	41674
2.	ERFB-BB-S 68	Zone 10	48.22	926	41717
3.	ERFB/BB-S 10M	Zone 10	48.220	926	41887
4.	ERFB/BB-S 7M	Zone 10	48.360	926	42155
	Base bleed simulation	Zone 10	48.00	926	42475

The BB drag reduction model indicated that significant increase in range could be achieved (up to 5%) with new design of BB unit compared to standard BB, if injection of combustion products in projectile's wake zone and afterburning effect are improved in region of high Mach numbers, especially at gun muzzle. Hence, M-REP projectile, as the solid rocket motor significantly influences projectile's trajectory profile, requires completely novel design of BB propellant grain as well as improved propellant formulation, as described in Chapter 3.3. Figure 3-45 represents modified drag reduction model with data derived from experiment and with parameters specific to novel composition of BB thermoplastic poly-plastisol composite propellant.

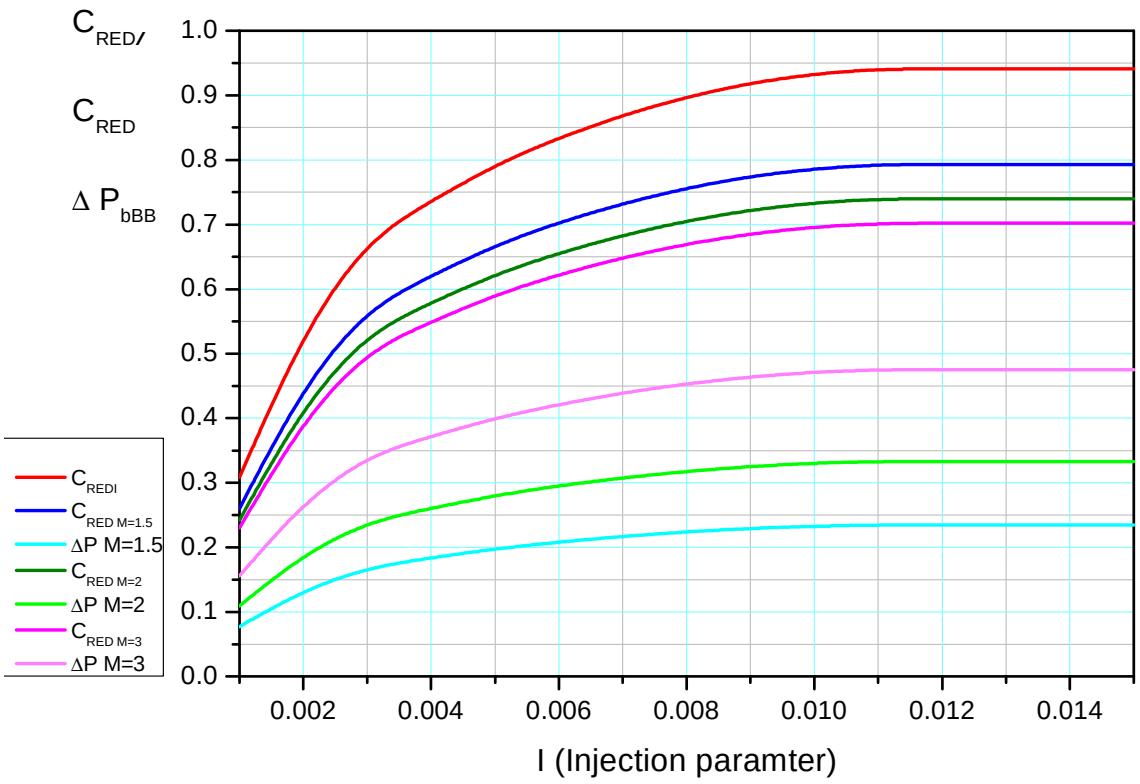

Figure 3-46 Functions of $C_{RED\,I}$, C_{RED} and $\Delta\overline{P}_{bBB}$ vs. injection parameter *I* and Mach number for novel poly-plastisol propellant

Drag reduction model, as described in Chapter 3.3.3 has been used to size and optimise M-REP BB grain shape, and therefore emanate shape of BB structural elements as well as arrangement inside BB unit (grain, O-rings, "sustainer", orifice sealing closure). Figure 3-46 shows comparison between the experimental (or "standard") BB grain burning surface development and novel design of M-REP's BB grain. At the muzzle, mass injection in wake of M-REP is increased 70% comparing to the "standard" BB. The M-REP grain has 20% more propellant then "standard" or any "contemporary" 155 mm BB grain, and it burn longer, approx. 45 second in flight (at max. range).

In the M-REP design, as it is modular configuration of a projectile, we can replace new BB unit with Boat Tail (BT) module, to reduce the range and to have configuration of rocket-assisted projectile (with SRM module), or, by

replacing the SRM module with precursor warhead we can obtain classical HE projectile.

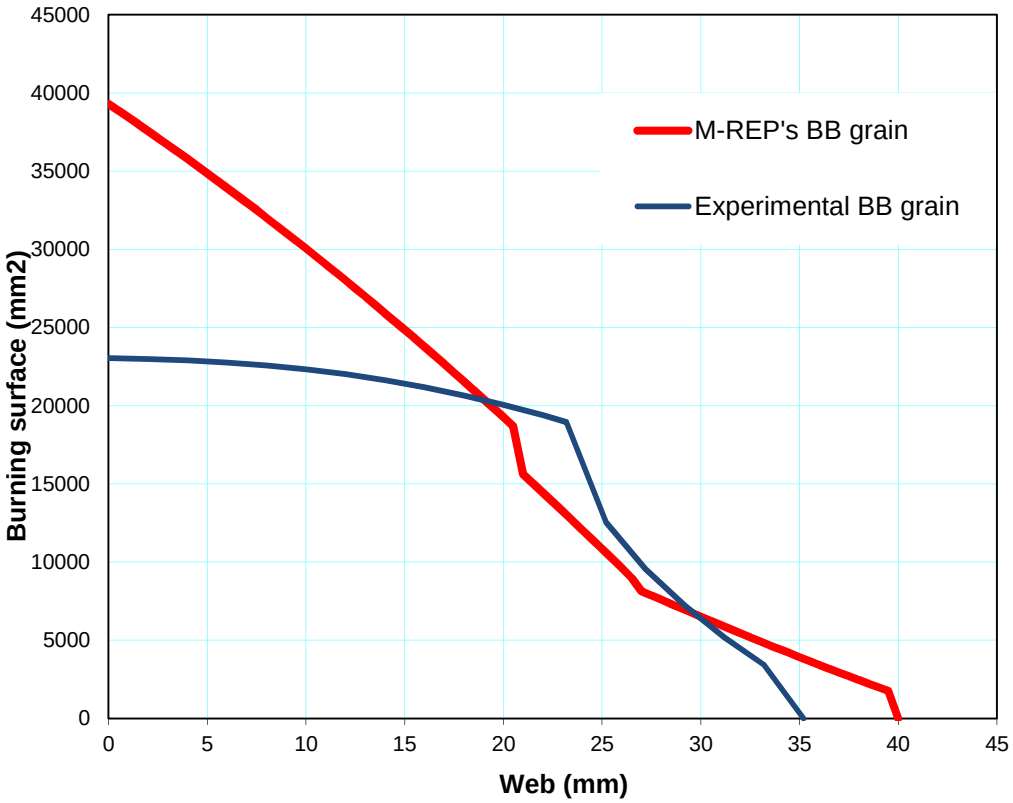

Figure 3-47 Burning surface development vs. web, M-REP BB propellant grain in comparison with Experimental (standard) BB grain.

Figure 3-48 Propellant mixture in powder form

3.5 Structural assessment of the M-REP's BB Unit elements

As part of the new BB unit design for M-REP, structural assessments of BBU's elements were conducted. In gun barrel, M-REP is subjected to high pressure and temperature loads from combustions of gun propellant charge and resulting acceleration. Simulation results of interior-ballistics for 155mm 52-calibre howitzer with M-REP projectile with "proof" pressure (most severe loading conditions) are presented in figures 3-47 to 3-49,.

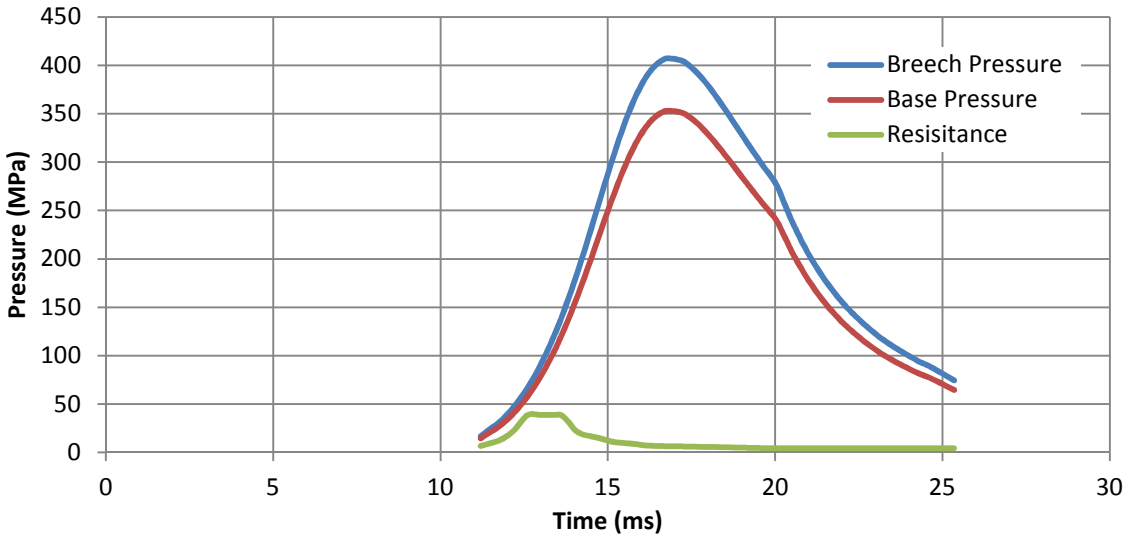

Figure 3-49 **Interior ballistics M-REP - Pressure vs. Time, 52 calibre gun.**

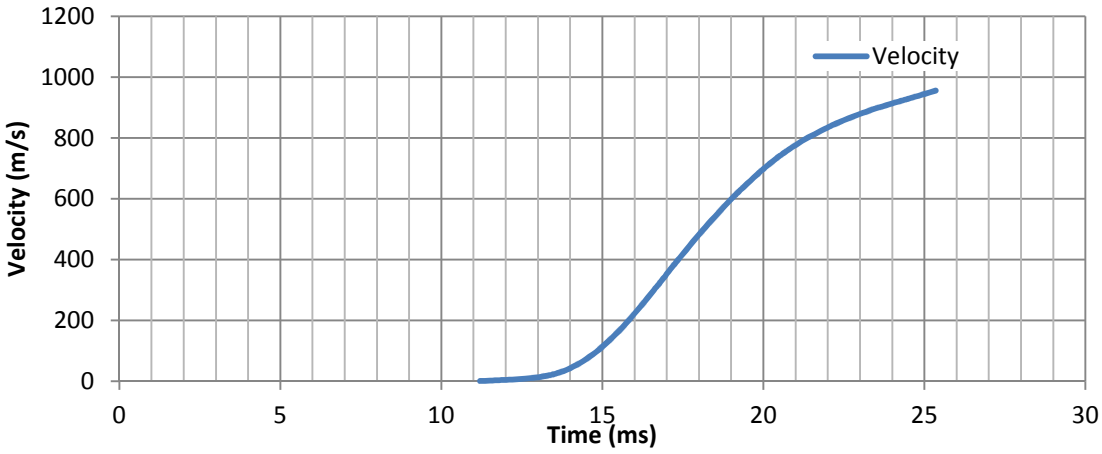

Figure 3-50 Interior ballistics – M-REP Axial Velocity vs. Time, 52 calibre gun.

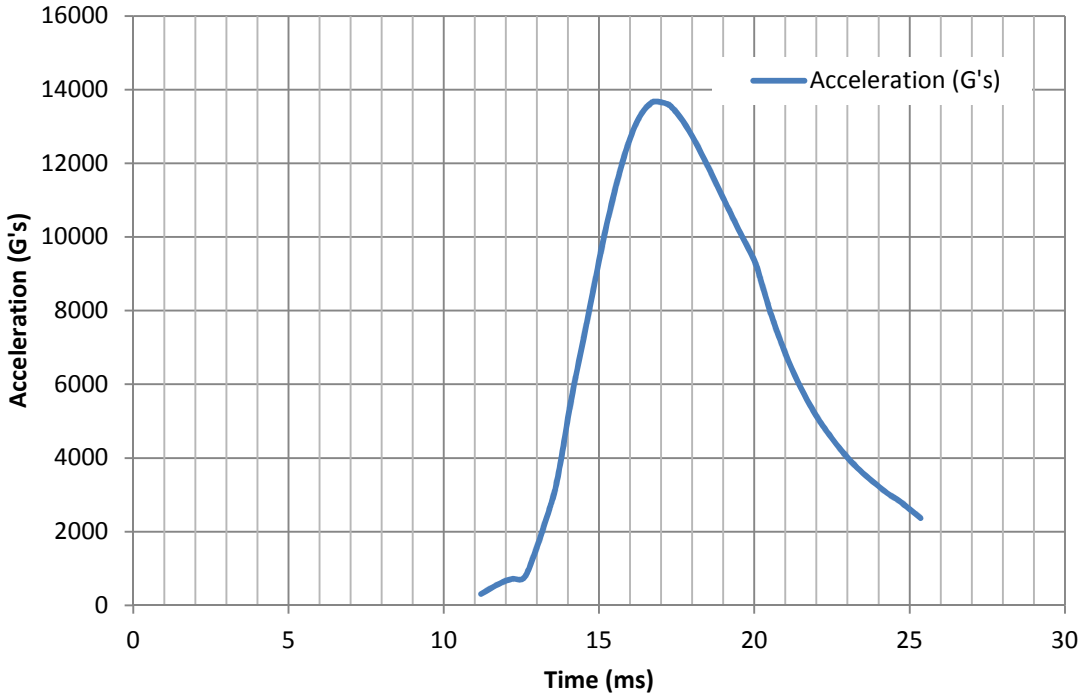

Figure 3-51 Interior ballistics- MREP Axial Acceleration vs. Time, 52 calibre gun.

Based on Interior Ballistic calculations, M-REP's BBU elements were analysed with finite element analysis (FEA) method using CAD/CAE software (PTC Creo and Ansys). Entire M-REP design model is generated and each element has been assigned appropriate mechanical properties. Main structural parts of BBU (BBU casing, and part of the projectile bottom) are designated as high-strength steel parts – steel grade SAE4340 for the casing, and AISI 9260 for the projectile body (payload). Applied loads (with safety factor) are: internal maximum base pressure and corresponding acceleration (boundary values) P_{max} = 430 MPa (equal to barrel "proof" pressure), acceleration corresponding to the projectile mass of 49.7 kg – a =169200 m/s^2. The BB propellant mechanical properties are modelled according to experiments presented in Chapter 3.3.2. The results of finite element analysis are presented in fig. 3-50. The average Von Mises stresses in projectile BBU steel elements are less than critical, i.e. the critical state of stresses is not reached for the design point (430 MPa pressure and corresponding ~17000 g acceleration) including 1.05 safety margin. The novel approach in design of the BBU and BB propellant grain

(radially divided propellant grain, gap for combustion gases to fill entire BB casing and equalise outer and inner pressure during firing sequence, “lower” grain inertial load on BB base), is successfully validated. With reference to modelling experiments (Chapter 3.3.2.), presented design solution can provide structural reliability of the BBU and required ignition of BB propellant and subsequent appropriate development of grain’s burning surface.

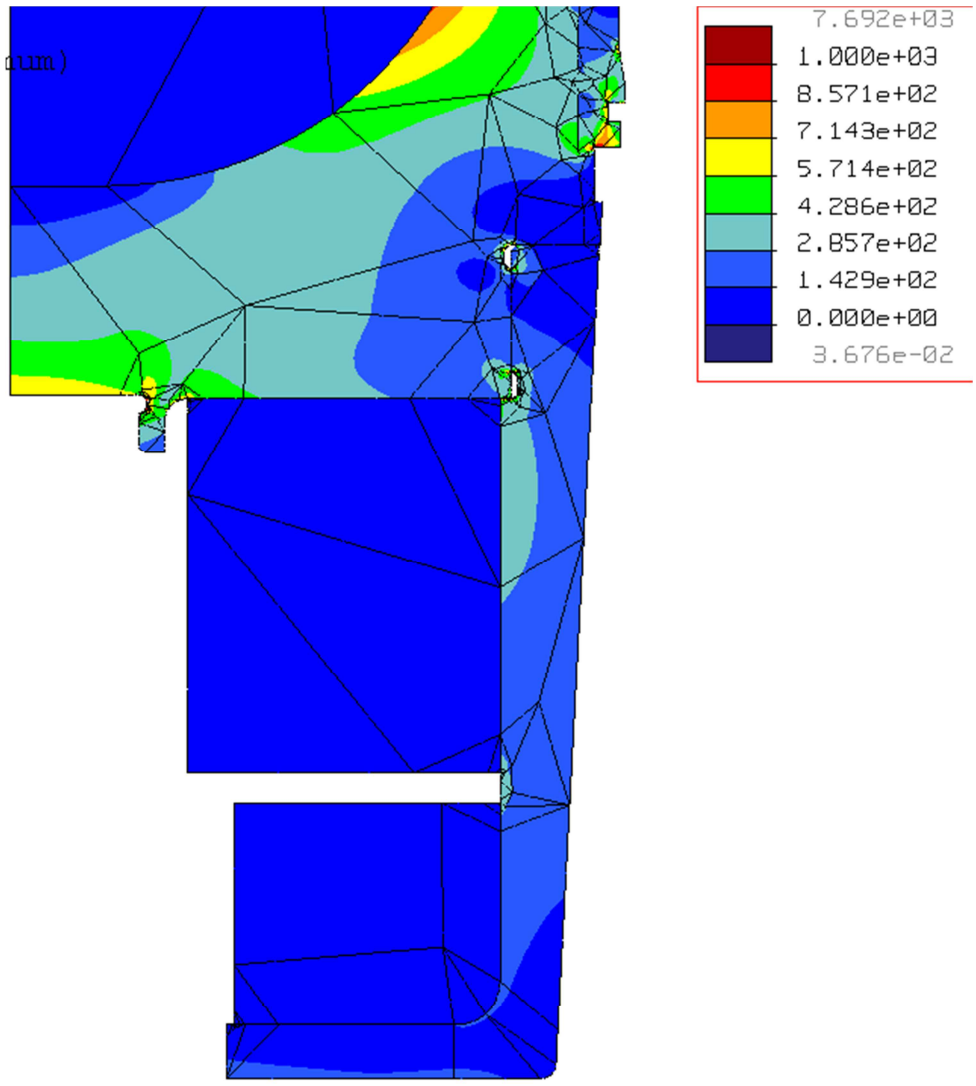

Figure 3-52 Average - combined stresses (von Mises [MPa]) in M-REP’s BB Unit during launch sequence

3.6 Summary of base bleed modelling and M-REP's BBU Designing and Optimisation

3.6.1 Findings

The M-REP BB Unit represents a novelty in design of BB, both from aspect of propellant formulation and performance (base drag reduction), and from the aspect of structural and re-ignition reliability of BB. Novel BB design contributes significantly to increment in M-REP range. The M-REP design already incorporates slender body with streamlined ogive (aspect ratio 4:1) and optimised boat-tail cone for drag reduction. The M-REP's base drag represents 50% to 60% of the total drag (depending on Mach number). The reduction of base-drag from 55% to 75% with optimised BB design, and in combination with "assisted" propulsion (SRM), results in range increase of 70%, (compared to the projectiles with low-drag ogive shape and standard boat tail fired from the same 52-calibre ordnance and Zone 10 powder charge). If we compare two artillery systems with same calibre (e.g. 155mm 39-calibre and 52-calibre howitzers), simulations and experiments showed that system with lower muzzle velocity requires smaller BB propellant grain. Also, BB's grain burning surface development should not be so regressive. The 52-calibre ordnance is chosen as "design ordnance" for M-REP, thus BB is "dimensioned" according to 52-calibre howitzer muzzle velocity and pressure inside barrel. Both aspects of design ("BB effect" and structural "reliability") are validated through mathematical modelling and simulations (FORTRAN Code, PRODAS, FEA). Resulting design is validated through comparison with experimental results [38] - Chapter 3.4, and new BB design is viable, range increment set as project "aim" can be achieved. Novel thermoplastic poly plastisol propellant represents a significant advance in solid rocket propellant technology for base bleed application. Novel formulation has significant improvement related to BB application: stable ignition at muzzle by combing propellant and pyrotechnic compound in the same grain; uniform combustion and functioning, increased after-burning effect due to balanced formulation of combustion products,

mechanical strength in combination with appropriate BBU installation. Further, method and model for BB optimisation represent useful tool for defining shape and dimensions of BB, beside that can be used as “testing” model for existing BB projectiles. BB mathematical model can be used to produce firing tables for projectiles with gas-generator, it is more accurate as it uses fewer empirical correction factors [84].

Regarding the range enhancement, it is indicative that if we want to reach far away targets with contemporary weapon systems, we must exploit all vantages that BB with thermoplastic poly plastisol propellant provides: easy production and performance “tuning,” high efficiency in drag reduction, low “consumption” of projectile’s volume.

3.6.2 Future directions in BB development

The field of “base bleed” is a vibrant research field with many of its aspects not clearly defined or not clearly explained, so far. Therefore, so much more can be investigated in this area. The aerodynamics of base-drag, injection of hot gases and after-burn effect in the wake, are some of the most intriguing phenomenon that could be investigated numerically. Contemporary CFD models [34, 85] do not yield satisfying results, especially form the aspect of mass injection with after-burning effect, i.e BB base drag reduction requires couple of times less reactive gas injection then anticipated by CFD models. Therewithal, new propellant formulation that could improve BB effect still can be found by exploring new energetic binders and plasticisers, and new oxidisers.

In relation to this work, authors future activities related to BB modelling will be focused on numerical simulation of BB effect (CFD), and investigation of improved propellant formulations.

4 METHODOLOGY FOR DEVELOPMENT AND DESING OF SOLID ROCKET MOTORS FOR GUN-LAUNCHED APPLICATIONS

4.1 Introduction

In order to increase range of artillery projectile, without interfering with gun itself, the most efficient way is to provide additional propulsion module within “existing” projectile, which will give additional boost at optimal point on trajectory, to reach maximum range for given gun and gun propelling charge combination. The “existing” projectile means that volume occupied by rocket motor must be minimal, i.e. SRM must not to interfere with efficiency of the payload in a way that the projectile becomes useless. Besides, for spin stabilised projectile “additional” module must not destabilise projectile (for spin stabilised projectile overall length of the projectile is function of projectile diameter and rarely exceeds seven calibres in length). The problem becomes evident when designer decide what will be configuration of projectile with SRM. Among the first artillery rocket assisted projectile successfully deployed in to “inventory” was 155mm M549(A1) [9] projectile, still in use in many armies around the world. The projectile configuration shown on figure 4-1, has SRM in the rear of the projectile, and nozzle protruding into the base cavity of boat tail.

Figure 4-1 155mm M549A1 projectile with SRM [9]

The setbacks of M549A1 arrangement is that the nozzle need to be sealed-off from the pressure inside the gun chamber once projectile is fired, as if combustion gases penetrate SRM cavity, it will certainly consume majority of SRM propellant while projectile is still in gun’s barrel. Further, SRM ignition

delay mechanism (pyrotechnic type) has to be ignited by gun propellant gases, as it is situated in SRM's nozzle. Dimensions of time delay element, do not allow pyrotechnic chain with prolonged delay time, so it is set to only 7 sec after projectile exits the muzzle. The arrangement of the SRM and propellant configuration has two separate propellant grains with central orifice. The grain is divided in to parts, to insert steel support as one unitary solid propellant grain will crack under own "weight" (acceleration loads) upon firing. The issue is with central orifice required for development of burning surface. Central-port will allow propellant grain to deform inward while subjected to high acceleration loads. Further, the projectile cannot be fired with max. propelling charge (Zone 10), due to structural issues both with payload and with SRM. The payload is similar in "size" with standard M107 artillery shell. The use of M549A1 is limited due to higher "dispersion", not because of projectile itself, but due to unreliable pyrotechnic chain and uncertain sealing of rocket engine.

Another similar artillery projectile is 155mm V-LAP [9] – figure 4-2. Solid rocket motor is in the rear. The SRM propellant is single grain, different to M549A1 two part grain, but with central orifice. The inertial forces acting on propellant grain during firing sequence is counteracted with gun pressure transmitting device, that is undisclosed. The smaller then standard BB unit is placed at the end of the projectile, but the action of the BB is disrupted by SRM that ignites approx.11 sec after the firing. The projectile has declared sea level range of >51000m.

Figure 4-2 155mm V-LAP projectile SRM [9]

In the next sections of Chapter Four, the methodology of the SRM development for range-enhanced projectile is described in order to give the insight in optimisation process of SRM design for gun-launched application.

4.1.1 Energy transformation in nozzle:

The Solid Rocket Motor represents “assembly” of two elements: solid rocket propellant packed into combustion chamber and nozzle. Chemical energy confined in solid rocket propellant, through combustion process and expansion of combustion products through rocket nozzle, according to the third Newton’s law (action-reaction) produces thrust to the projectile. Therefore, main role of nozzle is transformation of energy, and it can be explained with following postulates: nozzle converts potential energy of combustion products, generated in combustion chamber of rocket motor, through nozzle geometry, into kinetic energy of expanding combustion gases at nozzle exit. Combustion products represent mixture of gaseous products combined with fractions of liquid and/or solid particles, mixture accelerates in nozzle convergent part, reaching “critical” condition (Mach =1) at nozzle’s throat, then continue to accelerate even faster in nozzle’s divergent part obtaining maximum velocity at nozzle’s exit. In this process, characteristic parameters of flow are changing – pressure and temperature drop as gas stream accelerate towards the nozzle exit. Expanding pressure at nozzle exit, with respect to ambient pressure, can be differentiated into following flow conditions:

a) Under-expanded $(p_{ext}-p_a)>0$

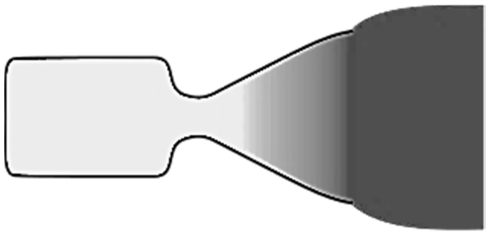

b) Fully-expanded (ambient) $(p_{ext}-p_a)=0$

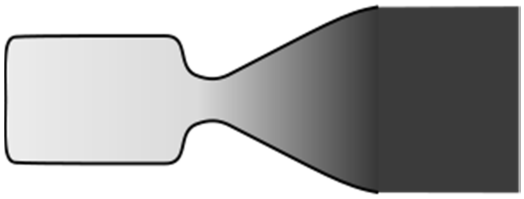

c) Over-expanded $(p_{ext}-p_a)<0$

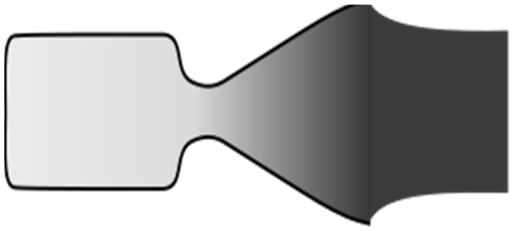

where p_{ext} represents the nozzle's exit pressure and p_a represents the ambient pressure.

Size of the nozzle throat and nozzle bell shape define combustion conditions in rocket motor chamber. Nozzle must be in compliance with combustion chamber in order to have "smooth" and uninterrupted process in the rocket motor. Transformation of chemical energy into potential energy of combustion gases occur in combustion chamber. To obtain thrust, potential energy of the combustion products converts via nozzle into the kinetic energy of the gaseous jet, which propels solid rocket motor. In order to explain how the rocket motor i.e. how the energy is transformed in nozzle, we should assume several theoretical hypothesis:

a) Combustion products are regarded as ideal gas (ideal gas flow conditions), so we can apply equation of the state for ideal gases.

b) Flow is frictionless, without heat exchange with surroundings, without mechanical work interchange or mass addition or subtraction.

c) The gas flowing though ideal nozzle represent mixture of combustion gases, without any liquid or solid particles. In case that particles do exist, they are in complete equilibrium – both kinetic (velocity) and thermal (temperature), with gaseous phase.

d) Regardless of high temperatures and pressures, combustion product do not interact, additional chemical reactions during expansion in the nozzle do not exist, i.e. chemical mixture of combustion gases in unchangeable – "frozen" [76]. The combustion gas along the nozzle has same molecular mass as the mixture of combustion products in

combustion chamber, and C_p – heat capacity at constant pressure, do not change as pressure and temperature change along the nozzle.

e) Nozzle Flow is quasi-stationary, i.e. pressure and temperature with do not change with time, or if variations exist, differences are small and without “peaks”.

f) Cross-sectional transitions in the nozzle are mild, without vortices and shock waves .

g) Nozzle Flow is quasi one-dimensional, pressure and temperature variations are of importance only in direction of nozzle axis of symmetry.

Under those premises, nozzle flow can be regarded as ideal gas flow, in order to calculate ideal nozzle performances [18-19, 86]. As ideal nozzle flow differs to real flow, difference between ideal and real expansion process in the nozzle can be rectified through appropriate correction factors. Basic equations of the nozzle flow are:

Mass conservation equation:

$$\rho \cdot v \cdot A = const \qquad \textbf{(4-1)}$$

in differential form:

$$\frac{1}{\rho}\frac{d\rho}{dx}+\frac{1}{v}\frac{dv}{dx}+\frac{1}{A}\frac{dA}{dx}=0 \qquad \textbf{(4-2)}$$

where are ρ- density, v- velocity, A- area (cross-section), x- longitudinal (axial) coordinate,

Momentum conservation equation:

$$\frac{d\left(\rho v^2 A\right)}{dx}=\frac{(-A\cdot dp)}{dx}=const \qquad \textbf{(4-3)}$$

in differential form:

$$\frac{1}{\rho}\frac{dp}{dx}+v\frac{dv}{dx}=0 \qquad \textbf{(4-4)}$$

Energy conservation equation:

$$\frac{v^2}{2} + C_p T = C_p T_0 \quad \textbf{(4-5)}$$

in differential form

$$C_p \frac{dT}{dx} + v\frac{dv}{dx} = 0 \quad \textbf{(4-6)}$$

where the T_0-represents the total temperature in combustion chamber.

Equation of state for perfect (ideal) gas:

$$p = \rho RT \quad \textbf{(4-7)}$$

in differential form:

$$\frac{1}{\rho}\frac{d\rho}{dx} + \frac{1}{T}\frac{dT}{dx} - \frac{1}{p}\frac{dp}{dx} = 0 \quad \textbf{(4-8)}$$

p-pressure, R-gas constant

Isentropic equation of state:

$$\frac{p}{\rho^{\kappa}} = const \quad \textbf{(4-9)}$$

where the κ-represents specific heat ratio for the combustion products

$M = \frac{v}{a}$ - Mach number **(4-10)**

$a = \sqrt{\kappa RT}$ - equation of for sonic conditions – sonic velocity **(4-11)**

In order to solve this system of equation, next equation's transformations are conducted in order to get relative changes of flow's parameters along the nozzle axis as function of relative changes of nozzle cross section:

Velocity change:

$$\frac{1}{v}\frac{dv}{dx} = -\frac{1}{1-M^2}\frac{1}{A}\frac{dA}{dx} \quad \textbf{(4-12)}$$

Relative change of static pressure:

$$\frac{1}{p}\frac{dp}{dx} = \frac{\kappa M^2}{1-M^2}\frac{1}{A}\frac{dA}{dx} \quad \textbf{(4-13)}$$

Relative change of static temperature:

$$\frac{1}{T}\frac{dT}{dx} = (\kappa - 1)\frac{M^2}{1-M^2}\frac{1}{A}\frac{dA}{dx} \quad \textbf{(4-14)}$$

Relative change of gas density with reference to static parameters:

$$\frac{1}{\rho}\frac{d\rho}{dx} = \frac{M^2}{1-M^2}\frac{1}{A}\frac{dA}{dx} \quad \textbf{(4-15)}$$

Above system of equations, determines change in the cross-section of nozzle, in order to achieve energy transformation (transformation of potential energy - pressure into kinetic energy – jet). Mach number in combustion chamber is less than 1, (the flow is subsonic), therefore to decrease static pressure i.e. to accelerate the flow, the cross-section “variation” gradient should be negative (eq. 4-13) – the flow channel is narrowing. We can describe this phenomenon with next mathematical equations:

$$\begin{aligned} &M < 1 \\ &\frac{1}{A}\frac{dA}{dx} < 0 \\ &\frac{1}{p}\frac{dp}{dx} < 0 \\ &\frac{1}{c}\frac{dc}{dx} > 0 \\ &\frac{1}{T}\frac{dT}{dx} < 0 \\ &\frac{1}{\rho}\frac{d\rho}{dx} < 0 \end{aligned} \quad \textbf{(4-16)}$$

For supersonic inlet flow, energy transformation of potential energy and increment of kinetic energy can be achieved with positive gradient of cross-section “variation”, i.e. by widening of the flow channel., Thus illation is that supersonic flow in the nozzle can be achieved if the nozzle is made of two parts: convergent nozzle where the flow is accelerated up to the sonic conditions and divergent part of the nozzle where the flow is further more accelerated to become supersonic. Zone where the flow corresponds to the sonic conditions corresponds to:

$$\frac{1}{A}\frac{dA}{dx} = 0 \quad \textbf{(4-17)}$$

and it is named critical cross section i.e. the nozzle throat. The Mach number in nozzle throat is defined as:

$M_t = 1$ M_t-critical Mach number **(4-18)**

This type of nozzle is named Laval's nozzle, and its geometry is given in figure 4-4. In critical section of the nozzle the static temperature can be found according to the premise that total temperature along the nozzle is constant:

$$T_0 = T_t\left(1+\frac{\kappa-1}{2}M_t^2\right) \quad \textbf{(4-19)}$$

where T_t represents static temperature in nozzle throat (critical flow conditions)

The equation between total temperature on the nozzle inlet and static temperature in the nozzle critical section, i.e. throat is:

$$\frac{T_t}{T_0} = \frac{2}{\kappa+1} \quad \textbf{(4-20)}$$

As we already defined flow as isentropic, other characteristic parameters of the flow in the cross-section can be found as:

$$\frac{P_t}{P_0} = \left(\frac{2}{\kappa+1}\right)^{\frac{\kappa}{\kappa-1}} \quad \textbf{(4-21)}$$

$$\frac{\rho_t}{\rho_0} = \left(\frac{2}{\kappa+1}\right)^{\frac{1}{\kappa-1}} \quad \textbf{(4-22)}$$

where p_t and ρ_t represents static pressure and density in the nozzle throat.

Similarly, we can find the characteristic flow parameters in other cross-sections of the nozzle. Considering the definition of Mach number the Mach number becomes:

$$\frac{1}{M}\frac{dM}{dx} = -\frac{1}{v}\frac{dv}{dx} - \frac{1}{2}\frac{1}{T}\frac{dT}{dx} \quad \textbf{(4-23)}$$

Substituting equations 4-12 and 4-14 in eq. 4-23, the relation between the Mach number and the cross-section is:

$$\left(\frac{1-M^2}{1+\frac{\kappa-1}{2}M^2}\right)\frac{1}{M}\frac{dM}{dx} = -\frac{1}{A}\frac{dA}{dx} \quad \textbf{(4-24)}$$

Again, solving previous equation, the relation between different cross-section of the nozzle and the Mach number becomes:

$$\frac{A_2}{A_1}=\frac{M_1}{M_2}\left(\frac{1+\frac{\kappa-1}{2}M_2^2}{1+\frac{\kappa-1}{2}M_1^2}\right)^{\frac{\kappa+1}{2(\kappa-1)}} \quad \textbf{(4-25)}$$

where indexes 1, 2 represents two different cross-sections of the nozzle.

Replacing sonic conditions in a throat and geometry of exit cross-section and throat section in eq 4-25, then expressions below define nozzle's flow:

$$A_1=A_t;\qquad M_1=M_t=1;\ \varepsilon_{ext}=\frac{A_{ext}}{A_t};\qquad M_2=M_{ext} \quad \textbf{(4-26)}$$

$$\varepsilon_{ext}=\left(\frac{2}{\kappa+1}\right)^{\frac{\kappa+1}{2(\kappa-1)}}\frac{1}{M_{ext}}\left(1+\frac{\kappa-1}{2}M_{ext}^2\right)^{\frac{\kappa+1}{2(\kappa-1)}} \quad \textbf{(4-27)}$$

where ε_{ext}- represent expansion ratio of the nozzle, and index "*ext*" represents conditions on the nozzle exit. As the divergent nozzle has

$$\varepsilon_{ext}>1 \quad \textbf{(4-28)}$$

and

$$M_{ext}>1 \quad \textbf{(4-29)}$$

In other words, by expanding the geometry in divergent nozzle, sonic flow in nozzle throat accelerate with static pressure and temperature drop, i.e. the conversion of potential energy into the kinetic is achieved on the nozzle exit. If we put the desired exit pressure we can define the exit area of the nozzle – or expansion ratio:

$$\varepsilon_{ext}=\frac{\left(\frac{2}{\kappa+1}\right)^{\frac{1}{\kappa-1}}\left(\frac{\kappa-1}{\kappa+1}\right)^{1/2}}{\left(\frac{P_{ext}}{P_0}\right)^{\frac{1}{\kappa}}\left[1-\left(\frac{P_{ext}}{P_0}\right)^{\frac{\kappa-1}{\kappa}}\right]^{1/2}} \quad \textbf{(4-30)}$$

Correlation between geometrical expansion ratio and for different specific ratio κ is given on diagram figure 4-3.

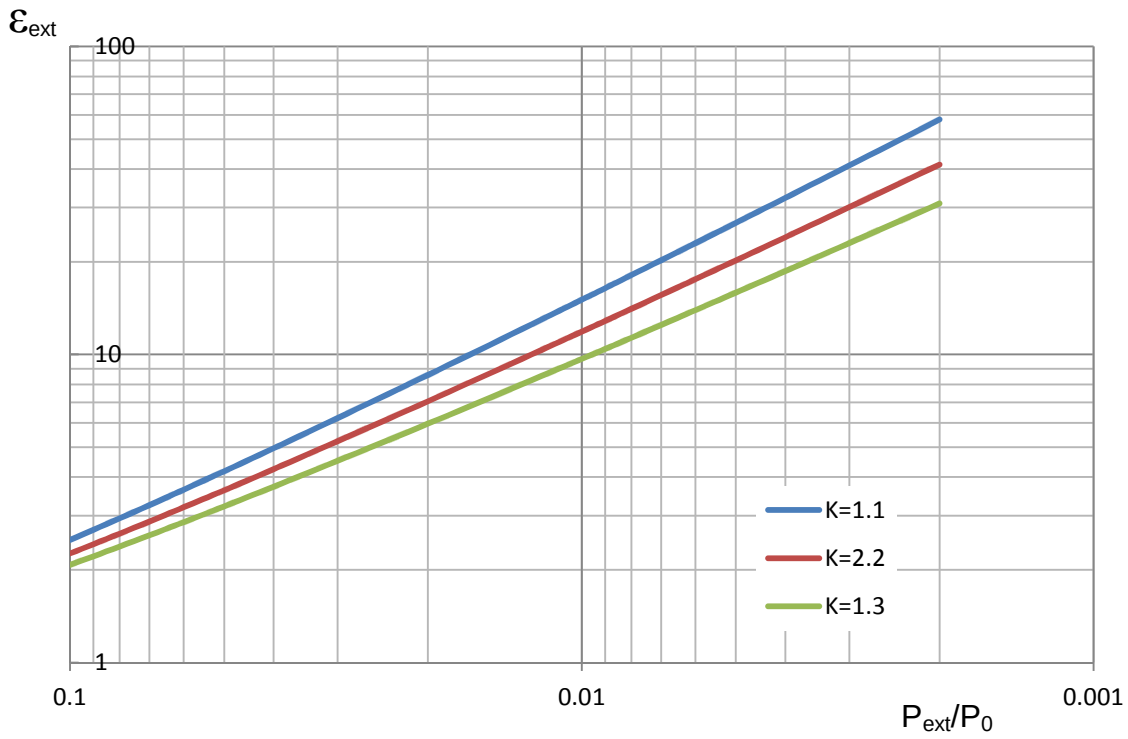

Figure 4-3 Pressure ratio P_{ext}/P_0 vs. ε_{ext}, for typical range of specific heat ratios of solid rocket propellant combustion products

4.1.2 Parameters of flow along "ideal" nozzle

Ideal nozzle flow conditions, under premise of "smooth" change of nozzle cross-sections (no sudden variations in nozzle geometry that can produce shock-waves or turbulence), can be described by following equations:

Constant mass flow:

$$\dot{m} = \rho v A \qquad \textbf{(4-31)}$$

Constant total pressure:

$$P_0 = p\left(1+\frac{\kappa-1}{2}M^2\right)^{\frac{\kappa}{\kappa-1}} \qquad \textbf{(4-32)}$$

Constant total temperature:

$$T_0 = T\left(1+\frac{\kappa-1}{2}M^2\right) \qquad \textbf{(4-33)}$$

According to equation 4-31, we can find the mass flow of combustion products in any cross-section of the nozzle (index $_0$ – stagnation or total flow parameters - combustion chamber):

$$\dot{m} = \frac{v}{a}\frac{a}{a_0}a_0 A\frac{\rho}{\rho_0}\rho_0 = M\sqrt{\frac{T}{T_0}}\sqrt{\kappa RT_0}\,A\frac{1}{\left(1+\frac{\kappa-1}{2}M^2\right)^{\frac{1}{\kappa-1}}}\frac{P_0}{RT_0} \qquad \textbf{(4-34)}$$

Solution of the equation 4-34 as follows:

$$\dot{m} = \sqrt{\kappa}\frac{P_0 A}{\sqrt{RT_0}}\frac{M}{\left(1+\frac{\kappa-1}{2}M^2\right)^{\frac{\kappa+1}{2(\kappa-1)}}} \qquad \textbf{(4-35)}$$

Replacing the part of equation 4-35, that entirely depends of Mach number with next equation

$$q(M) = \frac{M}{\left(1+\frac{\kappa-1}{2}M^2\right)^{\frac{\kappa+1}{2(\kappa-1)}}} \qquad \textbf{(4-36)}$$

then the flow in each cross section of the ideal nozzle can be described with:

$$\dot{m} = \sqrt{\kappa}\frac{P_0 A}{\sqrt{RT_0^*}}q(M) \qquad \textbf{(4-37)}$$

Analysing eq. 4-37, we can find a cross-section that has critical flow conditions (M =1). If we differentiate eq. 4-36 by “M”, and make first derivative (extreme) equal to 0, then:

$$1-\frac{\kappa+1}{2}\frac{M^2}{\left(1+\frac{\kappa-1}{2}M^2\right)} = 0 \qquad \textbf{(4-38)}$$

The solution is valid for:

$M = 1$ and critical cross section: $A = A_t$

If case that the difference between inlet pressure and exit pressure is greater than “critical”, then sonic conditions can be achieved and flow should be become supersonic. Therefore q(M) in the throat can be written as:

$$q(M=1)=\left(\frac{2}{\kappa+1}\right)^{\frac{\kappa+1}{2(\kappa-1)}} \quad \textbf{(4-39)}$$

Using the previous equation in solid rocket motor propulsion where the mass flow through critical cross-section of the nozzle is defined with equation:

$$\dot{m}=\frac{P_0 A_t}{C^*} \quad \textbf{(4-40)}$$

The parameter C^* is "characteristic velocity" and it is calculated for ideal nozzle as:

$$C^*=\frac{\sqrt{RT_0}}{\Gamma(\kappa)} \quad \textbf{(4-41)}$$

Where $\Gamma(\kappa)$ is:

$$\Gamma(\kappa)=\sqrt{\kappa}\left(\frac{2}{\kappa+1}\right)^{\frac{\kappa+1}{2(\kappa-1)}} \quad \textbf{(4-42)}$$

If the pressure ratio between inlet and exit pressure of the ideal nozzle is less then:

$$\frac{P_0}{p_a}<\left(\frac{\kappa+1}{2}\right)^{\frac{\kappa}{\kappa-1}} \quad \textbf{(4-43)}$$

thence, the flow is subsonic ,and the mass flow through cross-section is equal to:

$$\dot{m}=\sqrt{\frac{2\kappa}{\kappa-1}}\frac{P_0 A}{\sqrt{RT_0}}\sqrt{\left(\frac{P_a}{P_0}\right)^{\frac{2}{\kappa}}-\left(\frac{P_a}{P_0}\right)^{\frac{\kappa+1}{\kappa}}} \quad \textbf{(4-44)}$$

In solid rocket propulsion theory, the flow density "$\rho*$" is often used:

$$\rho^*=\frac{\dot{m}}{A}=v\rho \quad \textbf{(4-45)}$$

So with reference to eq. 4-36:

$$\rho^*=\sqrt{\kappa}\frac{P_0}{\sqrt{RT_0^*}}q(M) \quad \textbf{(4-46)}$$

Flow density is maximal in critical cross-section (nozzle throat):

$$\rho^*_t=\frac{P_0}{C^*} \quad \textbf{(4-47)}$$

Relative ratio of flow densities is written as:

$$\overline{\rho^*} = \frac{\rho^*}{\rho^*_t} = \frac{A_t}{A} = \left(\frac{\kappa+1}{2}\right)^{\frac{\kappa+1}{2(\kappa-1)}} q(M) \qquad \textbf{(4-48)}$$

4.1.3 Velocity change along the ideal nozzle

Absolute velocity change along the ideal nozzle can be found using eq. 4-32. equation 4-32. Resultant relation shows dependency between the velocity and the pressure drop along the nozzle:

$$M = \sqrt{\frac{2}{\kappa-1}\left[\left(\frac{P_0}{P}\right)^{\frac{\kappa-1}{\kappa}} - 1\right]} \qquad \textbf{(4-49)}$$

Considering previous relation, velocity in any cross section can be written as:

$$v = Ma = \frac{a}{a_0} a_0 M \qquad \textbf{(4-50)}$$

Replacing previous relation in eq. 4-49, the final expression for velocity along the nozzle is:

$$v = \sqrt{\frac{2\kappa}{\kappa-1} RT_0 \left[1 - \left(\frac{P}{P_0}\right)^{\frac{\kappa-1}{\kappa}}\right]} \qquad \textbf{(4-51)}$$

Nozzle exit velocity can be determined knowing the inlet conditions $(T_0 ; P_0)$, combustion products composition (κ, R) and exit pressure $p_{ext} = f(\varepsilon_{ext})$:

$$v_{ext} = \sqrt{\frac{2\kappa}{\kappa-1} RT_0 \left[1 - \left(\frac{P_{ext}}{P_0}\right)^{\frac{\kappa-1}{\kappa}}\right]} \qquad \textbf{(4-52)}$$

Eq. 4-52 indicates that the exit velocity can be increased if the inlet parameters are increased – total temperature T_0, decreasing the molecular weight of the combustion gases (increasing the R – specific gas constant), and decreasing the exit pressure. Solid rocket motors can achieve high value of exit velocities using the propellant with high combustion temperature T_0 (above

3200 K) and high inlet pressure P_0 (above 100 bars). Value of the V_{ext} in real conditions is:

$$v_{ext} = 2100 \div 2500 \cdot m/s$$

As example, figure 4-4 represents typical changes of nozzle parameters along the nozzle:

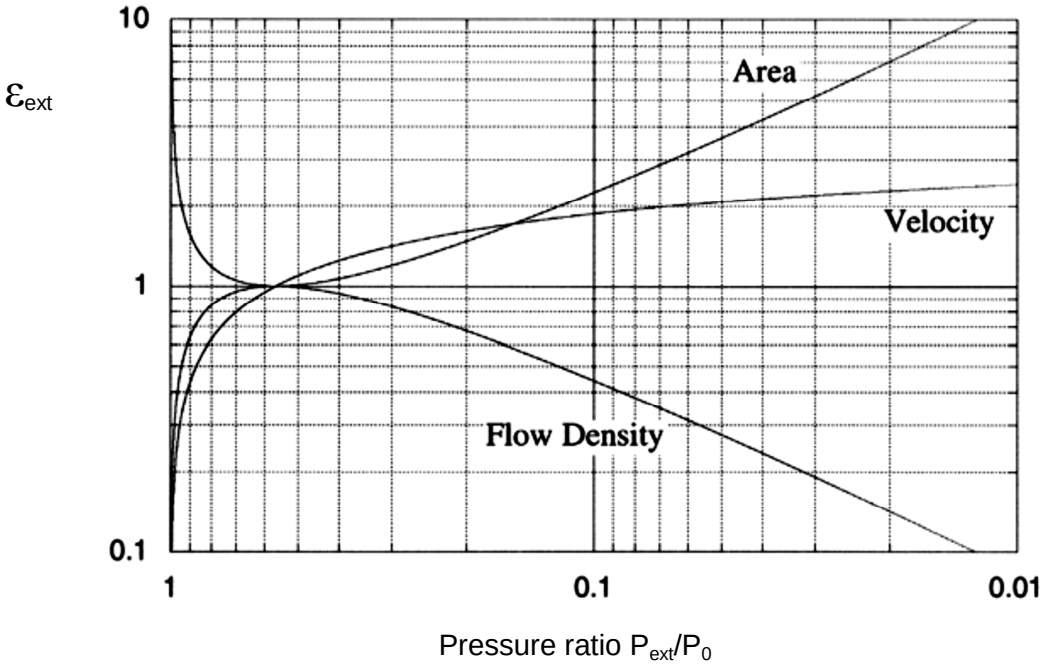

Figure 4-4 Pressure ratio P_{ext}/P_0 Vs. flow parameters [87]

4.1.4 Propulsive characteristics of ideal nozzle

Energy transformation (potential into kinetic) , done by the nozzle, is most utmost important function of the nozzle. Propulsion characteristic of the nozzle is defined through propulsion (thrust) coefficient C_F:

$$C_F = \frac{F}{P_0 A_t} \tag{4-53}$$

Substituting the expression for the propulsive force in above equation:

$$C_F = \frac{\dot{m} v_{ext}}{P_0 A_t} + \frac{A_{ext}}{A_t}\left(\frac{p_{ext}}{P_0} - \frac{p_a}{P_0}\right) \tag{4-54}$$

With reference to the eq. 4-30 and 4-40:

$$C_F = \frac{v_{ext}}{C^*} + \varepsilon_{ext}\left(\overline{p}_{ext} - \overline{p}_a\right) \quad \textbf{(4-55)}$$

If the expansion of the combustion gases is up the ambient pressure, then thrust coefficient has a value of:

$$C_F = \frac{v_{ext}}{C^*} \quad \textbf{(4-56)}$$

Thrust coefficient for the expansion in vacuum equals to:

$$C_F = \frac{v_{ext}}{C^*} + \varepsilon_{ext}\overline{p}_{ext} \quad \textbf{(4-57)}$$

Equation 4-57 substituted with eq. 4-30, 4-31 and 4-52 leads to:

$$C_F = \Gamma(\kappa)\sqrt{\frac{2\kappa}{\kappa-1}\left(1-\overline{p}_{ext}^{\frac{\kappa-1}{\kappa}}\right)^{1/2}} + \frac{\left(\frac{2}{\kappa+1}\right)^{\frac{1}{\kappa-1}}\left(\frac{\kappa-1}{\kappa+1}\right)^{1/2}}{\overline{p}_{ext}^{\frac{1}{\kappa}}\left[1-\overline{p}_{ext}^{\frac{\kappa-1}{\kappa}}\right]^{1/2}}\left(\overline{p}_{ext} - \overline{p}_a\right) \quad \textbf{(4-58)}$$

This gives:

$$C_F = \sqrt{\kappa}\left(\frac{2}{\kappa+1}\right)^{\frac{\kappa+1}{2(\kappa-1)}}\sqrt{\frac{2\kappa}{\kappa-1}\left[1-\left(\frac{p_{ext}}{p_0}\right)^{\frac{\kappa-1}{\kappa}}\right]} + \frac{\left(\frac{2}{\kappa+1}\right)^{\frac{1}{\kappa-1}}\sqrt{\frac{\kappa-1}{\kappa+1}}}{\left(\frac{p_{ext}}{p_0}\right)^{\frac{1}{\kappa}}\sqrt{1-\left(\frac{p_{ext}}{p_0}\right)^{\frac{\kappa-1}{\kappa}}}}\left(\frac{p_{ext}}{p_0} - \frac{p_a}{p_0}\right) \quad \textbf{(4-59)}$$

Expression 4-58 represents thrust coefficient as function of following parameters:

$$C_F = f\left(\overline{p}_{ext}, \overline{p}_a, \kappa\right) \quad \textbf{(4-60)}$$

or $C_F = f\left(\varepsilon_{ext}, \overline{p}_a, \kappa\right)$ **(4-61)**

The optimum (maximum) value of C_F is achieved when appropriate value of ε_{ext} has been chosen, i.e. when the

$$\overline{p}_{ext} = \overline{p}_a \quad \textbf{(4-62)}$$

Maximum value of the C_F can be written as:

$$C_{F\max} = \Gamma(\kappa)\sqrt{\frac{2\kappa}{\kappa-1}\left(1-\bar{p}_a^{\frac{\kappa-1}{\kappa}}\right)^{1/2}} \quad \textbf{(4-63)}$$

During M-REP flight , ambient pressure is changing with altitude, so the maximum thrust coefficient cannot be achieved during the entire active phase of the rocket flight, as M-REP's nozzle has fixed geometry (ε_{ext}=const.). M-REP-'s nozzle should be dimensioned for design point different to see level conditions in order to achieve optimum thrust along the desired trajectory. For the M-REP the ambient pressure correspond to the altitude at which the "ignition delay" activate/ignite the SRM. The nozzle should be adopted for those atmospheric parameters, however as the space for nozzles installation of are quite limited, the optimal solution has been elaborated in Chapter 4.1.5..

With defined flow and propulsive parameters of the nozzle we can determine specific impulse of the solid rocket motor as:

$$I_s = \frac{F}{\dot{m}} = \frac{C_F P_0 A_t}{\frac{P_0 A_t}{C^*}} = C_F C^* \quad \textbf{(4-64)}$$

Equation 4-64 indicates the "quality" of the solid rocket motor i.e. represents the quality of the transformation of energy in combustion chamber (C^*) and in the nozzle (C_F), relative to the total transformation of energy.

The specific impulse in vacuum is given by:

$$I_s^* = v_{ext} + C^* \varepsilon_{ext} \bar{p}_{ext} \quad \textbf{(4-65)}$$

4.1.5 Geometry of the M-REP's nozzle

Geometry of the convergent-divergent nozzle(s) for M-REP's SRM is one of the crucial design task. The nozzle design should provide optimal geometry to achieve required thrust for augmented range and de-spinning moment for stabilization of the projectile Optimization of nozzle design is complex process, primarily directed by design features of projectile itself (free volume in which we

can install the nozzles), and other requirements such as nozzle's throat erosion, heat transfer in the nozzle, and potential thrust misalignment. Regarding convergent-divergent nozzle and in particular the "scarfed" nozzle profile, several types of the nozzle configurations are considered:

- Conical Laval's nozzle with profiled convergent nozzle part as well as profiled throat segment (fig. 4.5);
- Conical Laval nozzle with immersed conical part into the combustion chamber;
- Profiled Laval nozzle, , specifically divergent part of the nozzle in order to achieve minimum losses, induced by 2D flow and nonparallel flow on the nozzle exit for nozzle with oblique exit planes;
- Different types of Laval's nozzles that are used for inducing the spinning moments or inducing the force under the angle toward projectile's axis of symmetry, as well as different types of nozzles for thrust vector control.

Nozzle geometry influence thrust losses and nozzle's heat transfer, as well as defines mass of the nozzle, which is critical for M-REP's overall design. Beside elementary requirements to produce thrust, minimize the losses and withstand enormous heat flux, M-REP's nozzle geometry is directed by additional design criteria such as oblique cut-off of nozzle exit and effective length of divergent part as nozzles intersect with projectile's ogive. To appreciate design of convergent-divergent nozzle with conical scarfed divergent part and profiled convergent part and throat segment, the nozzle configuration-geometry should be described with system of mathematical equations. The calculation method for scarfed nozzle performance is presented in following paragraphs.

Scarfed nozzle geometry model is represented as combination of "basic" Laval's nozzle and nozzle extension (figure 4-5) [88-89]. Due to geometrical constraints of the M-REP's ogive (size and the profile of the ogive surface), as well as manufacturing constraints (drilling techniques for divergent part of the nozzle's geometry situated on ogive part of the projectile), a few different shapes of the nozzle geometry were considered - figure 4-6 [88].

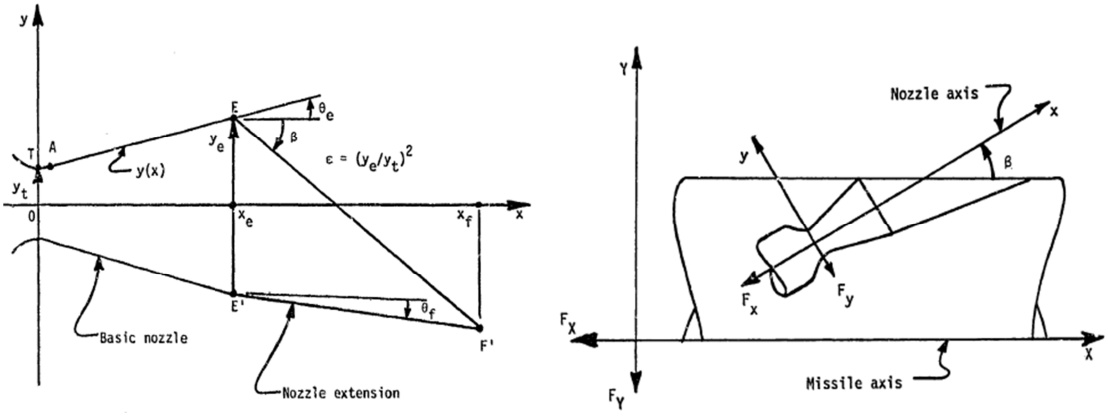

Figure 4-5 Geometry of the Scarfed Nozzle [88]

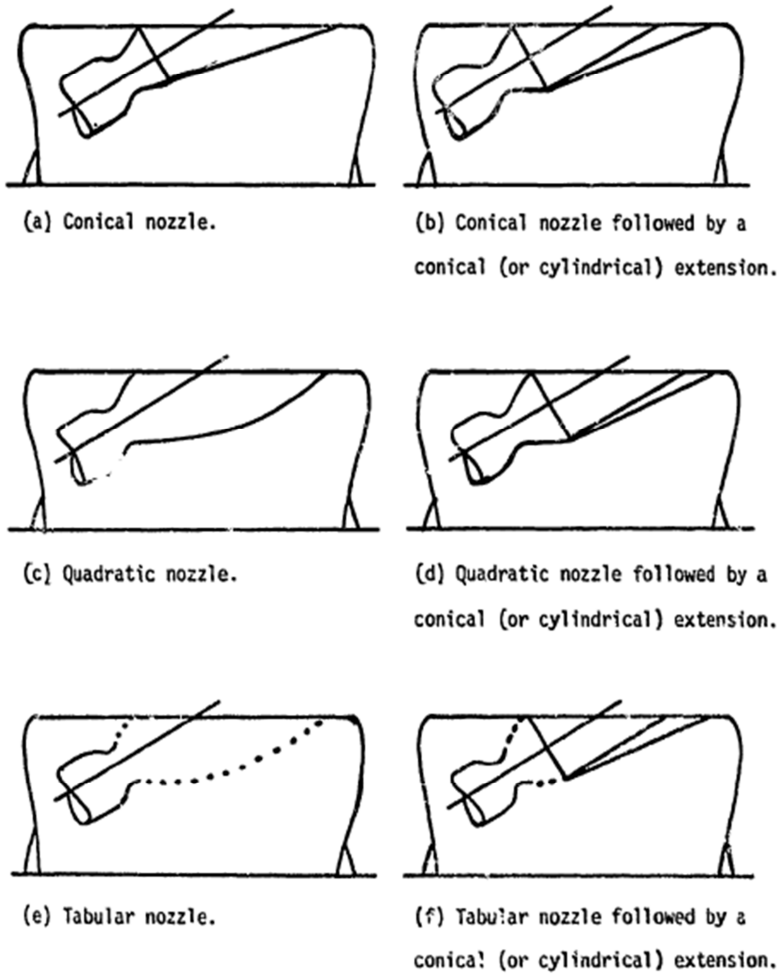

Figure 4-6 Nozzle geometric models considered [88]

Selected nozzle configuration with regards to the thrust losses and optimal manufacturing-drilling method is conical nozzle – figure 4-6 (a). Certainly, chosen model is far from simple looking at manufacturing aspects of the design, but it is optimal considering the aspects of maximising thrust coefficient and imparting projectile's de-spinning, which importance is described in Chapter 5. The "basic" Laval's nozzle geometry is directed with following design parameters and their recommended values, given in Table 4-1 and figure 4-7.

Table 4-1 Geometry of Laval's Nozzle

Geometry parameter	*Recommended values*	*Criterion*
$(D_0/D_t)^2$	2.5-20 1.5-2.5 -immersed	Combustion chamber compatibility
r_{1m}/D_t	0.5-1.0	min. the loses in convergent part
r_{2m}/D_t	0.5-2.0	min. the losses and 2D flow in convergent part
r_{3m}/D_t	0.25-1.0	min. losses
β_c	35-45 (deg)	min. loses, min. mass
α_d	12-15 (deg)	min. loses, min. mass
ε_{exit}	4-20	Expansion factor referenced by the calibre of the projectile
D_t	with reference to the design point (design pressure and flow)	

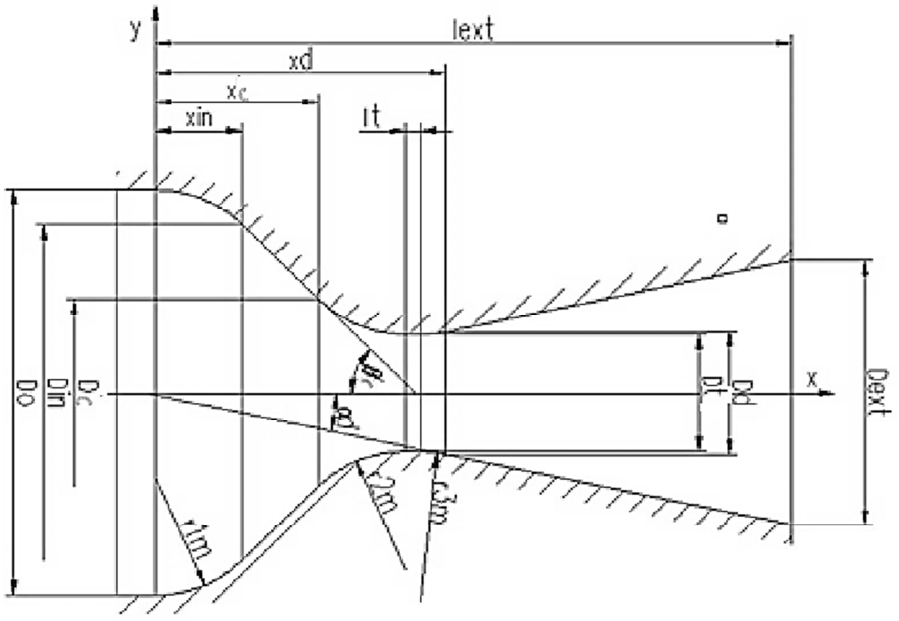

Figure 4-7 Geometry of the "basic" Laval's nozzle

Significant contributors to the nozzle design represent heat transfer and pressure loads induced by combustion of solid rocket propellant and supersonic flow of combustion products. In order to achieve optimal overall geometry of the nozzle, i.e. inner and outer contour of the nozzle, stress analysis (thermal and pressure loads) must be performed and incorporated in nozzle desing.

Geometry of the “basic” nozzle can be described with following system of equations (4-66 to 4-75):

Convergent section of the nozzle – inlet:

$$\begin{aligned} \overline{D}_{in} &= \frac{D_{in}}{D_t} = \overline{D}_o - 2\bar{r}_{1m}\left(1-\sin\beta_k\right) \\ \bar{x}_{in} &= \frac{x_{in}}{D_t} = \bar{r}_{1m}\cos\beta_k \end{aligned} \qquad \textbf{(4-66)}$$

Convergent section:

$$\begin{aligned} \overline{D}_c &= \frac{D_c}{D_t} = 1+2\bar{r}_{2m}\left(1-\sin\beta_c\right) \\ \bar{x}_c &= \frac{x_c}{D_t} = \bar{r}_{1m}\cos\beta_c + \frac{\overline{D}_o-1}{2}tg\beta_c - \left(1-\sin\beta_c\right)\left(\bar{r}_{1m}+\bar{r}_{2m}\right)tg\beta_c \end{aligned} \qquad \textbf{(4-67)}$$

Profiled throat section:

$$\begin{aligned} \overline{D}_d &= \frac{D_d}{D_t} = 1+2\bar{r}_{3m}\left(1-\cos\alpha_d\right) \\ \bar{x}_d &= \frac{x_d}{D_t} = \bar{x}_k + \bar{r}_{2m}\cos\beta_k + \bar{l}_t + \bar{r}_{3m}\sin\alpha_d \end{aligned} \qquad \textbf{(4-68)}$$

Divergent section:

$$\begin{aligned} \overline{D}_{ext} &= \frac{D_{ext}}{D_t} = \sqrt{\varepsilon_{ext}} \\ \bar{x}_{ext} &= \bar{l}_{ext} = \frac{l_{ext}}{D_{cr}} = \frac{\sqrt{\varepsilon_{ext}} - 1 - 2\bar{r}_{3m}\left(1-\cos\alpha_d\right)}{2tg\alpha_d} + \bar{x}_d \end{aligned} \qquad \textbf{(4-69)}$$

Cross section variations or relative diameter variations, along the “basic” nozzle axis of symmetry is specified for each section of the nozzle as follows:

Inlet:

$$0 \le \bar{x} \le \bar{x}_{in}$$
$$\bar{D} = \bar{D}_o - 2\left(\bar{r}_{1m} - \sqrt{\bar{r}_{1m}^2 - \bar{x}^2}\right) \quad \textbf{(4-70)}$$

Convergent section:

$$\bar{x}_{in} \le \bar{x} \le \bar{x}_c$$
$$\bar{D} = \bar{D}_o - 2\bar{r}_{1m}\left(1 - \sin\beta_c\right) - \frac{2\left(\bar{x} - \bar{r}_{1m}\cos\beta_c\right)}{tg\beta_c} \quad \textbf{(4-71)}$$

Throat section:

$$\bar{x}_c \le \bar{x} \le \bar{x}_d + \bar{r}_{2m}\cos\beta_c$$
$$\bar{D} = 1 + 2\left[\bar{r}_{2m} - \sqrt{\bar{r}_{2m}^2 - \left(\bar{r}_{2m}\cos\beta_c - \bar{x} + \bar{x}_c\right)^2}\right] \quad \textbf{(4-72)}$$

$$x_c + \bar{r}_{2m}\cos\beta_c \le \bar{x} \le \bar{x}_k + \bar{r}_{2m}\cos\beta_c + \bar{l}_t$$
$$\bar{D} = 1 \quad \textbf{(4-73)}$$

$$x_c + \bar{r}_{2m}\cos\beta_c + \bar{l}_t \le \bar{x} \le \bar{x}_d$$
$$\bar{D} = 1 + 2\left[\bar{r}_{3m} - \sqrt{\bar{r}_{3m}^2 - \left(\bar{x} - \bar{x}_k - \bar{r}_{2m}\cos\beta_c - \bar{l}_t\right)^2}\right] \quad \textbf{(4-74)}$$

Divergent section:

$$\bar{x}_d \le \bar{x} \le \bar{l}_{ext}$$
$$\bar{D} = \bar{D}_d + 2\left(\bar{x} - \bar{x}_d\right)tg\alpha_d \quad \textbf{(4-75)}$$

The geometry of the nozzle "extension" is defined by the D_{ext}, and attachment point (x_e,y_e) the angle of the conical extension θf , and the length of conical extension x_f. The angle of conical extension for M-REP nozzle design is same as the angle of "basic" nozzle divergent section, that implies Mach line propagation and the oblique shock wave at scarfed surface, which produces thrust deflection angle θ [89] and "side" force and moment in nozzle plane of symmetry. However, as M-REP has 6 symmetrically distributed nozzles around the designated perimeter of the ogive, side forces and moments are annulled, therefore thrust deflection angle results as additional axial thrust loss factor.

4.1.6 Propulsion characteristics of real scarfed nozzle

Real flow processes in the scarfed nozzle can be calculated through correction factor for thrust coefficient (loss coefficient)

$$C_F^* = \varphi_{cf} C_F ; \quad 0.9 \le \varphi_{cf} \le 0.97 \qquad \textbf{(4-76)}$$

The factor φ_{cf} characterise real (non-ideal) process in the nozzle and it is always less than 1.

In a first instance we should calculate the loss coefficient for “basic” nozzle, then we should add the thrust “deflection” due to scarfed nozzle. Several theories take into account number of factors influencing the real nozzle flow, however in most cases the experimental relations are more accurate in predicting the nozzle losses. Those experimental equations correlate nozzle geometry, propellant characteristics and real flow parameters. Empirical equation [90] that yields satisfactory results for solid rocket motor performance calculations, i.e. loss coefficient for “basic” part of scarfed nozzle is given by:

$$\begin{aligned}\varphi_{CF} &= 1.1336 + 0.0122\ln(Dt) - 0.0465\ln(\alpha_d) - 0.230\,Al - \\ &- 0.0048\ln(\varepsilon) + 0.0153\ln(1-S) - 0.00842\ln(ASUB) - \\ &- 0.00548\ln(P) + 0.0033\ln(R_u)\end{aligned} \qquad \textbf{(4-77)}$$

Variables in equation above are:

D_t – throat diameter, [in inch]

$\alpha_d = \dfrac{\bar{\theta} + 2\theta_e}{3}$ represents the value of the angle of divergence of Laval’s nozzle [in degrees], for “bell” shape of divergent nozzle, and for factor $\bar{\theta} = \arctan\left[\dfrac{D_t\left(\varepsilon^{0.5} - 1\right)}{2L_n}\right]$_[deg] , and L_n - divergent section length, [in inch]

θ_e exit angle, [in degree]

Al – the mass fraction of the aluminium in propellant

ε - expansion ratio

S – submergence fraction

ASUB – inlet area ratio

P – pressure, [in psi]

R_u – radius of curvature, non-dimensional - R/R_t

For conical nozzle, expression for loss coefficient is:

$$\varphi_{CF} = 1.0605 + 0.0111\ln\left(\frac{Dt}{25.4}\right) - 0.0328\ln(\alpha_d) - 0.254(Al) - 0.00617\ln(\varepsilon_{ext}) \quad \textbf{(4-78)}$$

where α_d – represents the value of the angle of divergence of Laval's nozzle in degrees for conical nozzles.

Regarding the losses of the scarfed nozzle, with reference to "scarf" angle and initial expansion ration, for particular value of specific heat ratio for combustion products the thrust deflection angle can be found [89].

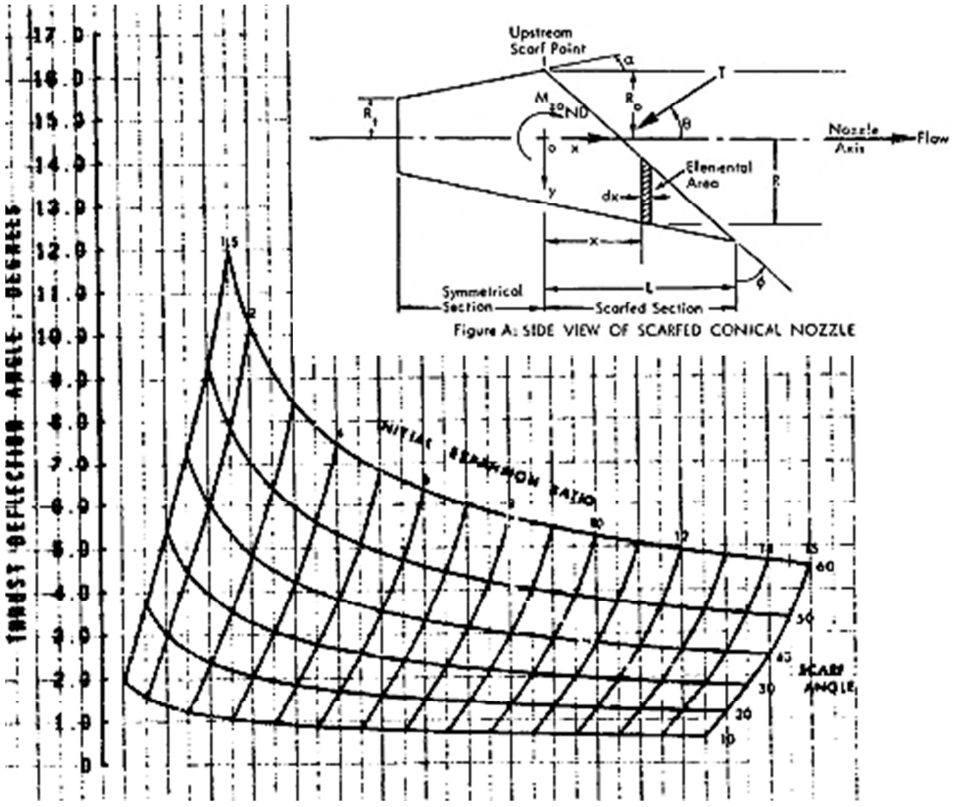

Figure 4-8 **Relations between scarf angle, expansion ration ant thrust deflection angle, for κ= 1.22 [89]**

4.1.7 Interior Ballistics of M-REP's Solid Rocket Motor

Basic technical requirement for any solid rocket motor beside geometrical dimensions mass, centre of gravity, and moments of inertia is total impulse - I_{tot} of SRM. In addition, some specific solid rocket motor design may require thrust vectoring or different thrust levels during active phase of rocket flight (booster and sustainer thrust levels).

Total impulse of solid rocket motor represents thrust-time integral during "active" time of solid rocket motor:

$$I_{tot} = \int_0^{\tau} F(t) \cdot dt \qquad \textbf{(4-79)}$$

Solid rocket motor thrust is given by:

$$F(t) = \dot{m}(t)\, v_{ext}(t) + \left(p_{ext}(t) - p_a(t,h)\right) A_{ext} \qquad \textbf{(4-80)}$$

Median rocket thrust for the active phase of solid rocket motor is calculated using following equation:

$$F = C_F \cdot P_0 \cdot A_t \qquad \textbf{(4-81)}$$

Mass flow rate for the specific propellant and solid rocket motor configuration can be written as:

$$\dot{m} = \frac{P_0 \cdot A_t}{C^*} \qquad \textbf{(4-82)}$$

Replacing the eq. 4-82 into 4-81, the thrust is written as:

$$F = C_F \cdot C^* \cdot \dot{m} \qquad \textbf{(4-83)}$$

The characteristic velocity C^* is property of solid rocket propellant type and the C_F is defined by the nozzle geometry, thus for known type of propellant and know nozzle configuration, in order to achive the required thrust levels we must obtain appropriate mass flow rate by designing solid propellant burning surface..

For homogenous propellant, combustion develops at each "singular" burning point at the burning surface, and combustion progress in all directions

from burning singularities, as shown in fig. 4-9. By intersecting combustion singularities at burning surface, the burning layer is produced, with tendency to burn in parallel stratums relative to initial burning area, as represented on fig. 4-10. Initial burning area is determined according to design criteria for solid rocket motor, therefore some of the burning surfaces can disappear (burn-out), but some burning surfaces can appear, as it is represented on fig. 4-11.

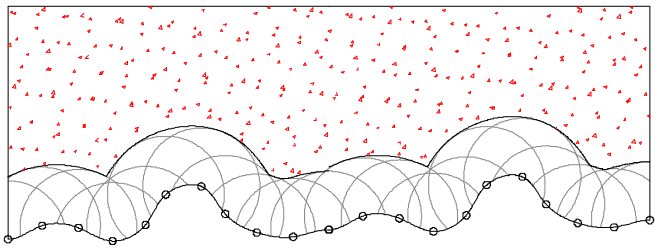

Figure 4-9 Burning singularities

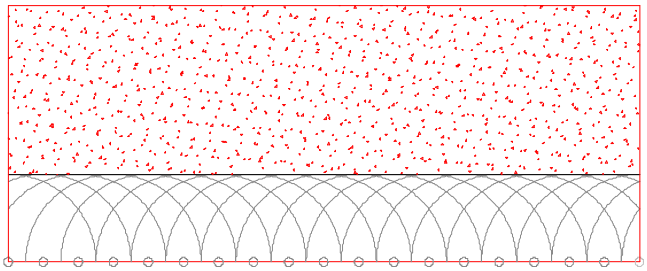

Figure 4-10 Burning layer

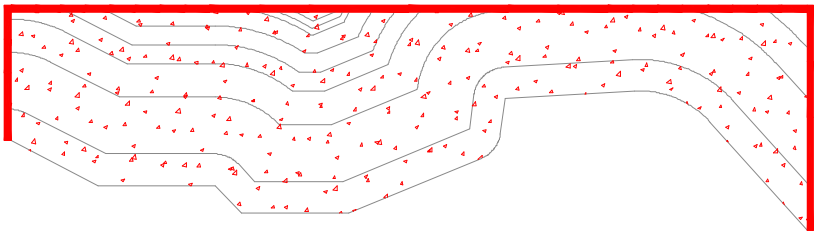

Figure 4-11 Development of burning area.

Mass flow generated at homogenous propellant burning surface can be calculated knowing the area of the burning surface A_{burn}, burning rate r at different burning pressures, and density ρ_{sp} of the solid rocket propellant.

By dividing propellant grain into smaller, finite elements (figure 4-12) , we can make assumption that those finite elements has own burning conditions. The “Finite Element” approach is important with propellant grains that have high aspect ratio L/D (diameter vs. length), i.e. the burning conditions along the central-port channel significantly vary along the grain’s longitudinal axis. However, as the propellant grain is shortened, particularly for propellant grains with end burning (burning “forehead”), the burning conditions can be assumed uniform in each burning point. Knowing propellant characteristics, and according to eq. 4-31 (mass conservation law), we can find pressure distribution in solid rocket motor that produces required SRM thrust.`

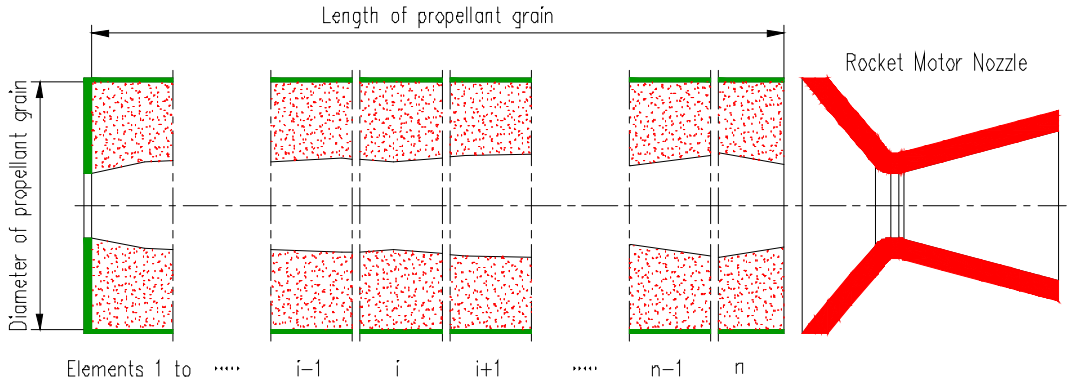

Figure 4-12 Approximation with one-dimensional “flow” finite elements

Based on previous premise, mass flow rate for each finite element can be given as:

$$\dot{m}^{i} = \rho_{SP}^{i} \cdot r^{i} \cdot A_{burn}^{i} \qquad \textbf{(4-84)}$$

and total mass flow generated at burning area:

$$\dot{m} = \sum_{i=0}^{n} \rho_{SP}^{i} \cdot r^{i} \cdot A_{burn}^{i} \qquad \textbf{(4-85)}$$

where ρ_{SP}^{i} - *solid* propellant density in “i” segment, A_{burn}^{i} - burning area (sum of burning surfaces in “i” segment), r^{i} – burning rate in “i” segment.

According to the conservation law, mass flow through nozzle must be equal to the mass flow generated at burning surface-area, under hypothesis

that free volume of combustion chamber and generated combustion pressure are changing under finite, “quasi-stationary” conditions.

$$\sum_{i=0}^{n} \rho_{SP}^{i} \cdot r^{i} \cdot A_{burn}^{i} = \frac{p_0 \cdot A_t}{C^*} \quad \textbf{(4-86)}$$

For homogenous propellant, density is constant:

$$\rho_{SP} \cdot \sum_{i=0}^{n} r^{i} \cdot A_{burn}^{i} = \frac{p_0 \cdot A_t}{C^*} \quad \textbf{(4-87)}$$

Under assumption that combustion pressure at each burning point of the burning surface/area is equal, meaning uniform burning rate over entire burning area, therefore eq. 4-87 becomes:

$$\rho_{SP} \cdot r \cdot A_{burn} = \frac{p_0 \cdot A_t}{C^*} \quad \textbf{(4-88)}$$

The burning rate can be written as exponential law function:

$$r = b \cdot p^{n} \quad \textbf{(4-89)}$$

where: p – combustion pressure (in general),

b – linear coefficient in burning rate law

Burning rate law also can be written as:

$$r = a + b \cdot p^{n} \quad \textbf{(4-90)}$$

Constant “a” in the burning rate law (eq. 4-90) represents burning rate in “vacuum”, and it is widely neglected (a=0), except for subsonic, low pressure burning conditions such as base bleed burning described in Chapter 3.

Finally, equation for steady-state burning of solid rocket propellant that defines the pressure inside the combustion chamber is given as:

$$P_o = \left(\rho_{SP} \cdot b \cdot C^* \cdot \frac{A_{burn}}{A_t} \right)^{\left(\frac{1}{1-n}\right)} \quad \textbf{(4-91)}$$

Burning rate, can “shift” due to variation of environmental or storage temperature (initial temperature of the propellant grain). Temperature sensitivity of propellant burning rate σ_p can be defined as follows:

$$\sigma_p = \frac{1}{r} \cdot \left(\frac{\partial r}{\partial T} \right)_{p=const} \quad \textbf{(4-92)}$$

Solving previous equation, for known burning rate at “referent” storage temperature, burning rate at current temperature is given as:

$$r = r_0 \cdot e^{\sigma_p \cdot (T_P - T_{P0})} \quad \textbf{(4-93)}$$

where:

r - burning rate at “current” environment/storage temperature – T_P

r_0 - burning rate for “reference” storage temperature - T_{P0}

Using eq. 4-93, we can find propellant coefficient of temperature sensitivity as:

$$\sigma_p = \frac{\ln(r) - \ln(r_0)}{T_P - T_{P0}} \quad \textbf{(4-94)}$$

The “standard” , referent, temperature for solid rocket propellant interior ballistics tests is $T_{P0} = 15^0$C (288.15 K) , but “current” ambient temperatures can vary from -43^{0}C to +60^{0}C according to ammunition qualification standard [91]. After finding the burning rate law at several different temperatures, median value of temperature sensitivity coefficient can be calculated, for given temperature range and pressures (“median value” due to fact that σ_p can vary both with pressure and temperature). If exponential coefficient in burning rate law “*n*” does not deviate with temperature (usual case), then σ_p is pressure “independent” and it can be written as :

$$\sigma_p = \frac{\ln(b) - \ln(b_0)}{T_P - T_{P0}} \quad \textbf{(4-95)}$$

Therefore the burning rate law of solid rocket propellant is defined as:

$$r = b_0 \cdot p^n \cdot e^{\sigma_p \cdot (T_P - T_{P0})} \quad \textbf{(4-96)}$$

Accordingly, M-REP's SRM interior ballistics calculation algorithm (general structure of computer code) is as follows:

Input data required for the calculation:

Propellant characteristics:

- Temperature of combustion T_0
- Propellant Density ρ_{sp}
- Molecular weight of combustion products M
- Specific heat ratio κ
- Linear coefficient in burning rate law b_0
- Exponent coefficient in burning rate law n
- Temperature sensibility σ_p
- Referent "storage" propellant temperature T_{P0}
- Current "storage" propellant temperature T_{P0}
- Mass fraction of Aluminium m_{Al} or ("*Al*")

Motor characteristics:

- Number of nozzles NN
- Diameter of throat D_t
- Nozzle expansion ratio ε_{ext}
- Angle of nozzle divergence α_d
- Scarf angle Φ
- Nozzle(s) inclination angle β
- Burning surface vs. burnt web ("e") function $A_{burn}=f(e)$

Algorithm:

Characteristic velocity:

$$\Gamma(\kappa)=\sqrt{\kappa}\left(\frac{2}{\kappa+1}\right)^{\frac{\kappa+1}{2(\kappa-1)}} \longrightarrow \quad C^{*}=\frac{\sqrt{RT_0}}{\Gamma(\kappa)}$$

system of eq. (4-97)

↓

Combustion pressure calculation:

$$p_o(e)=\left(\rho_{SP}\cdot b\cdot C^{*}\cdot\frac{A_{burn}(e)}{A_t}\right)^{\left(\frac{1}{1-n}\right)}$$

↓

Calculation of propellant burning rate:

$$r\,(e)=b_0\cdot p_0(e)^{n}\cdot e^{\sigma_p\cdot\left(T_p-T^{*}_0\right)}$$

↓

Calculation of time between two burnt web points:

$$\Delta t_i(e_i)=\frac{e_i-e_{i-1}}{[(r(e_i)+r(e_{i-1}))/2]}$$

↓

Burning time:

$$t\;(e_i)=t(e_{i-1})+\Delta t(e_i)$$

↓

Exit pressure ratio $\frac{p_{ext}}{p_0}$ is function of ε_{ext} :

$$\varepsilon_{ext}=\left(\frac{2}{\kappa+1}\right)^{\frac{\kappa+1}{2(\kappa-1)}}\frac{1}{M_{ext}}\left(1+\frac{\kappa-1}{2}M_{ext}^{2}\right)^{\frac{\kappa+1}{2(\kappa-1)}}$$

$$\frac{p_{ext}}{p_0}=\left(1+\frac{\kappa-1}{2}M_{ext}{}^{2}\right)^{-\frac{\kappa}{\kappa-1}}$$

↓

system of eq. (4-98) cont.

Thrust coefficient - ideal:

$$C_F = \sqrt{\kappa}\left(\frac{2}{\kappa+1}\right)^{\frac{\kappa+1}{2(\kappa-1)}}\sqrt{\frac{2\kappa}{\kappa-1}\left[1-\left(\frac{p_{ext}}{p_0}\right)^{\frac{\kappa-1}{\kappa}}\right]}+\frac{\sqrt{\left(\frac{\kappa-1}{2}\right)\left(\frac{2}{\kappa+1}\right)^{\frac{\kappa+1}{\kappa-1}}}}{\left(\frac{p_{ext}}{p_0}\right)^{\frac{1}{\kappa}}\sqrt{1-\left(\frac{p_{ext}}{p_0}\right)^{\frac{\kappa-1}{\kappa}}}}\left(\frac{p_{ext}}{p_0}-\frac{p_a}{p_0}\right)$$

↓

Correction factor (real nozzle) for thrust coefficient, for "basic" nozzle configuration:

$$\varphi_{CF_B} = 1.0605 + 0.0111\ln\left(\frac{D_t}{25.4}\right) - 0.0328\ln(\alpha_d) - 0.254(Al) - 0.00617\ln(\varepsilon)$$

Correction factor for thrust coefficient, including "scarfed" nozzle configuration and nozzle inclination:

$$\varphi_{CF} = \varphi_{CF_B} \cdot \varphi_{CF_{SCARFED}}(\Phi, \beta)$$

↓

Thrust coefficient (real nozzle):

$$C_F^* = \varphi_{CF} \cdot C_F$$

↓

Thrust:

$$F(e) = C_F^* \cdot p_0(e) \cdot A_t$$

↓

Total impulse:

$$I_{tot} = \int_0^t F(e) \cdot dt$$

4.2 Propellant grain with embedded metal wires – "M-REP" application

The SRM for Modular Range Enhanced Projectile is designed according to technical requirements to deliver projectile beyond 40km when it is "fired" from 39 calibres howitzer, or 50km when fired from 52 calibres howitzer. Required value of total impulse for M-REP's solid rocket motor should be higher than 6000Ns (thrust required for firings at sea level altitude), deployed at optimal

time interval on the designed trajectory for “targeted” max. range. The amount of required total impulse were calculated using the exterior ballistics model described in Chapter Five. Furthermore, SRM’s propellant grain must withstand severe launching conditions in the gun-barrel (high axial acceleration and high spin rate), to have shortest possible working time and to minimise thrust misalignment to prevent disturbances on the trajectory. In addition SRM should occupy as small as possible projectile’s free volume, thus minimising the impact of reduced payload volume on projectile’s lethality.

The M-REP conceptual design indicated that SRM should be composed of combustion chamber, nozzle section with igniter and propellant grain. Two concepts were envisaged:

- Concept No.1 - rear location of SRM, and
- Concept No.2 front – “tractor” configuration of SRM

In concept No. 1 SRM combustion chamber also supports rotating (driving) band, as well as connection thread for BB casing. Concept No. 1 occupies more important part of projectile from aspect of lethality, as explained in Chapter Eight. Therefore, the concept No. 2 has been chosen as optimal deployment of M-REP design (figure 4-13).

Chosen material for combustion chamber is high-strength steel (e.g. AISI 4340) that can withstand high loads imparted by acceleration in the barrel and internal pressures during the combustion of the SRM, with minimal thickness of the chamber wall. Titanium alloys were not considered in order to keep manufacturing cost low, opposite to other contemporary designs of extended range projectiles [4, 9], where unit cost of the projectile is high . Nozzle section comprises high-strength steel body with nozzle inserts made from high-temperature resistant material (refractory metal Mo and its alloys Moly TZM [92]). Design calculations indicated that for shortest possible active time of rocket motor, and projectile volume that SRM would occupy, high pressure SRM (>150 bar) has to be designed. Therefore, within couple of design iterations, solution with six nozzles having nominal 4mm critical diameter and

9mm exit area diameter (for ”basic” nozzle desing) has been selected. The nozzles are angled at 30 degrees to the projectile axis, in order to shorten the length of the nozzles, but also to decrease thrust losses due to nozzle inclination. Possible thrust misalignment, which could induce high angles of attack and projectile instability, has been minimised or avoided, by dividing potential thrust eccentricity - misalignment into six fractions, in comparison to configurations with only one nozzle. Furthermore, nozzle “cant” angle (angle perpendicular to the projectile’s axis of symmetry) is introduced to impart opposing spin (de-spinning – described in Chapter Five.) that will “actively” improve projectile’s stability and dispersion at descend part of the trajectory..

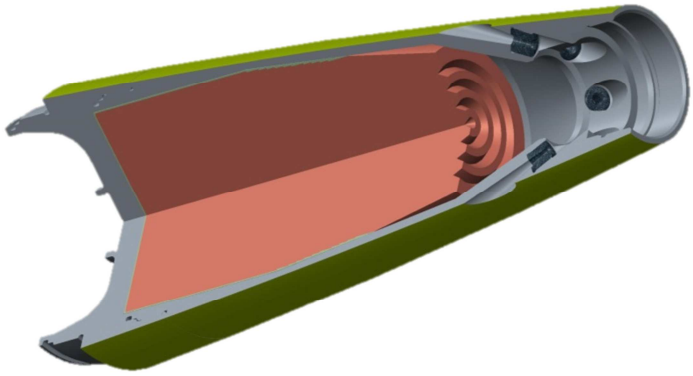

Figure 4-13 SRM for M-REP

The SRM propellant shape is optimised against launching (firing) conditions. High acceleration in gun barrel acts upon propellant, and it tends to “squeeze” the propellant under own weight. The conceptual design of propellant grain shape started with following hypothesis: if we manage to confine a propellant grain in a way that dilatations (deformations) ε (eq. 4-99) under active loads are small, i.e. loads acting upon propellant grain do not induce stress (eq. 4-100 and 4-101) or induce stress that is below “yield” margin for given propellant mechanical characteristics, we are on the right path to design propellant shape that will withstand enormous acceleration loads (eq. 4-102) . Therefore, monolithic propellant grain, which takes up “entire” volume of proposed combustion chamber, is designed. Such grain should withstand axial acceleration loads and high spin load, by restricting grain displacements as

propellant grain should fit into chamber with minimum gap required only for assembling.. The stress analysis is presented in Sixth Chapter.

$$\varepsilon = \frac{\Delta l}{l}$$ - relative deformation **(4-99)**

$$\sigma = \frac{F}{A}$$ - generalised stress equation **(4-100)**

$\sigma = E \cdot \varepsilon$ - induced stress **(4-101)**

(Young's module as paradigm)

$$\lim_{\varepsilon \to 0} \sigma(\varepsilon) \approx 0$$ **(4-102)**

The propellant grain has "cylindrical" from with front-end shaped in cone with engraved forehead. Rear-end of propellant grain is flat to mate with appropriate wall on combustion chamber closure, which also represents the payload's closure. Rear-end and outer diameter of propellant grain are inhibited, allowing only grain's forehead and front cone to burn. Propellant grain has high volumetric loading factor (i.e. $\varepsilon_V \approx 1$), it occupies almost entire free volume of the combustion chamber. Grain itself do not possess internal orifices (central-port), usually required for development of burning surface and desired pressure/thrust profile. Instead of "standard" propellant grain shapes (orifices - trumpet, slots, star, wagon wheel, finocyl shape configuration [86]), for burning surface evolvement, M-REP's required thrust profile is achieved by using "heat conductors" - wires embedded in propellant grain [72-74] Heat conductors "augment" propellant burning rate along the wires, which result in high thrust and reduced total active time of the SRM.

Ignition delay of SRM is based on electro/mechanical/pyrotechnic chain initiated in gun barrel during the launch (mechanical fuze "arming" function). Ignition delay ignites SRM between 17 sec. and 32 sec depending on required projectile flight profile (trajectory). Time delay can be optimised for max. range at optimal elevation, and for given altitude of firing position. For other trajectory

profiles time delay can be adjusted, as the ignition delay “mechanism” is in the projectile nose and it can be easily set in the same manner as the electro/mechanical “time-fuze” is set for illuminating projectiles[100].

4.2.1 Interior ballistics of the M-REP propellant grain with embedded metal wires

4.2.1.1 Combustion process of propellant with embedded metal wires

Solid rocket propellant grains have two basic configurations. First and most common configuration is central-port burning grain, with majority of combustion products generated at evolving central port cross section such as cylinder/trumpet, slot, star shape, or wagon wheel profile. Second type of grain shape configuration is end burning propellant grain that develops (evolve) its burning surface from one end of propellant grain (forehead), perpendicular to the main axis of symmetry. The main difference between those two configurations is combustion (burning) time. For end-burning propellant grain burning time is much longer comparing to the central-port burning grains with same (similar) L/D – aspect ratio and burning rate. However, the mass fraction ratio or volumetric loading factor is much higher with end-burning grains comparing to the central-port grains (more propellant can be packed in the same volume). Therefore SRM designers sometimes find as issue, “long” active time of end-burning grain and “low” thrust levels. The common solution is to increase burning rate using high energetic propellant in order to decrease active time and increase thrust level. However, this approach has, as a consequence, high pressure and thermal loads, which sometimes cannot be solved with standard engineering materials that are used in rocket motor design. Apart from using high energetic propellant, there is another, more exotic solution: inserting metal wires that allow increase in burning rate along the wires embedded in the propellant, practically enabling creation of new burning surfaces. Thereby, overall burning surface increases, thrust level increases, but burning time decreases and still a propellant with lower energetic properties can be used.

Pioneering work in investigation of the metal wires enhanced burning of solid rocket propellant is done in 1950s and 1960s, and it is discovered that the metal wires with high thermal diffusivity have positive influence in burning rate augmentation along the wire [93, 94].

The theoretical background for the propellant burning rate has been discussed by many researchers, to establish the correlation between the nominal burning rate and “augmented” burning rate along the heat conductors [15,73, 74, 93-96]. The mechanism of increasing burning rate along the wire is essentially the passage of heat, i.e. thermal diffusion in propellant around the wire. As heat propagates through wire faster than through propellant, then volume of the propellant, influenced by heat flux conducted by the wire, takes conical shape. This zone is represented on figure 4-14.

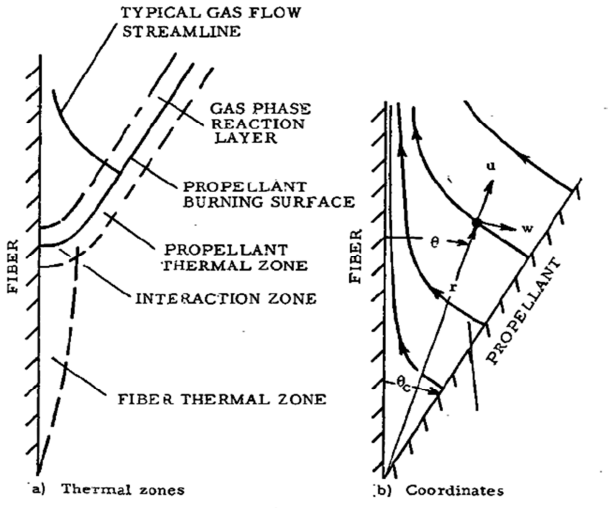

Figure 4-14 Combustion model geometry [94]

Although theoretical models has been devised [15, 73, 74, 93-96] and some of them yield matching results with particular trials (figures 4-15 and 4-16), eventually, actual burning rate augmentation factor must be determined experimentally, i.e. for each combination of propellant and heat conductor type, the experimental relation have to be found to establish accurate combustion model.

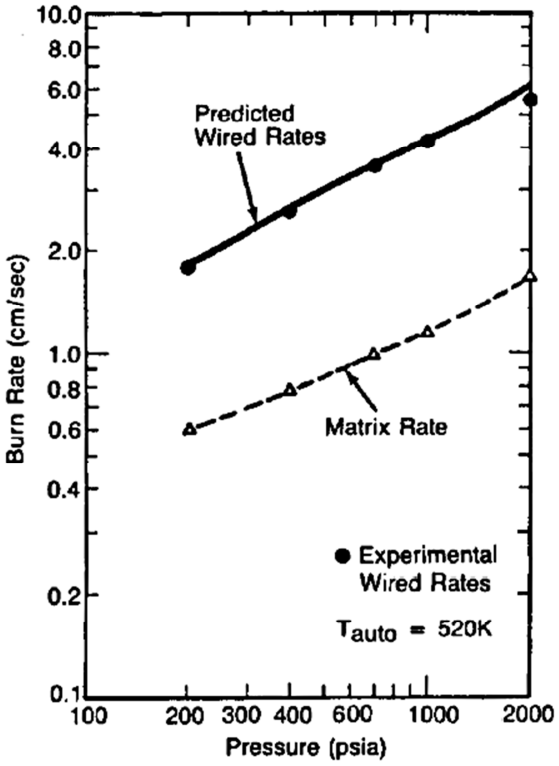

Figure 4-15 Combustion model data comparison – composite Plastisol-AP propellant with W-wires [73]

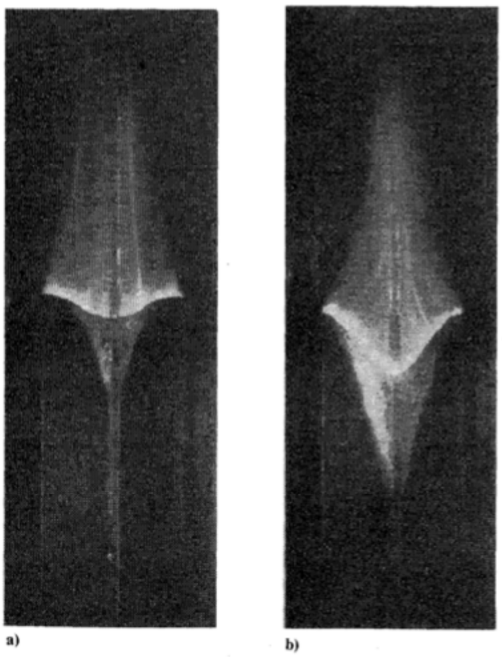

Figure 4-16 IR image of propellant with embedded wire, left - ignition sequence, right – development of burning cone [74]

The burning rate enhancement along the metal wire can be represented with following system of equations (fig. 4-17.):

$$\sin\chi = \frac{e_1}{w_1} = \frac{e_2}{w_2} = \frac{e_m}{w_2 - w_1} \quad \textbf{(4-103)}$$

$$e_1 = r_0 \cdot t_1 \rightarrow e_2 = r_0 \cdot t_2 \rightarrow e_m = r_0 \cdot (t_2 - t_1) \quad \textbf{(4-104)}$$

$$w_1 = r_w \cdot t_1 \rightarrow w_2 = r_w \cdot t_2 \rightarrow \frac{e_1}{w_1} = \frac{e_2}{w_2} = \frac{r_0}{r_w} \quad \textbf{(4-105)}$$

where:

- χ - half angle of the burning cone, e_1, w_1, and e_2, w_2, (e_m), burnt web and burnt web along the wire for time intervals t_1 and t_2, respectively
- r_0 - burning rate of the propellant (basic burning rate)
- r_w - burning rate of propellant along wire

$\sin\chi = \frac{r_0}{r_w}$ - angle of augmentation ratio **(4-106)**

The enhancement factor E_w of the burning rate along a metal wire is given as:

$$E_w = \frac{r_w}{r_0} = \frac{1}{\sin\chi} = const. \quad \textbf{(4-107)}$$

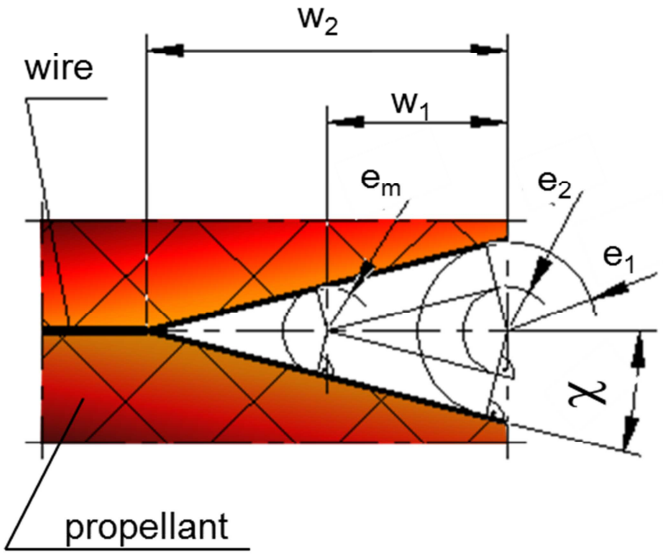

Figure 4-17 Development (evolution) of the burning surface for propellant with embedded metal wires

Augmentation (enhancement) factor is function of metal wire material (metal thermal diffusivity/conductivity), diameter of the wire, type of the propellant, self-ignition temperature of the propellant, and for the composite type of solid rocket propellant, function of oxidiser particle size [73-74]. The relation between enhancement factor and "basic" propellant burning rate can be obtained by experiment, with data acquisition apparatus for measuring interior ballistic properties of rocket propellant, so called BATES (**Ba**llistic **Tes**ts Motor for propellant burn rate experimental investigation [38, 97]). For that purpose, propellant grain is experimental, thick cylinder with outer diameter D_p and only one forehead inhibited. The other forehead is free of inhibitor to develop burning surface, and to induce combustion along the wire. Burning area for single centrally positioned metal wire (fig. 4-17), is written as:

$$A_{burn}(e) = \frac{D_p^2}{4}\cdot\pi + (E_W - 1)\cdot e^2 \cdot \left(\tan(\frac{\pi}{4} - \frac{\chi}{2})\right)^2 \quad e < 0.5\cdot D_P \cdot \left(\tan(\frac{\pi}{4} - \frac{\chi}{2})\right)^{-1} \qquad \textbf{(4-108)}$$

$A_{burn}(e) = E_w \cdot \frac{D_p^2}{4}\cdot\pi = const.$ - otherwise,

Therefore, to reach equilibrium burning surface instantaneously, the number of embedded metal wires must be increased. The heat conductors should be uniformly distributed across the burning forehead (fig 4-18). The optimal number of wires is function of basic burning rate, diameter of the propellant grain, enhancement factor, propellant ignition sensitivity, free volume-characteristic length of the rocket motor (free volume inside SRM versus throat area A_t). Fully evolved burning area with optimal number of embedded wires is equal to:

$$0 \le e \le web_{\max} \quad \rightarrow A_{burn}(e) = E_w \cdot \frac{D_p^2}{4}\cdot\pi \qquad \textbf{(4-109)}$$

as burning cones intersect with each other.as shown in figure 4-19. At the start of combustion process i.e. for burnt web e=0 , volumetric loading factor of the propellant grain is $\varepsilon_v(0) = 1$.

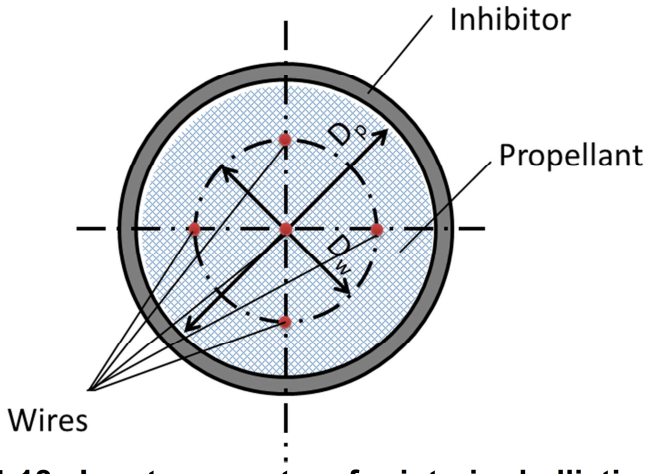

Figure 4-18 Input parameters for interior ballistic analysis

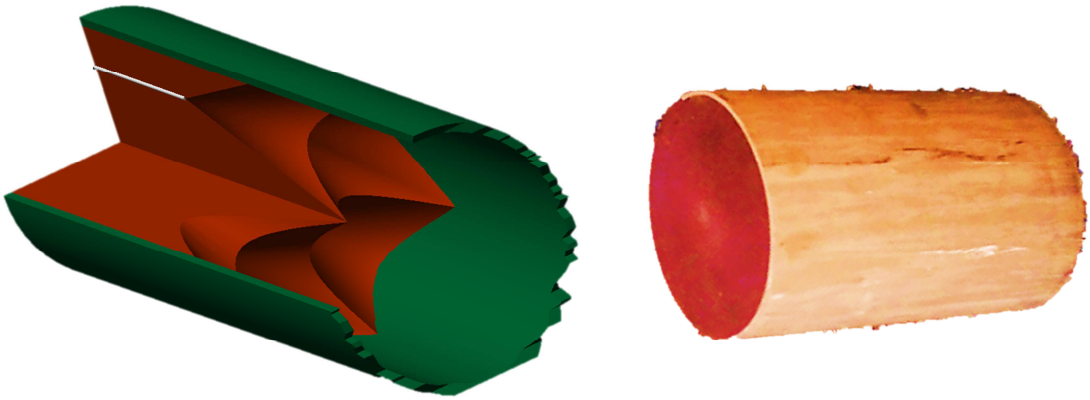

Figure 4-19 Right: Fully evolved burning surface for small diameter propellant grain with embedded wires (CAD model), Left: end-burning propellant grain with embedded wires

Specifically, for M-REP SRM propellant grain desing, in order to shorten time required to achieve fully developed burning area, 49 metal wires were inserted into the propellant grain.

Furthermore, new propellant formulation has been considered for M-REP SRM. Afresh, novel thermoplastic “poly-plastisol” propellant based on ammonium-perchlorate as oxidiser, has been devised. The content of the ammonium perchlorate in the propellant is about 75%, to achieve good ratio between energetic and mechanical properties. A small amount of aluminium powder up to 1%, has been introduced to improve heat conduction into the propellant, and in conjunction with embedded wires.

To validate the new formulation of propellant both experimental and and mathematical methods for propellant characterization were conducted. The propellant SRM is based on the same binder system as base bleed propellant, i.e. thermoplastic/elastomeric “Poly-Plastisol”, composite propellant developed with vinyl resin, vinyl copolymers, solid and liquid inert plasticizers, again with or without addition of energetic plasticiser (Low Molecular Weight GAP). The performance of the chosen propellant/binder system has been theoretically evaluated using modified Computer Program for Calculation of Complex Chemical Equilibrium Compositions and Applications – CEA and ICT Code [76, 99]. Energetic properties of different types of propellant can be compared using product of propellant density and specific impulse ($\rho \cdot I_{sp}$ Ns/m^3), so called volume specific impulse. Figure 4-20 represents comparison between theoretical volume specific impulse of HTPB/AP propellant, and thermoplastic/elastomeric/AP propellant with or without energetic plasticiser – GAP – supplement..

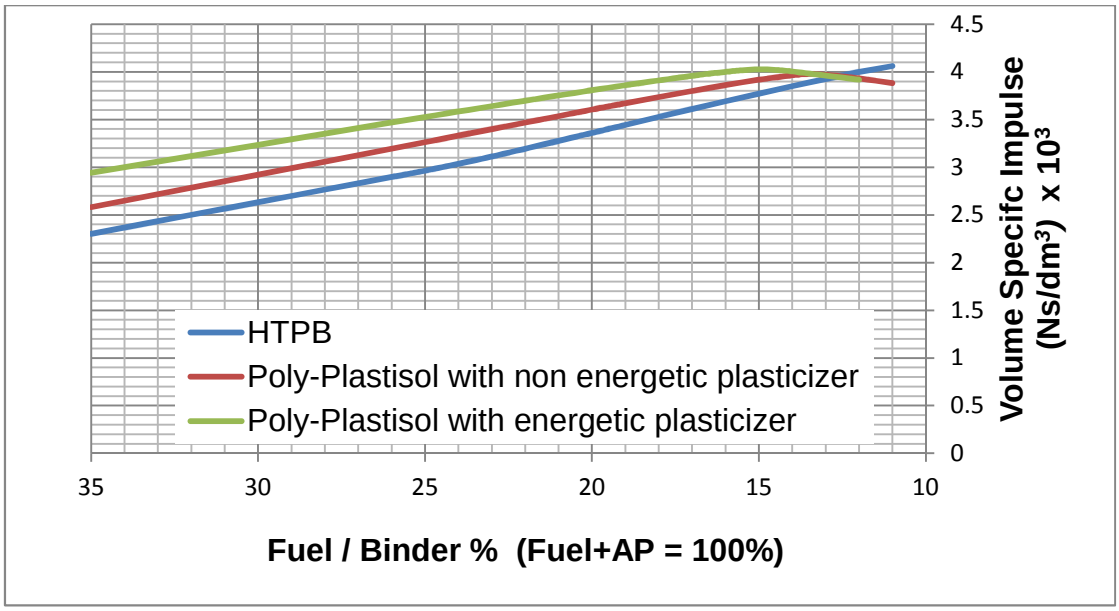

Figure 4-20: Volume Specific Impulse comparison between “Poly-Plastisol”/AP an HTBP/AP propellants (ref. combustion pressure 7 MPa)

Variable is ammonium perchlorate content in the propellant formulation. The comparison has been calculated for the nominal 70 bar pressure inside combustion chamber and expansion of the combustion gases to 1 bar

(atmospheric pressure). Results of the theoretical calculations indicate that the thermoplastic/elastomeric propellants without energetic plasticiser have better volume specific impulse in comparison to HTPB/AP propellant with same amount of binder. The thermoplastic/elastomeric propellants with energetic plasticiser (GAP) have even better volume specific impulse. The volume specific impulse of thermoplastic/elastomeric differs to the HTPB/AP propellant in range from 3% to 9% (they have higher values of VI_{sp} comparing to the HTPB propellant with same amount of binder). For all propellant formulations, higher percentage than 1% of aluminium powder, as energetic additive, is not considered, due to small diameter of the nozzle throat, as condensed phase solid particles Al_2O_3 would clog the throat. Likewise, combustion products has been compared for different ratios of binder with GAP and AP as oxidiser and results are presented on figure 4-21. Each column set represents specific combustion product for given amount of AP (no Al particles). The binder/GAP mixture is same in all propellant formulations: AP% content 50% in formula No. (151/1), AP60% in formula No. (151/4) , AP65% in formula No. (151/7), AP70% in formula No. (151/10), AP74% in formula No. (151/13), AP75% in formula No. (151/16), AP80% in formula No. (151/19), AP83% formula in No. (151/22) and AP 85% in formula No. (151/25).

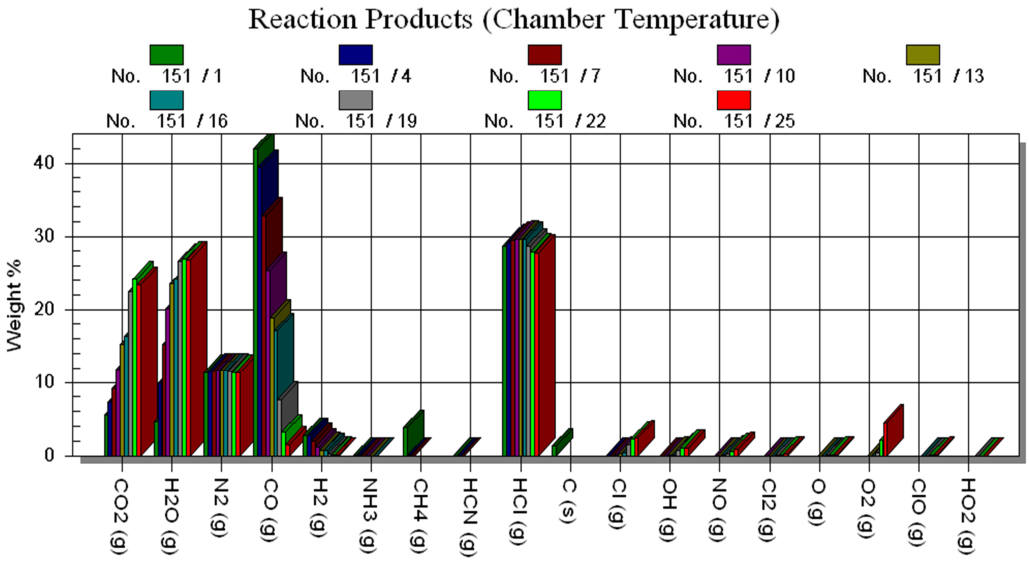

Figure 4-21: Combustion product in relation with AP% content for Poly-Plastisol propellant with GAP [99]

Furthermore, combustion products has been compared for different ratios of non-energetic binder and AP and results are presented on figure 4-22. Each column set is for specific combustion product and amount of AP (no Al particles). The binder mixture is same in all propellant composition. AP% content 50% (111/1), AP 60%(111/4), AP 65%(111/7), AP 70%(111/10), AP 74%(111/13), AP 75% (111/16), AP 80%(111/19), AP 83%(111/22) and AP 85%(111/25).

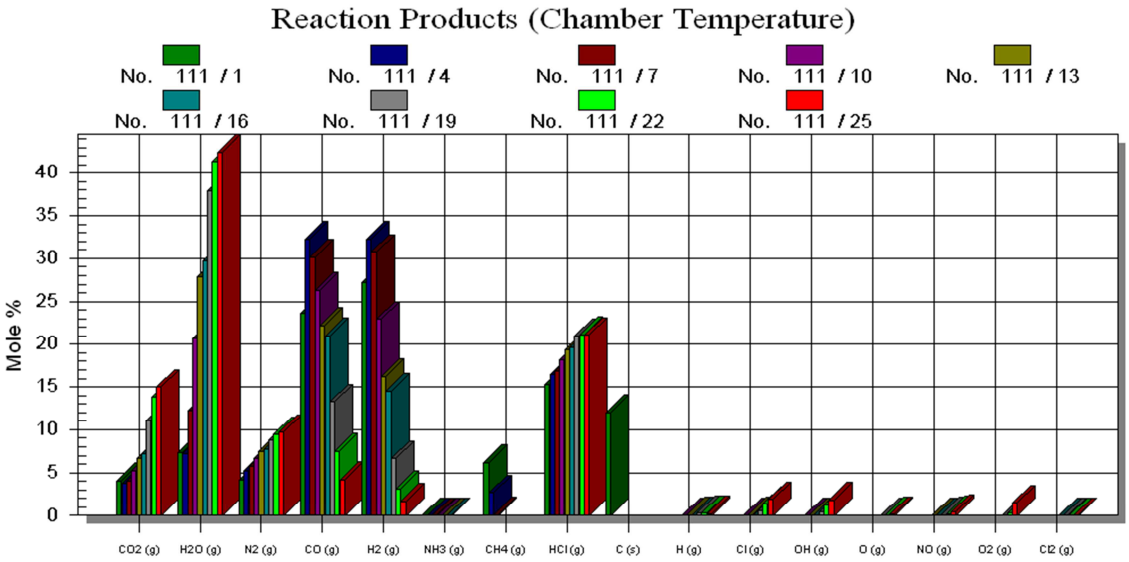

Figure 4-22: Combustion product in relation with AP% content for PolyPlastisol propellant without GAP [99]

Optimal propellant composition considered for solid rocket motor has ammonium perchlorate (AP) as oxidiser in amount of 825 phr, relative to the PVC content in binder (PVC = 100 phr) as reference compound, It is same both for binder with energetic, and for binder without energetic plasticiser. Optimal compound of novel solid rocket motor propellant with GAP energetic plasticiser contains 74% of AP, and its equivalent formula is $C_{1.55}H_{5.18}O_{2.61}Cl_{0.68}N_{0.74.}$ Weight ratios of the elements in a compound are:

- C 18.60 %
- H 5.22 %
- O 41.79 %
- Cl 23.99 %
- N 10.40 %

The equivalent formula of the basic compound of novel thermoplastic/elastomeric composite propellant for M-REP's solid rocket motor with 74% of AP but without GAP, is $C_{2.31}H_{5.99}O_{2.39}Cl_{0.58}N_{0.51}$, and weight ratios of the elements in formulation are:

- C 27.78%
- H 6.05 %
- O 38.40 %
- Cl 20.70 %
- N 7.07 %

The theoretical rocket performance of the propellant with energetic plasticiser (GAP) has been calculated for pressures in working domain of designed SRM (150 bars). The results are presented in table 4-2:

Table 4-2 THEORETICAL ROCKET PERFORMANCE OF THERMOPLASTIC POLY PLASTISOL PROPELLANT WITH ENERGETIC PLASTICISER (GAP), ASSUMING FROZEN COMPOSITION DURING EXPANSION

MIXTURE THEORETICAL DENSITY 1698.9 kg/m3

	CHAMBER	THROAT	EXIT	EXIT
P_0/P	1	1.791	150	34.85
P, bar	150	83.751	1	4.3042
T, K	2488.7	2232.5	900.3	1238.9
ρ, kg/m3	18.5387	11.5387	0.3416	1.0686
H, KJ/kg	-2723.65	-3170.55	-5312.29	-4808.02
U, KJ/kg	-3532.76	-3896.37	-5605	-5210.82
G, KJ/kg	-25849.1	-23915.5	-13678.2	-16320.5
S, KJ/kgK	9.2922	9.2922	9.2922	9.2922
M, MOL WT	25.574	25.574	25.574	25.574
MOL WT (GAS)	25.301	25.301	25.301	25.301
C_P, kJ/kgK	1.7581	1.7298	1.4341	1.5406
κ (S)	1.2269	1.2314	1.2932	1.2675
κ (IS)		1.2291	1.2546	1.2444
a, m/s	996.3	945.4	615.2	714.5
MACH NUMBER	0	1	3.698	2.858
Aext/At		1	14.033	5
C*, m/s		1375	1375	1375
C_F (ideal)		1.239	1.654	1.595
I_{VAC}, Ns/kg		1713.1	2404	2239
I_{VAC}/I_{VAC}*		1	1.403	1.307
I_{SP}, Ns/kg		945.4	2275.4	2041.7
I_{SP}(SL), Ns/kg		1714	2275.4	2195.2

Similarly, the theoretical rocket performance of propellant with non-energetic plasticiser has been calculated for working pressures of 150 bars. The combustion model [76] is based on one-dimensional ideal flow - perfect (ideal) gas, i.e. one dimensional form of conservation laws: mass-energy and momentum conservation, zero velocity of gas in combustion chamber, complete combustion process, adiabatic combustion, isentropic expansion process in the nozzle, homogenous mixing of gaseous and liquid/solid particles. For the rocket performance, an equilibrium compositions are based on hypothesis of instantaneous chemical equilibrium during the expansion in the nozzle. Frozen performances are based on assumption that composition remains frozen during expansion – all chemical reactions finish in combustion chamber. The results of computations are presented in Table 4-3 and 4-4:

Table 4-3 THEORETICAL ROCKET PERFORMANCE ASSUMING EQUILIBRIUM COMPOSITION DURING EXPANSION FOR POLY-PLASTISOL PROPELLANT WITHOUT ENERGETIC PLASTICISER

Theoretical density: 1661.3 kg/m^3, COMBUSTION PRESSURE 150.0 bars

	CHAMBER	THROAT	EXIT	EXIT
P_0/P	1	1.794	150	34.434
P, bar	150	83.612	1	4.3562
T, K	2433.2	2186.7	937.7	1228.1
ρ, kg/m3	17.9289	11.1252	0.312	1.0327
H, KJ/kg	-2471.11	-2934.97	-5165.46	-4624.44
U, KJ/kg	-3307.75	-3686.52	-5485.98	-5046.26
G, KJ/kg	-25771.2	-23874.7	-14144.5	-16384.5
S, KJ/kgK	9.5761	9.5761	9.5761	9.5761
M, MOL WT	24.18	24.191	24.323	24.206
MOL WT (GAS)	23.922	23.928	24.044	23.929
C_P, kJ/kgK	1.8882	1.8215	2.4853	1.762
κ (S)	1.2269	1.2344	1.1995	1.2437
κ (IS)		1.2236	1.235	1.2395
a, m/s	1013.1	963.2	620.1	724.3
MACH NUMBER	0	1	3.744	2.865
Aext/At		1	14.796	5
C*, m/s		1400	1400	1400
C_F (ideal)		1.239	1.657	1.594
I_{VAC}, Ns/kg		1743.5	2459.4	2278.5
I_{VAC}/I_{VAC}*		1	1.411	1.307
I_{SP}, Ns/kg		963.2	2321.4	2075.3
I_{SP}(SL), Ns/kg		1744.4	2321.4	2233.9

Table 4-4 THEORETICAL ROCKET PERFORMANCE ASSUMING FROZZEN COMPOSITION DURING EXPANSION FOR POLY-PLASTISOL PROPELLANT WITHOUT ENERGETIC PLASTICISER

COMBUSTION PRESSURE 150.0 bars

	CHAMBER	THROAT	EXIT	EXIT
P_0/P	1	1.7972	150	35.749
P, bar	150	83.461	1	4.1959
T, K	2433.2	2173	847.3	1173.9
ρ, kg/m3	17.9289	11.1701	0.3432	1.0395
H, KJ/kg	-2471.11	-2934.95	-5108.44	-4613.52
U, KJ/kg	-3307.75	-3682.13	-5399.79	-5017.17
G, KJ/kg	-25771.2	-23743.8	-13222.6	-15855
S, KJ/kgK	9.5761	9.5761	9.5761	9.5761
M, MOL WT	24.18	24.18	24.18	24.18
MOL WT (GAS)	23.922	23.922	23.922	23.922
C_P, kJ/kgK	1.7977	1.7671	1.4618	1.5665
κ (S)	1.2365	1.2416	1.3076	1.2812
κ (IS)		1.239	1.2667	1.255
a, m/s	1017.1	963.2	617.2	719.1
MACH NUMBER	0	1	3.721	2.878
Aext/At		1	13.648	5
C*, m/s		1394	1394	1394
C_F (ideal)		1.24	1.646	1.591
I_{VAC}, Ns/kg		1738.9	2423.5	2265
I_{VAC}/I_{VAC}*		1	1.394	1.303
I_{SP}, Ns/kg		963.2	2296.7	2070
I_{SP}(SL), Ns/kg		1739.7	2296.7	2220.5

For the frozen expansion, parameter of flow can be calculated, as follows:

Specific gas constant:

$$R = \frac{R_0}{M} = \frac{8315}{24.18} = 343.88$$

Specific heat (p=const.) in combustion chamber:

$$C_p = \frac{\kappa_o}{\kappa_o - 1} R = \frac{1.236}{0.236} 343.88 = 1800.1 \left(\frac{J}{kg \cdot K} \right)$$

Heat of combustion (total enthalpy in combustion chamber):

$$Q_c = H_o = C_p T_o = 1800.1 \cdot 2433.2 = 4.382(MJ/kg)$$

Characteristic velocity:

$$C^* = \frac{\sqrt{RT_o}}{\Gamma(\kappa_o)} = \frac{\sqrt{343.88 \cdot 2433.2}}{0.65543} = 1394(m/s)$$

Coefficient Γ (κ_0) :

$$\Gamma(\kappa_o) = \sqrt{\kappa_o}\left(\frac{2}{\kappa_o + 1}\right)^{\frac{\kappa_o + 1}{2(\kappa_0 - 1)}} = \Gamma(1.236) = 0.65543$$

Expansion ratio:

$$\varepsilon_{ext}(\kappa_I) = \frac{\left(\frac{2}{\kappa_I + 1}\right)^{\frac{1}{\kappa_I - 1}} \sqrt{\frac{\kappa_I - 1}{\kappa_I + 1}}}{\left(\frac{p_{ext}}{p_o}\right)^{\frac{1}{\kappa_I}} \sqrt{1 - \left(\frac{p_{ext}}{p_o}\right)^{\frac{\kappa_I - 1}{\kappa_I}}}} = \varepsilon_{ext}(1.255) = 5$$

For the ambient expansion:

$$\varepsilon_{ext}(\kappa_I) = \frac{\left(\frac{2}{\kappa_I + 1}\right)^{\frac{1}{\kappa_I - 1}} \sqrt{\frac{\kappa_I - 1}{\kappa_I + 1}}}{\left(\frac{p_a}{p_o}\right)^{\frac{1}{\kappa_I}} \sqrt{1 - \left(\frac{p_a}{p_o}\right)^{\frac{\kappa_I - 1}{\kappa_I}}}} = \varepsilon_{ext}(1.255) = 13.68$$

Laval's number for the given pressure ratio:

$$\lambda_{ext} = \sqrt{\frac{\kappa_I + 1}{\kappa_I - 1}\left[1 - \left(\frac{p_{ext}}{p_o}\right)^{\frac{\kappa_I - 1}{\kappa_I}}\right]} = \lambda_{ext}(1.255) = 2.136$$

Nozzle exit velocity:

$$v_{ext} = \sqrt{\frac{2\kappa_I}{\kappa_I - 1} RT_o \left[1 - \left(\frac{p_{ext}}{p_o}\right)^{\frac{\kappa_I - 1}{\kappa_I}}\right]} = 2070(m/s)$$

Specific impulse for the given expansion ratio:

$$I_s = v_{ext} + C^* \varepsilon_{ext} \left(\frac{p_{ext}}{p_o} - \frac{p_a}{p_o} \right) = 2220.3 \left(\frac{Ns}{kg} \right)$$

Specific impulse for ambient expansion ($p_{ext}=p_a$), is given as:

$$v_{ext} = \sqrt{\frac{2\kappa_I}{\kappa_I - 1} RT_o \left[1 - \left(\frac{p_a}{p_o} \right)^{\frac{\kappa_I - 1}{\kappa_I}} \right]} = 2296 \left(m/s \right)$$

$$I_s = v_{ext} = 2296 \cdot (Ns/kg)$$

Vacuum specific impulse for expansion ratio equivalent for ambient expansion:

$$I_s = v_{ext} + C^* \varepsilon_{ext} \frac{p_{ext}}{p_o} = 2423 \left(\frac{Ns}{kg} \right)$$

Thrust coefficient as follows:

$$C_F = \frac{I_s}{C^*}$$

Sea level:

$$C_F = \frac{2220.3}{1394} = 1.59$$

Ambient expansion:

$$C_F = \frac{2296}{1394} = 1.647$$

Subsequently, thrust loss coefficient calculations (eq.4-78) with inclusion of losses due to nozzle inclination and due to oblique shape of exit cross section of scarfed nozzle, yield value of φ_{CF} = 0.965, and C_F^* =1.328 (real).

The propellant with 26% of the binder has been chosen because of good mechanical properties required for extreme loading conditions of the SRM during gun launch. The difference in density specific impulse for particular propellant with and without energetic plasticisers has been in range of 2% in

favour of propellant with GAP. However, as requirements for SRM total impulse is just 5500 Ns, the necessity for better mechanical properties that can be achieved with non-energetic-plasticiser prevailed in decision to further investigate binder formulation without GAP.

In order to validate mathematical model and the method, and to establish referent ratio for burning rate augmentation with wires, raw experimental data [101] have been used. The experimental binder system is based on polyvinylchloride resin and the AP as oxidiser similar to referent base bleed propellant [38]. First step is to determine basic propellant burning rate, and method used is BATES motor [97]. The cylindrical specimen, inhibited form all sides, with bore diameter 16mm and 50mm outer diameter is fired The results of interior ballistic test are shown on Figure 4-23., and calculated burning rate has been presented on Figure 4-24.

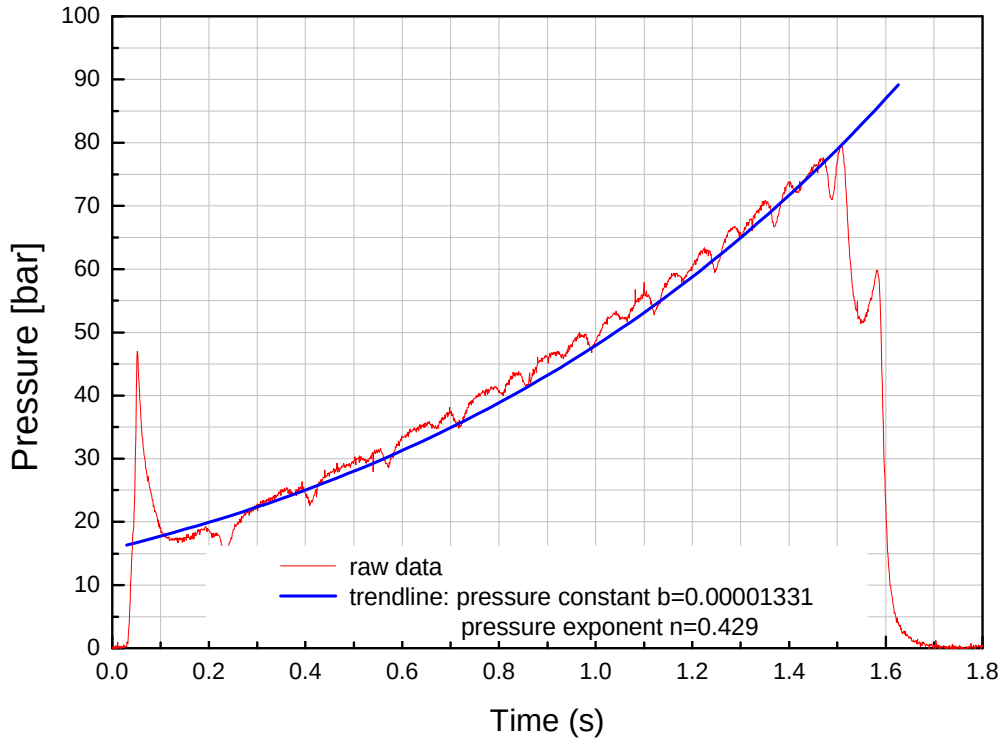

Figure 4-23: Experimental Burning Rate measurement for PVC propellant, 74 AP% content, pressures in range between 2 MPa and 9 MPa

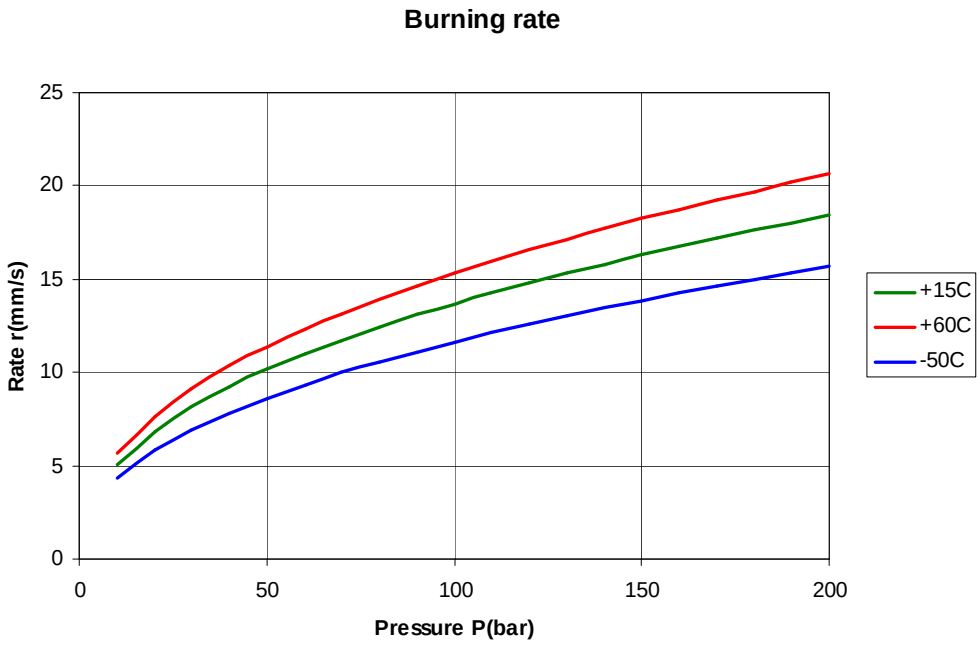

Figure 4-24: Calculated Burning Rate for SRM ref. propellant, 74 AP% content, the burning rate has been calculated for the temperature sensitivity coefficient σ_p= 0.25%/K

The burning rate parameters, obtained from the interior ballistic test for the new thermoplastic “poly-plastisol” propellant are:

- Linear coefficient in burning rate law: $b_0 = 0.00001331$
- Exponential coefficient in burning rate law: $n = 0.429$
- Temperature sensitivity coefficient (estimated) σ_p= 0.25% per K

Experimental propellant grain for “wire” burning rate model validation contains 5 embedded wires along entire length of the propellant, burning conical forehead and inhibited outer diameter and rear end of the grain (Figure 4-25). The wires used in the experiment were copper (Cu) wire plated with silver (Ag). Diameter of the wire is 0.25mm (SWG 33). The development of the burning surface for the given propellant grain dimensions and propellant burning rate factor augmentation is programmed inside the PTC Creo Paramteric software [102] (Figure 4-26) and burning surface diagram is in figure 4-27. The nozzle is made of refractory metal molybdenum (Moly TZM) ASTM B-386, B-387. diameter of the nozzle is Ø3.9mm.

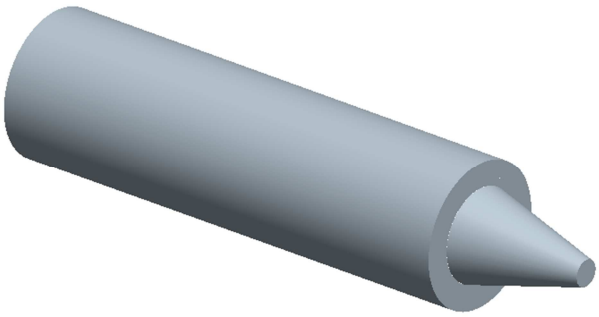

Figure 4-25: Experimental propellant grain with 5 copper wires, radially distributed at diameter Ø30mm, outer diameter of the propellant is Ø46.3 mm, inhibitor thickness 1.5mm, length of the propellant 200mm

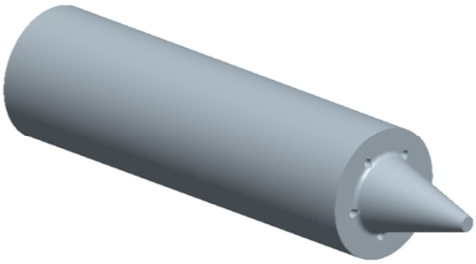

a) Burnt web e = 2 mm

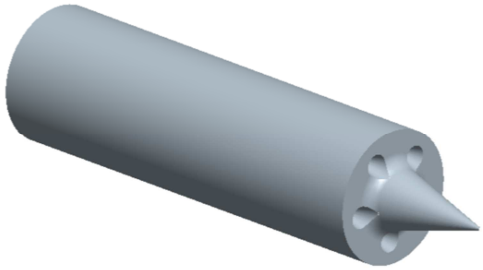

b) Burnt web e = 5 mm

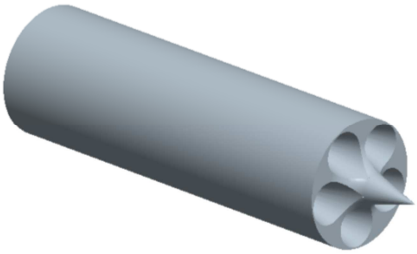

c) Burnt web e = 10 mm

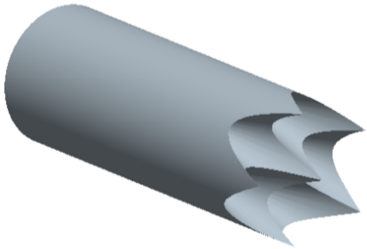

d) Burnt web e = 20 mm

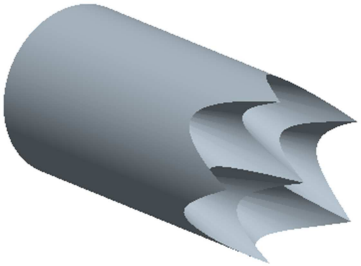

e) Burnt web e = 30 mm

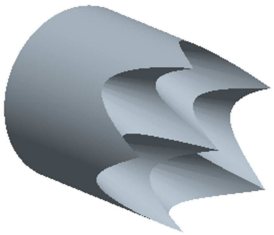

f) Burnt web e= 40 mm

g) Burnt web e=50 mm

Figure 4-26: Burning surface- area evolution for experimental propellant grain.

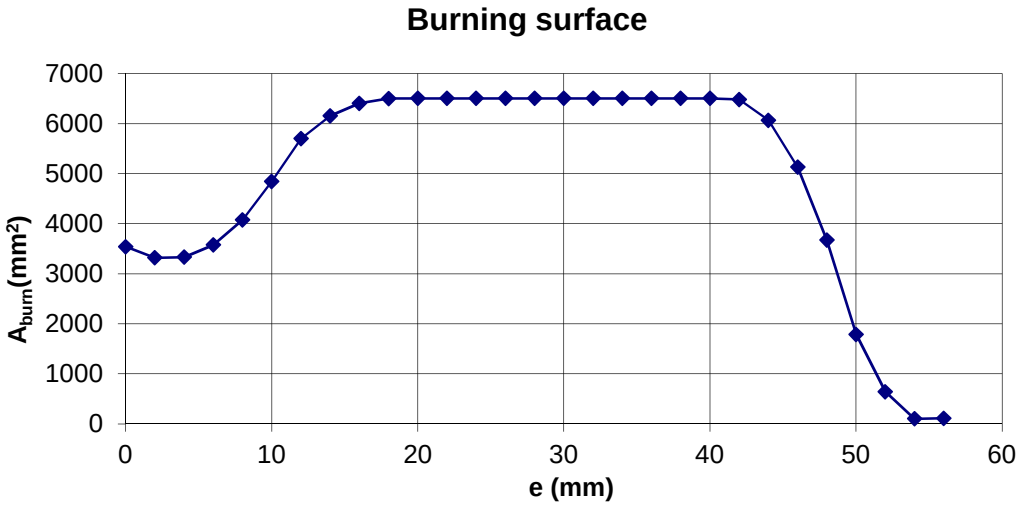

Figure 4-27 Burning surface Vs. burning web - experimental rocket motor

Analysis of experimental pressure data [101] in conjunction with theoretical burning model, yielded value of burning rate augmentation coefficient E_w: for silver plated copper wires – augmentation factor is 3.85, i.e. the burning rate augmentation angle $\chi \approx 15^0$. The comparison between the theoretical model pressure curve and experimental pressure diagram is given on Figure 4-28.

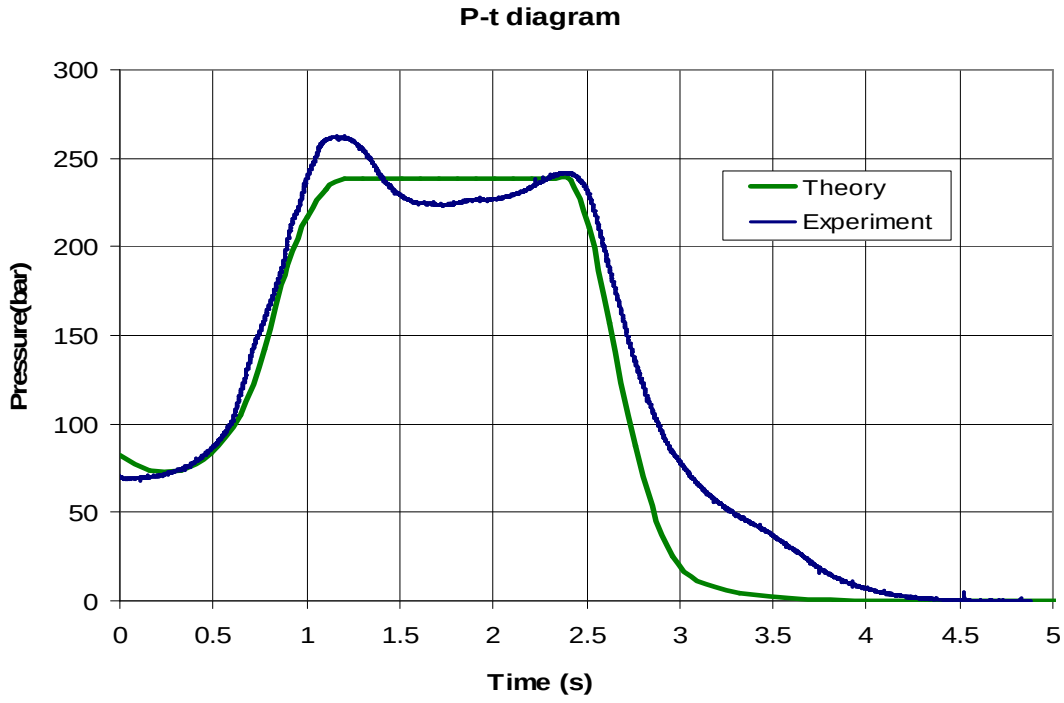

Figure 4-28: Model rocket motor performance: pressure vs. time

The experimental results are in good agreement with theoretical model for polyvinylchloride-AP propellant [73]. The method and values from experimental evaluation [101] and literature [73] indicate that similar level of burning rate augmentation could be expected from novel poly-plastisol propellant. Post-test nozzle dimension check, suggests that under high thermal loads, nozzle changed throat diameter, i.e. the entire nozzle insert expanded outward and inward due to high thermal absorption, but it managed to withstands enormous heat flux without any other anomalies. This phenomenon is clearly shown on pressure diagram – figure 4-27 (about 1 second from start). The difference between calculated and the real test direct us to the fact that nozzle change the geometry after 1 second of burning time - after accumulating heat (throat diameter variations, in theoretical model, are not taken in account in a first place). Variations in combustion pressure during the rocket burn correspond to nozzle throat geometry change as well as to defects in manufacturing of propellant grain. Wires probably wrinkled-buckled during the homogenisation of the propellant grain. The burning area deviated from theoretical burning surface evolution, however the “basic” burning rate and the augmentation of burning rate along the wires were in compliance with the basic burning rate law and *Ew*. The pressure diagram indicates that difference was about 1% to 4% due to increased burning surface. At “sliver” part of the diagram, the difference between calculated pressure and experimental pressure is mainly caused by nozzle geometry change due to high thermal load, as well as by inhibitor melting causing clogging in the nozzle throat. Measurement of nozzle throat immediately after test, points that initial 3.90-3.95mm, were changed to 3.4-3.5mm, which explains the pressure increment in descending part of the pressure-time curve. Losses in the nozzle (nozzle throat) has been derived from the experiment. The test verified compatibility of multi wire propellant grain with requirements set for M-REP’s SRM

Based on previous calculations (both exterior and interior ballistics of the M-REP) and experimental results, the “final” design of SRM is optimised. The figure 4-29, represents the cut-out view of entire SRM for M-REP. The SRM for M-REP is placed in the ogive part of the projectile, occupying volume that

minimally affects efficiency of the payload. The acceleration force during the firing sequence will act on the propellant grain pushing it against the walls of combustion chamber.

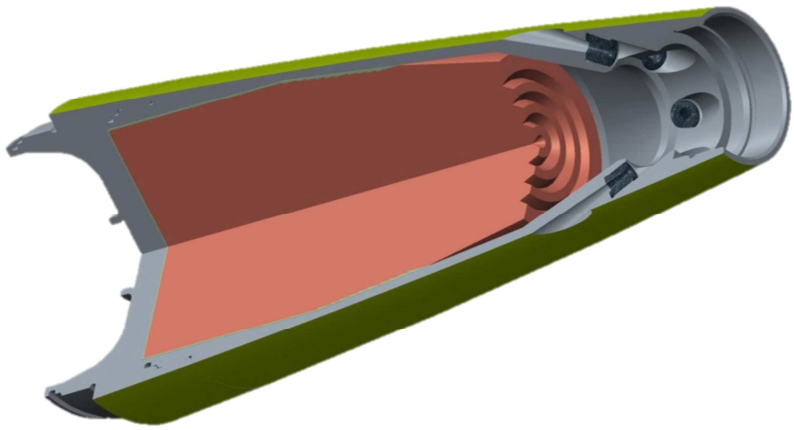

Figure 4-29 “Optimal Design” of SRM for M-REP

However, due to tiny technological gap (0.1mm) required for SRM assembling , the propellant grain will dilate under the acceleration only to fill the technological gap, and it will compress in itself as much as the propellant bulk modulus allows, but it will not compromise structural integrity of the propellant grain itself. The front conical part of the motor casing will prevent propellant to “spring” back once the projectile start to decelerate after leaving muzzle. The nozzle section contains 6 nozzle pieces, made form Molybdenum Alloy - Moly TZM. The material has been proved during the experiment, and it is able to withstand high heat fluxes and temperatures. The nozzle section is represented on figure 4-30. Total impulse obtained is 6297 Ns.

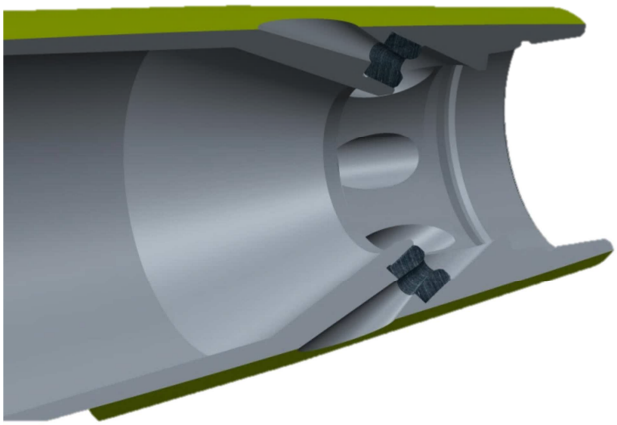

Figure 4-30 “Optimal Design” of SRM for M-REP - nozzle section

Figure 4-31 and 4-32 represent the burning surface evolution for "optimal design" of propellant grain and diagrams on figures 4-33 and 4-34 show interior ballistic calculations for such SRM..

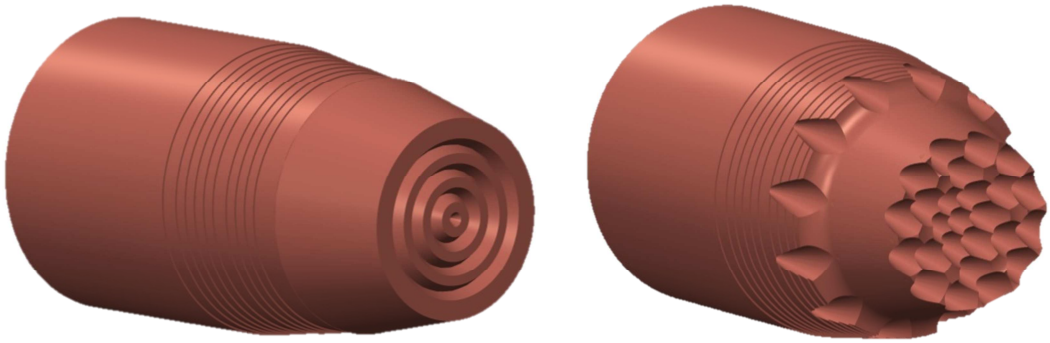

a) Burnt web e = 0 mm

b) Burnt web e = 10 mm

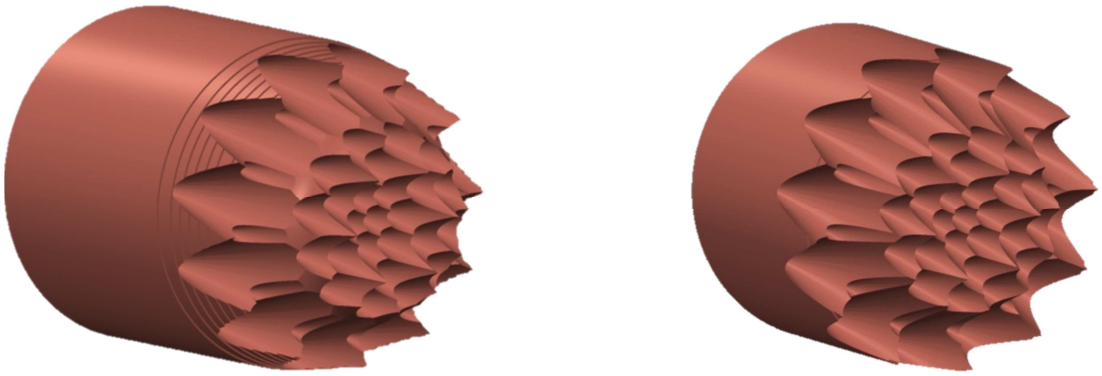

c) Burnt web e = 20 mm

d) Burnt web e = 30 mm

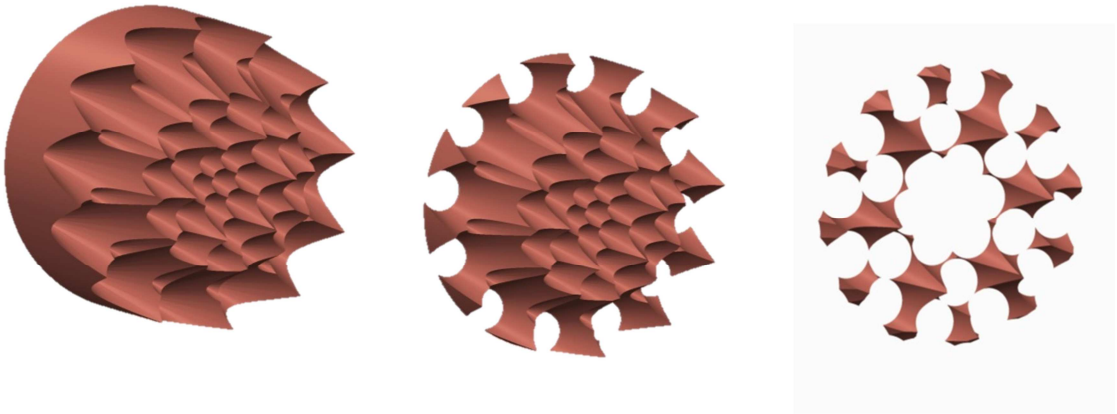

e) Burnt web e = 40 mm

f) Burnt web e= 50 mm

g) Burnt web e=60 mm

Figure 4-31: Burning surface development for "optimal design" of SRM propellant grain

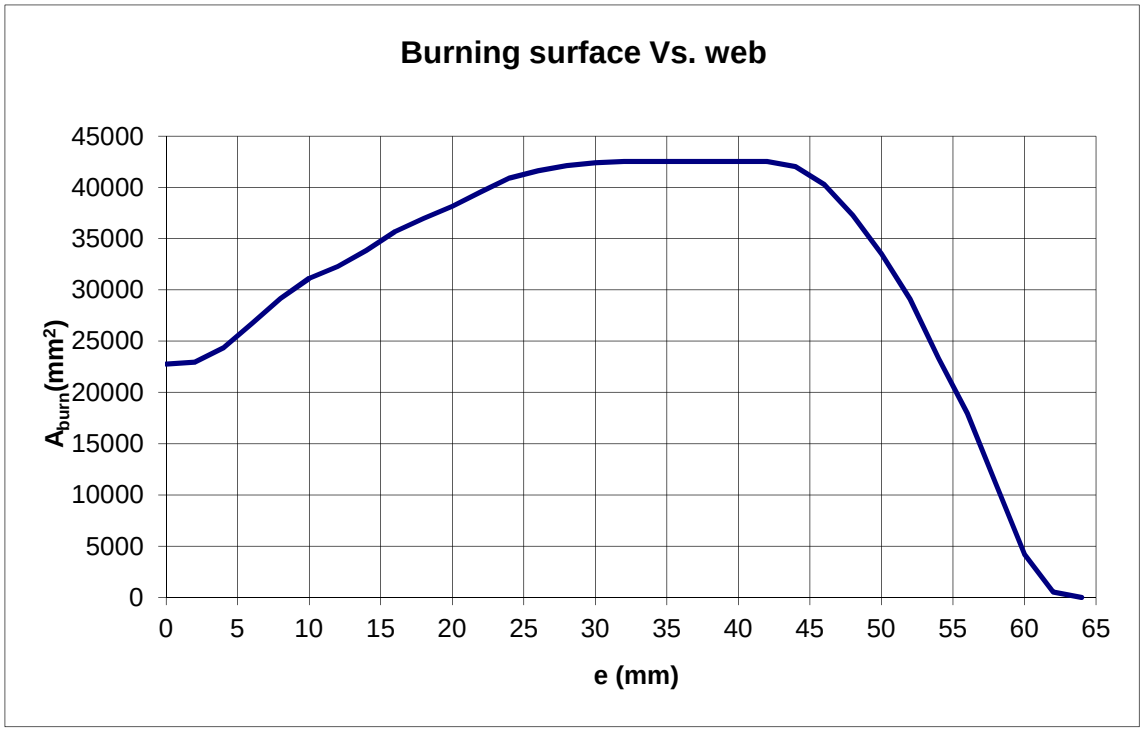

Figure 4-32 **Burning surface Vs. web – "Optimal Design" SRM**

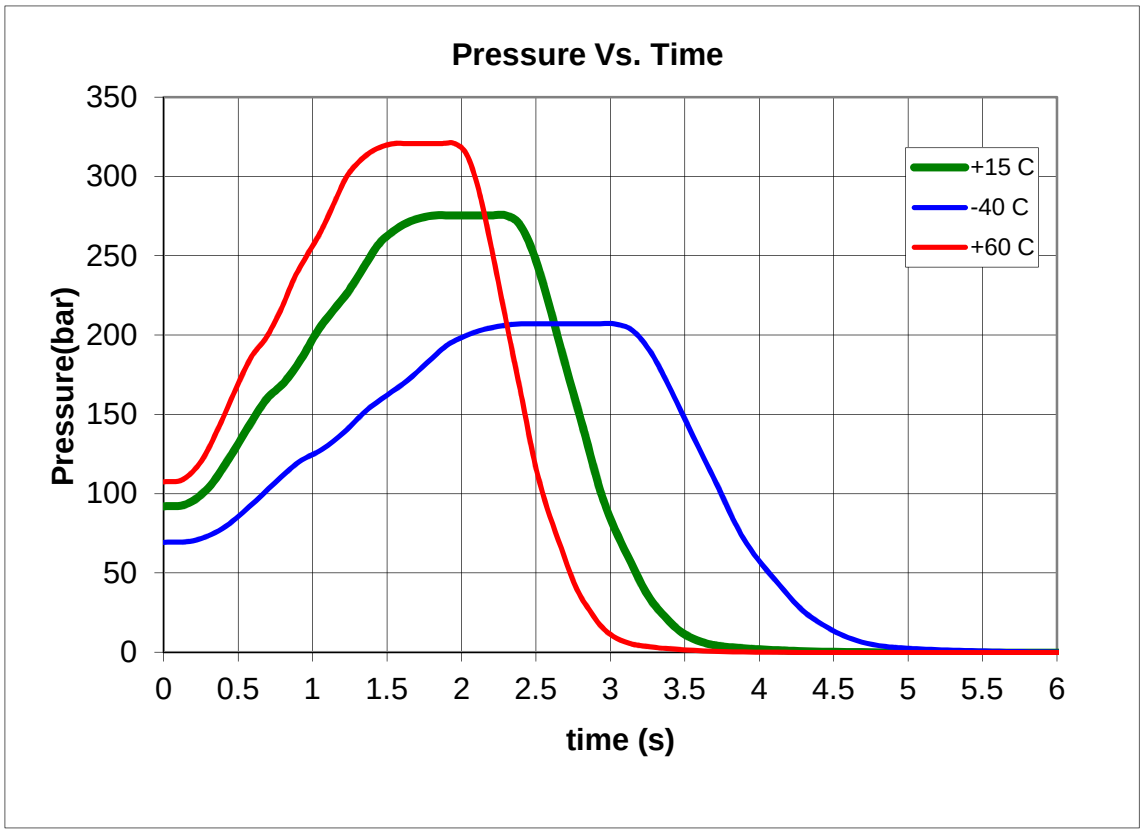

Figure 4-33 "Optimal Design" SRM performance: pressure vs. time

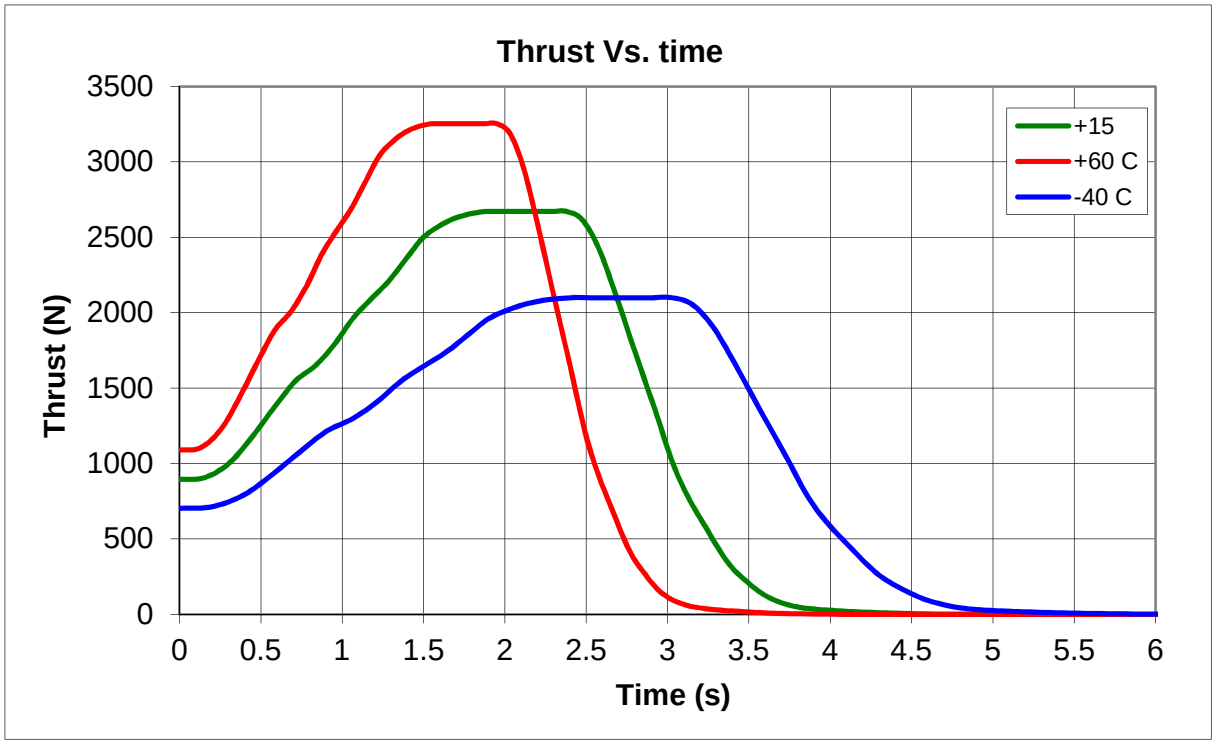

Figure 4-34 "Optimal Design" SRM performance: thrust vs. time

Following interior ballistic assessment of the design, mechanical properties of novel thermoplastic "poly-plastisol" propellant for M-REP's SRM application have been investigated. Due to high axial and radial loads (axial acceleration, angular/radial acceleration and radial velocity - spin), propellant grain is under great stress and strain. In order to withstand gun firing loads, the propellant grain has to maintain good mechanical properties and flexibility at all operating temperatures (from -40^{o}C to +60^{o}C). Therefore, with appropriate grain geometry and arrangement inside SRM combustion chamber, the propellant grain should withstand inertial loads upon firing. Mechanical properties of the novel thermoplastic/elastomeric poly-plastisol propellant for M-REP, have been tested on Universal Testing Machine with constant strain rate (cross-head speed) and in environmental chamber for specimens tempering. Uniaxial/Isothermal tensile tests were performed using JANNAF dog bone specimens "C" and appropriate procedure according to STANAG 4506 [103] at ambient temperature +20^{o}C with strain rate of 50 mm/min, as well as on -30^{o}C and +50^{o}C with same strain rate. Tension force and elongation were measured with load cell and extensometer in temperature-controlled chamber. Acquired

data has been analysed, and maximum stress (tensile strength)- σ_m, strain at maximum stress- ε_m, and initial tangent modulus- E_o, were calculated as average values from several measurements. The results of tensile tests are presented on Figures 4-35 to 4-37.

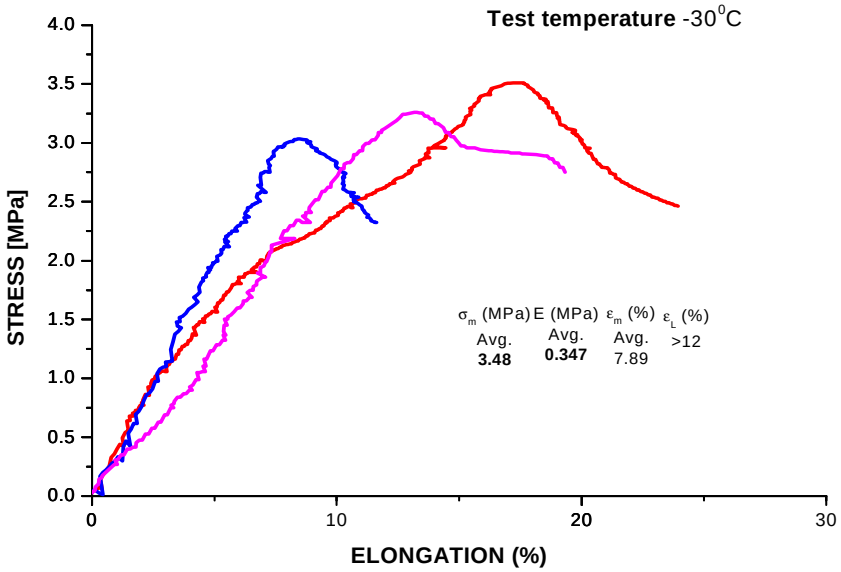

Figure 4-35: Thermoplastic/elastomeric SRM propellant, 74 AP% content, Tensile Properties Test -30 °C

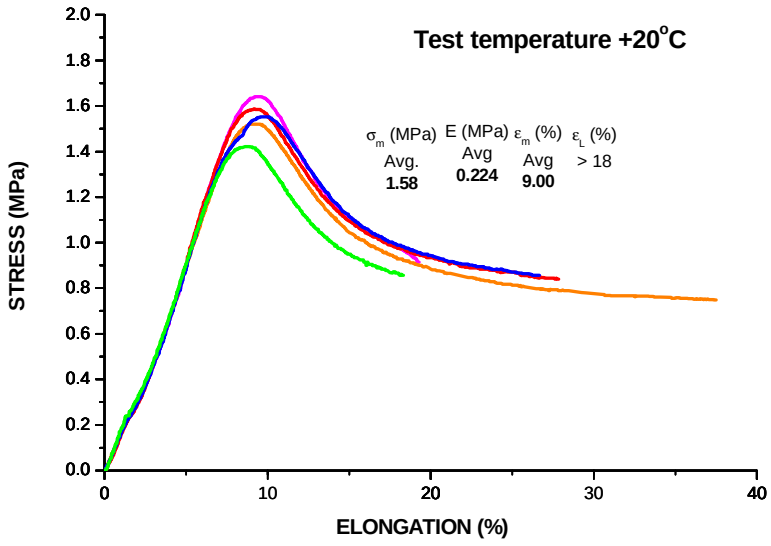

Figure 4-36: Thermoplastic/elastomeric SRM propellant, 74 AP% content, Tensile Properties Test +20 °C

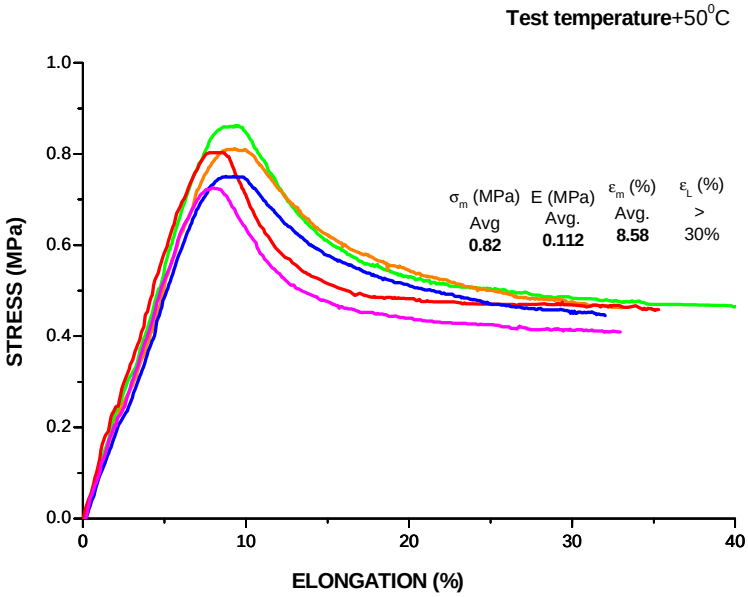

Figure 4-37: Thermoplastic/elastomeric SRM propellant, 74 AP% content, Tensile Properties Test +50°C

In order to establish glass transition temperature (T_g) and visco-elastic properties of thermoplastic/elastomeric propellant for SRM ,required for grain structural analysis, the DMA (dynamic material analysis) tests have been conducted. The temperature scans and frequency scans has been performed in order to establish the glass transition temperature and parameters for William-Landel-Ferry WLF equation [77-78], which describes time-temperature-superposition phenomenon of visco-elastic material. Tests have been carried out on specimens with same binder composition as “energetic” propellant but with inert filler ($CaCO_3$ instead of AP) figure 4-38 .

Figure 4-38: SRM propellant sheet for DMA specimens

Apparatus for DMA tests is shown on figure 4-39, and results of DMA tests are presented on Figures 4-40 and 4-41. The T_g (temperature of transition

from "glassy" to visco-elastic material behaviour) has been established for SRM propellant, and it is below temperature of -60^{o}C. figure 4-40. The master curve is obtained (fig. 4-41) and WLF coefficients are C_1=95.5 and C_2=556.5 for reference temperature T_0= -10 ^{o}C.

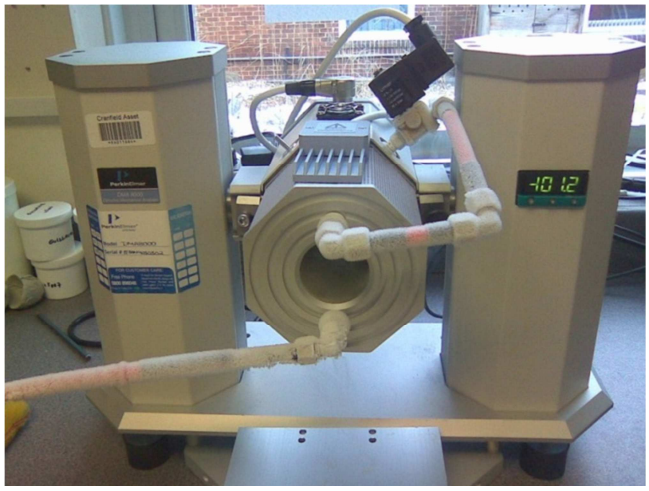

Figure 4-39: DMA apparatus used for establishing the visco-elastic properties of propellant

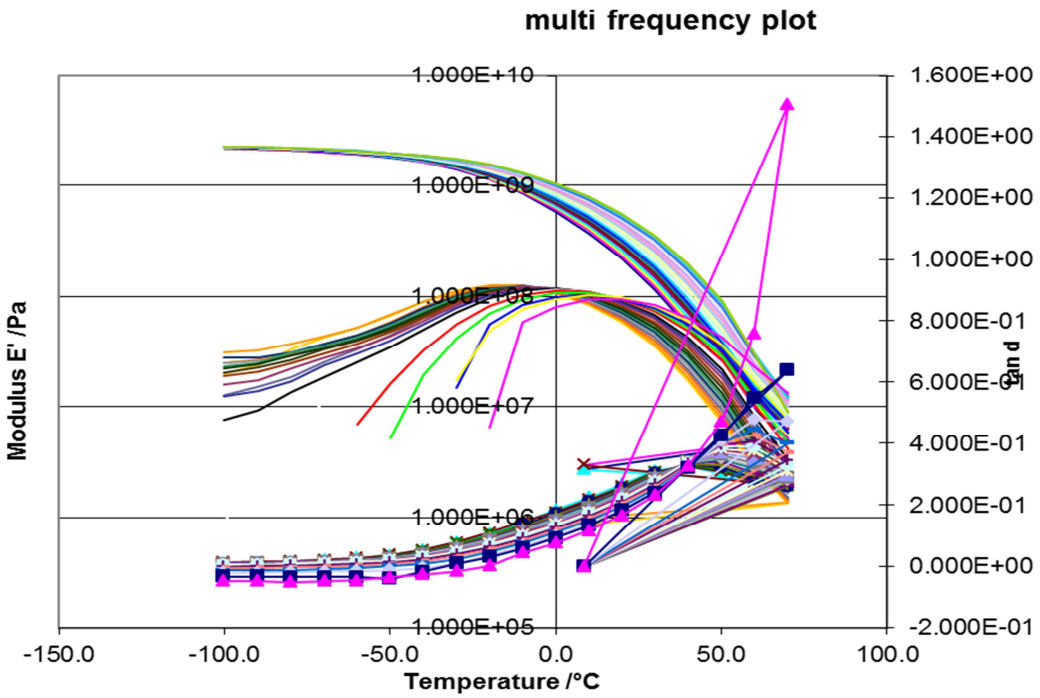

Figure 4-40: Frequency scan for thermoplastic/elastomeric SRM propellant, without energetic plasticiser, multiple frequencies. "Glass" transition temperature found is below -60^{o}C

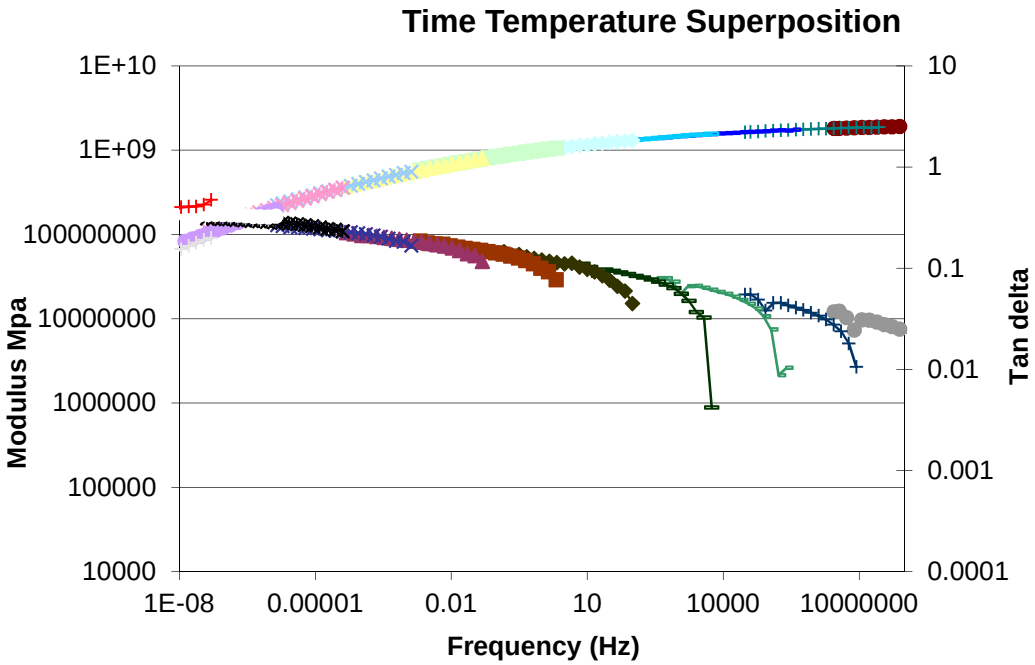

Figure 4-41: Frequency scan for thermoplastic/elastomeric SRM propellant, without energetic plasticiser, time-temperature-superposition master curve

4.3 SRM Findings

The SRM design for M-REP is successfully established and verified. The rocket motor total impulse required to propel M-REP beyond 50 km by exterior ballistics calculation, has been affirmed by interior ballistics calculations. Combustion model and burning surface evolution model is validated through comparison with experiment.

Optimal SRM design includes novel propellant formula novel arrangement of propellant grain and nozzle in rocket motor. Energetic and mechanical properties of new propellant in combination with motor layout satisfy basic technical requirements for gun launched rocket assisted projectile, structural integrity in gun barrel and required total impulse. New propellant grain design includes multitude of heat conductors to augment the burning rate, which resulted in short active time of SRM, therefore less disturbances on trajectory due to rocket motor ignition and working time..

5 OPTIMISATION OF FLIGHT MECHANICS PARAMETERS FOR MODULAR RANGE ENHANCED PROJECTILE

5.1 Introduction

Design process of artillery projectiles utilises many scientific disciplines in order to achieve optimum shell configuration. First of all, disciplines that cover specific domains of defence engineering, such as projectile aerodynamics, interior ballistics of guns, exterior ballistics, and ballistics on target. General mechanical and structural engineering. follow, but without knowledge of thermodynamics (combustion and heat transfer), chemistry, process engineering, manufacturing etc., the projectile design would be incomplete and faulty. Therefore, we can say that environment in which projectile design evolves is complex matrix, with all these disciplines intertwined, and changing one aspect of the design can profoundly change the overall performance of the projectile. Sometimes, the focus is on one discipline or particular problem, but we must not forget the overall projectile “picture” Optimal design of artillery shell should provide long range, as little as possible dispersion and adequate target defeating capability. In case of M-REP, the main design goal is extended range, therefore, projectile’s exterior ballistics is primary “probe” in the loop of the design process algorithm. The exterior ballistics calculations are expected to provide feedback regarding the given goal set i.e. to validate the “success” of the overall projectile design.

The 155mm M-REP design represents extended range artillery shell integrated with optimised propulsion elements (solid rocket motor and base bleed unit) in order to achieve maximum ranges from given 155mm ordnance (52 and 39 calibre gun-howitzers, towed or self-propelled) and corresponding propelling charge systems. The JBMoU [1] guidelines have been used as design requirements for projectile shape, weight and performance. Additional design goals, but not regarded as lower level design aims are accuracy and

lethality. The goal is to keep dispersion of M-REP within the limits that will allow successful use of 1D and 2D trajectory correction systems. Moreover, lethality of a projectile should be kept at level similar to existing 155mm “standard” ammunition (such as M107, L15, ERFB-BT, etc. [9]), or level comparable with more complex and more expensive systems such as Excalibur or Volcano [4,9], Moreover, M-REP should be better than M549A1 or V-LAP ammunition [9], i.e. projectile’s lethality should be adequate for required target defeating capability, which is basically counter-batting and engaging third echelon targets The 155mm M-REP should be regarded as supplement to existing pallet of 155mm HE ammunition, but also it can be considered as solution to replace existing ammunition. Modular projectile can perform different roles (HE, cargo, BT, BB, incendiary, illuminating, thermobaric modules), and with additional enhancement in range that M-REP provides existing howitzer becomes updated, modernized systems without any upgrade to the gun itself whatsoever. Projectile handling do not require additional training for gun-crew, or additional logistics preparation then standard one. Projectile can be fitted with trajectory correction fuze (TCF) in order to increase accuracy (dispersion – both lateral and in range). Trajectory Correction Fuze, i.e method of trajectory correction can be exercised as supplement to the design solution of the projectile.

Technical characteristics of 155mm M-REP projectile:

General:

- Marking 155mm M-REP
- Calibre 155 mm
- Ordnance gun-howitzer 39 (45 or 52) calibre
- Propellant Charge Zone 9(8S) – 39 calibre, Zone 10 (45-52 calibre)
- Fuze Point Detonating (PD), Proximity or TCF
- Temperature range $-40 \div +63^{o}C$

Weight:

- Total Weight LT. 49.75 kg
- Without PD fuze LT. 49.10 kg
- PD fuze weight LT. 0.65 kg

- HE weight cca. 6 kg
- Weight of Base Bleed Grain LT. 1.3 kg
- Weight of Solid Propellant Grain LT. 3.6 kg

Dimensions

- Outer diameter-calibre 154.74 mm
- Fuzed length cca. 920 mm
- Unfuzed length cca. 824 mm
- Rotating band dia. 157.86 mm

Ballistics:

- Muzzle velocity V_0 required 821 m/s (39 calibre), 930 m/s (52 calibre)
- Max. range (at sea level) 40.7 km(39), 51.4km (52)
- Max. barrel pressure ~345 MPa (39), ~380MPa (52)
- Dispersion lateral LT. 0.75 %
- Dispersion in range LT. 0.15 %

Interior ballistic of solid rocket motor required for the exterior ballistics is defined in Chapter Four. Figure 5-1 represent thrust diagram for solid rocket motor that will be used in this phase of validation of M-REP performance.

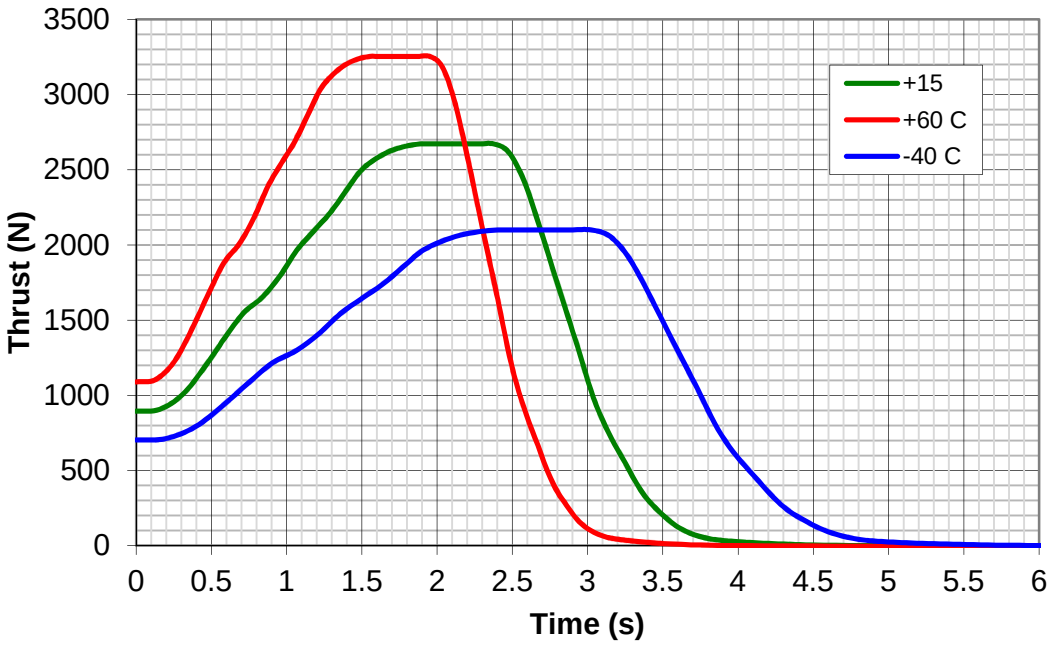

Figure 5-1 Thrust vs. Time for M-REP's SRM

5.1.1 Projectile design

Projectile 155 mm MREP (fig. 5-2) design, comprise:

- Fuze (PD – “graze”, Proximity, TCF)

- Solid Rocket Motor (SRM)

- Warhead (Payload)

- Rotating Band

- Base Bleed Unit (BB)

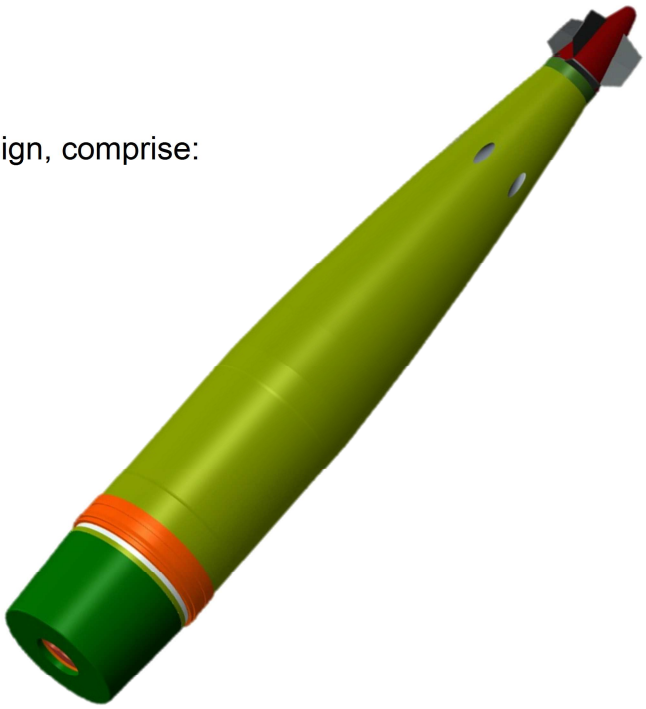

Figure 5-2. 3D representation of the projectile

The M-REP design features separate modules for propulsion, payload and base bleed i.e. their functions are independent of each other, especially regarding SRM and BB unit, in order to be reliable and not to interfere with each other, both in barrel and at the trajectory. Further, the M-REP stands for interchangeability and modularity, i.e. the SRM can be replaced with supplementary warhead, and BB can be replaced with boat tail (BT), with result that M-REP becomes “standard” 155mm HE projectile.

Solid Rocket Motor

The SRM (fig. 5-3) features combustion chamber, nozzle section and propellant grain. Combustion chamber is in the ogive part of the projectile and it is fitted with time delay ignition mechanism, but also it can accommodate an TCF. Material of combustion chamber is high-strength steel that can withstand high loads imparted by acceleration in the barrel and internal pressures during the combustion of the SRM. Nozzle section features machined ogive body with nozzle inserts made from high-temperature resistant material - refractory metal Mo or Mo-Ti alloy - Molly TZM. Nozzles having 4mm throat diameter and 9mm

exit area diameter (basic, not oblique-scarfed nozzle exit area), total number of nozzles is 6, nozzles are angled to the projectile axis at 30 deg,

The SRM's propellant grain has cylindrical shape with front-end shaped in cone, as described in Chapter 4. Rear-end of propellant grain is flat to mate with appropriate surface on payload closure. Rear-end and outer diameter of propellant grain are inhibited, forehead of the propellant grain is burning from one side, however, required thrust profile is obtained with "heat conductors" – copper wires embedded in the "fuel" in order to augment propellant's burning rate. Total impulse of SRM is I_{tot}=6297Ns, "real" specific impulse is I_{sp}=1748Ns/kg. Burning time of propellant grain is cca. 4 sec. Ignition delay device for SRM is based on electronic or mechanical timer fuze (electro-mechanical device) similar to those used for illuminating or cluster ammunition. Ignition delay ignites SRM in range between 17 sec. and 32 sec of projectile flight (projectile trajectory). Time delay settings depends on requested range in conjunction with gun elevation. Longest range at sea level can be achieved with several combinations of time delay and elevations.

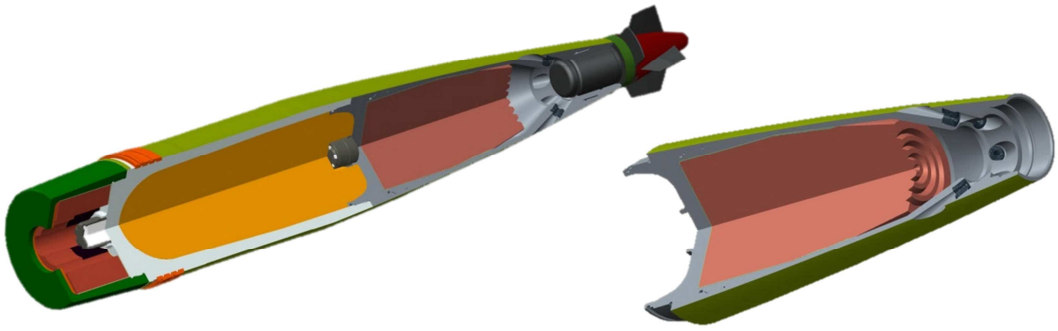

Figure 5-3 SRM in M-REP's assembly and separately

Base Bleed (as part of the M-REP)

Base Bleed (fig. 5-4) case is designed of high-strength steel capable to withstand high acceleration and pressure in gun-barrel. Base Bleed grain is two part cylindrical shape with central port, inhibited at outer diameter, and rear-end. Combustion of the Base Bleed propellant grain allows reduction of projectile's base drag on the trajectory, by injecting the hot gases in the wake zone. Burning time of BB is cca. 44 sec. at optimal elevation. Ignition of the BB is in

gun-barrel during the firing sequence, and with help of BB igniter/sustainer, ignition is reliable and BB works immediately, at the muzzle, without delay. The BB reliable ignition contributes to significant reduction of drag at initial part of trajectory. The BB can be replaced with BT, or it can be a part of expelling bottom for cluster or illuminating ammunition.

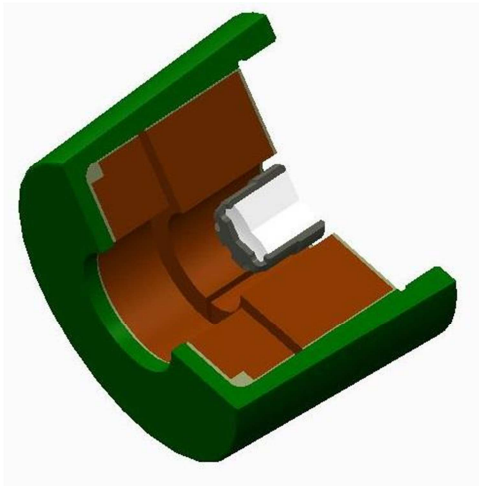

Figure 5-4 Base Bleed Unit for M-REP

Warhead

Basic payload design is HE warhead that serves against enemy personnel, light armoured vehicles and fortifications, intended for targets displaced deep in enemy territory. Metal jacket is made from natural-fragmenting steel HF1, weight of explosive is cca. 6 kg of aluminised TNT (or more brisance explosive e.g. COMP B – 6.3 kg.). Figure 5-5 shows represents simplified fuze, i.e. space an position occupied by the payload fuze required to initiate the detonation.

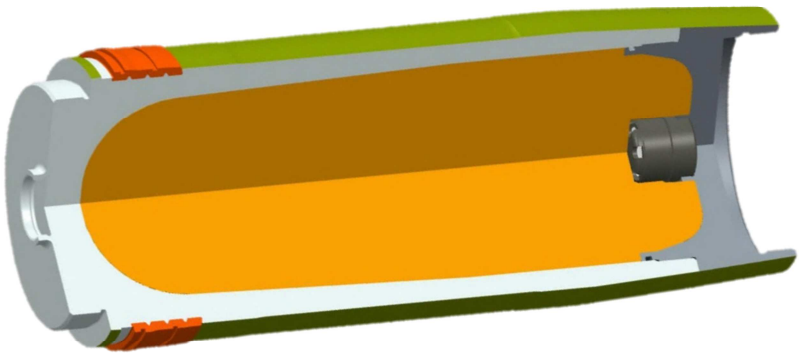

Figure 5-5 Warhead

Fuze

There are two fuzes on the projectile, one simple percussion fuze with “graze” function (precursor initiate the explosive charge on deceleration, either with instantaneous or “delay” function) or inductive electronic fuze with timer assembled into the warhead. Second fuze is required to initiate the SRM and to complement fuze in warhead with additional fuze options such as proximity function or super quick action. The fuze on top of the projectile is interchangeable with Trajectory Correction Fuze (TCF) [9]. The TCF corrects flight path and dispersion both in range and lateral. Warhead Fuze should be fitted into projectile before the SRM is screwed onto the payload module; it can be factory fitted whether with “graze” fuze, multifunction fuze (in combination with nose fuze) or electronic fuze. The fuze in the warhead should be designed to use Inductive Artillery Fuze Setter [9]. Arming of warhead’s fuze is done by acceleration setback, i.e. mechanically. Handling and maintenance of the M-REP should be the same as standard HE shell.

Figure 5-6 Mockup fuze for M-REP – PGK XM1156 [9,104]

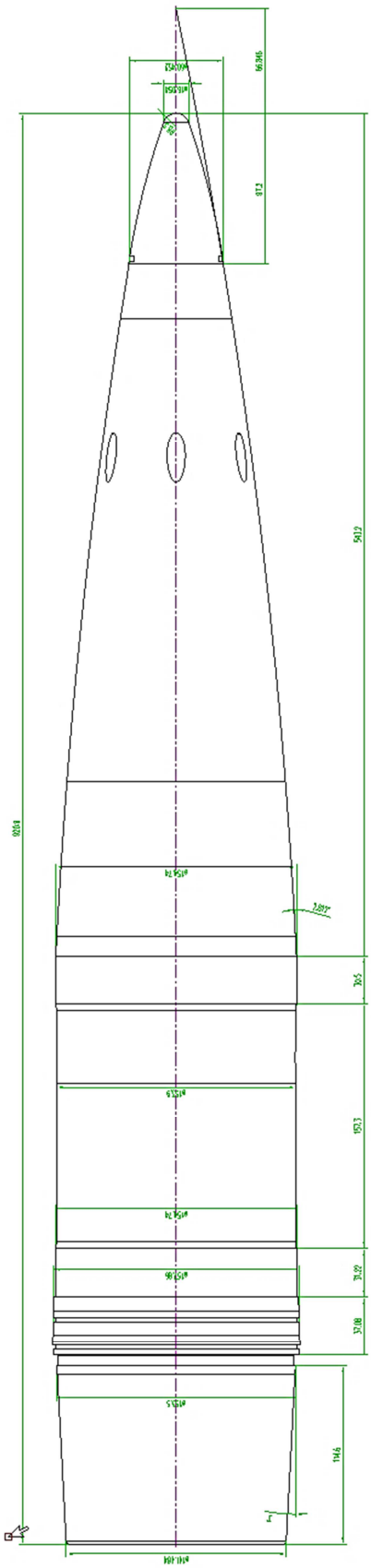

Figure 5-7 Geometry and aero model of M-REP projectile with PD fuze and aerodynamic cap.

5.2 Exterior ballistics of Modular – Range Enhanced Projectile

The guidelines stated in the strategic documents such as JBMoU [1], and parameters of the existing ordnances and their propelling charges, directed in a straightway manner optimisation path of M-REP's exterior ballistics. Under aforementioned constrains, the new projectile configuration has emerged utilizing additional propulsion elements (SRM and BB) to achieve longer ranges and active control of projectile angular motion to affect projectile's stability.

To optimise M-REP's trajectory for increased range, the base bleed and rocket propulsion need to be "synchronized". The base bleed allows significant increase in range, by decreasing the base drag, which represents the largest portion of overall projectile drag, as presented in Chapter Three. Hence, prolonged and uninterrupted base bleed effect has profound influence on trajectory range and dispersion, as decrease in overall drag reduces effects of atmospheric disturbances (gust wind, turbulences). The Solid Rocket Motor, as additional projectile's propulsion generates "boost," which increases projectile's kinetic energy, required for range extension.

In spite of individual contributions to range increment, without harmonization between Base Bleed, Solid Rocket Motor and gun related parameters (muzzle velocity and induced projectile spin), the effort to maximise projectile's range can be futile. Therefore, we should determine for each specific type of gun or howitzers, optimal ignition time for SRM and optimal gun elevation that produce maximum ranges for chosen ordnance and charge system.

The analysis of projectile's exterior ballistics is not finished by calculation of projectile range. The design must be further validated by determining the static and dynamic stability of the projectile, as well as angular movements of a projectile. Those parameters have direct influence on trajectory "shape" and projectile dispersion on target.

The novel approach to aeroballistics modelling of gun-launched-free-flight-artillery projectiles has been developed in order to incorporate and validate all novel features of M-REP design (novel base bleed unit, novel rocket assisted concept, and active de-spinning or up-spinning of a projectile) that differentiate M-REP's exterior ballistic when compared with "classical" projectile aeroballistics. Mathematical model of M-REP's aeroballistics trajectory includes "in-flight" calculation of base bleed effect, calculation of rocket thrust contribution to the trajectory profile with reference to time delay function and altitude, "active" control of projectile's spin with rocket motor to achieve more stable flight and to decrease the dispersion on target, and use of aerodynamic brakes as form of guidance mechanism. The trajectory model is based on six-degrees-of-freedom rigid body differential equations of motion.

The 6DOF mathematical model (programmed in FORTRAN) is devised to include most relevant aerodynamic forces and moments acting on spin stabilised projectiles, base-bleed effect, forces and moments produced by the solid rocket motor, variable inertial characteristics of a projectile including mass imbalance, properties of atmosphere [105] and gravity field model. Flight stability analysis is incorporated using the derived equations from linearised pitching and yaw motion [22, 23, 26, 106] for rotationally symmetric spin stabilised projectiles, by calculating the dynamic and gyroscopic stability factors, and total angle of attack. Trajectory model has been validated by comparing the experimental data [38] from "live firing" of reference projectile 155mm ERFB-BB (figure 3-25) with computational results as described in Chapter 3.4. In addition, the series of mathematical experiments were conducted and compared with results from literature [22, 26, 34, 3, 107]. Furthermore, trajectory model simulation results are compared with the output of PRODAS [79, 108] as benchmark software for exterior ballistics (Appendix A). Input parameters for M-REP's trajectory simulations are calculations of SRM's interior ballistics, presented in Fourth Chapter, base drag reduction model presented in Third Chapter, and 3D modelling using CAD software package PTC Creo Paramteric [102]). The 6DOF mathematical model and results of simulations are presented in section 5.2.5.

5.2.1 M-REP's Equations of Motion

The main direct task of flight mechanics is calculation (prediction) of projectile's trajectory for given set of input data and initial conditions. The inverse task of flight mechanics is to define input parameters (projectile or gun features) that will anticipate desired output such as range, or accuracy. In case of M-REP, aeroballistics model is devised to combines both tasks, model can calculate range from given input data, but also in can conduct parametric optimisation of projectile trajectory to find required values for thrust and drag reduction to achieve primary design goal – range increase above 50 km, as well as to check flight parameters that will keep dispersion at the required level.

To accomplish the exterior ballistics tasks, following input data for the projectile need to be defined up-front:

- Aerodynamic properties of the projectile (aerodynamic forces and aerodynamic moments coefficients versus Mach number)
- Propulsion (thrust forces, thrust moments, and propellant consumption versus time)
- Inertial characteristics (weights, moments of inertia, and centre of mass versus time, as SRM and BB propellant grains are consumed along the trajectory)
- Properties of the Atmosphere (standard, polar/cold or tropical/hot atmosphere, atmospheric pressure, temperature and humidity deviations, wind data)
- Earth model (flat, spherical or ellipsoid model and appropriate gravity field model)
- Initial parameters (firing position – longitude and latitude, weapon azimuth and elevation, muzzle velocity, etc.)

After defining input data, the mathematical model of a projectile dynamic motion can be described with a system of differential equations, three equations for translational and three equation of rotational movement of a projectile – six degrees of freedom 6DOF [106]. The equations of motion for

6DOF trajectories of M-REP represent a complex system of differential equations. The projectile is assumed as unconstrained rigid body, and the rotational movement is described around the projectiles centre of gravity (mass). Furthermore, system of equation describes flight path and flight dynamics of rotationally symmetric, spinning REP projectile with addition of base bleed effect, thrust forces and thrust moments generated by SRM, as new features of M-REP. The projectile motion is described with reference to the Earth, as M-REP covers long distances, and influence of Earth rotation and curvature should be taken into account when the trajectory is calculated. The coordinate systems, in which projectile motion is described, are chosen with according to adopted practices in atmospheric flight mechanics of space vehicles [22] and practices in defining the exterior ballistics of artillery projectiles [26, 84]. Several “different” coordinate systems are utilised in order to describe M-REP trajectory: “Local” coordinate system (Figure 5.8) – rectangular, right-handed, Earth-fixed coordinate system with origin at the gun muzzle; “Body-Fixed”, “Plane-Fixed” and “Aeroballistics” coordinate systems, again rectangular and right handed, with origin at the projectile centre of mass, which travels with the projectile.

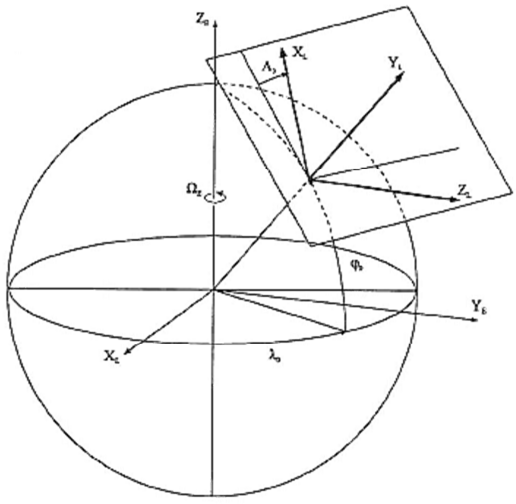

Figure 5-8 Local coordinate system [26]

Local coordinate system has the X_L axis coincident with firing direction looking down range and Y_L axis vertically upward and orthogonal to the plane

that is tangent to the Earth curvature at the origin of the local coordinate system. With reference to the Earth, the azimuth (*AZ*) of firing direction is measured against direction of the North, and it is positive in clock-wise rotation. The latitude (*LT*) of the Local coordinate system is measured against the Equator.

The Aeroballistics coordinate frame (figure 5-9), is plane-fixed but utilises projectile body-axis . Aeroballistics coordinate system has *x* axis aligned with the projectile longitudinal axis of symmetry, positive in forward direction. The aeroballistics coordinates can pitch and yaw with the body, however it cannot roll with the body. One axis is always in vertical plane (in this case $\tilde{z}$ axis), and this assumption is made because of the high rotational speed (several order greater than other projectile's angular velocities) of spin-stabilised projectiles.

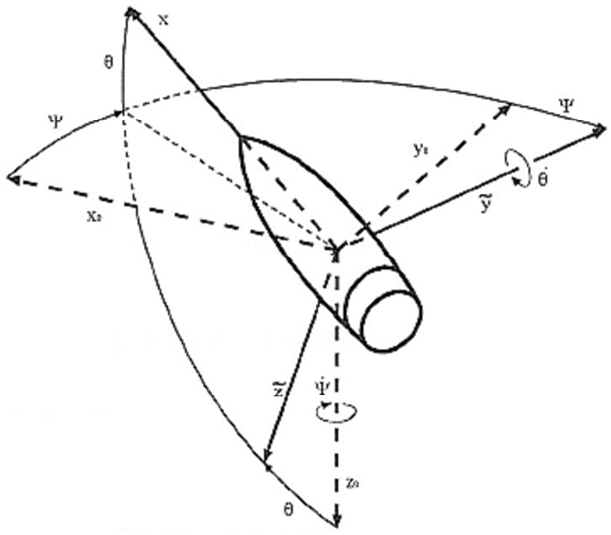

Figure 5-9 Aeroballistics coordinate system [22]

The fast spinning will interfere with numerical computations, as the gravity component projects itself onto aeroballistics coordinate frame, and it will be trailed-across the computations. This smearing of the gravitation force can be avoided by using very small time step for calculations, that in the other hand, drastically increase computation time. Body and Plane-Fixed coordinate systems travel with the projectile (figure 5-10), originate in the projectile centre of mass, but for Plain-fixed frame coordinate axes stay parallel to Local

coordinate system during flight (non-roll coordinate system). In Plain-fixed coordinate system, we are describing projectile motion around its centre of mass. Body-fixed coordinate frame has coordinate axes aligned with projectile inertial axes. In addition, to describe aerodynamic forces and moments, the "wind" or "aerodynamic" coordinate frame is used with the origin at the projectile's centre of the mass and $\bar{x}$ axis aligned with the resulting velocity vector.

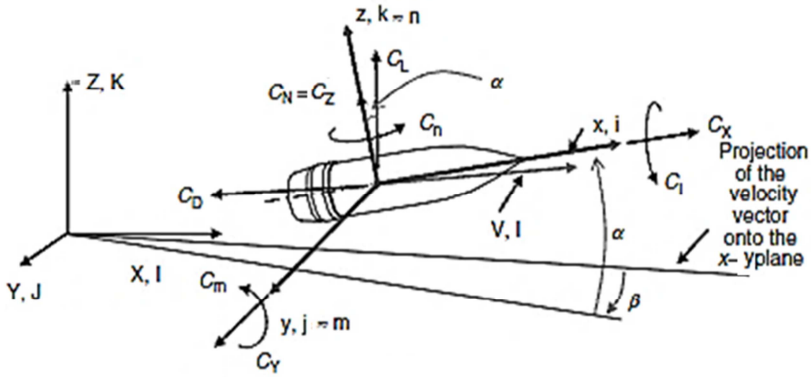

Figure 5-10 Physical model of the projectile [22,26]

Projectile's trajectory model is represented with four differential vector equation: a) derivation (relative) of position vector $\bar{r}$, b) vector equation of projectile centre of mass relative motion, c) vector equation of motion around the projectile's centre of mass, and d) relation between the angular velocities and angles derivation (system of eq. 5-1).

$$\begin{aligned}
&\dot{\vec{r}} = \frac{d\vec{r}}{dt} = \vec{V} \\
&m \cdot \ddot{\vec{r}} = m \cdot \frac{d\vec{V}}{dt} = \sum_{i=1}^{n} \vec{F}_i = \vec{R} + \vec{T}^F + m\vec{g} - 2 \cdot m \cdot \vec{\Omega}_E \times \vec{V} \\
&\frac{d\vec{H}}{dt} = \vec{M} + \vec{M}^F \\
&\vec{\Omega} = \vec{\Omega}_E + \dot{\vec{\lambda}}_{LT} + \dot{\vec{\varphi}}_{LA} + \dot{\vec{\phi}} + \dot{\vec{\theta}} + \dot{\vec{\psi}}
\end{aligned} \qquad \textbf{(5-1)}$$

The external forces that are defining motion of the M-REP are: aerodynamic forces summarised as vector $\vec{R}$, projectile thrust $\vec{T}^F$ (feature of M-REP), gravity $m\vec{g}$, and Coriolis force. As the Earth rotates around its Z axis,

velocity of the projectile's centre of mass $\vec{V}$, that is relative to the Earth, represents the velocity in moving coordinate system – "Local coordinate system". The Coriolis inertial force is vector product of the projectile relative velocity and rotational speed of the Earth: $-2 \cdot m \cdot \vec{\Omega}_E \times \vec{V}$, and value of angular velocity of Earth rotation is $\Omega_E = 7.27 \cdot 10^{-5}$ 1/s. The Coriolis force and the gravity force does not produce the moments as they are acting in the centre of the projectile's mass. Angular momentum $\vec{H}$, as well as the sum of aerodynamic moments $\vec{M}$ and sum of thrust moments $\vec{M}^F$ (novel feature of M-REP, comparing to the flight dynamics of standard free flight artillery projectile) have been reduced to the projectile centre of mass, with the same analogy. Usually, the angular velocity of the Plain-Fixed coordinate system relative to the Earth is equal to the Earth rotation Ω_E, as the components $\dot{\vec{\lambda}}_{LT} + \dot{\vec{\varphi}}_{LA}$ (transfer angular velocity) are negligible with regards to range of artillery projectiles. Further, value of Coriolis acceleration could be taken out from trajectory calculations of giro-stabilised projectiles, as for number of cases, for large spin-stabilised projectiles with range up to ~80 km, influence of Coriolis force is rather small. Therefore, the assumption can be made that the Earth is not moving (rotating) and projectile resultant velocity $\vec{V}$ is absolute velocity relative to the Earth.

In order to solve system of vector equations (eq. 5.1), equations need to be transformed into system of scalar equations, i.e. by projection of vector equations to coordinate axes of chosen coordinate systems (Local, Body-fixed, Plain-Fixed, Air-Path and Aeroballistics coordinate systems). The transformed system of scalar equations represents 6DOF trajectory model. The 6DOF trajectory model includes 12 basic differential equations (eq. system 5.2): first 6 equations are used to compute derivatives of projectile's translational and rotational velocities, following 3 equations describe relations between projectile's rotational velocities and derivatives of projectile's angular position with reference to the aeroballistics coordinate system. The last 3 eqautions (with reference in Local coordinate system) transform projectile's velocity from

Aeroballistics to Local coordinate system, in order to integrate data for Range, Altitude, and Drift.

$$\dot{u} = -q \cdot w + r \cdot v + \frac{T_{\tilde{X}}^{F} - R_{\tilde{X}}}{m(t)} - g \cdot \sin\theta - a_{Cor\tilde{X}}$$
$$\dot{v} = -r \cdot w \cdot tg\,\theta - r \cdot u + \frac{R_{\tilde{Y}} + T_{\tilde{Y}}^{F}}{m(t)} - a_{Cor\tilde{Y}}$$
$$\dot{w} = r \cdot v \cdot tg\,\theta + q \cdot u + \frac{R_{\tilde{Z}} + T_{\tilde{Z}}^{F}}{m(t)} + g \cdot \cos\theta - a_{Cor\tilde{Z}}$$

$$\dot{p} = \frac{M_{\tilde{X}} + M_{\tilde{X}}^{F}}{I_X(t)}$$
$$\dot{q} = -r^2 \cdot tg\,\theta + \frac{-I_X(t) \cdot p \cdot r + M_{\tilde{Y}} + M_{\tilde{Y}}^{F}}{I_Y} \qquad \textbf{(sys. eq. 5-2)}$$
$$\dot{r} = -r \cdot q \cdot tg\,\theta + \frac{I_X(t) \cdot p \cdot q + M_{\tilde{Z}} + M_{\tilde{Z}}^{F}}{I_Y(t)}$$

$$\dot{\phi} = p + r \cdot tg\,\theta$$
$$\dot{\theta} = q$$
$$\dot{\psi} = \frac{r}{\cos\theta}$$

$$\dot{x} = V_{X_L} = u \cdot \cos\theta \cdot \cos\psi - v \cdot \sin\psi + w \cdot \sin\theta \cdot \cos\psi$$
$$\dot{y} = V_{Y_L} = u \cdot \cos\theta \cdot \sin\psi + v \cdot \cos\psi + w \cdot \sin\theta \cdot \sin\psi$$
$$\dot{z} = V_{Z_L} = -u \cdot \sin\theta + w \cdot \cos\theta$$

Coriolis acceleration components in Aeroballistics coordinate system are calculated as follows:

Components of the Earth rotation in Aeroballistics coordinate system:

$$\Lambda_{\tilde{X}} = \Omega_E \cdot (\cos\theta \cdot \cos\psi \cdot \cos AZ \cdot \cos LT - \cos\theta \cdot \sin\psi \cdot \sin AZ \cdot \cos LT + \sin\theta \cdot \sin LT)$$
$$\Lambda_{\tilde{Y}} = \Omega_E \cdot (-\sin\psi \cdot \cos AZ \cdot \cos LT - \cos\psi \cdot \sin AZ \cdot \cos LT) \qquad \textbf{(5-3)}$$
$$\Lambda_{\tilde{Z}} = \Omega_E \cdot (\sin\theta \cdot \cos\psi \cdot \cos AZ \cdot \cos LT - \sin\theta \cdot \sin\psi \cdot \sin AZ \cdot \cos LT + \cos\theta \cdot \sin LT)$$

After transformations, components of the Coriolis acceleration in Aeroballistics coordinate system are described as follows:

$$\begin{aligned} a_{Cor\tilde{X}} &= 2 \cdot (-\Lambda_{\tilde{Z}} \cdot v + \Lambda_{\tilde{Y}} \cdot w) \\ a_{Cor\tilde{Y}} &= 2 \cdot (\Lambda_{\tilde{Z}} \cdot u - \Lambda_{\tilde{X}} \cdot w) \\ a_{Cor\tilde{Z}} &= 2 \cdot (-\Lambda_{\tilde{Y}} \cdot u + \Lambda_{\tilde{X}} \cdot v) \end{aligned} \qquad \textbf{(5-4)}$$

In order to calculate aerodynamic velocity of a projectile (velocity relative to the air), the components of the wind are transformed into Aeroballistics coordinate system. According to the flight mechanic practise, the assumption is made, that the wind is always horizontal, i.e. there is no vertical movement in the atmosphere.

$$\begin{aligned} u_W &= u - (V_W \cdot \cos AZ_W \cdot \cos\theta \cdot \cos\psi + V_W \cdot \sin AZ_W \cdot \cos\theta \cdot \sin\psi) \\ v_W &= v - (-V_W \cdot \cos AZ_W \cdot \sin\psi + V_W \cdot \sin AZ_W \cdot \cos\psi) \\ w_W &= w - (V_W \cdot \cos AZ_W \cdot \sin\theta \cdot \cos\psi + V_W \cdot \sin AZ_W \cdot \sin\theta \cdot \sin\psi) \end{aligned} \qquad \textbf{(5-5)}$$

Next step is to calculate the resulting velocity of the projectile required for calculation of aerodynamics forces and moments:

$$V = \sqrt{u_w{}^2 + v_w{}^2 + w_w{}^2} \qquad \textbf{(5-6)}$$

Respectively, projectiles pitch and yaw angles in aeroballistics coordinate system are:

$$\begin{aligned} \alpha &= arctg \frac{w_w}{u_w} \\ \beta &= \arcsin \frac{v_w}{V} \end{aligned} \qquad \textbf{(5-7)}$$

For small values of pitch and yaw angle, the total angle of attack in aeroballistics coordinate system is:

$$\alpha_t = \sqrt{\alpha^2 + \beta^2} \qquad \textbf{(5-8)}$$

Further step is to define the external forces acting upon the projectile in flight – aerodynamic drag, lift and side force, aerodynamic moments and thrust. For the M-REP, thrust can be ambiguous: thrust generated by SRM and "thrust" obtained by Base-Bleed. Thrust generated by the BB represent "difference" between the drag force in "gas bleed–on" or "gas bleed–off" mode. However, BB effect can be treated as part of aerodynamics, i.e. as component of aerodynamic drag coefficient. Thus for M-REP aeroballistics model, the thrust will be considered as thrust generated by the SRM only.

Definition of aerodynamic forces and moments for M-REP's dynamic equations of motion and gun-launched projectiles in general, are described in flowing Chapter 5.2.2. The, axial (drag) force with BB effect is described in detail in the Chapter 3.

5.2.2 Aerodynamic forces and moments acting at the M-REP projectile in motion

Total aerodynamic force $\vec{R}$ and total aerodynamic moment $\vec{M}$ are results of projectile motion through atmosphere, and in case of M-REP the contribution of BB effect to the aerodynamics of the projectile. Aerodynamics forces magnitude, direction, and position of centre of pressures depend largely on projectile geometry, as well as on projectile orientation relative to the free air-stream, air density, pressure, temperature, and atmospheric disturbances (wind). The resultant aerodynamic force $\vec{R}$ is sum of drag $\vec{D}$, lift $\vec{L}$ and side force $\vec{N}$ (Magnus Force). Other forces with random character are neglected, as their influence on the M-REP trajectory is negligible .

$$\vec{R} = \vec{D} + \vec{L} + \vec{N} \qquad \textbf{(5-9)}$$

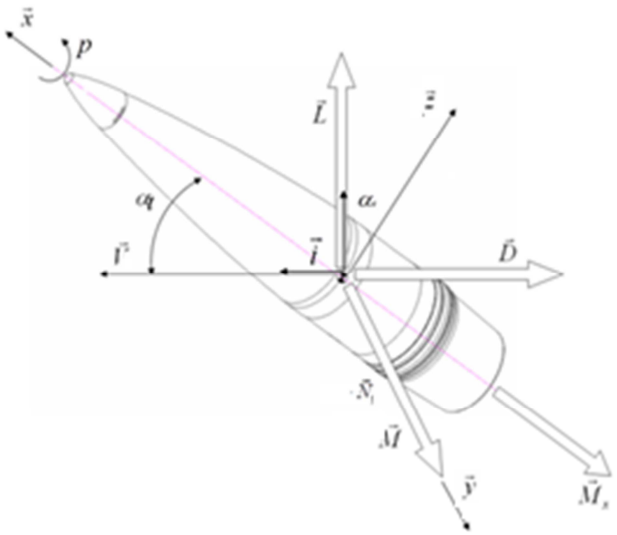

Figure 5-11 Aerodynamic forces and moments

Figure 5-11 represents aerodynamic model of projectile in flight, where direction of unit vector $\vec{x}$ in Body-Fixed or Aeroballistics coordinate system is angled to the projectile resulting velocity $\vec{V}$ by the angle α_t. Angle between $\vec{V}$ and $\vec{x}$, α_t represents projectile's total angle of attack.

Components of aerodynamic forces are represented as follows:

Drag – intensity of drag is usually described in aerodynamics as:

$$\vec{D} = -\frac{1}{2} \cdot \rho \cdot S_{ref} \cdot (C_{D0} + C_{D\alpha^2} \cdot \alpha_t^{\,2}) \cdot V \cdot \vec{V} \qquad \textbf{(5-10)}$$

The scalar value of the drag force is

$R_D = \frac{1}{2} \cdot \rho V^2 \cdot C_D \cdot S_{ref}$ in air-path coordinate system **(5-11)**

or, axial force

$R_{\tilde{X}} = \frac{1}{2} \cdot \rho \cdot V^2 \cdot C_X \cdot S_{ref}$ in aeroballistics coordinate system **(5-12)**

where are, reference area $S_{ref} = \frac{d_{ref}^{\,2} \cdot \pi}{4}$, and ρ – air density of free stream, d_{ref} – calibre (ref diameter of the projectile), V – resulting velocity of projectile's centre of mass, C_D – non-dimensional drag coefficient, C_X – non-dimensional axial force coefficient. The $\vec{V}$ represents the projectile's velocity

vector, direction of the drag force is aligned with vector $\vec{V}$ in projectile's "Aeroballistics" coordinate system. Although there is difference between the drag force coefficient and axial force coefficient, due to small value of total angle of attack α_t, for the trajectory calculations approximation of $C_X = -C_D$ is satisfactory.

The drag/axial force in Aeroballistics coordinate system is given as:

$$R_{\tilde{X}} = \frac{\rho \cdot V^2}{2} \cdot S_{ref} \cdot (C_{X_0} + C_{X_{\alpha^2}} \cdot \alpha_t^{\,2}) \qquad \textbf{(5-13)}$$

Angle of attack induces additional projectile drag, and drag magnitude is correlated with angle of attack - squared. Coefficient of induced drag is $C_{X\alpha^2}$, induced drag is result of asymmetrical airflow around projectile, intensity of induced drag is $C_{X_{\alpha^2}} \cdot \alpha^2$, thus drag coefficient is as follows:

$$C_X = C_{X_0} + C_{X_{\alpha^2}} \cdot \alpha_t^{\,2} \qquad \textbf{(5-14)}$$

Lift – projectile's aerodynamic lift is caused by asymmetric air flow around a projectile, when it flies under total angle of attack α_t. Lift intensity is equal to:

$$L = \frac{\rho \cdot V^2}{2} \cdot S_{ref} \cdot C_{\bar{L}\alpha} \cdot \sin(\alpha_t) \qquad \textbf{(5-15)}$$

where $C_{\bar{L}\alpha}$ - represents non-dimensional gradient of lift coefficient

Lift force acts in pitch plane of projectile motion ("angle of attack" plane) and it is perpendicular to the projectile direction of motion. Vector $\left[\vec{V} \times (\vec{x} \times \vec{V})\right]$, that describes lift force is perpendicular to velocity vector $\vec{V}$, i.e. belongs to the plane that is formed by $\vec{V}$ and $\vec{x}$, with intensity $V^2 sin(\alpha_t)$. Thus, lift in vector form is written as:

$$\vec{L} = \frac{\rho \cdot V^2}{2} \cdot S_{ref} \cdot C_{\bar{L}\alpha} \cdot \left[\vec{V} \times (\vec{x} \times \vec{V})\right] \qquad \textbf{(5-16)}$$

By aligning components of resulting aerodynamic force along directions of unit vectors relative to the projectile's geometry (i.e ,along vector $\vec{x}$ and perpendicular to $\vec{x}$ instead along direction of $\vec{V}$ and perpendicular to $\vec{V}$), then resulting aerodynamics force consists of axial and normal aerodynamics force . The Normal force is component that introduces projectile's overturning aerodynamic moment.

$$R_N = \frac{\rho \cdot V^2}{2} \cdot S_{ref} \cdot C_{\bar{N}\alpha} \cdot \sin(\alpha_t) \quad \textbf{(5-17)}$$

Normal force and axial force can be "mapped" into the selected coordinate system, for air-path or aeroballistics coordinate system transformation equations are as follows:

$$D = R_{\bar{N}} \cdot \sin(\alpha_t) - R_X \cdot \cos(\alpha_t) \quad \textbf{(5-18)}$$

$$L = R_{\bar{N}} \cdot \cos(\alpha_t) + R_X \cdot \sin(\alpha_t)$$

If we exclude the common multipliers in both equations, the aerodynamic coefficients can be represented as follows:

$$C_{\bar{D}} = C_{\bar{N}_\alpha} \cdot \sin^2(\alpha_t) - C_X \cdot \cos(\alpha_t) \quad \textbf{(5-19)}$$

$$C_{\bar{L}_\alpha} = C_{\bar{N}_\alpha} \cdot \cos(\alpha_t) + C_X$$

For small values of angle of attack, the relations between axial and drag coefficients, as well as for lift and normal force coefficients can be represented with:

$$C_{\bar{D}} \cong -C_X \quad \textbf{(5-20)}$$

$$C_{\bar{L}_\alpha} \cong C_{\bar{N}_\alpha} + C_X$$

Overturning moment - destabilising aerodynamic moment is result of projectile's aerodynamic lift not "passing" through the centre of projectile mass. Position of normal force vector for ogive shapes is closer to the projectile's nose, producing aerodynamic overturning moment. The moment arm represent distance between the projectile's centre of mass and centre of pressure – the "point" on projectile ogive where normal force acts. Intensity of overturning moment is calculated as follows:

$$C_{\bar{Z}\alpha} = -C_{\bar{N}\alpha} \quad \textbf{(5-21)}$$

$C_{\bar{Z}\alpha}$- normal force coefficient in “aeroballistics” coordinate system.

$$C_{\bar{m}\alpha} = -C_{\bar{Z}\alpha} \cdot (X_{CG} - X_{CP}) \quad \textbf{(5-22)}$$

where $C_{\bar{m}\alpha}$ represents non-dimensional gradient of overturning moment coefficient in “wind” coordinate system, and X_{CP} distance from the nose to the normal force centre of pressure and X_{CG} distance from the nose to the centre of mass, in calibres.

Overturning moment vector is perpendicular to the pitch plane ($\vec{V}$ and $\vec{x}$ plane) and direction is defined by vector product $\vec{V} \times \vec{x}$ with intensity of $Vsin(\alpha_t)$. Further overturning moment can be represented as:

$$\vec{M}_{\bar{Y}(C_{\bar{m}_\alpha})} = \rho \frac{\pi \cdot d_{ref}^{\,3}}{8} \cdot C_{\bar{m}\alpha} \cdot V \cdot (\vec{V} \times \vec{x}) \quad \textbf{(5-23)}$$

and it intensity as:

$$M_{\bar{Y}(C_{\bar{m}_\alpha})} = \rho \frac{\pi \cdot d_{ref}^{\,3}}{8} \cdot C_{\bar{m}\alpha} \cdot V^2 \cdot \sin(\alpha_t) \quad \textbf{(5-24)}$$

Spin (or roll) dumping moment – is result of viscous friction on the surface of rotational projectile. Spin dumping moment has effectively reduce spinning of a projectile (spinning around longitudinal axis).As the roll dumping moment is opposite to the axial rotation, its direction is aligned with unit vector $\vec{x}$. Vector equation of roll dumping moment is

$$\vec{M}_x = -\rho \frac{\pi \cdot d_{ref}^{\,4}}{16} \cdot C_{lp} \cdot p \cdot V \cdot \vec{x} \quad \textbf{(5-25)}$$

Intensity of the moment is written as:

$$M_x = \rho \frac{\pi \cdot d_{ref}^{\,4}}{16} \cdot C_{lp} \cdot p \cdot V \quad \textbf{(5-26)}$$

Where C_{lp} – represent non-dimensional gradient of roll dumping moment coefficient for referent angular velocity (spin rate) $C_{lp} = f(p^*)$, $p^* = \frac{p \cdot d_{ref}}{2 \cdot V}$

Pitch dumping moment occurs as result of transversal angular movement associated with yawing motion of the projectile, and aerodynamic resistance to that motion. The pitch dumping moment is associated with pitching velocity *q* and time derivation of the angle of attack (its rate of change) - $\dot{\alpha}_t = \frac{d\alpha_t}{dt}$.The pitch dumping moment in aerodynamic is represented as sum of two coefficients $(C_{\overline{m}\dot{\alpha}} + C_{\overline{m}q})$,i.e. sum of pitch dumping coefficient due to pitch velocity and pitch dumping coefficient due to angular velocity change (derivation) of the angle of attack:

$$M_{\tilde{Y}(C_{\overline{m}_{\dot{\alpha}}}+C_{\overline{m}_q})} = \rho\frac{\pi\cdot d_{ref}^{\ 3}}{8}\cdot V^2\cdot\left[\left(\frac{\dot{\alpha}_t\cdot d_{ref}}{V}\right)\cdot C_{\overline{m}_{\dot{\alpha}}} + \left(\frac{q\cdot d_{ref}}{V}\right)\cdot C_{\overline{m}_q}\right] \qquad \textbf{(5-27)}$$

However, as the $C_{\overline{m}\dot{\alpha}} << C_{\overline{m}q}$, usually the part related to the $\dot{\alpha}_t$ is negligible and the pitch dumping moment is given as:

$$M_{\overline{Y}_{(C_{\overline{m}_{\dot{\alpha}}}+C_{\overline{m}_q})}} = \rho\frac{\pi\cdot d_{ref}^{\ 3}}{8}\cdot V^2\cdot(C_{\overline{m}_{\dot{\alpha}}} + C_{\overline{m}_q})\cdot\left(\frac{q\cdot d_{ref}}{V}\right) \qquad \textbf{(5-28)}$$

As result of aerodynamic testing, the approximations of the pitch dumping moment coefficients are given in several forms with reference to the influencing parameters in coefficient weighting functions. Fitting function [21, 22] that covers most aerodynamic configurations of gun launched projectiles is given a :

$$(C_{\overline{m}\dot{\alpha}} + C_{\overline{m}q}) = \begin{cases} -2\cdot\left[C_{\overline{N}_\alpha}\cdot\left(X_{CG} - X_{CP}\right)^2 + 0.633\right] \rightarrow M > 1 \\ -2\cdot(0.77 + 0.23M^2)\cdot(L_P\cdot\sqrt{0.77 + 0.23M^2} - X_{CG}) \rightarrow M < 1 \end{cases} \qquad \textbf{(5-29)}$$

Side force and moment – Magnus force and moment. Magnus force **[21, 22]** occurs as result of viscous interaction between the surface of the projectile and air in boundary layer of spinning projectile, The interaction outcome is uneven pressure distribution around the projectile. The Magnus force act in the yaw plane, and it is referred as “side” force in aeroballistics coordinate system.

The Magnus force intensity is equal to:

$$R_{\bar{Y}_\alpha} = \frac{\rho \cdot V^2}{2} \cdot S_{ref} \cdot C_{\bar{Y}_{P\alpha}} \cdot \left(\frac{p \cdot d_{ref}}{2 \cdot V} \right) \cdot \sin(\alpha_t) \qquad \textbf{(5-30)}$$

where $C_{Y_{P\alpha}} = f(p^*)$ represents non-dimensional Magnus force coefficient reduced to non-dimensional angular velocity $p^* = \frac{p \cdot d_{ref}}{2 \cdot V}$, i.e. $C_{\bar{Y}\alpha} = C_{Y_{P\alpha}} \cdot \frac{p \cdot d_{ref}}{2V}$

As Magnus force (similar to the overturning moment, but in the yaw plane) does not “pass” through the centre of projectile’s mass, the induced moment is Magnus moment, or side force moment. The moment arm is distance between the centre of mass X_{CG} and centre of pressure of Magnus force $X_{NP.}$(distances measured from projectile’s nose)

$$C_{\bar{n}\alpha} = C_{\bar{Y}\alpha} \cdot (X_{CG} - X_{NP}) \qquad \textbf{(5-31)}$$

In most cases Magnus force is irrelevant for the trajectory calculations of spinning projectiles, as the force magnitude is very small, however resulting Magnus moment has profound influence on angular - swerving motion and dynamic stability of the projectile, and cannot be null out of the equations of motion

The Magnus moment intensity is equal to:

$$M_{\bar{Z}_{P\alpha}} = \rho \frac{\pi \cdot d_{ref}^{\ 3}}{8} \cdot V^2 \cdot (C_{\bar{n}_\alpha}) \cdot \left(\frac{p \cdot d_{ref}}{2 \cdot V} \right) \cdot \sin(\alpha_t) \qquad \textbf{(5-32)}$$

The approximations of the Magnus coefficients are given in the literature [22,26,103,107], in form of tabular data. The M-REP trajectory model incorporates calculation of Magnus moment.

The final set of aerodynamic equations required for the M-REP’s 6DOF trajectory model, i.e. the aerodynamic model in aeroballistics coordinate frame is given with following system of equations:

$$
\begin{aligned}
R_{\tilde{X}} &= \frac{\rho \cdot V^2}{2} \cdot S_{ref} \cdot (C_{X_0} + C_{X_{\alpha^2}} \cdot \alpha_t^{\,2}) \\
R_{\tilde{Y}} &= \frac{\rho \cdot V^2}{2} \cdot S_{ref} \cdot (C_{\bar{Y}_\alpha} \cdot \alpha + C_{\bar{Z}_\alpha} \cdot \beta) \\
R_{\tilde{Z}} &= \frac{\rho \cdot V^2}{2} \cdot S_{ref} \cdot (-C_{\bar{Y}_\alpha} \cdot \beta + C_{\bar{Z}_\alpha} \cdot \alpha) \\
M_{\tilde{X}} &= \frac{\rho \cdot V^2}{2} \cdot S_{ref} \cdot d_{ref} \cdot (C_{lp} \cdot p \cdot \frac{d_{ref}}{2 \cdot V}) \\
M_{\tilde{Y}} &= \frac{\rho \cdot V^2}{2} \cdot S_{ref} \cdot d_{ref} \cdot \left[C_{\bar{m}\alpha} \cdot \alpha + C_{\bar{n}\alpha} \cdot \beta + (C_{\bar{m}\dot{\alpha}} + C_{\bar{m}q}) \cdot q \cdot \frac{d_{ref}}{V}) \right] \\
M_{\tilde{Z}} &= \frac{\rho \cdot V^2}{2} \cdot S_{ref} \cdot d_{ref} \cdot \left[-C_{\bar{m}\alpha} \cdot \beta + C_{\bar{n}\alpha} \cdot \alpha + (C_{\bar{m}\dot{\alpha}} + C_{\bar{m}q}) \cdot r \cdot \frac{d_{ref}}{V}) \right]
\end{aligned}
\qquad \textbf{(5-33)}
$$

5.2.3 Trajectory modelling for optimization of base bleed effect and additional propulsion

Optimization of base bleed unit and optimization of additional propulsion module for M-REP represent inverse task for exterior ballistic calculations. The input parameter is desired range and output from calculations are required size of base bleed propellant grain and total impulse of SRM. Beside BB and SRM parameters algorithm requires mathematical modelling to estimate projectile stability and to find optimal method to reduce dispersion on target. Therefore optimization algorithm should use most appropriate method that provides fast convergence toward solution, in this case it is modified point mass trajectory model [84, 107-114] that ,includes calculation of yaw of repose vector or approximate angle of yaw [26, 109, 112, 114]. Angle yaw of repose has profound influence on projectile stability and dispersion. Further, in order to validate results of optimization, the stability of M-REP are validated by calculating total angle of attack and gyroscopic and dynamics stability factors [26] using 6DOF trajectory model, as well as median angle of nutation δ_r [110, 111], i.e. angle between velocity vector and the axis of projectile's dynamic balance if it is not aligned with projectile axis of symmetry. The modified point mass trajectory model is assembled for fast calculation of base bleed effect on

the trajectory as well as for estimation of required rocket thrust and effect of SRM ignition delay.

The MPTM [84, 112-114] includes in calculations all significant aerodynamics forces and moments with addition of spin imparted by gun riffling (figure 5-11).

The following conditions are assumed for MPMT:

- Projectile represents rigid body of revolution geometrical axis of symmetry is aligned with projectile's dynamic balance axis of inertia;
- Projectile is dynamically stable (S_d>1) – in order to check the dynamic stability we can use following equation [22,26,84, 107-114]:
- $$S_d = \frac{2 \cdot \left(C_{L_\alpha} + \frac{m(t) \cdot d_{ref}^{\,2}}{2 \cdot I_x(t)} \cdot C_{n\alpha} \right)}{C_{L_\alpha} - C_D - \frac{m(t) \cdot d_{ref}^{\,2}}{2 \cdot I_y(t)} \cdot (C_{m\dot{\alpha}} + C_{mq})}$$ **(5-34)**
- Initial total angle of attack at the gun muzzle, is negligible and its influence on the projectile trajectory is insignificant.

Furthermore, direction of projectile motion is determined by unit vector $\vec{i} = \frac{\vec{V}}{V}$ (fig 5-11). The $\vec{i}$ originate in projectile's centre of mass and it is aligned with resulting velocity vector $\vec{V}$ (projectile velocity in "wind" coordinate system). Then $\left| \vec{x} \times \vec{i} \right| = \sin(\alpha_t) = \alpha_t$, which is valid for first order approximation and small angles of attack. However for the higher order and to estimate larger yaw angles, vector of yaw of repose is more appropriate. The vector has same direction and orientation as lift force. i.e yaw of repose vector orientation is defined as vector product:

$$\vec{\alpha}_e = \vec{i} \times (\vec{x} \times \vec{i}) = \vec{x} - \cos(\alpha_t) \cdot \vec{i} \qquad \textbf{(5-35)}$$

as $\vec{\alpha}_e \perp \vec{i}$, i.e. they are perpendicular vectors, then their product is $\vec{\alpha}_e \cdot \vec{i} = 0$, i.e. the yaw of repose vector is oriented from $\vec{i}$ to $\vec{x}$ (right thumb rule). Assuming that rate of change of total angle of attack $\dot{\vec{\alpha}}_t$ is negligible as

explained in relation to eq. 5-28, i.e. $\dot{\alpha}_t \approx 0$, $\ddot{\alpha}_t \approx 0$ by differentiating eq. 5-35, the following relations are written:

$$\dot{\vec{x}} = \cos(\alpha_t) \cdot \dot{\vec{i}} \;\; ; \;\; \ddot{\vec{x}} = \cos(\alpha_t) \cdot \ddot{\vec{i}} \qquad \textbf{(5-36)}$$

In order to determine vector of angle of yaw of repose we can use system of equation 5-1 – equations of projectile motion. As pitch angular velocity several order of magnitude smaller then projectile spin rate , i.e.we can neglect transversal component of momentum, that why the total momentum can be represented as:

$$\vec{H} = I_x \cdot p \cdot \vec{x} \qquad \textbf{(5-37)}$$

Momentum equation from equations system 5-1 becomes:

$$\frac{d\vec{H}}{dt} = I_x \cdot \frac{dp}{dt} \cdot \vec{x} \; + I_x \cdot p \cdot \dot{\vec{x}} \; = \vec{M}_x + \vec{M}_x^F + \vec{M}_{\bar{Y}(C_{\bar{m}_\alpha})} + \vec{M}_{\tilde{Y}(C_{\bar{m}_{\dot{\alpha}}} + C_{\bar{m}_q})} \qquad \textbf{(5-38)}$$

Projectile spin gradually slowdown as result of roll dumping moment M_x, this phenomenon is order of magnitude slower than change of pitch angle due to overturning moment, The active de-spinning by SRM - M^F_x influences the change of kinetic momentum, however does it is acting in very short period of time in comparison with overall flight time of the projectile. Pitch dumping moment is insignificant in comparison to overturning moment, thus eq. 5-38 can be simplified as follows:

$$\frac{d\vec{H}}{dt} = I_x \cdot p \cdot \dot{\vec{x}} = \vec{M}_{\bar{Y}(C_{\bar{m}_\alpha})} \text{ during the “passive” phase of flight}$$
$$\frac{d\vec{H}}{dt} = I_x \cdot \frac{dp}{dt} \cdot \vec{x} \; + I_x \cdot p \cdot \dot{\vec{x}} \; = \vec{M}_x^F + \vec{M}_{\bar{Y}(C_{\bar{m}_\alpha})} \text{, active SRM de-spin} \qquad \textbf{(5-39)}$$

For “passive” flight phase equation 5-39 is given as :

$$I_x \cdot p \cdot \dot{\vec{x}} \; = \rho \frac{\pi d^3}{8} \cdot C_{\bar{m}\alpha} \cdot V \cdot (\vec{V} \times \vec{x}) \qquad \textbf{(5-40)}$$

Inclusion of eq. 5-35 and eq. 5-36 in eq 5-40 produces: :

$$I_x \cdot p \cdot \cos(\alpha_t) \cdot \dot{\vec{i}} = \rho \frac{\pi d^3}{8} \cdot C_{\bar{m}\alpha} \cdot V \cdot \left[\vec{V} \times (\vec{\alpha}_e + \cos(\alpha_t) \cdot \vec{i})\right] \qquad \textbf{(5-41)}$$

Since $\left[\vec{V} \times (\vec{\alpha}_e + \cos(\alpha_t) \cdot \vec{i})\right] = \vec{i} \times \vec{\alpha}_e$, therefore eq. 5-41 is written as follows:

$$\vec{\alpha}_e \times \vec{I} = -\frac{8 \cdot I_x \cdot p \cdot \cos(\alpha_t)}{\rho \pi d^3 \cdot C_{\bar{m}\alpha} \cdot V_r^2} \cdot \dot{\vec{I}} \quad \textbf{(5-42)}$$

Arranging and manipulating eq. 5 - 42 it becomes:

$$\vec{\alpha}_e = -\frac{8 \cdot I_x \cdot p \cdot \cos(\alpha_t)}{\rho \pi d^3 \cdot C_{\bar{m}\alpha} \cdot V^4} \cdot (\vec{V} \times \dot{\vec{V}}) \quad \textbf{(5-43)}$$

For small angles of total attack $\cos(\alpha_t) = 1$, therefore:

$$\vec{\alpha}_e = -\frac{8 \cdot I_x \cdot p}{\rho \pi d^3 \cdot C_{\bar{m}\alpha} \cdot V_r^4} \cdot (\vec{V} \times \dot{\vec{V}}) \quad \textbf{(5-44)}$$

Velocity is difference between absolute velocity of projectiles centre of mass in aeroballistics coordinate system and atmospheric wind

$$\vec{V} = \vec{V}_a - \vec{W} \quad \textbf{(5-45)}$$

$$\dot{\vec{V}} = \dot{\vec{V}}_a - \dot{\vec{W}} \quad \textbf{(5-46)}$$

$\vec{W}$, $\dot{\vec{W}}$, - represent wind's velocity and wind acceleration vectors.

Wind intensity, direction and orientation is measured with meteorological "probe" that supplies "raw" atmospheric data (wind profile vs. altitude). By knowing the wind data we can calculate wind disturbances along the projectile trajectory. However, for the calculation purposes, the "median" or "mean" ballistic wind is used for finding the firing corrections (for range and deflection). Another assumption is that wind is horizontal do not have vertical component of the velocity. Furthermore, wind is relatively constant phenomenon in time (relative to time of flight), therefore wind acceleration $\dot{\vec{W}}$ is irrelevant, i.e. $\dot{\vec{V}}_r = \dot{\vec{V}}$.

Regarding firing projectile in real conditions, wind is stochastic atmospheric phenomenon, so wind's intensity, direction and orientation are changing along flight trajectory. Vector of angle of yaw of repose $\vec{\alpha}_e$ represents qualitative parameter of the projectile's trajectory, especially for projectiles with base bleed unit and solid rocket motor. Thereafter, to establish the trajectory model for optimization of base bleed and rocket motor parameters system of equation must be set as follows:

Equation of Motion for projectile's centre of mass including aerodynamic forces and thrust:

$$m(t)\cdot\frac{d\vec{V}}{dt}=-\rho\frac{\pi d^2}{8}\cdot(C_{D0}+C_{D\alpha^2}\cdot\alpha_d^2)\cdot V\cdot\vec{V}+\rho\frac{\pi d^2}{8}\cdot C_{L\alpha}\cdot V^2\cdot\vec{\alpha}_e+m\cdot\vec{g}+\vec{T} \quad \textbf{(5-47)}$$

Equation of approximation of vector of yaw of repose:

$$\vec{\alpha}_e=-\frac{8\cdot I_x\cdot p}{\rho\pi d^3\cdot C_{\bar{m}\alpha}\cdot V^4}\cdot(\vec{V}\times\dot{\vec{V}}) \quad \textbf{(5-48)}$$

Projectile's spin:

$$I_x(t)\cdot\frac{dp}{dt}\cdot\vec{x}=-\rho\frac{\pi d^4}{16}\cdot C_{lp}\cdot p\cdot V\cdot\vec{x}+\vec{T}_L \quad \textbf{(5-49)}$$

Relative air velocity:

$$\vec{V}=\vec{V}_a-\vec{W} \quad \textbf{(5-50)}$$

Position vector relative to the Fixed Plane (Earth) Coordinate system:

$$\dot{\vec{r}}=\vec{v} \quad \textbf{(5-51)}$$

Position vector in Fixed Plane Coordinate system, absolute velocity and acceleration are:

$$\vec{r}=x\vec{i}+y\vec{j}+z\vec{k}$$

$$\vec{V}_a=V_x\vec{i}+V_y\vec{j}+V_z\vec{k} \quad \textbf{(5-52)}$$

$$\frac{d\vec{V}_a}{dt}=\dot{V}_x\vec{i}+\dot{V}_y\vec{j}+\dot{V}_z\vec{k}$$

Wind vector is equal to:

$$\vec{W}=W_x\vec{i}+W_y\vec{k} \quad \textbf{(5-53)}$$

Wind component *Wz* is zero under presumption that vertical movements in atmosphere are negligible. Final system of equation adopted for solving with numerical methods in Fixed Plane Coordinate system is:

$$\dot{V}_x=-\rho\frac{\pi d^2}{8\cdot m(t)}\cdot(C_{D0}+C_{D\alpha^2}\cdot\alpha_e^2)\cdot V\cdot(V_x-W_x)+\rho\frac{\pi d^2}{8}\cdot C_{L\alpha}\cdot V^2\cdot(-\frac{8\cdot I_x(t)\cdot p}{\rho\pi d^3\cdot C_{\bar{m}\alpha}\cdot V^4})\cdot\left[V_z\cdot\dot{V}_y-(V_y-W_y)\cdot\dot{V}_z\right]+\frac{T_x}{m(t)}$$

$$\dot{V}_y=-\rho\frac{\pi d^2}{8\cdot m(t)}\cdot(C_{D0}+C_{D\alpha^2}\cdot\alpha^2)\cdot V\cdot(V_y-W_y)+\rho\frac{\pi d^2}{8}\cdot C_{L\alpha}\cdot V^2\cdot(-\frac{8\cdot I_x(t)\cdot p}{\rho\pi d^3\cdot C_{\bar{m}\alpha}\cdot V^4})\cdot\left[(V_x-W_x)\cdot\dot{V}_z-V_z\cdot\dot{V}_x\right]+\frac{T_y}{m(t)}$$

$$\dot{V}_z=-\rho\frac{\pi d^2}{8\cdot m(t)}\cdot(C_{D0}+C_{D\alpha^2}\cdot\alpha_d^2)\cdot V\cdot V_y+\rho\frac{\pi d^2}{8}\cdot C_{L\alpha}\cdot V^2\cdot(-\frac{8\cdot I_x(t)\cdot p}{\rho\pi d^3\cdot C_{\bar{m}\alpha}\cdot V^4})\cdot\left[(V_y-W_y)\cdot\dot{V}_x-(V_x-W_x)\cdot\dot{V}_y\right]-g+\frac{T_z}{m(t)}$$

$$V = \sqrt{(V_x - W_x)^2 + (V_y - W_y)^2 + V_z^2}$$

$$V_a = \sqrt{V_x^2 + V_y^2 + V_z^2}$$

$$\alpha_e = \left(-\frac{8 \cdot I_x(t) \cdot p}{\rho \pi d^3 \cdot C_{\overline{m}\alpha} \cdot V_e^4}\right) \cdot \sqrt{\left[V_z \cdot \dot{V}_y - (V_y - W_y) \cdot \dot{V}_z\right]^2 + \left[(V_y - W_y) \cdot \dot{V}_x - (V_x - W_x) \cdot \dot{V}_y\right]^2 + \left[(V_x - W_x) \cdot \dot{V}_z - V_z \cdot \dot{V}_x\right]^2}$$

$$\dot{X} = V_x$$

$$\dot{Y} = V_y$$

$$\dot{Z} = V_z$$

$$\dot{p} = -\rho \frac{\pi d^4}{16 \cdot I_x(t)} \cdot C_{lp} \cdot V \cdot p + \frac{T_L}{I_x(t)}$$

Aerodynamic coefficients required for trajectory calculation can be obtained from experimental and semi-empirical methods and equations [16-29, 32-38,41-47,107-114]. The Aerodynamic coefficients should be calculated for entire range of projectile's Mach numbers.

With presented model for trajectory calculation (modified point mass), it is possible to obtain all significant parameters of projectile flight, including the parameters that are related to the base bleed combustion along the trajectory. Numerical method for calculation is chosen in way that the fast and accurate calculation of trajectory parameters can be obtained. Additional correction factors can be derived from experiments as it is presented in Third and Fourth Chapter.

5.2.4 Exterior Ballistics Results

Table 5-1 Mass and geometry model input:

Mass	Transverse Inertia	Axial Inertia	CG from Nose	Diameter
kg	kg-m^2	kg-m^2	mm	mm
Flight Vehicle (at muzzle):				
49.77621	2.071840	0.1710571	578.1742	154.7400
Flight Vehicle: (after burnout)				
44.96712	1.904437	0.1618871	594.7363	154.7400

Table 5-2 Aerodynamic Features of the Flight Vehicle:

Projectile Length	920.9 mm
Ogive Length	543.2 mm
Ogive Radius	4000 mm
Meplat Diameter	10.7 mm
Boattail Length	114.2 mm
Boattail Diameter	141.286 mm
Rotating Band Length	37.08 mm
Rotating Band Diameter:	157.582 mm

Results of the basic Aerodynamics calculations [8,25, 38, 79,108]:

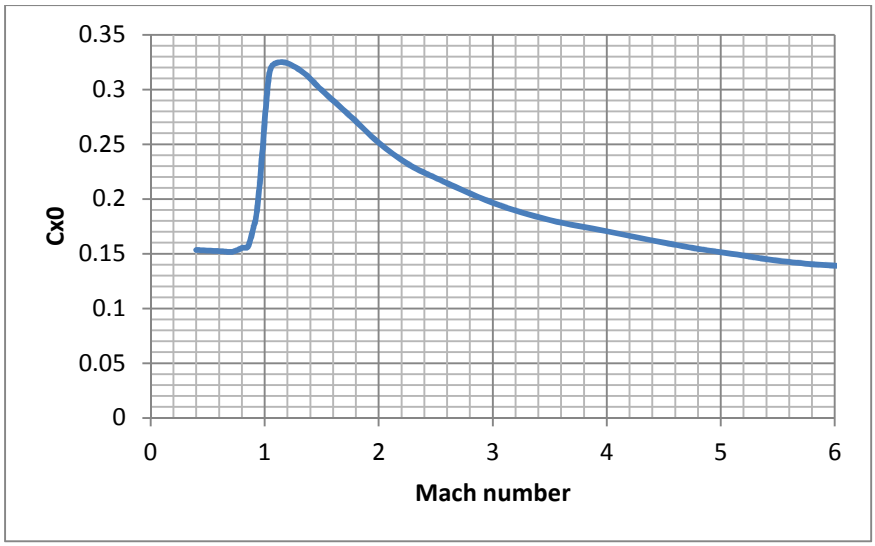

Figure 5-12 Diagram Zero Yaw Drag Vs. Mach number

The input parameters for calculations as well as the output from PRODAS [79] calculations can be found in Appendix A. For base drag reduction, Base Drag Cx_B coefficient is calculated using analytical equations [25], and method for $Cx_{B\text{-}BB}$ is derived from theory and experiments [38], as presented in Third Chapter. The difference ΔCxB required for trajectory calculations is presented on next diagram. Figure 5-13 shows ΔCx_B for muzzle velocities 835m/s and 921m/s. The calculations are made in FORTRAN program designed to calculate drag reduction for given flight trajectory.

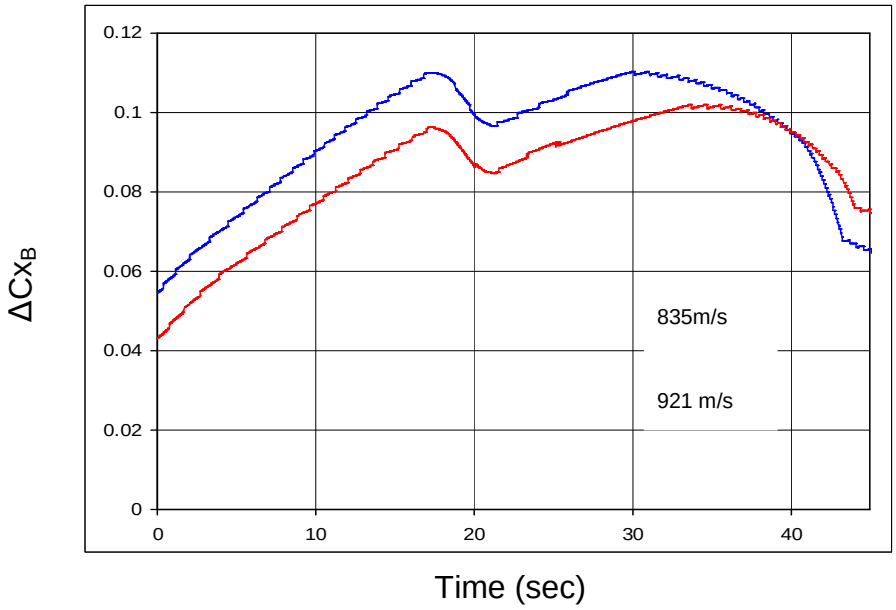

Figure 5-13 ΔCx_B v.s time (sec)

Stability for the projectile is calculated using the equations related to the Spin Stabilised Projectiles Stability Analysis, according to the PRODAS [79,108] and references [5,22,26,79, 108-114]:

The gyroscopic stability factor, is as follows:

$$S_g = \left(\frac{I_x}{I_x}\right)\left(\frac{p \cdot d_{ref}}{V}\right)^2\left(\frac{2 \cdot I_x}{\rho \cdot \pi \cdot d^5{}_{ref} \cdot C_{\overline{m}\alpha}}\right) > 1 \qquad \textbf{(5-64)}$$

At gun muzzle, the value of the gyroscopic stability factor should be within limits $1.5<S_g<3.5$ (recommended values) [5,26]. The gyroscopic stability factor represents least but not last condition for stable flight of spin-stabilised projectiles. For stable flight, dynamic stability factor S_d (equation 5-36) should be calculated and the value required for stable flight is given by following inequality $\mathbf{1/S_g < S_d(2-S_d)}$ [22,26,107]. Dynamic stability factor S_d should be in range $0<S_d<2$ (for gyro-static stable projectile). Furthermore, max. angle of yaw of repose, angle of dynamic equilibrium δ_p (precession angle) or total angle of α_t should be less than $\alpha_t < 2^0(4^0)$ – on the muzzle ore at the apogee respectively.

$$\delta_p = \frac{2 \cdot I_x \cdot p \cdot g \cdot \cos\gamma}{\rho \cdot V^3 S_{ref} \cdot d \cdot C_{\overline{m}\alpha}} \qquad \textbf{(5-65)}$$

For the given initial firing conditions, stability factors are calculated with in developed FORTRAN MPMT and 6 DOF trajectory codes. Few representative flight cases are presented with 6DOF calculations results. The time delay and active control of projectile stability factors are presented on diagrams from 5-14 to 5-25, as provide insight in the methodology of M-REP trajectory optimisation

Results for 6DOF trajectory calculations for optimal elevation angles of firing (max. ranges) and maximum gun charges, are as follows:

- 39 calibre gun, muzzle velocity 835m/s, standard atmosphere conditions, H=0m - sea level, time delay -18s, without active de-spinning, 50 deg elevation
- 52 calibre gun, muzzle velocity 921 m/s, standard atmosphere conditions, H=0m - sea level, time delay -18s, without active de-spinning, 54 deg elevation
- 52 calibre gun, muzzle velocity 921 m/s, standard atmosphere conditions, H=0m - sea level, time delay -31s, with active de-spinning, 54 deg elevation

Further the trajectory model and stability calculations are validated by comparing results with PRODAS [79] output for same firing conditions. The 6DOF fixed plain trajectory calculations in PRODAS are used, with input for Base Bleed effect (base drag reduction) made in separate FORTRAN program, that calculates base drag reduction on the trajectory for given Base Bleed and SRM configuration. Results from PRODAS [79, 108] software are presented in Appendix A

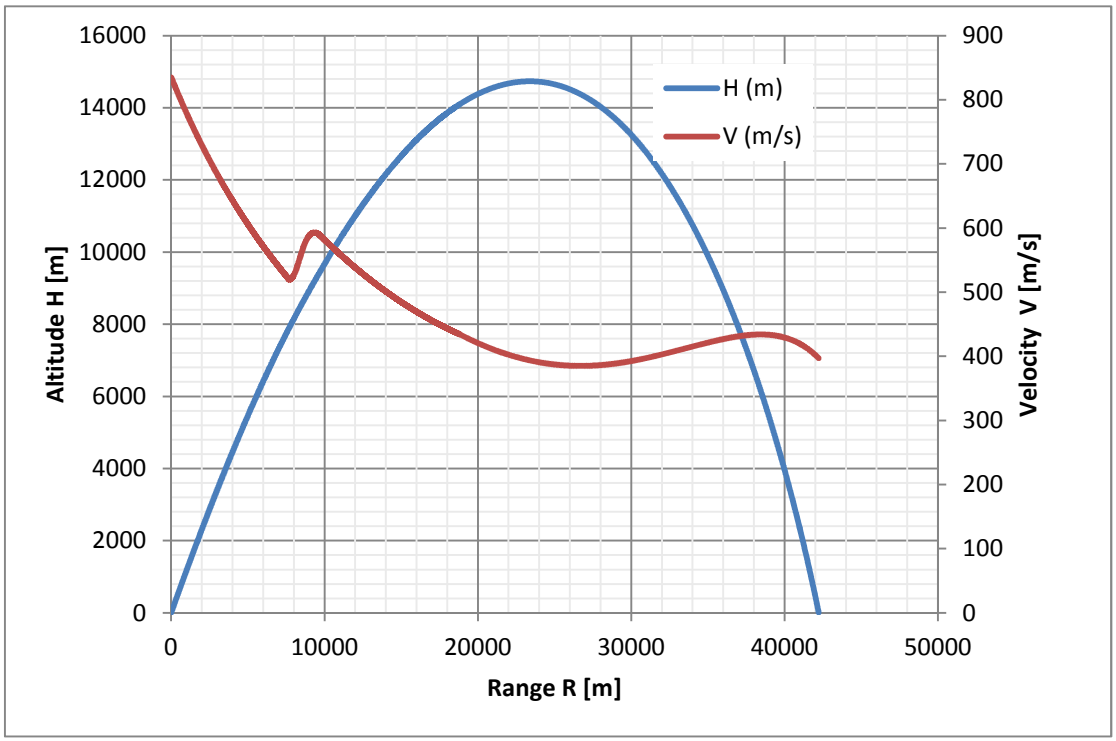

Figure 5-14 Range vs. Altitude, Velocity, 39 calibre gun, max. range

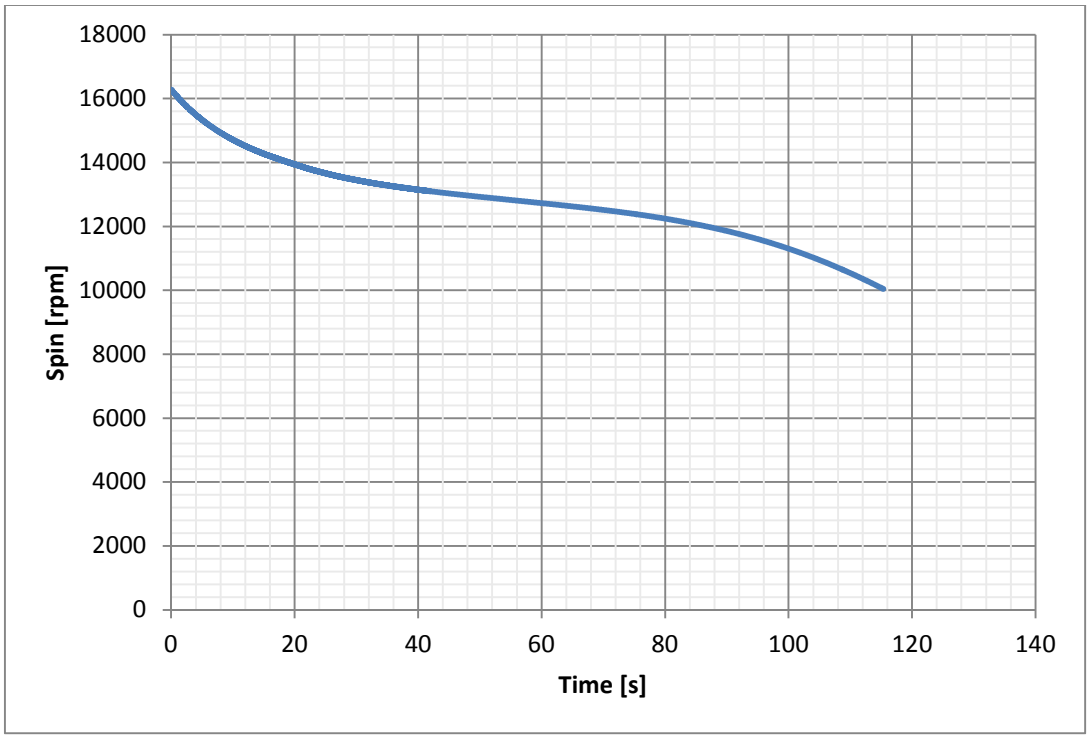

Figure 5-15 Time vs. Spin, 39 calibre gun, max. range

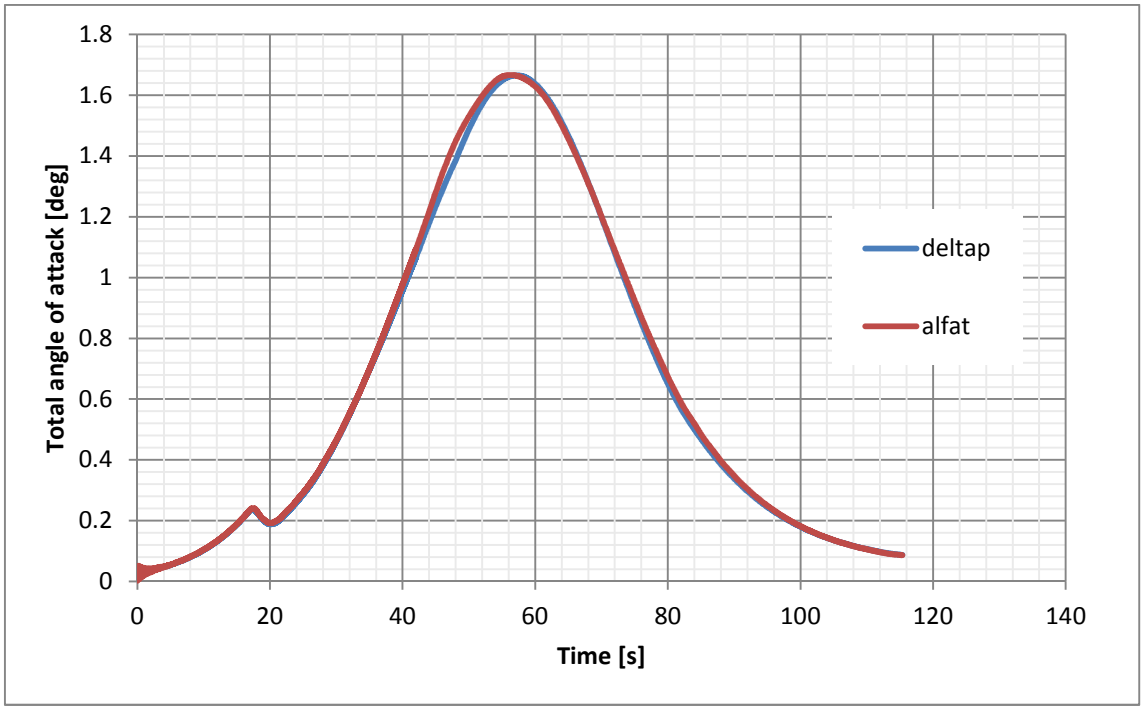

Figure 5-16 "Total" angle of attack history, 39 calibre gun, max. range

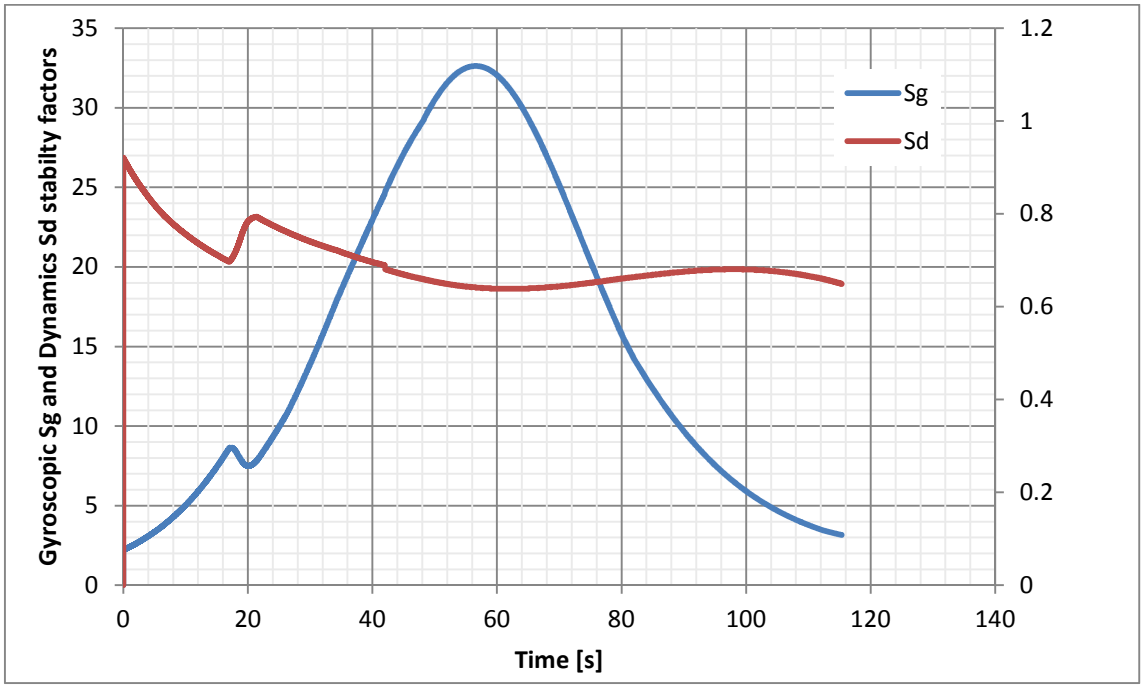

Figure 5-17 Gyro and Dynamic stability factor history, 39 calibre gun, max. range

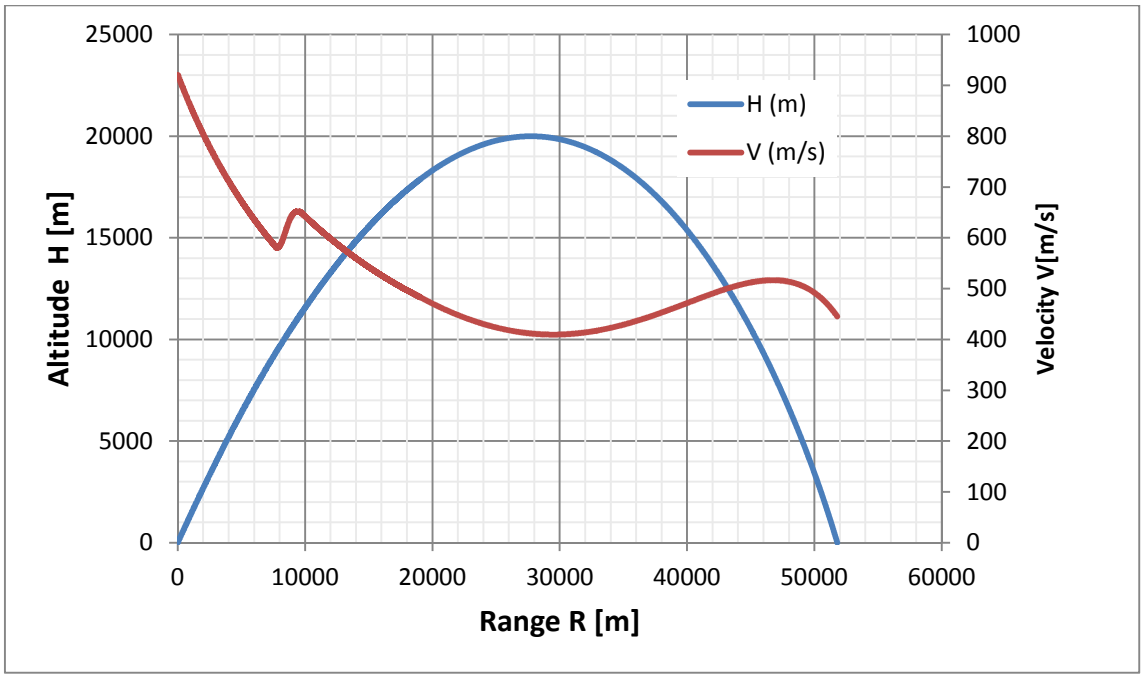

Figure 5-18 Range vs. Altitude, 52 calibre gun, max. range, std. atmos., time delay 18 s, no de-spinning

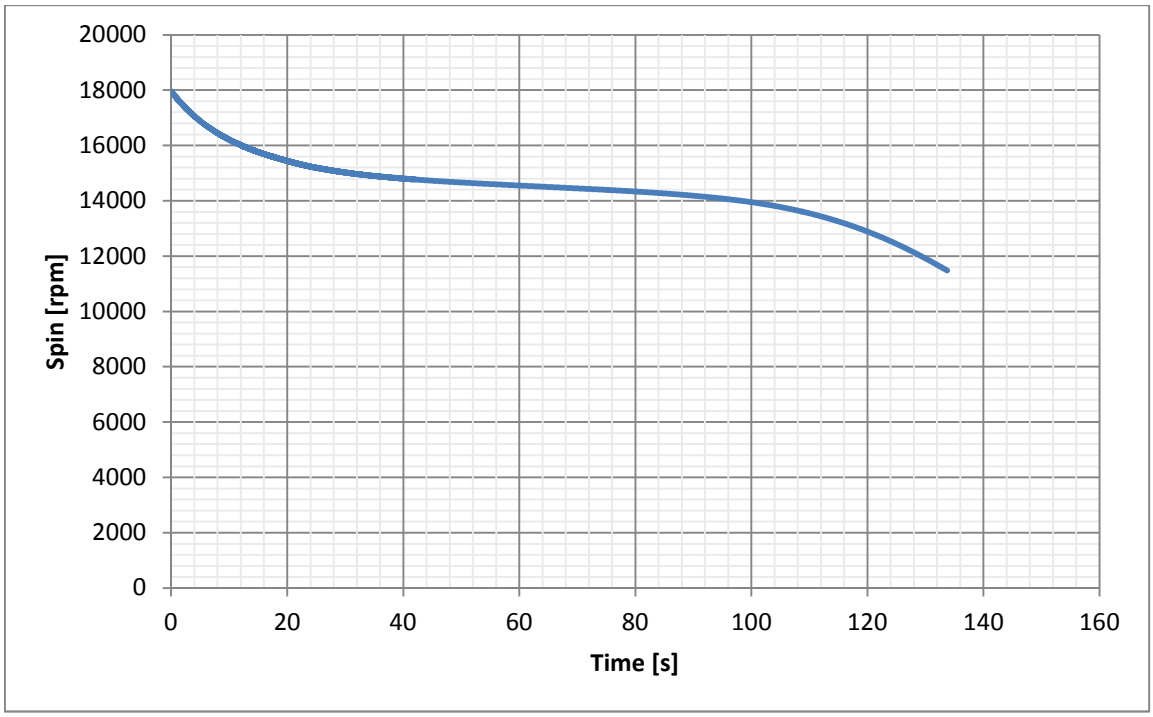

Figure 5-19 Spin history, 52 calibre gun, max. range, std. atmos., time delay 18 s, no de-spinning.

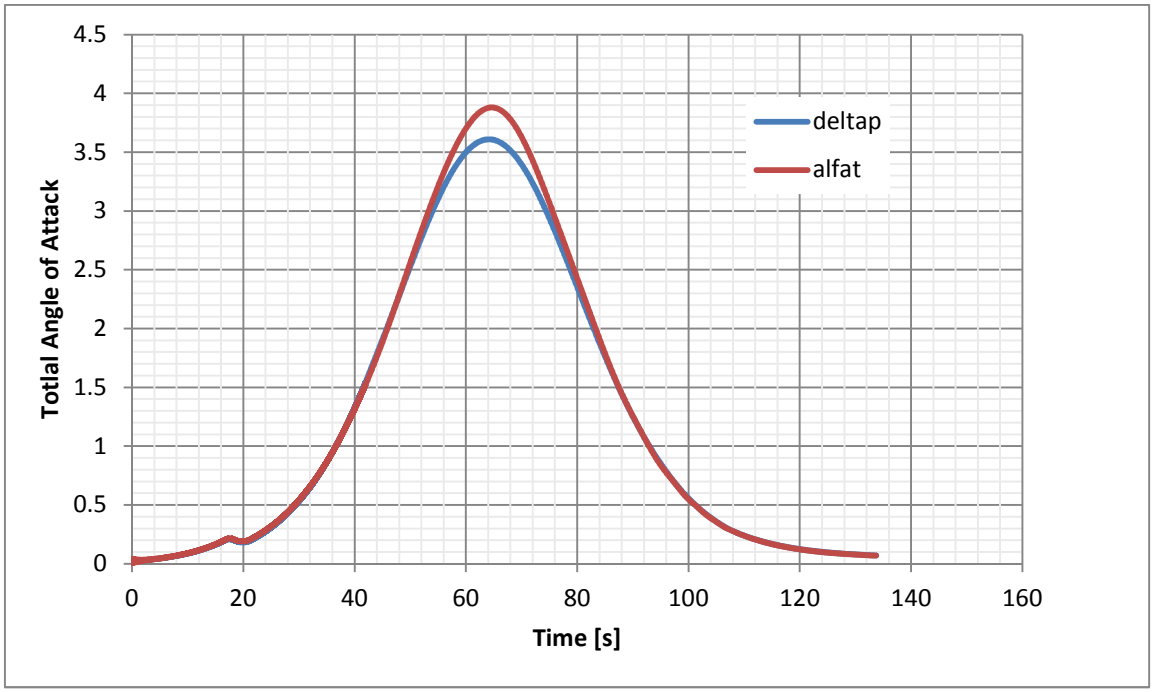

Figure 5-20 "Total" angle of attack history, 52 calibre gun, max. range, std. atmos., time delay 18 s, no de-spinning

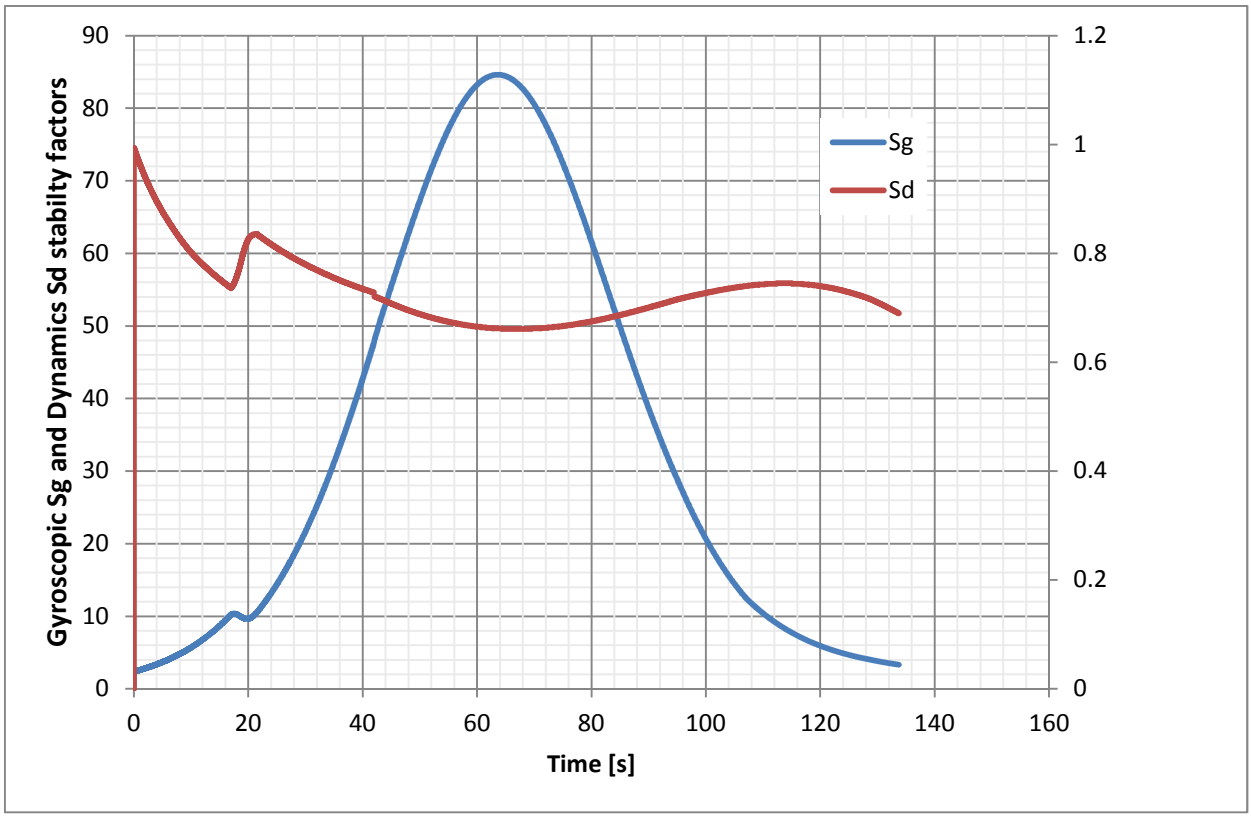

Figure 5-21 Gyro and Dynamic stability factor history, 52 calibre gun, max. range, std. atmos., time delay 18 s, no de-spinning

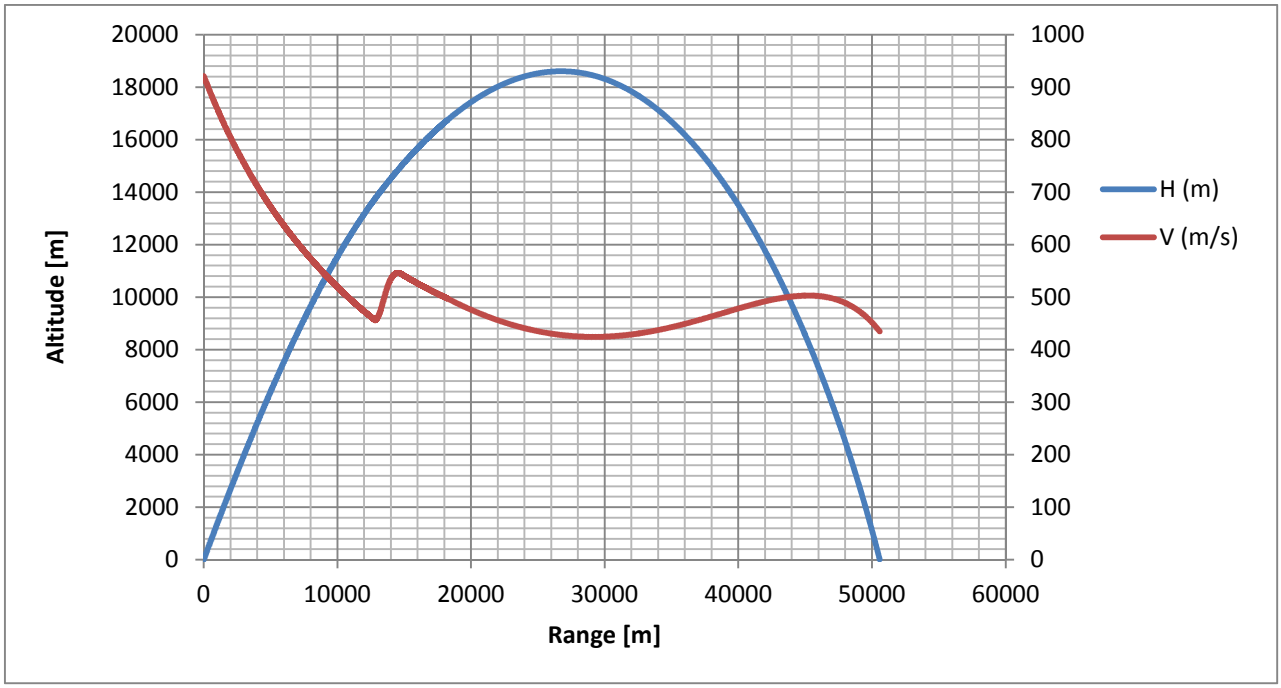

Figure 5-22 Range vs. Altitude, 52 calibre gun, max. range, std. atmos.,time delay 31 s, active de-spinning

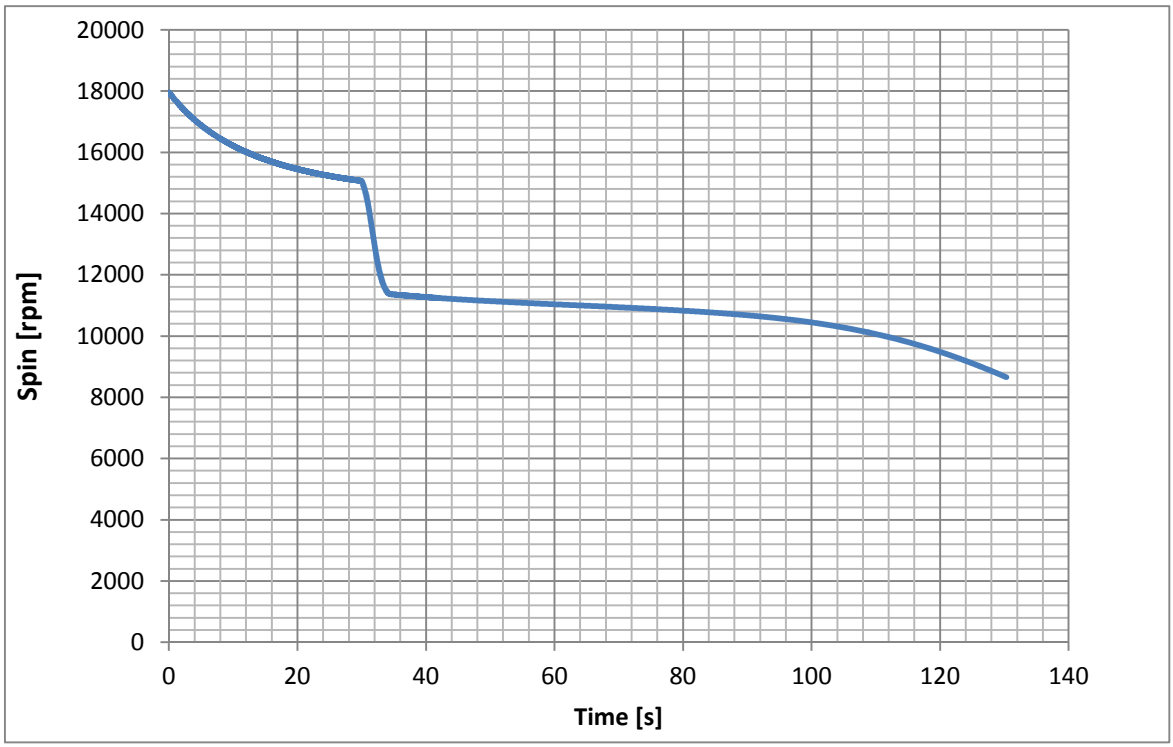

Figure 5-23 Spin history, 52 calibre gun, max. range, std. atmos., time delay 31 s, active de-spinning.

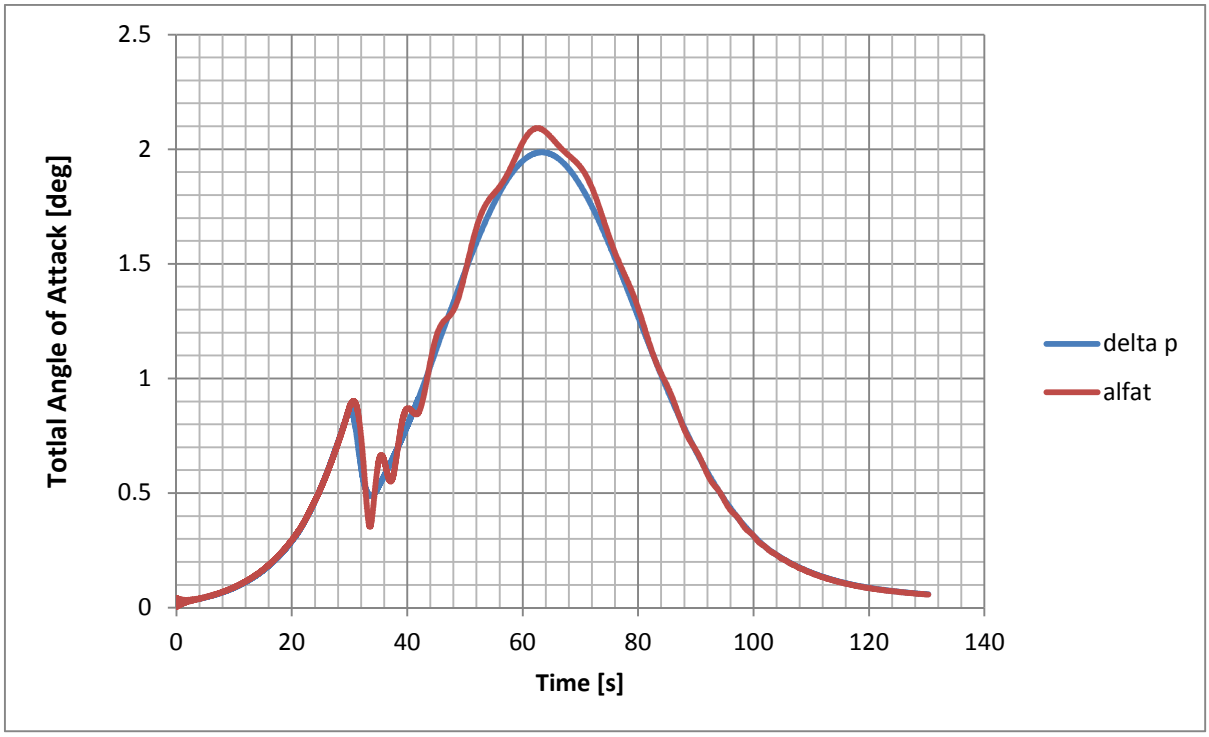

Figure 5-24 "Total" angle of attack history, 52 calibre gun, max. range, std. atmos., time delay 31 s, active de-spinning.

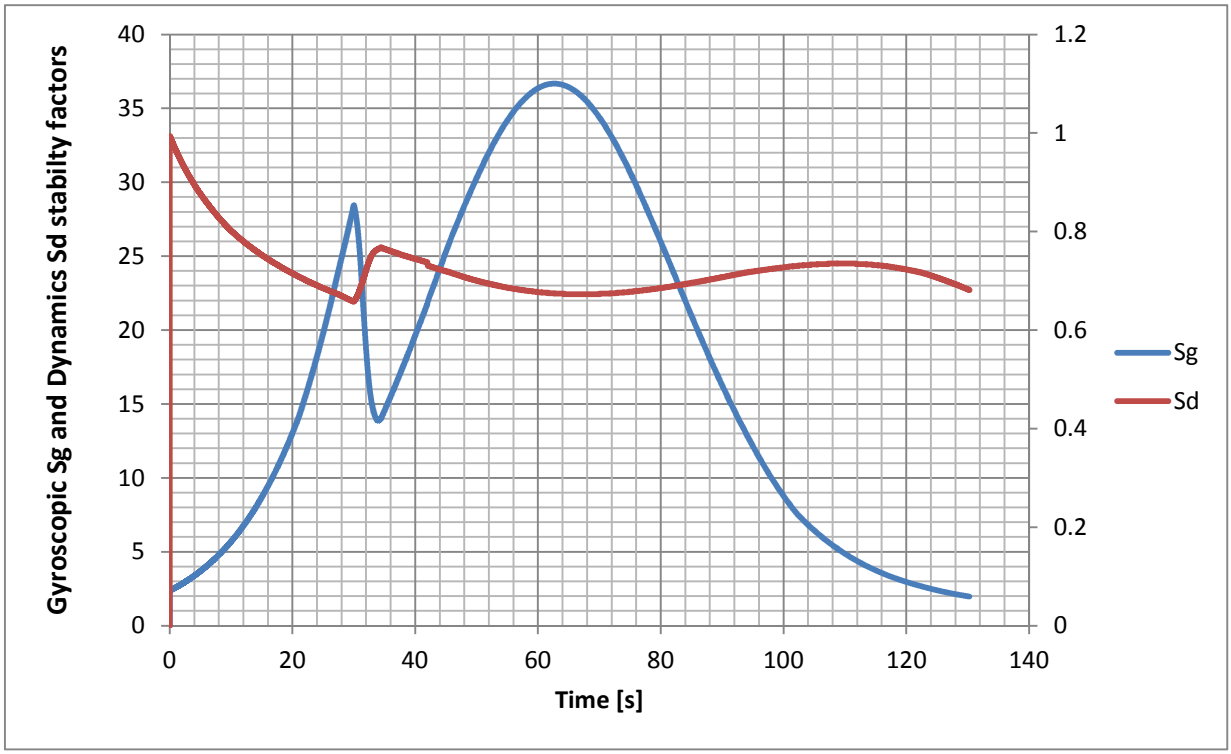

Figure 5-25 Gyro and Dynamic stability factor history, 52 calibre gun, max. range, std. atmos., time delay 31 s, active de-spinning.

5.3 Exterior ballistic - conclusion

Proposed design of M-REP artillery projectile with SRM and BB modules is feasible from the aspect of projectile's exterior ballistics. Trajectory models, both made in FORTRAN and PRODAS yielded results which confirms significant range extension and sufficient stability at trajectory. Stability factors recommended limits are fulfilled in both cases, whether M-REP is launched from 39 or 52 calibre systems. With appropriate selection of active spin control parameters, both time delay and de-spinning feature of the rocket motor can be combined and it will yield stable long range flight with decreased dispersion. The combination of optimal SRM ignition at 18 sec, without de-spinning, produces max. range from 52 howitzer, however total angle of attack has border values closer to 4 deg, that might induce larger lateral, dispersion. The concept has been numerically proven and the detailed firing tables can be made for the each type of the ordnances.

6 M-REP'S STRUCTURAL ASSESSMENT - SRM PROPELLANT GRAIN AND METAL JACKET (BRIEF OVERVIEW)

6.1 Finite element analysis

6.1.1 Acceleration loads

During firing sequence, we can distinguish two types of loads exerted on a projectile in gun barrel: first type - active loads (or pressure loads) and second type- reactive (or inertial loads). Active loads result from pressure build up due to combustion of gun propelling charge in barrels' combustion chamber and continued combustion in the barrel. Projectile elements in front of driving (rotating) band are subjected to severe inertial loads (acceleration, axial and radial). At bottom of a projectile (BB and payload bottom), pressure generated by gun powder charge is "counteracting" inertial loads along with rifling resistance of driving band. In order to determine structural strength of the components including payload's metal jacket and the SRM's elements, M-REP projectile components are analysed with finite element method. Entire projectile is generated in CAD, meshing is simplified to reduce the computational time and to increase calculation accuracy, method used is axisymmetric loading case for structural analysis. The calculations are backed up with hand calculations for critical design features such as thread connection between motor and the payload. Main structural parts (combustion chamber, base bleed case and payload closure) are designated as high-strength steel parts made of AISI 4340 Q&T and AISI 9260 Q&T. Applied analytical loads are: Internal peak barrel pressure and corresponding acceleration (never exceeded pressure in gun barrel), i.e. P_{max} = 430 MPa, and acceleration corresponding to the projectile mass of 49.7 kg - a=169200 m/s^2. The payload metal jacket is high-fragmenting structural steel HF1, with many of mechanical properties identical to AISI 9260. The aim of this chapter is to validate structural viability of the M-REP design..

The most stressed projectile module is bottom of a projectile, especially as the bottom features the thread that connects the BBU, as well as the igniter-sustainer for base bleed. The positive feature of the design is that entire BB unit is immersed into the gun combustion chamber, behind the driving band, so that the gun pressure surrounds the BB casing, i.e. pressure do not impart significant pressure loads onto the BB elements. Figure 6-1, represents the stress concentration at the bottom of the payload where the BB is attached. The results form FEA are satisfactory, for tormenting pressure inside the gun combustion chamber and appropriate inertial loading the stresses are below the yield stress for the steel grade of choice (Yield stress HF-1 > 1250 N/mm^2)

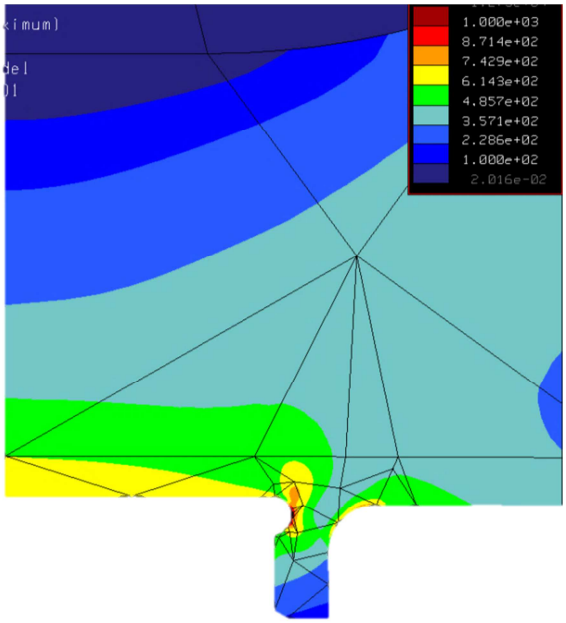

Figure 6-1 Combined stress (detail - bottom of waehead metal jacket support – value in the middle of section 743 N/mm^2.

Figure 6-2 shows detail on the payload where stress concentration exist due to change in geometrical cross section, i.e., transition from cylinder to bourlett before the rotating band – dia.153.9mm to dia. 154.74mm. This is region where driving ban represents support , i.e where active and reactive forces “meat”. The FEA stress value is 1178 N/mm^2. Payload cross section shown on Figure 6 -2 is the most loaded as this particular cross section of metal jacket bears all inertial loads (W=m*a – “a”- acceleration in the barrel)

exerted by the M-REP elements before the bourllet. Stress concentration value is high due to small dimensional transition and due to constrain that exist in that region (simulation of barrel wall) – i.e. it is single point of stress concentration. Yield stress for high-strength steel is higher than values of stress in the concentration, although some increment in the thickness of material in that area can improve the stress distribution.

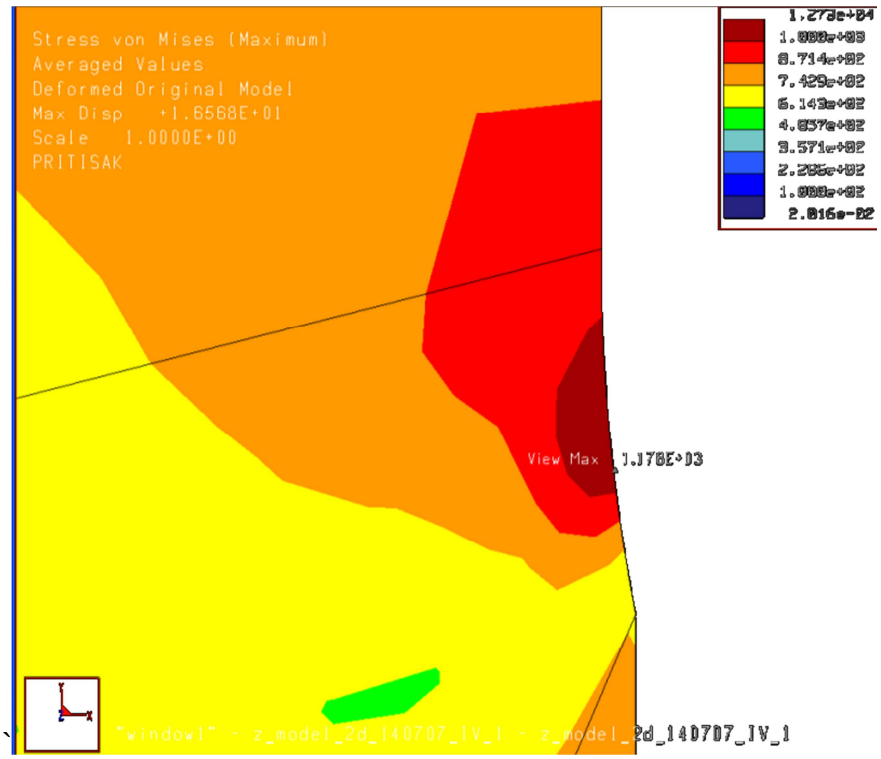

Figure 6-2 Stresses (combined) – detail: payload body - transition from bourllet to the driving band

On figure 6-3, the FEA results indicate that the most loaded part of the projectile is inner transitional radius inside payload cavity at the bottom of the projectile. The stress values show that the part does not yield under given load: the von Mises stress value is 964 N/mm^2, which indicates good dimension for the projectile bottom and cavity.

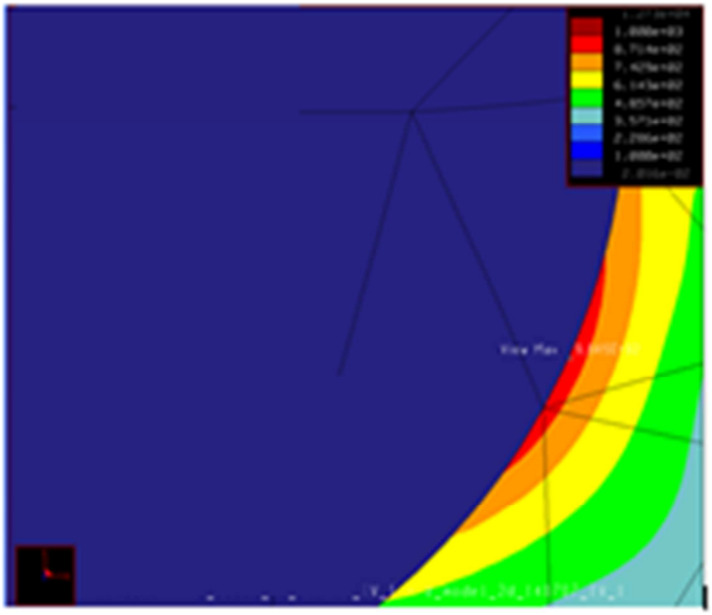

Figure 6-3: Stresses (combined) – detail bottom of the payload cavity - radius 50mm – stress value 964 N/mm^2.

To test the stress concentration in ogive part with holes for divergent nozzle, equivalent load equal to augmented weight of elements in front of the of the nozzles, due to acceleration, i.e. 4.566 kg x acceleration 169200 m/s^2,= 78.75 t, and simplified model has been analysed – Figure – 6-4 Stress value in a cross section with full profile does not exceed 334.25 N/mm^2.

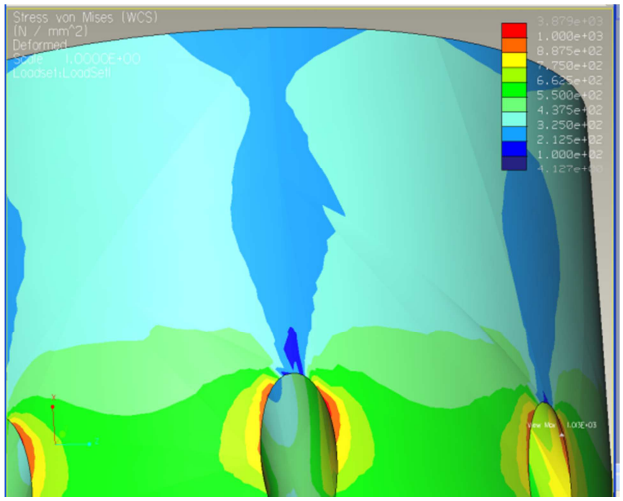

Figure 6-4 Combined stresses: Detail – stress concentrations on the holes – exit area on the nozzles: 497 N/mm^2. Singular point 713 N/mm^2.

Conclusion: all elements structurally validated against projectile focal point of design (max. load), do not have critical stresses that are higher than proportionality limit and yield strength of high strength steel SEA 4340/SAE 9260 (ref. $Rp_{0.2}$ = 1100 N/mm^2, Rm = 1250 N/mm^2).

6.2 Stress analysis for thread M128x2 under the load of internal pressure of 100 MPa

The connecting thread between the SRM and the payload is critically loaded by internal pressure, as soon as the SRM is ignited. The internal pressure is high as 300 bar (with safety factor – 100 bar), and to validate the strength of the thread, thread bearing capacity is calculated by hand calculations.

The thread teeth load bearing capacity:

Internal (combustion) pressure: 100 MPa

Material high-strength steel:

$R_m \geq$ 1250 N/mm^2, $R_{0.2} \geq$ 1100 N/mm^2, A_5=10%, Z=40%, $KU^{300/3}$=35 J.

R_1=62.6 mm- max. inner diameter of combustion chamber cavity

R_2=76.4 mm –min. outer diameter of combustion chamber

$E = 210000 \frac{N}{mm^2}$ -Young's module of elasticity for high-strength carbon steel

μ =0.3 –Poisson coefficient for steel

Knowing the geometry of the thread, stresses in the thread's teeth can be determined by:

$$\tau = \frac{F_{\max}}{A_{kr}} = \frac{0.22 \cdot F}{2 R_{kr} \cdot \pi \cdot \delta_1} = \frac{0.22 \cdot (62.6)^2 \pi \cdot 100}{2 \cdot 64 \cdot \pi \cdot 1.749} = 385.098 \frac{N}{mm^2} \quad \textbf{(6-1)}$$

According to the theory of threads, first teeth are bearing 22% of total axial force that loads the thread.

$$\sigma_m = 1250\frac{N}{mm^2} \Rightarrow \tau_m \approx 0.625 \cdot \sigma_m = 781.25\frac{N}{mm^2} \quad \textbf{(6-2)}$$

Safety factor:

$$\nu = \frac{\tau_m}{\tau} = \frac{781.25}{385.098} = 2.03 \quad \textbf{(6-3)}$$

Shear stresses in critical cross-section of thread on nozzle support:

$$\tau = \frac{F_{\max}}{A_{kr}} = \frac{0.22 \cdot F}{2R_{kr} \cdot \pi \cdot \delta} = \frac{0.22 \cdot (62.6)^2 \pi \cdot 100}{2 \cdot 62.641 \cdot \pi \cdot 1.5} = 458.776\frac{N}{mm^2} \quad \textbf{(6-4)}$$

$$\sigma_m = 1250\frac{N}{mm^2} \Rightarrow \tau_m \approx 0.625 \cdot \sigma_m = 781.25\frac{N}{mm^2} \quad \textbf{(6-5)}$$

$$\sigma_{0.2} = 1100\frac{N}{mm^2} \Rightarrow \tau_{0.2} \approx 0.625 \cdot \sigma_{0.2} = 687.5\frac{N}{mm^2} \quad \textbf{(6-6)}$$

Safety factors are:

$$\nu = \frac{\tau_m}{\tau} = \frac{781.25}{458.776} = 1.7$$
$$\nu = \frac{\tau_{0.2}}{\tau} = \frac{687.5}{458.776} = 1.5 \quad \textbf{(6-7)}$$

6.3 Conclusion

According to the projectile's technical drawings and calculations made for focal point of design (loads P_{max}=430 MPa, equivalent acceleration for projectile mass of 49.737 kg a= 169200 m/s^2), elements are dimensioned in a way that the stresses do not exceed proportionality limit (yield strength) of materials chosen for construction of SRM, as well as in the other elements of the projectile's assembly. The safety factor is at least 1.5. Due to fact that the pressures in the gun barrel in 52-23 calibre systems do not exceed 380MPa (breech pressure), the design has space to be improved from the aspect of strength and dimensions, however the fragmentation effect of the projectile metal jacket should be taken in consideration too. With the right choice of shape

and deployment of propellant grain in combustion chamber (by minimising the gaps), it can be achieved that load acting upon the propellant grain do not produce critical stresses for given mechanical properties of the propellant. The Finite Element Method that is used in this Chapter for evaluation of M-REP elements are not elaborated in minute details, although results of simulations exists, it is considered to be too elaborative for scope of the research in this thesis.

7 BRIEF OVERVIEW OF INTERIOR BALLISTICS OF GUN-HOWITZER WITH M-REP (IB - COMPATIBLITY ASSESMENT)

7.1 Introduction

Interior ballistics of gun-projectile system represents complex problem. The M-REP with its own weight comes at top of “weight zones” for 155mm artillery shells. Therefore, compatibility of new design need to be assessed in conjunction with existing ordnances. Simulations of the interior ballistics have been conducted both for firing from 39 calibre howitzer with 19 litre chamber volume, and 52 calibre with 23 litre chamber volume. The nominal weight of the projectile with M-REP fuze is 49.7 kg. The simulations were carried out using Baer-Frankle analysis in PRODAS[79, 108]. The aim of this Chapter is to present whether the new M-REP design is in compliance with interior ballistics of existing howitzers and resulting gun dynamics (recoil). Gun propellant charges has been computationally “modified”, in order to reach required muzzle velocities. Results of Interior ballistic calculations for M-REP with 155mm howitzers, 39-19 and 52-23, are shown in Chapter 7.2 and Chapter 7.3. The results of simulation are found to be satisfactory.

7.2 Interior ballistics of 155mm 39-19 calibre gun with M-REP

The M-REP fired from 39-19 howitzer, should reach velocity of 821 m/s at the muzzle. Hence, the gun propellant charge should be tailored to enable projectile to accelerate in gun barrel, and to achieve nominal muzzle velocity of 821 m/s with charge Zone 8. However standard weight of propelling charge Zone 8 (M203) is not enough to provide required exit velocity due to “weight zone” of the M-REP, thus propelling charge should be increased. Computed weight of propellant charge is 12.46 kg, 19 holes - perforated grains, named Zone 8S. The projectile length of travel in the barrel is 5080 mm, twist angle 8.9^{o} (20 cal/rev). Results are presented in table 7-1 and 7-2 and figures 7-1 to 7-3.

Table 7-1 Propellant Charge Characteristics for 39-19 155mm Howitzer

Type: Modified M203 Zone 8S Propellant charge		
Time Delay	(sec)	0.0100
Weight	(kg)	12.46
Impetus	(MJ/kg)	1.091
Gamma		1.25
Co-volume	(m^3/kg)	0.0011
Flame Temperature	(K)	3040.
Density	(g/cm^3)	1.66
Burn Rate Exponent		0.6700
Initial Burn Rate	(cm/sec/bar)	0.06860
Final Burn Rate	(cm/sec/bar)	0.06860

Parameters of 39 calibre gun:

- Barrel Length (without chamber) 5080 mm
- Chamber Volume 0.019 m^3
- Bore Diameter 154.9910 mm
- Bore Area 19248.65mm^2 Rifling/Twist Parameters:
  - Initial Twist 8.9^o
  - Exit Twist 8.9^o
  - Number of Lands or Grooves 48

Calculated Interior Ballistics of 39-19 howitzer with M-REP:

- Muzzle Velocity 822.60 m/s
- Muzzle Pressure 79.38 MPa
- Maximum Acceleration 11895.70 G's
- Maximum Breech Pressure 346.76 MPa
- Travel at Max. Breech Pressure 442.29 mm
- Time at Max. Breech Pressure 16.60 ms
- Maximum Base Pressure 308.18 MPa
- Travel at Max. Base Pressure 442.29 mm
- Time at Max. Base Pressure 16.60 ms
- Impulse at Projectile Exit 44550.84 Ns

The calculated breech pressure with M-REP do not exceed the maximum permissible chamber pressure in 39-19 gun howitzers of 3700 bars.

Table 7-2 Interior Ballistics of 39-19 155mm Howitzer with M-REP, as function of time

Time	Travel	Breech Pressure	Base Pressure	Velocity	Temp	Volume	Resist Pressure	Linear Accel	Spin	Mass % Prop1
ms	mm	MPa	MPa	m/s	K	m^3	MPa	G's	rad/sec	
11.000	0.124	14.8	13.1	1.	2850.	0.0115	6.4	264.	1.37	0.008
11.600	1.156	29.0	25.8	3.	2940.	0.0114	11.8	552.	6.17	0.020
12.200	4.063	50.8	45.1	7.	2982.	0.0114	26.8	721.	13.75	0.038
12.600	7.350	70.4	62.6	10.	2998.	0.0113	38.7	944.	19.64	0.055
13.000	12.176	94.9	84.4	15.	3009.	0.0113	38.7	1802.	30.27	0.075
13.200	15.553	109.1	97.0	19.	3013.	0.0113	38.7	2299.	38.30	0.086
13.400	19.824	124.6	110.7	24.	3015.	0.0113	38.7	2841.	48.39	0.099
13.600	25.203	141.3	125.6	30.	3016.	0.0113	38.7	3427.	60.70	0.113
13.800	31.947	159.2	141.5	38.	3016.	0.0113	25.9	4557.	76.36	0.129
14.000	40.445	178.0	158.2	47.	3013.	0.0114	21.8	5377.	95.91	0.146
14.200	51.041	197.5	175.5	59.	3008.	0.0115	18.1	6208.	118.79	0.164
14.400	64.056	217.3	193.1	72.	3000.	0.0116	16.8	6952.	144.72	0.183
14.600	79.783	237.1	210.7	86.	2990.	0.0117	15.3	7704.	173.60	0.204
14.800	98.515	256.4	227.9	102.	2978.	0.0119	13.5	8451.	205.45	0.226
15.000	120.543	274.7	244.2	119.	2964.	0.0122	11.4	9178.	240.20	0.250
15.200	146.147	291.6	259.2	137.	2947.	0.0125	10.4	9810.	277.65	0.275
15.400	175.576	306.7	272.6	157.	2928.	0.0129	9.8	10362.	317.42	0.300
15.600	209.043	319.6	284.1	178.	2907.	0.0133	9.2	10840.	359.21	0.327
15.800	246.733	330.1	293.4	199.	2884.	0.0139	8.4	11238.	402.73	0.354
16.000	288.803	338.1	300.5	222.	2860.	0.0145	7.6	11549.	447.63	0.383
16.200	335.371	343.4	305.2	244.	2834.	0.0152	6.9	11761.	493.58	0.411
16.400	386.520	346.2	307.7	267.	2807.	0.0159	6.7	11869.	540.13	0.440
16.800	502.699	345.2	306.8	314.	2752.	0.0178	6.3	11847.	633.72	0.499
17.000	567.720	341.8	303.8	337.	2724.	0.0188	6.3	11732.	680.16	0.528
17.200	637.311	336.9	299.4	359.	2696.	0.0199	6.2	11564.	726.04	0.557
17.400	711.408	330.8	294.0	382.	2668.	0.0212	6.1	11352.	771.17	0.586
17.600	789.928	323.7	287.6	404.	2641.	0.0225	6.0	11108.	815.40	0.615
17.800	872.776	315.8	280.7	425.	2615.	0.0239	5.9	10838.	858.61	0.643
18.000	959.848	307.5	273.3	446.	2589.	0.0253	5.7	10550.	900.73	0.670
18.200	1051.033	298.8	265.6	466.	2565.	0.0269	5.6	10251.	941.70	0.697
18.400	1146.214	290.0	257.7	486.	2540.	0.0285	5.5	9947.	981.48	0.724
18.600	1245.273	281.1	249.8	505.	2517.	0.0303	5.4	9641.	1020.06	0.750
18.800	1348.091	272.3	242.0	523.	2495.	0.0321	5.2	9337.	1057.45	0.775
19.200	1564.536	255.1	226.7	559.	2453.	0.0359	4.9	8744.	1128.68	0.824
19.600	1794.629	238.7	212.1	592.	2414.	0.0400	4.6	8183.	1195.38	0.871
20.000	2037.498	223.4	198.6	622.	2378.	0.0443	4.5	7654.	1257.80	0.916
20.400	2292.321	209.4	186.1	651.	2345.	0.0490	4.5	7160.	1316.20	0.958
21.000	2695.296	185.6	165.0	691.	2287.	0.0564	4.5	6328.	1396.59	1.000
21.400	2976.502	165.9	147.4	714.	2233.	0.0618	4.5	5636.	1443.71	1.000
21.800	3266.526	149.1	132.6	735.	2183.	0.0673	4.5	5050.	1485.81	1.000
22.200	3564.452	134.9	119.9	754.	2138.	0.0730	4.5	4551.	1523.66	1.000
22.800	4024.481	117.2	104.2	779.	2076.	0.0818	4.5	3931.	1573.75	1.000
23.400	4498.374	103.0	91.5	800.	2021.	0.0909	4.5	3431.	1617.27	1.000
24.115	5080.000	89.5	79.5	822.	1964.	0.1020	4.5	2959.	1661.86	1.000

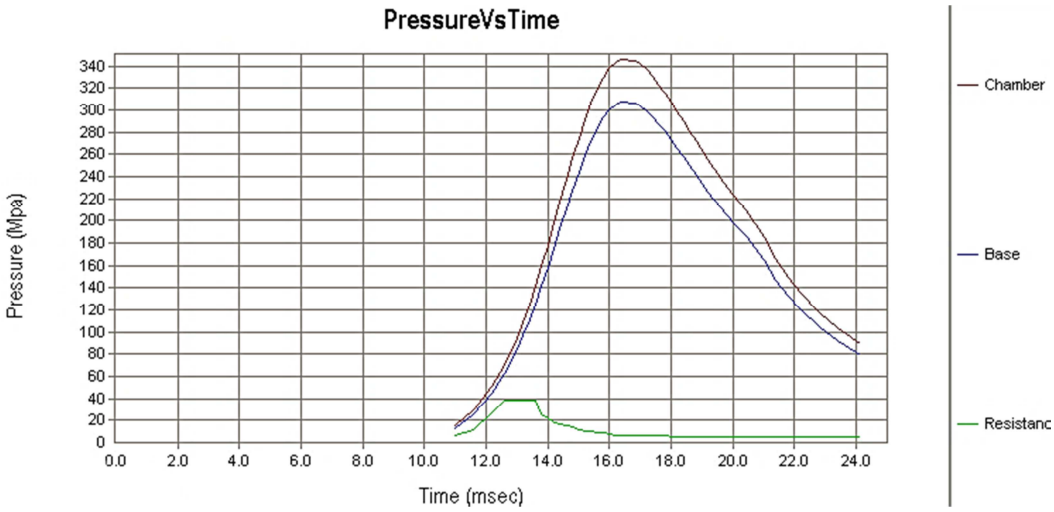

Figure 7-1. IB pressure vs. time, 39 calibre gun with MREP

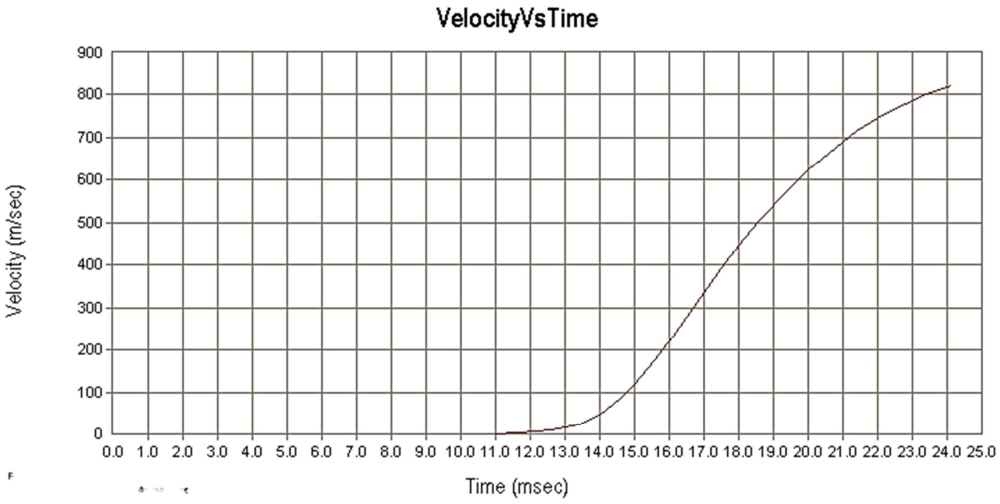

Figure 7-2 IB, axial velocity vs. time, 39 calibre gun with MREP

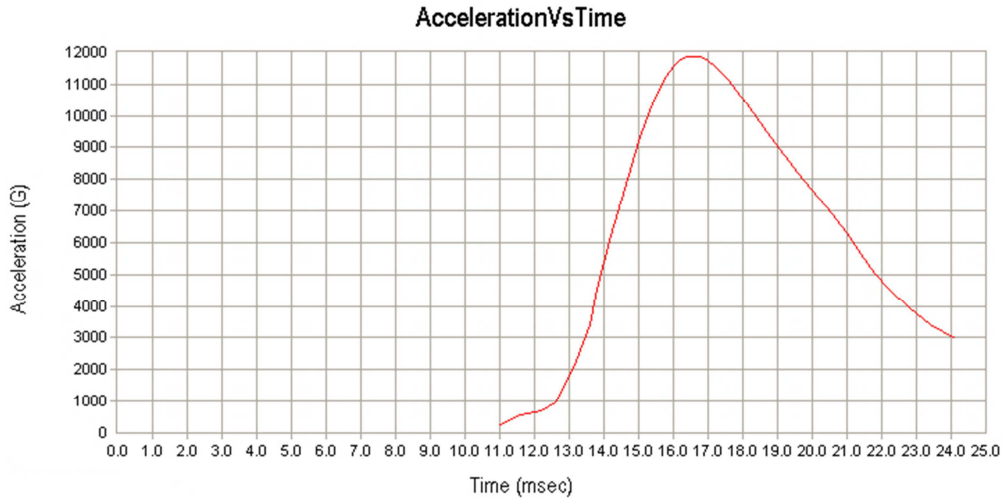

Figure 7-3 IB axial acceleration vs. time, 39 calibre gun with MREP

7.3 Interior ballistics of 52-23 howitzer with M-REP

The M-REP fired from 52-23 howitzer, should reach velocity of 930 m/s at the muzzle. Hence, the gun propellant charge should be tailored to enable projectile to accelerate in gun barrel, and to achieve nominal muzzle velocity of 930 m/s with charge Zone 10. Standard weight of propelling charge Zone 10 (M11C) is enough to provide required exit velocity as the "weight zone" of the M-REP is within the limits of standard ERFB-BB ammunition, so variation on propelling charge weight can be tolerated. Computed weight of propellant charge required to achieve 930 m/s is 15.23 kg, with 19 holes - perforated grains. The projectile length of travel in the barrel is 6900 mm, twist angle 8.9^{o} (20 cal/rev). The howitzer with 52-25 litre barrel and rifling angle of 22.5 cal/rev, has been investigated, too. Results are presented in table 7-3 and 7-4 and figures 7-4 to 7-6.

Table 7-3 Propellant Charge Characteristics for 52-23 155mm Howitzer

Type: Modified Zone 10 Propellant charge		
Time Delay	(sec)	0.0100
Weight	(kg)	15.23
Impetus	(MJ/kg)	1.091
Gamma		1.25
Co-volume	(m^3/kg)	0.0011
Flame Temperature	(K)	3040
Density	(g/cm^3)	1.66
Burn Rate Exponent		0.6700
Initial Burn Rate	(cm/sec/bar)	0.06860
Final Burn Rate	(cm/sec/bar)	0.06860

Parameters of 52 calibre gun:

- Barrel Length (without chamber) 6900 mm
- Chamber Volume 0.023 m^3
- Bore Diameter 154.9910 mm
- Bore Area 19248.65mm^2
- Rifling/Twist Parameters:
  - Initial Twist 8.9^{o}
  - Exit Twist 8.9^{o}
  - Number of Lands or Grooves 48

Table 7-4 Interior Ballistics of 52-23 155mm Howitzer with M-REP, as function of time

Time	Travel	Breech Press.	Base Press.	Vel.	Temp	Volume	Resist	Linear Accel	Spin	Mass Prop1
ms	mm	MPa	Mpa	m/sec	deg K	m^3	Mpa	G's	rad/s	
11.2	0.2	16.7	14.5	1.0	2898	0.0138	6.7	308	2.0	0.011
11.8	1.4	32.5	28.2	4.0	2965	0.0137	13.1	593	8.1	0.023
12.2	3.3	47.4	41.1	6.0	2988	0.0136	23	716	12.1	0.036
12.6	6.3	66.7	57.8	9.0	3003	0.0136	38.5	764	18.2	0.051
13.0	10.7	91.0	78.9	13.0	3013	0.0135	38.7	1587	26.3	0.071
13.4	17.5	120.9	104.8	21.0	3019	0.0135	38.7	2609	42.4	0.094
13.6	22.4	138.0	119.7	27.0	3020	0.0135	38.7	3195	54.6	0.108
13.8	28.4	156.6	135.8	34.0	3021	0.0135	32.6	4072	68.7	0.124
14.0	36.1	176.5	153.1	43.0	3019	0.0135	23.9	5096	86.9	0.14
14.2	45.8	197.6	171.4	54.0	3016	0.0135	19.3	6000	109.1	0.158
14.4	57.8	219.6	190.5	66.0	3010	0.0136	17.4	6825	133.4	0.178
14.6	72.5	242.3	210.1	81.0	3002	0.0137	16	7653	163.7	0.199
14.8	90.1	265.1	229.9	96.0	2993	0.0138	14.3	8501	194.0	0.221
15.0	111.1	287.7	249.5	114.0	2981	0.0141	12.3	9352	230.3	0.245
15.2	135.7	309.5	268.4	133.0	2967	0.0143	10.6	10166	268.7	0.271
15.4	164.3	330.1	286.3	153.0	2951	0.0146	10.1	10892	309.2	0.298
15.6	197.1	348.9	302.6	175.0	2933	0.015	9.4	11561	353.6	0.326
15.8	234.4	365.5	317.0	198.0	2913	0.0155	8.7	12160	400.1	0.355
16.0	276.5	379.6	329.2	223.0	2890	0.0161	7.8	12674	450.6	0.385
16.2	323.5	390.9	339.0	248.0	2867	0.0167	7	13093	501.1	0.416
16.4	375.6	399.2	346.3	274.0	2842	0.0174	6.8	13386	553.6	0.448
16.6	432.9	404.7	351.0	300.0	2815	0.0183	6.6	13581	606.2	0.481
16.8	495.5	407.3	353.2	326.0	2788	0.0192	6.4	13679	658.7	0.513
17.2	636.7	405.0	351.3	380.0	2733	0.0214	6.2	13609	767.8	0.579
17.4	715.3	400.7	347.6	406.0	2705	0.0226	6.1	13466	820.4	0.611
17.6	799.1	394.7	342.4	432.0	2678	0.0239	6	13265	872.9	0.644
17.8	888.1	387.4	336.0	458.0	2651	0.0254	5.8	13018	925.4	0.676
18.0	982.2	378.9	328.6	483.0	2624	0.0269	5.7	12734	975.9	0.708
18.2	1081.2	369.6	320.6	507.0	2598	0.0286	5.6	12422	1024.4	0.739
18.4	1185.0	359.8	312.1	531.0	2572	0.0303	5.4	12092	1072.9	0.769
18.6	1293.6	349.6	303.2	554.0	2547	0.0321	5.3	11749	1119.4	0.799
18.8	1406.8	339.3	294.2	577.0	2524	0.0341	5.1	11400	1165.9	0.829
19.0	1524.4	328.8	285.2	599.0	2500	0.0361	5	11049	1210.3	0.858
19.2	1646.3	318.4	276.2	620.0	2478	0.0382	4.8	10701	1252.8	0.886
19.6	1902.5	298.2	258.6	660.0	2436	0.0427	4.5	10021	1333.6	0.94
20.0	2174.3	279.0	241.9	698.0	2397	0.0475	4.5	9364	1410.4	0.991
20.2	2315.8	264.1	229.0	716.0	2368	0.0501	4.5	8855	1446.7	1
20.4	2460.7	247.2	214.4	733.0	2335	0.0529	4.5	8277	1481.1	1
20.6	2608.8	231.8	201.0	748.0	2303	0.0557	4.5	7751	1511.4	1
21.0	2914.0	205.0	177.8	777.0	2243	0.0615	4.5	6836	1570.0	1
21.4	3229.9	182.7	158.4	802.0	2188	0.0675	4.5	6071	1620.5	1
21.8	3555.3	163.9	142.1	824.0	2138	0.0738	4.5	5428	1665.0	1
22.2	3889.1	147.9	128.3	845.0	2092	0.0801	4.5	4882	1707.4	1
22.8	4404.0	128.2	111.2	871.0	2030	0.09	4.5	4208	1759.9	1
23.4	4933.8	112.4	97.5	894.0	1975	0.1001	4.5	3667	1806.4	1
24.2	5659.9	95.8	83.1	920.0	1911	0.1141	4.5	3098	1858.9	1
24.7	6090.0	88.1	76.4	934.0	1878	0.1223	4.5	2835	1887.2	1
25.4	6900.0	74.5	64.6	956.0	1824	0.1344	4.5	2368	1931.7	1

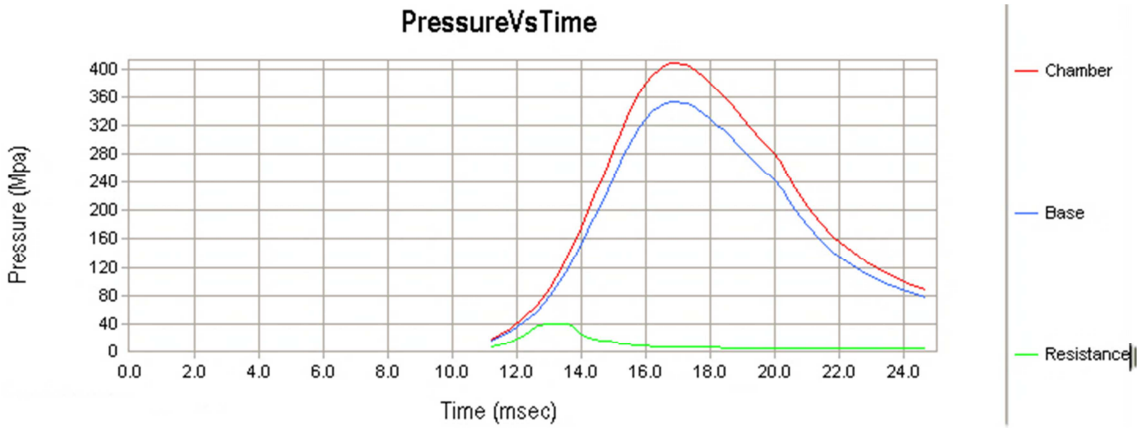

Figure 7-1 IB pressure vs. time, 52 calibre gun with MREP.

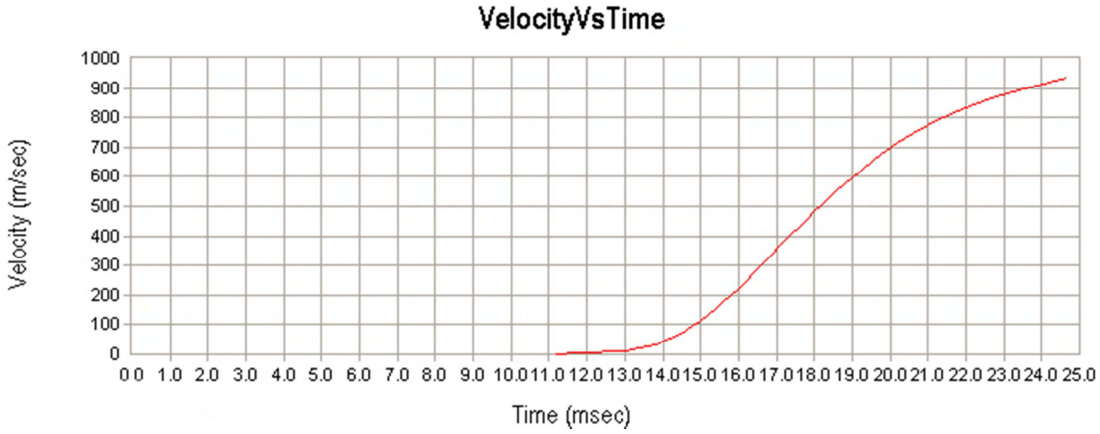

Figure 1-2 IB axial velocity vs. time, 52 calibre gun with MREP

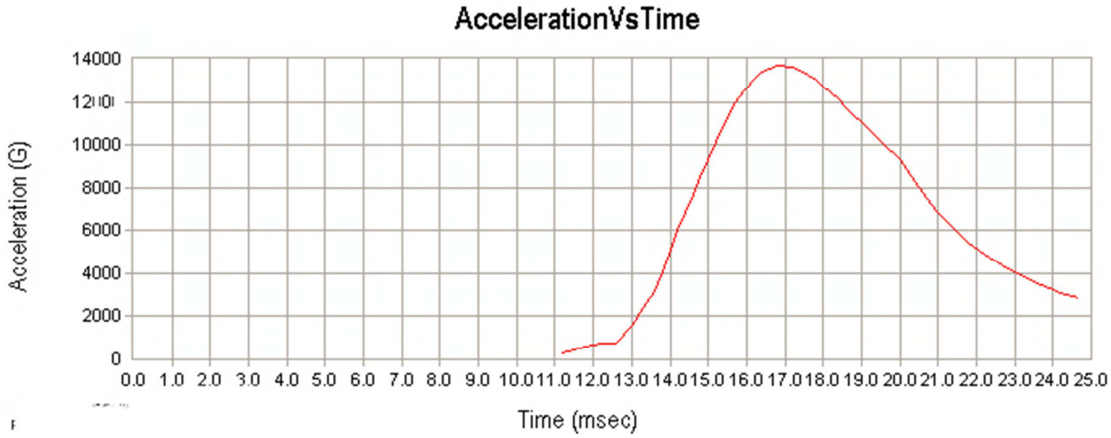

Figure 1-3 IB axial acceleration vs. time, 52 calibre gun with MREP

Calculated Interior Ballistics of 52-23 howitzer with M-REP:

- Muzzle Velocity 934 m/s (956 m/s)
- Muzzle Pressure 76.24 MPa
- Maximum Acceleration 13683.78 G's
- Maximum Breech Pressure 407.33 MPa
- Travel at Max. Breech Pressure 563.47 mm
- Time at Max. Breech Pressure 17.00 ms
- Maximum Base Pressure 353.28 MPa
- Travel at Max. Base Pressure 563.47 mm
- Time at Max. Base Pressure 17.00 ms
- Impulse at Projectile Exit 52287.92 Ns

The calculated breech pressure with M-REP do not exceed the maximum permissible chamber pressure in 52-23 gun howitzers of 4400 bars.

7.4 Interior Ballistic assessment - Conclusion

The objective of assessing MREP compatibility with existing ordnances has been successfully achieved through simulation. The new M-REP artillery shell complies with interior ballistics of contemporary ordnances in 39 and 52 calibre, as required by JBMoU. The projectile should not alter gun dynamics when it is fired from standard 155 mm howitzers such as AS-90, PzH2000, M777, ATMOS, etc. Further work in field of IB should address the compatibility and potentially longer ranges with 52-25 howitzer systems with rifling of 22.5 cal/rev.or 24 cal/rev.

8 BRIEF OVERVIEW AND ASSESMENT OF WARHEAD DESIGN AND TERMINAL BALLISTICS

The aim of this Chapter objective is to provide insight in design of the payload module and lethality assessment of module with fragmentation effect. As the large part of the M-REP's volume is occupied with Base Bleed Unit and Solid Rocket Motor, the effect on target can be compromised. Modular Range Enhanced Projectile shape is governed by aerodynamic requirements (streamlined ogive), and overall mass of the projectile. With projectile's volume occupied by BB and SRM, there is a limited "space" for payload design. Therefore, MREP's design must be optimized and enhanced to match terminal effect of contemporary ammunition. The focus is on Natural Fragmenting Payload module (warhead), although for future developments, concepts of pre-fragmenting warhead, cluster scattering warhead, blast effect or thermo-baric warhead should be investigated in order to increase terminal effect of a payload. Again, the module itself can be "filled" with illuminating or incendiary mixtures, or packed with guided sub-munitions.

The High Explosive Natural Fragmentation lethality assessment is conducted using the analytical equations [7, 60], PRODAS [79,108] software and modified Fragmentation Analysis Tool [61, 115]. The aim is to establish indication of M-REP payload effectiveness in terms of fragment velocity, fragment mass and distribution, and most important lethality effect according to the chosen lethality function [61,115]. Initial fragment velocity derived from blast effect is determined by the charge-to-mass ratio (C/m) [7, 60, 108]. The *C* is weight of the explosive and the *m* is the mass of the metal surrounding it. Velocity of fragments is calculated using the Gurney's equation [61, 108]:

$$V_{Fi} = K\sqrt{\frac{(C/m)_i}{1+0.5(C/m)_i}} \qquad \textbf{(8-1)}$$

where V_{fi} - initial fragment velocity

K – Gurney's constant for explosive type

$(C/m)_i$ – ratio of explosive filling vs. metal jacket mass(section)

The Gurney's equation is based on cylindrical shape of a payload, so alternative methods are used [60, 61, 115] and compared to each other, to take in account mass distribution and direction of fragment velocity vectors affected by external and internal shapes of a warhead and material used in manufacturing of metal jacket - payload body. Both utilised methods [60, 61,115] are based on empirical equations, to calculate fragment mass distribution. Analytical approach to design of a fragmenting process in Modified Fragmentation Analyses Tool yields accurate predictions of payload's fragmentation lethality effect. Results of fragment distribution analysis have been presented in Chapter 8.1 and values of lethality in comparison to referent shell 155mm M107 HE are presented in Chapter 8.2.

8.1 Calculation of fragment distribution and velocities for Range Enhanced Projectile

Fragment distribution has been calculated using PRODAS [79]. The materials used for simulations are: explosive filling Comp B (RDX/TNT); The MREP's metal jacket material is AISI (SAE) 9260 - Quenched and Tempered, High Strength - High Fragmentation Steel; M107metal jacket is AISI (SAE) 1055. The firing conditions and corresponding terminal velocities are given for M-REP fired form 39, 45 and 52 calibre howitzers at QE for max range at sea level (muzzle velocity , 821 m/s, 897 m/s and 930 m/s respectively), and for M107 for 39 calibre howitzer.

The Gurney's constant has been selected for Comp B, K = 8800 and the velocity of detonation of 7860 m/s has been assigned. Computations for 155mm M107 yielded next results:

Charge Weight:	6639.150 gm
Metal Weight:	29363.094 gm (HEI Cavity Only)
Charge Weight / Metal Weight:	0.2261
Number of Fragments:	2756.7
Average Fragment Weight :	10.6408 g
Fragment Velocity-Sectional :	1292.2 m/sec
Fragment Velocity-Total:	1208.9 m/sec

Table 8-1 Analysis of M-REP' Payload Fragment distribution

Payload Section	HE Weightgt	Metal Weight	Ratio	Frag. Velocity	Avg. Weight	Spray angle
	g	g	C/M	m/sec	g	deg
1	378.26	1194.69	0.3166	1402.3	10.342	82.1
2	392.18	1133.63	0.346	1456.7	9.167	81.9
3	406.35	1071.45	0.3793	1514.5	8.078	81.7
4	394.4	1006.6	0.3918	1535.3	7.25	92.6
5	356.09	940.92	0.3784	1513.1	6.653	93.2
6	318.52	876.9	0.3632	1487.1	6.098	93.3
7	283.04	814.66	0.3474	1459.3	5.573	93.4
8	249.65	754.2	0.331	1429.4	5.078	93.6
9	218.38	695.56	0.314	1397.2	4.612	93.7
10	189.17	638.63	0.2962	1362.4	4.175	93.9
11	162.07	583.52	0.2778	1324.6	3.766	94.1
12	137.07	530.19	0.2585	1283.4	3.385	94.3
13	114.16	478.63	0.2385	1238.2	3.03	94.7
14	93.35	428.87	0.2177	1188.4	2.701	95.6
15	72.88	388.53	0.1876	1110.8	2.537	99.3

Fragment Numbers by Weight Groups vs. Zone									
Weight Class (gm)									
Lower Weight	0.032	0.096	0.36	1.231	2.527	4.666	8.877	20.4	45.1
Upper Weight	0.096	0.36	1.231	2.527	4.666	8.877	20.47	45.1	
Average Weight--	0.061	0.21	0.73	1.81	3.484	6.503	13.53	30.0	67.7
Ave Velocity m/sec	1322.176	1322.6	1322.	1322.	1319.	1314.	1299.	1263	1047
Polar Zone (deg)	Number of Fragments								
27.5-47.5	1.682	3.312	4.559	3.197	2.804	2.744	2.827	1.66	2.04
47.5-57.5	4.673	9.199	12.66	8.88	7.789	7.623	7.852	4.62	5.67
57.5-67.5	24.113	47.469	65.34	45.82	40.19	39.33	40.51	23.8	29.3
67.5-77.5	10.094	19.871	27.35	19.18	16.82	16.46	16.96	9.99	12.2
77.5-87.5	13.832	27.23	37.48	26.28	23.05	22.56	23.24	13.6	16.8
87.5-97.5	38.506	75.803	104.3	73.17	64.18	62.81	64.69	38.1	46.7
97.5-107.5	63.554	125.111	172.	120.7	105.	103.7	106.	62.92	77.2
107.5-122.5	13.271	26.126	35.	25.	22.	21.	22.	13.	16.
122.5-157.5	10.841	21.342	29.38	20.60	18.0	17.68	18.21	10.7	13.1
Charge	Weight	:	6025	g					
Metal	Weight	:	18495	g	(HEI Cavity Only)				
Charge Weight/Metal	Weight: 0.325								
Number	of	Fragments	:5662						
Average	Fragment	Weight	:4.01						
Fragment	Velocity-Sectional	:1285		m/sec					
Fragment	Velocity-Total	:1282		m/sec					

The results obtained from terminal ballistic calculations using PRODAS gave similar results in comparison of two projectiles. The average velocity of the fragments for both projectiles are similar, however the size and the number of fragments is in favour of M-REP, due to better “explosive to metal” ratio. The computations using PRODAS model are deficient, although including Shapiro’s formula for spatial distribution of a fragments, the terminal velocity, and rotation speed of a projectile has not been taken in account.

8.2 Lethality Comparison between M-REP and M107 projectile

The model of the M-REP projectile is compared with M107 - standard artillery round for 155mm howitzers. Two models are investigated for M-REP projectile: (i) model that complies with PRODAS model – computes lethality of part of the projectile that is filled with HE, but includes base bottom - M-REP”A”; (ii) Model that takes in account the both modules of the M-REP. i.e. payload with explosive filling and cavity for SRM - M-REP”B”; (iii) M107 projectile. Simulation were exercised to include Proximity Fuze (8 m burst altitude) and Point Detonating Fuze (0m burst altitude), for Modular Range Enhanced Projectiles fired at optimal angle for maximum range from 39, 45 and 52 calibre howitzer, and M107 fried from 39 calibre gun. The results are presented in figures 8-2 to 8-21.

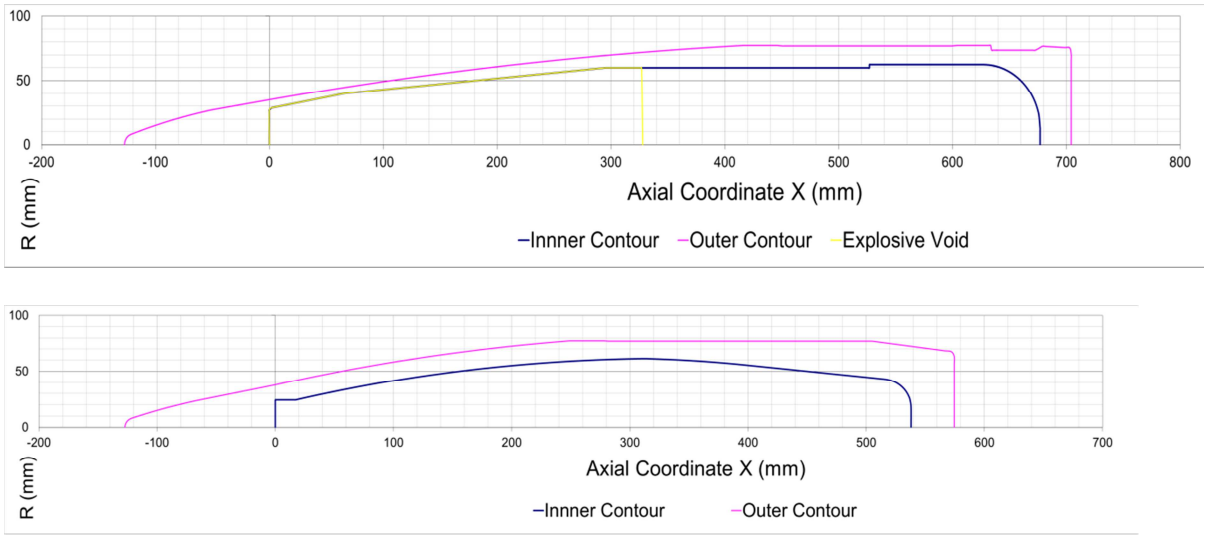

Figure 8-1 M-REP (top) and M107 (bottom) fragmentation models for modified Fragmentation Analysis Tool [61, 115]

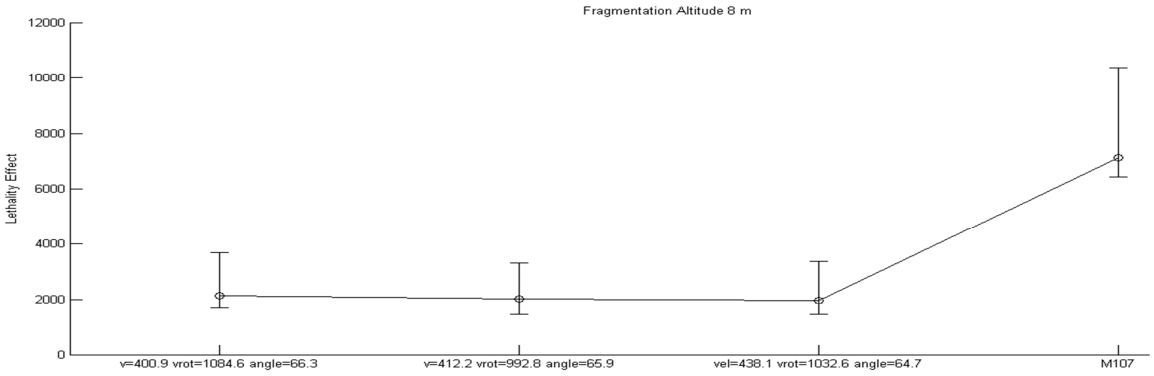

Figure 8-2 Lethality effect for the REP-A and M107 at burst altitude of 8m

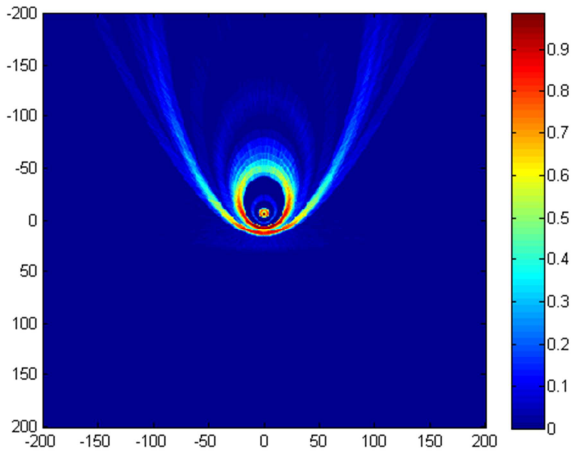

Figure 8-3 MREP-A: Burst alt.=8m V=400.9m/s ω=1084.6 rad/s Impact angle=66.3^o

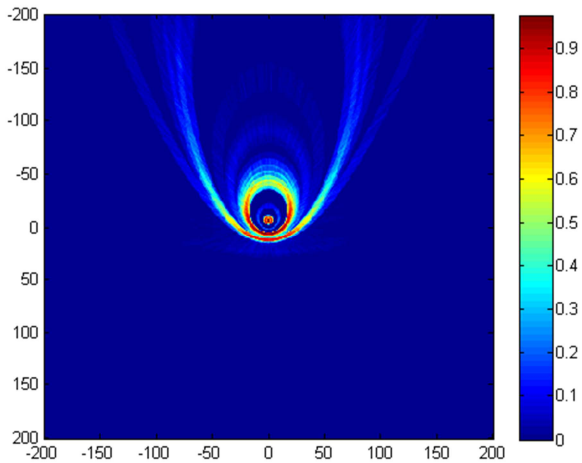

Figure 8-4 MREP-A: Burst alt.=8m V=412.2m/s ω=992.8 rad/s Impact angle=65.9^o

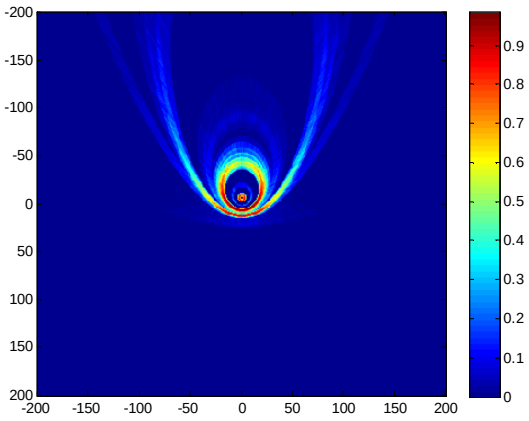

Figure 8-5 MREP-A: Burst alt.=8m V=438.1m/s ω=1032.6 rad/s Impact angle=64.7^o

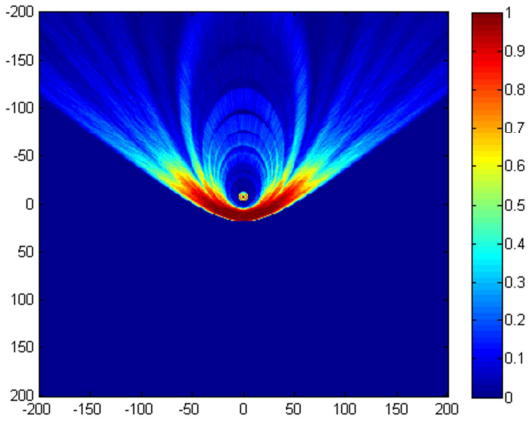

Figure 8-6 Projectile M107: Burst alt.=8m V=333.3m/s ω=1119.7 rad/s Impact angle=63.7^o

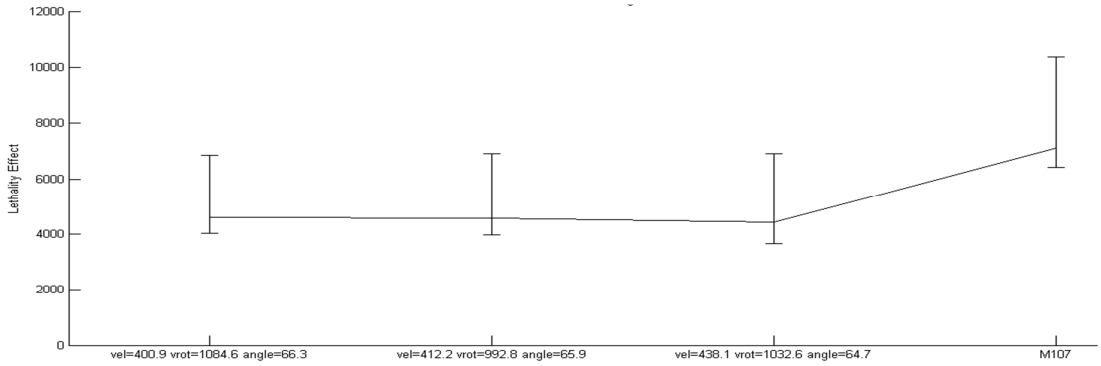

Figure 8-7 Lethality effect for the REP-B and M107 at burst altitude of 8m

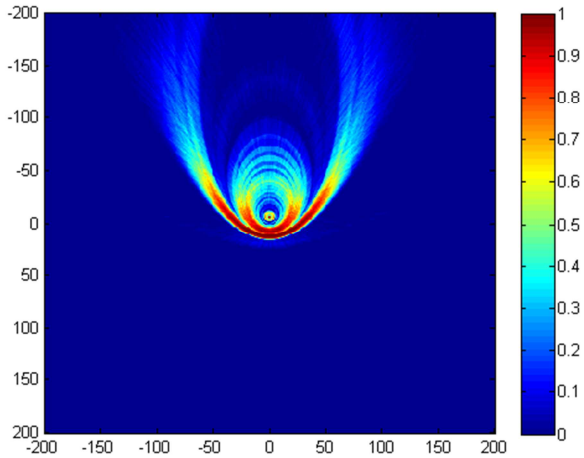

Figure 8-8 MREP-B: Burst alt.=8m V=400.9m/s ω=1084.6 rad/s Impact angle=66.3^{o}

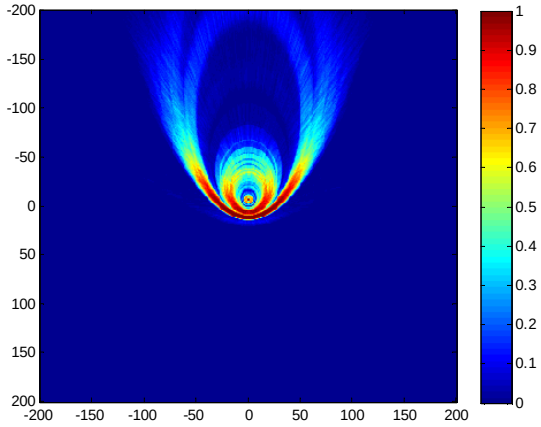

Figure 8-9 MREP-B: Burst alt.=8m V=412.2m/s ω=992.8 rad/s Impact angle=65.9^{o}

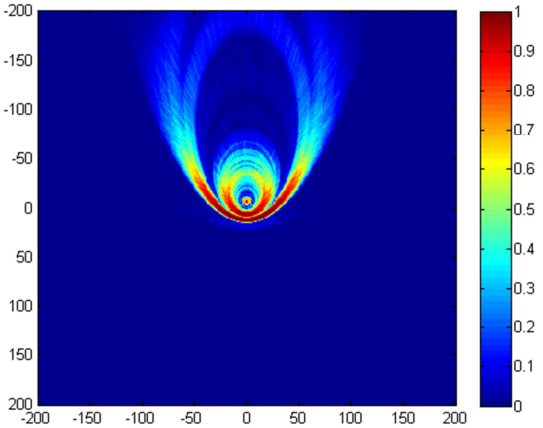

Figure 8-10 MREP-B: Burst alt.=8m V=438.1m/s ω=1032.6 rad/s Impact angle=64.7^{o}

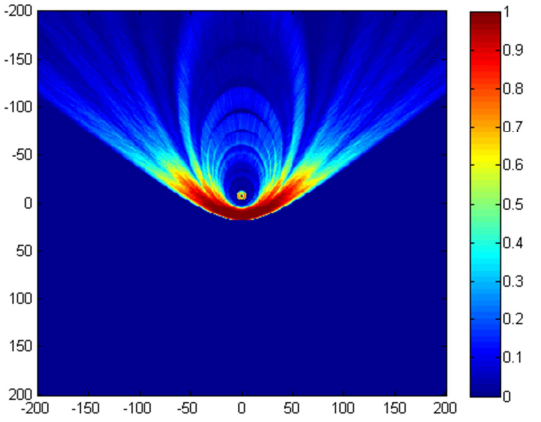

Figure 8-11 Projectile M107: Burst alt.=8m V=333.3m/s ω=1119.7 rad/s Impact angle=63.7^{o}

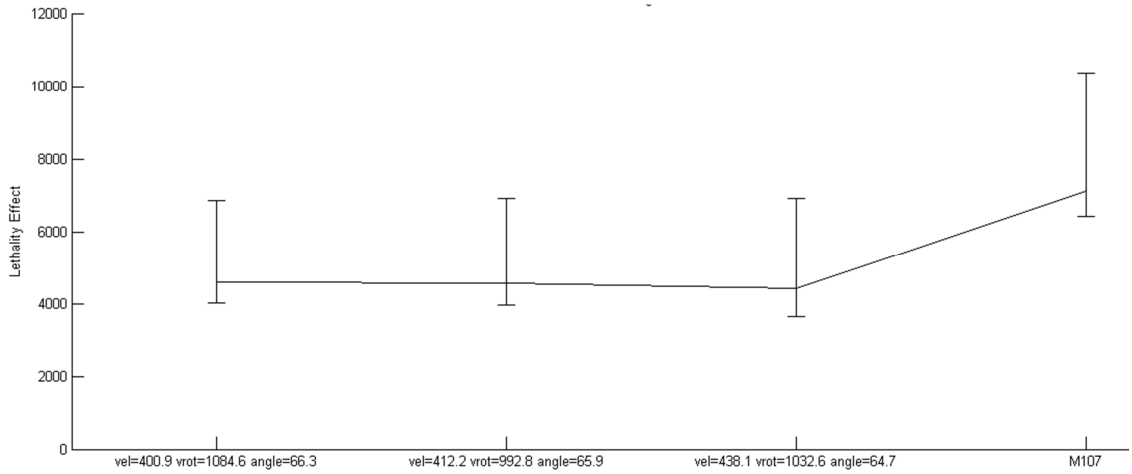

Figure 8-12 Lethality effect for the REP-A and M107 at burst altitude of 0m

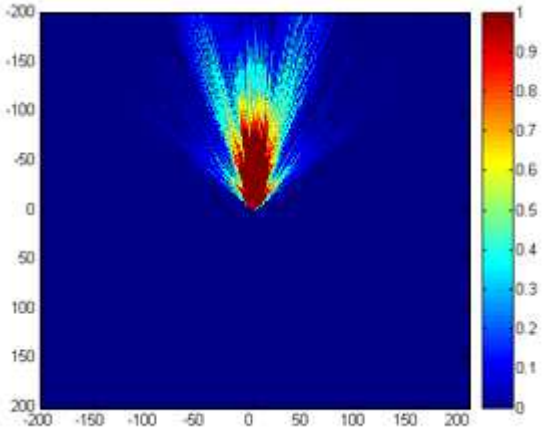

Figure 8-13 MREP-A: Burst alt.=0m V=400.9m/s ω=1084.6 rad/s Impact angle=66.3^{o}

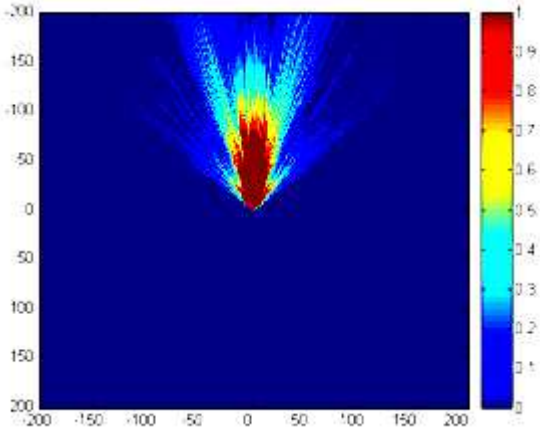

Figure 8-14 MREP-A: Burst alt.=0m V=412.2m/s ω=992.8 rad/s Impact angle=65.9^{o}

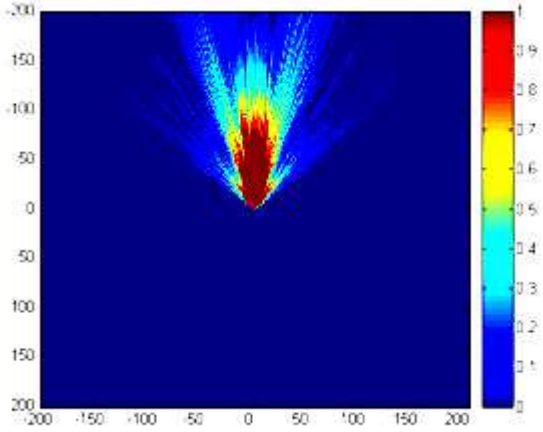

Figure 8-15 MREP-A: Burst alt.=0m V=438.1m/s ω=1032.6 rad/s Impact angle=64.7^{o}

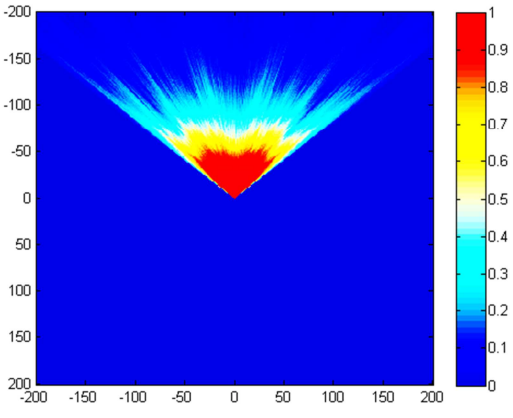

Figure 8-16 Projectile M107: Burst alt.=0m V=333.3m/s ω=1119.7 rad/s Impact angle=63.7^{o}

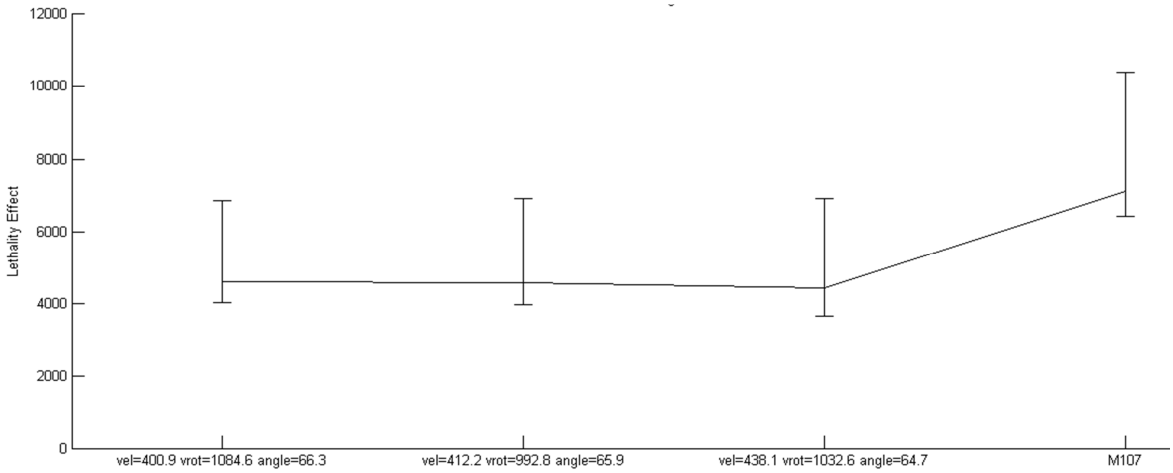

Figure 8-17 Lethality effect for the MREP-B and M107 at burst altitude of 0m

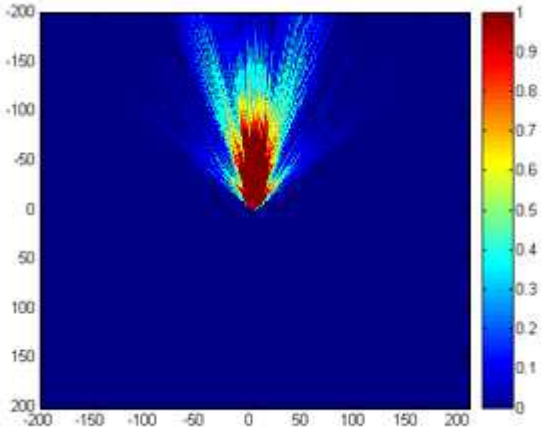

Figure 8-18 MREP-B: Burst alt.=0m V=400.9m/s ω=1084.6 rad/s Impact angle=66.3^{o}

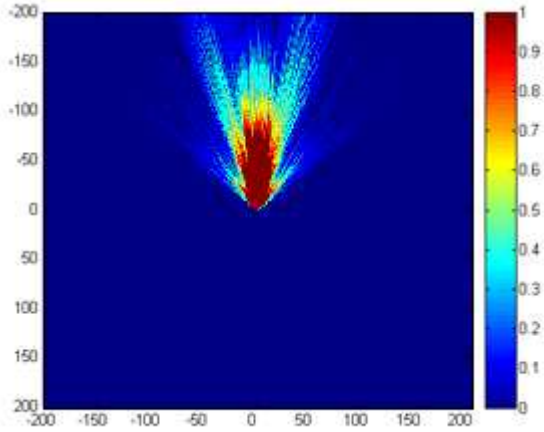

Figure 8-19 REP-B: Burst alt.=0m V=412.2m/s ω=992.8 rad/s Impact angle=65.9^{o}

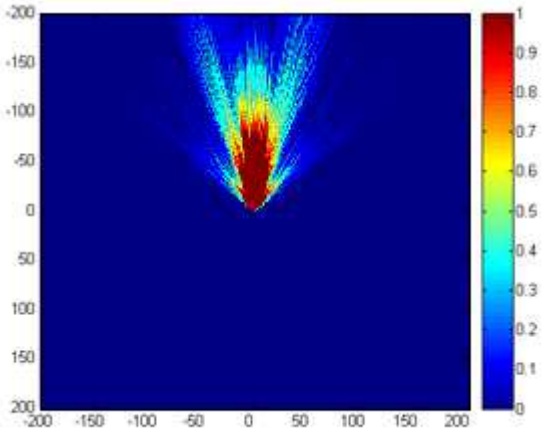

Figure 8-20 MREP-B: Burst alt.=0m V=438.1m/s ω=1032.6 rad/s Impact angle=64.7^{o}

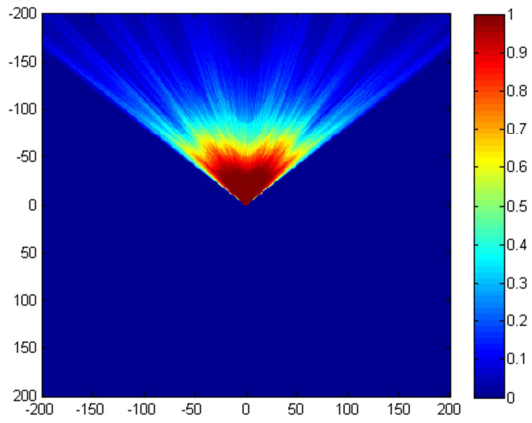

Figure 8-21 Projectile M107: Burst alt.=0m V=333.3m/s ω=1119.7 rad/s Impact angle=63.7^{o}

8.3 Lethality assessment - conclusion

Proposed design of modular artillery projectile with SRM in front part of a projectile and BB unit at the rear of a projectile, from the aspect of target defeating capability by fragmentation effect, has similar efficiency as standard 155mm M107 projectile. It is considered that M-REP would be initiated by Point Detonating Fuze – with “graze” function (precursor with initiation by deceleration, time delay set to ”0”), or Proximity Fuze set to appropriate bust height. The time fuzes has not been investigated in case of fragmentation payload module, but it will have application for smoke, illumination or cargo module for M-REP. The comparison between fragmentation effects of M-REP (both fragmentation variants A and B) is less due to 30% higher impact velocity (more projectile volume-fragments are coming into the ground), but the blast effect should be the similar as the mass of the explosive is only 5% less than M107 projectile. There is no significant difference in lethality effect if the front part, the ogive where SRM is situated, is taken in account for fragmentation (without explosive filling). The lethality and effect on target regarding the fragmentation entirely depends on the M-REP module filled with HE. However, the ogive part, can be significant in penetration into the fortified structures as it will contribute to the kinetic effect itself due to high supersonic impact velocity. Additional optimisation of the payload can be conducted in a way to have pre-fragmented payload in order to increase fragmentation effect on target, as well as to improve metal jacket and C/m ratio. There is a space to design “cargo” version of the payload, as well as illumination, incendiary or payload with thermobaric effect.

9 Conclusions and Recommendations

9.1 Overview

The future of artillery systems and related artillery ammunition is to make them efficient, precise as tactical use of a artillery system requires, and to enable operators more distant stand-off between them and potential targets. In addition, the future projectiles are “referred” to utilise more of the existing delivery systems, to be more “economical”. Modular Range Enhanced Projectile and presented Design and Optimisation Methodology for gun launched projectiles with SRM and BB are tackling all problems related to advancement in ammunition design, proposing feasible solution for effective range increment. The described methodology and “technology” is also looking at the cost factor of gun-projectile system, as majority of other contemporary solutions for range extension are using high end solutions to achieve the goal, making them unviable in terms of cost effective performance. Limiting conditions (existing gun systems) are not exceeded, the M-REP shell design is kept within boundaries of existing ordnances (overall projectile’s dimensions, mass and working pressures). The goal of this work was to present the novelty in design of artillery projectiles as a whole, but also to contribute to advancement in design of base bleed units and solid rocket motor for gun-launched application. Keeping “significant range enhancement” in focus, the M-REP design has been modelled both mathematically (computations), and by testing main contributors to range increment, i.e. SRM and BB has been validated against the experiments.

9.2 Conclusions

The thesis has shown that 155mm M-REP model, represents improvement in design of artillery shells (direct outcome of the thesis). Modular concept of an entire projectile is novelty in design of the artillery shells, enabling diverse use of the projectile, such as blast, fragmentation, thermobaric, incendiary, illumination, cargo, or combination of those effects on a target. The particular fragmentation terminal effect of M-REP has been satisfyingly

validated through lethality simulations. The 155 mm M-REP can supplement artillery ammunition inventories, enhancing range and minimising requirement for different projectiles, just by interchanging the modules. The projectile does not require any additional training for gun-crew, nor does require additional preparation in comparison with a standard round. The results included in the thesis show that M-REP artillery shell with innovative SRM and BB can be fired form standard 155 mm ordnance (39, 45 and 52-calibre gun-howitzers, towed or self-propelled), without any limitations in “size” of gun-propelling charges. Further, thesis results indicate that most benefits will be with “39-calibre” systems, as range of 40+ km using M-REP gives capability to 39 calibre system users to compete with 52-calibre howitzers (direct outcome of the thesis) i.e. reduction of base drag from 65% to 80% with optimised BB design, and with progress in SRM design, result in a range increase of 70% in comparison to standard artillery . The results show that efficiency of projectile is comparable to similar contemporary but significantly more expensive projects, i.e. range and lethality is adequate for required set of targets (counter-battery and engaging third echelon targets), suggesting that the goal set for this thesis has been met successfully.

The additional outcome of this thesis is new rocket propellant formulation that can be used for other propulsion units. Thermoplastic/elastomeric poly plastisol composite propellant with novel binder system, based on modified copolymer technology, have been successfully investigated. The binder based on commercially available ingredients allows simplified production process, but without compromise with propellant performances. The binder can be improved with energetic plasticisers to gain higher specific impulse but for particular applications of base bleed propellant grain and propellant grain with embedded wires, the improvement in combustion characteristics can be weighed against propellant with non-energetic plasticiser, as the propellants without energetic plasticiser may have better mechanical properties. The research shown that novel thermoplastic/elastomeric poly-plastisol propellants have better performance than similar HTPB compositions, corresponding range of burning rate, and adequate mechanical properties. The density specific impulse is

higher - in comparison to HTPB propellant, giving lower grain volume for the same total impulse, which is important for the “volume” restricted gun launched projectiles. The novel propellant shaped in propellant grains, can be easily machined to a geometry required for optimal burning surface development for base bleed. The novel formulation investigated in the thesis, indicated contribution to all significant aspects of BB design: stable ignition, uniform combustion and functioning, after-burning effect, and mechanical strength in combination with an appropriate BB Unit arrangement. The BB modelling methodology contributes to better understating of base bleed effect and most influencing parameters. Further, technique of embedding wires into novel propellant allows design of SRM’s grain with high volumetric factor, without compromising thrust level, and novel approach in modelling of such propellant grain, is contribution to the knowledge in solid rocket propulsion. Again, advantages of such propellant grain design for gun launched application have been established. The thesis has shown that the flight mechanic of the long range projectile can be altered with combination of time delay – de-spinning effect of SRM. The high angle of attack at apogee (that causes increased dispersion), due to high spin rate induced by legacy rifling in gun barrels, can be minimised by setting the appropriate timing sequence with or without de-spinning torque of SRM. The model of projectile with BB and SRM has been partially validated with experimental results, and it can contribute to future researches related to exterior ballistics domain of defence engineering.

9.3 Recommendations and Future work

The M-REP concept represents an inventive “step forward” in artillery projectile design, and very cost–effective innovation. The M-REP is still “core” fire support projectile with its “economical” design, and not a guided missile, Future work should be directed in way that the design methodology for M-REP could be optimised for different calibres. The “benefits” of the "thermoplastic poly plastisol technology" that M-REP’s BB and SRM utilise, can be disseminated for any application in defence or space engineering, where Solid Rocket Propellant Propulsion is required.. The novel thermoplastic binders and

propellants (with or without energetic plasticizers) are “easy” to produce, have high specific impulse and their performance can be "tuned" by simple methods, so future work can be also directed toward production of more insensitive and environmental friendly rocket propellants and explosives. In perspective, as modelled M-REP has capacity for upgrade, it could be fitted with a trajectory correction device in the nose of a projectile, similar to trajectory correction fuze (TCF) in order to increase accuracy (dispersion – both lateral and in range), or Semi Active Laser guidance fuze, producing long range “precision on target” weapon. Prospective investigations, utilising the M-REP exterior ballistic model, can be expanded with guidance and control module.

REFERENCES

[1] Memorandum of Understanding Between the UNITED STATES OF AMERICA and OTHER GOVERNMENTS, TREATIES AND OTHER INTERNATIONAL ACTS SERIES 09-1218, 2009

[2] Grignon C., Cayzac R., Heddadj S., *IMPROVEMENT OF ARTILLERY PROJECTILE ACCURACY*, 23rd INTERNATIONAL SYMPOSIUM ON BALLISTICS, TARRAGONA, 2007

[3] Bo Janzon et al. *THE FUTURE OF WARHEADS, ARMOUR AND BALLISTICS*, 23rd INTERNATIONAL SYMPOSIUM ON BALLISTICS TARRAGONA, 2007

[4] Flyer, *XM 982/EXCALIBUR*, Copyright BAE Systems Bofors AB, 2007

[5] Carlucci, Donald E., *Ballistics: theory and design of guns and ammunition*, CRC Press Taylor & Francis Group, New York 2008

[6] Stiefel L. *Gun Propulsion Technology*, AIAA Publishing, Vol. 109. TL507.P75, Washington DC, USA, 1988.

[7] Richard M. Lloyd, *Conventional Warhead Systems Physics and Engineering Design*, V-179 AIAA, 1998

[8] Z. Jelic, A. Hameed, R. Sheldon, “Design Optimisation of a Range Enhanced Projectile”, conference paper, NASA Glenn Research Centre - 62nd Aeroballistics Range Association Annual Meeting, Cleveland, Ohio, USA, 2011.

[9] Jane’s Ammunition handbook, [documents on the Internet], IHS Publishing, no date [cited 2013, February 02]. Available from https://janes.ihs.com

[10] Hongbing Xiao, Shiyi Li, Qiang Shen, Huquan Li and Qin Wang, *Automatic Positioning of Spinning Projectile in Trajectory Correction Fuze via GPS/IMU Integration*, Proceedings of the 2007 IEEE International Conference on Mechatronics and Automation August 5 - 8, 2007, Harbin, China

[11] Ćuk V. Danilo, *KOREKCIJA PUTANJE ŽIROSKOPSKI STABILISANOG PROJEKTILA PRIMENOM PROPORCIONALNE NAVIGACIJE*, Vojnotehnicki glasnik 2010-1, januar-mart, Beograd 2010 (in Serbian)

[12] Craig A. Phillips, *Guidance Algorithm for Range Maximization and Time-of-Flight Control of a Guided Projectile*, JOURNAL OF GUIDANCE, CONTROL, AND DYNAMICS Vol. 31, No. 5, September–October 2008

[13] K.D. Thomson, *WIND TUNNEL TESTS ON A TUBE-LAUNCHED MISSILE CONFIGURATION WITH A DEFLECTABLE NOSE CONTROL AND A NOVEL WRAP-AROUND FIN STABILISER*, WSRL-0327-TR, 1983

[14] Zhongyuan Wang et al., *The design and experiments of aerodynamic shapes for extended-range projectile,* 23rd INTERNATIONAL SYMPOSIUM ON BALLISTICS TARRAGONA, 2007

[15] Kubota N., *Propellants and Explosives – Thermochemical Aspects of Combustion*, „Wiley-Verlag GmbH“, 2002.

[16] Anderson, D. John. *Fundamentals of Aerodynamics*, McGraw – Hill, Inc. New York, 1991.

[17] Brebner G. G., Anderson J. C., Bartlett R., Moore T.W.F. *Missile Aerodynamics*, series 67, Von Karman Institute for Fluid Dynamics, Brissel, 1974.

[18] Dragović T. *Aerodinamika projektovanja letelica*, Univerzitet u Beogradu, Beograd, 1997. (in Serbian)

[19] Dragović T. *Aerodinamika*, Teorijske osnove projektovanja letelica, I deo, Beograd, 1992. (in Serbian)

[20] Hermann Schlichting, *Boundary Layer Theory*. McGraw–Hill Book Co., New York, 7th edition, 1979. ISBN 0–07–055334–3.

[21] Janković S. *Aerodinamika projektila (Projectile Aerodynamics)*, Mašinski fakultet u Beogradu, 1979. (in Serbian)

[22] Janković S. *Spoljna balistika (Exterior Ballsitics)*, Vojnoizdavački zavod, Beograd 1977. (in Serbian)

[23] Lieske R.F. and McCoy R.L., *Equations of Motion of a Rigid Projectile*, BRL Report No. 1244, 1964.

[24] Mason, L., Devan L., Moore F. G., McMillan D., *Aerodynamics Design Manual for Tactical Weapons*, NSWC TR. 81-1156, Naval Surface Weapons Center, Dahlgren, VA, 1981.

[25] McCoy R. L., *"MC DRAG"- A Computer Program for Estimating the Drag Coefficients of Projectiles*, Ballistic research laboratory, 1981.

[26] McCoy R. L.. *Modern Exterior Ballistics*, Schiffer Publishing, Atglen, PA, USA, 1999.

[27] Military Handbook – 762. *Design of Aerodynamically stabilized free rockets*, US Army Missile Command, Department of Defense, Redstone Arsenal, AL 35809, 1990.

[28] Moore, F. G., *Body Alone Aerodynamics of Guided and Unguided Projectiles at Subsonic, Transonic and Supersonic Mach Numbers*, Naval weapons laboratory, Dahlgren, Virginia, 1973.

[29] N.F. Krasnov, *Aerodynamics of Bodies of Revolution*, American Elsevier Publishing Company Inc. New York 1970.

[30] Robert T. Whyte, SPIN-73, AN UPDATFD VERSION OF THE SPINNER COMPUTER PROGRAM, AD915628, PICATINNY ARSENAL, 1973

[31] White, F. M. *Viscous Fluid Flow*, McGraw – Hill, New York, 1974.

[32] F. G. Moore and L. Y. Moore, *Improved Aerodynamics for Configurations with Boattails*, JOURNAL OF SPACECRAFT AND ROCKETS, Vol. 45, No. 2, March–April 2008

[33] C. J. Bourdon and J. C. Dutton, *Turbulence Structure of a Compressible Base Flow with a Central Bleed Jet*, JOURNAL OF SPACECRAFT AND ROCKETS, Vol. 41, No. 3, May–June 2004

[34] C.-K. Kim and J.-Y. Choi, *NUMERICAL STUDY ON THE BASE DRAG CHARACTERISTICS OF A BASE BLEED PROJECTILE WITH A CENTRAL PROPULSIVE JET*, 22nd International Symposium of Ballistics, 2001

[35] Charles J. Nietubicz and Howard J. Gibeling, *Navier–Stokes Computations for a Reacting M864 Base Bleed Projectile*. In 31st Aerospace Sciences Meeting, Reno, NV, Jan. 1993. AIAA Paper 93–0504.

[36] F. G. Moore and L. Y. Moore, *Improvements to Power-On Base Pressure Prediction for the Aeroprediction Code,* JOURNAL OF SPACECRAFT AND ROCKETS, Vol. 47, No. 1, January–February 2010

[37] Joel P. Kuehner, Blake B. Anderson and Jonathan G. Flittner, *Characteristics of a Central Bleed Jet in Supersonic Axisymmetric Base Flow*, JOURNAL OF SPACECRAFT AND ROCKETS Vol. 44, No. 2, March–April 2007

[38] Jelic, Z., Razvoj inženjerske metode za proračun optimalnog oblika punjenja gasogeneratora za granate, Magisterial Thesis, Mašinski fakultet u Beogradu, 2006 (in Serbian)

[39] Kenneth K. Kuo. *Base Bleed: First International Symposium on Special Topics in Chemical Propulsion*. Hemisphere Publishing Corporation, NewYork, 1988. ISBN 0–89116-937-7.

[40] L. Svanberg et al. *NUMERICAL MODELING AND EXPERIMENTAL VERIFICATION OF A NOVEL BASE BLEED DESIGN*, 23rd INTERNATIONAL SYMPOSIUM ON BALLISTICS TARRAGONA, 2007

[41] Larry R. Rollstin, *Measurement of In-Flight Base Pressure on an Artillery-Fired Projectile*, J. SPACECRAFT, VOL. 27, NO. 1, JAN.-FEB. 1990

[42] Sahu Jubaraj and Heavey Karen R., *Numerical Investigation of Supersonic Base Flow with Base Bleed*. Journal of Spacecraft and Rockets, Vol. 34, No. 1, pp. 62–69, Jan.-Feb. 1997.

[43] Sahu Jubaraj, and Danberg James E., *Navier–Stokes Computations of Transonic Flows with a Two-Equation Turbulence Model*. AIAA Journal, Vol. 24, No. 11, pp. 1744–1751, Nov. 1986.

[44] Sahu Jubaraj, Nietubicz Charles J., and Steger Joseph L., *Navier–Stokes Computations of Projectile Base Flow with and without Mass Injection*. AIAA Journal, Vol. 23, No. 9, pp. 1348–1355, Sep. 1985

[45] Tarun Mathur and J. Craig Dutton, *Base-Bleed Experiments with a Cylindrical Afterbody in Supersonic Flow*. Journal of Spacecraft and Rockets, Vol. 33, No. 1, pp. 30–37, Jan.-Feb. 1996.

[46] Young-Ki Lee et al., *Optimization of Mass Bleed for Base-Drag Reduction*, AIAA JOURNAL Vol. 45, No. 7, July 2007

[47] Zesheng Ding, Shaosong Chen, Yafei Liu, Rong Luo, and Jingyuan Li. *Wind Tunnel Study of Aerodynamic Characteristics of Base Combustion*. Journal of Propulsion and Power, Vol. 8, No. 3, pp. 630–634, May-June 1992.

[48] NASA/SP-8039, *Solid Rocket Motor Performance Analysis and Prediction*, NASA SPACE VEHICLE DESIGN CRITERIA (Chemical Propulsion), NASA (Washington, DC, United States), May, 1971

[49] NASA/SP-8064, *Solid propellant selection and characterization*, NASA SPACE VEHICLE DESIGN CRITERIA (Chemical), NASA (Washington, DC, United States), June, 1971

[50] NASA/SP-8073, *Solid propellant grain structural integrity analysis*, NASA SPACE VEHICLE DESIGN CRITERIA (Chemical), NASA Lewis Research Center (Cleveland, OH, United States), June, 1973

[51] NASA/SP-8075, *Solid propellant processing factor in rocket motor design*, NASA SPACE VEHICLE DESIGN CRITERIA (Chemical), NASA (Washington, DC, United States), October, 1971

[52] NASA/SP-8076, *Solid propellant grain design and internal ballistics*, NASA SPACE VEHICLE DESIGN CRITERIA (Chemical), NASA Lewis Research Center (Cleveland, OH, United States), March, 1972

[53] Sutton, George P.; Biblarz, Rocket Propulsion Elements, John Wiley & Sons, 2001.

[54] Kenneth K. Kuo. Principles of Combustion. John Wiley & Sons, Inc., New York, 1986. ISBN 0–471–62605–8.

[55] Stockenström, NUMERICAL MODEL FOR ANALYSIS AND SPECIFICATION OF A RAMJET PROPELLED ARTILLERY PROJECTILE, 19th International Symposium of Ballistics, 2001

[56] ASHER SIGAL, JAMES E. DANBERG, AERODYNAMICS ANALYSIS OF SOLID FUEL RAMJET PROJECTILES, ADA196755, 1988

[57] R. Oosthuizen, J.J. du Buisson, G.F. Botha, SOLID FUEL RAMJET (SFRJ) PROPULSION FOR ARTILLERY PROJECTILE APPLICATIONS – CONCEPT DEVELOPMENT OVERVIEW, 19th International Symposium of Ballistics, 2001

[58] R.G. Veraar and K. Andersson, FLIGHT TEST RESULTS OF THE SWEDISH-DUTCH SOLID FUEL RAMJET PROPELLED PROJECTILE, 19th International Symposium of Ballistics, 2001

[59] Seo Won Choi et al., Simultaneous Internal/External Flow Calculation of a Solid Fuel Ramjet Projectile: a Design Analysis, KSME International Journal, Vol. 12, No. 3, pp. 479-485, 1998

[60] Carleone J., Tactical missile warheads, American Institute of Aeronautics and Astronautics, Inc., 1993

[61] Z. Jelic, A. Zagorecki, A. Hameed, S. Nandecha, “Fragmentation and Lethality Analysis Tool for Natural and Controlled Fragmentation, and Pre-Fragmented Warheads”, conference paper, 27th International Symposium on Ballistics, Frauhofer EMI, Freiburg, Germany, 2013.

[62] Frank Fresconi and Peter Plostins, Control Mechanism Strategies for Spin-Stabilized Projectiles ARL-TR-4611 September 2008

[63] Thomas Pettersson, Richard Buretta, and David Cook AERODYNAMICS AND FLIGHT STABILITY FOR A COURSE CORRECTED ARTILLERY ROUND, 23rd INTERNATIONAL SYMPOSIUM ON BALLISTICS TARRAGONA, 2007

[64] Flyer, 155 mm VULCANO (BER nad GLR), OTO Melara, Italy, 2013

[65] Jeong-Yeol Choi et al, Numerical Study of Base-Bleed Projectile with External Combustion, 41st AIAA/ASME/SAE/ASEE Joint Propulsion Conference & Exhibit, Tucson, Arizona, 10 - 13 July 2005

[66] Krüger T., Leap Ahead – 52 cal. Artillery System, Presentation at the International Armaments Technology Symposium – 16 June 2004

[67] Zhou C., Meng H., Ju, Y., Zhu G., Analysis on Grain’s Integrity of Ramjet Assisted projectile under High Overload. Proceeding to the 3rd ICMEM, Beijing, 2009

[68] P. Sunitha, Z. Jelic, S. Kumar, A. Hameed, M. Gibson, A. Ali, J. Ram Mohan, “Analysis on Grain’s Structural Integrity of Gun Launched Rocket Assisted Projectile – Range Enhanced Projectile (REP)”, conference paper, 8th International High Energy Materials Conference & Exhibit (HEMCE-2011), Chandigarh, India.

[69] D. E. Coats, IMPROVEMENTS TO THE SOLID PERFORMANCE PROGRAM (SPP), 39th AIAA/ASME/SAE/ASEE Joint Propulsion Conference AIAA-2003-4504 Huntsville, 2003

[70] G. Püskülcü, A. Ulas, 3-D grain burnback analysis of solid propellant rocket motors: Part 1 – ballistic motor tests, Aerospace Science and Technology 12 (2008) 579–584

[71] G. Püskülcü, A. Ulas, 3-D grain burnback analysis of solid propellant rocket motors: Part 2 – modeling and simulations, Aerospace Science and Technology 12 (2008) 585–591

[72] H. G. Darabkhanid and N. S. Mehdizadeh, Solid propellants burning enhancement using foil embedding method, THE AERONAUTICAL JOURNAL, VOLUME 112 NO 1138, DECEMBER 2008

[73] King M., Analytical Modelling of effects of Wires on Solid Motor Ballistics, Journal of Propulsion, Vol. 7, May-June.1991. pp. 312-321

[74] Kubota N., Ichida M., Fujisawa T., Combustion Processes of Propellants with Embedded Metal Wires, AIAA Journal, Vol. 20, Jan.1982. pp. 116-121

[75] Michael A. Willcox, Solid Rocket Motor Internal Ballistics Simulation Using Three-Dimensional Grain Burnback, JOURNAL OF PROPULSION AND POWER Vol. 23, No. 3, May–June 2007

[76] McBride B. J. and Gordon S., Computer Program for Calculation of Complex Chemical Equilibrium Compositions and Applications, Part I: Analysis, NASA RP–1311, 1994.

[77] Williams, Malcolm L.; Landel, Robert F.; Ferry, John D. (1955). "The Temperature Dependence of Relaxation Mechanisms in Amorphous Polymers and Other Glass-forming Liquids". J. Amer. Chem. Soc. 77 (14): 3701–3707

[78] L. C. E. Struik, Physical aging in amorphous polymers and other materials, Elsevier Scientific Pub. Co. ; New York, 1978.

[79] Siewert J., Prodas User Manual, Arrow Tech Associates, 2010

[80] Tanaka, M. et al., Combustion characteristic of solid propellants in vacuum, International Journal of Energetic Materials and Chemical Propulsion, Vol 8(3), 2009

[81] Miller, M.S. and Holmes, H.E., Subatmospheric Burning Rates and Critical Diameters for AP/HTPB Propellant., ARMY BALLISTIC RESEARCH LAB ABERDEEN PROVING GROUND MD, Dec 1988

[82] R. A. BATTISTA, L. H. CAVENY, IU. A. GOSTINTSEV, H. ISODA, N. KUBOTA, and M. SUMMERFIELD. "Theory of dynamic extinguishment of solid propellants with special reference to nonsteady heat feedback law", Journal of Spacecraft and Rockets, Vol. 8, No. 3 (1971), pp. 251-258.

[83] Tanaka M et al. "Combustion of solid propellants at low pressure", 36th AIAA/ASME/SAE/ASEE Joint Propulsion Conference and Exhibit, Joint Propulsion Conferences, 2000.

[84] STANAG 4355 JAIS (EDITION 3) - THE MODIFIED POINT MASS AND FIVE DEGREES OF FREEDOM TRAJECTORY MODELS, NATO, 2009

[85] Kaurinkoski, P. and Hellsten, A., “Numerical Simulation of a Supersonic Base-Bleed Projectile with Improved Turbulence Modelling,” Journal of Spacecraft and Rockets, Vol. 35, No. 5, Sep-Oct. 1998, pp.606-611

[86] Davenas, A. Solid Rocket Propulsion Technology, 1st Edition, Pergamon Press, 1992

[87] Turner M.J.L., “Rocket and Spacecraft Propulsion”, Springer Praxis Books, 2008

[88] Hoffman J.D. *A Computer Program for the Performance Analysis of Scarfed Nozzles,* Technical Report, BATTELLE COLUMBUS LABS RESEARCH TRIANGLE PARK NC , 1984

[89] Phillips, William W. ; Fiedler, Ross A. ; Hopcroft, Robert G., *THRUST COEFFICIENTS, THRUST DEFLECTION ANGLES, AND NONDIMENSIONAL MOMENTS FOR NOZZLES WITH OBLIQUE EXIT PLANES,* BOEING AEROSPACE CO SEATTLE WA, 1968

[90] Landsbaum et al., Specific Impulse Prediction of Solid-Propellant Motors, J of Spacecraft, Vol.17, No.05, AIAA, 1980

[91] Environmental Engineering Considerations and Laboratory Tests; MIL-STD-810G; U.S. Department of Defense USA, 2008.

[92] Smallwood, R.E., at al Refractory Metals and Their Industrial Applications: A Symposium, Issue 849 ASTM International, 1984.

[93] Rumbel, K.E., “Poly(vinyl chloride) Plastisol Propellants,” Propellants Manufacture, Hazards, and Testing, Advances in Chemistry Series, American Chemical Society, No. 88, Washington, D.C., 1969, pp. 36-66.

[94] Caveny, L. H., and R. L. Glick. “Influence of Embedded Metal Fibers on Solid Propellant BurningRate.” Journal of Spacecraft 4.1 (1967): 79-85.

[95] Gosant, B., et al. “Theoretical Calculus of Burning Rate Ratio in Grains with Embedded Metal Wires.’Paper presented at the 24th AIAA/ASME/SAE/ASEE Joint Propulsion Conference, 1988

[96] Winch, P.C., et al. “Forced Cone Burning for Active Control of Solid Propellant Burning Rate.” Paper presented at the 22nd IAA/ASME/SAE/ASEE Joint Propulsion Conference, June 16-18,1986, Huntsville

[97] Geisler, R., Beckman, C. "The History of the BATES Motors at the Air Force Rocket Propulsion Laboratory". Paper presented at the 34th AIAA/ASME/SAE/ASEE Joint Propulsion Conference, 1998

[98] SciFinder, [documents on the Internet], CAS – division of American Chemical Society, no date [cited 2012, September 04]. Available from https://www.cas.org

[99] Bathelt, H., Volk, F.: “User’s Manual for the ICT-Thermodynamic Code” Fraunhofer-Institut für Chemische Technologie ICT, 2012

[100] Reutech Fuchs Electronics Product Catalogue - Fuzes, [documents on the Internet], Reutech Fuchs, no date [cited 2012, December 05]. Available from http://www.fuchs.co.za/

[101] Jelic Z. et al., Raw Data [unpublished] , 2007

[102] PTC Creo Parametric - online documentation, [documents on the Internet], PTC Co., no date [cited 2012, June 17]. Available from http://www.ptc.com

[103] STANAG 4506 (Ed 1), Explosive Materials, Physical/Mechanical Properties Uniaxial Tensile Test, NATO, 2000

[104] Burke, P.J., Pergolozzi, A. *XM1156 Precision Guidance Kit (PGK), overview for 2010 Fuze Conference*, 2010, [document on the Internet], [cited 2013, February 18]. Available from http://dtic.mil

[105] The ISO Standard Atmosphere, 1975, ISO 2533

[106] Amoruso, M.J., *Euler Angles and Quaternions in Six Degree of Freedom Simulations of Projectiles*, March 1996, U.S. Army Armament, Aeroballistics Branch.

[107] Baranowski, L. *Numerical Testing of Flight Stability of Spin-Stabilized Artillery Projectiles*, Military University of Technology, Faculty of Mechatronics and Aerospace, Warsaw, Poland, Journal of Theoretical and Applied Mechanics 51, 2, pp. 375-385, Warsaw 2013.

[108] Siewert J., Prodas V3 Technical Manual, Arrow Tech Associates, 2010

[109] BALON R, KOMENDA J, ANALYSIS OF THE 155 MM ERFB/BB PROJECTILE TRAJECTORY, Advances in MT, 10/2006

[110] Dmitrievskii A.A., External Ballistics , Mashinostroenie, Moscow 2005 [in Russian]

[111] Lebedev A.A. *Flight Dynamics*, Mashinostroenie, Moscow 1973 [in Russian]

[112] Lieske R.F. Reiter M., *Equations of Motion for a Modified Mass Point Traject*ory, BRL Report No. 1314 1966.

[113] Baranowski, L. *EQUATIONS OF MOTION OF A SPIN-STABILIZED PROJECTILE FOR FLIGHT STABILITY TESTING*, JOURNAL OF THEORETICAL AND APPLIED MECHANICS 51, 1, pp. 235-246, Warsaw 2013

[114] Pekic Z. *PREDICTION THE BALLISTIC TRAJECTORY OF SPIN-STABILISED PRIJECTILES BY METHOD OF MODIFIED POINT MASS, RIM'99, Bihac, 1999*

[115] Zagorecki, A., Hameed, A., and Shukla, A. *Lethality Analysis Based on a Fragmentation Model for Naturally Fragmenting Shells*, IBS 2011.

[116] Z. Jelic, A. Hameed, *A Case Study to Investigate the Propulsion Aspects of Air-Intercept-Missile (AIM) Conversion into Surface-to-Air Missile (SAM) for Air-Defence*, conference paper, International Symposium on Air Defence 2020+, The Air Defence Forces Institute, Jeddah, Saudi Arabia, 2011.

APPENDICES

Appendix A Results of PRODAS Simulations of M-REP Exterior Ballistics

Table A-1 AERODYNAMIC COEFFICEINTS FOR M-REP - PRODAS [79]

Ref Dia	Ref CG	Total Length	Ogive Length	Ogive Radius	Boattail Length	Boattail Dia	Meplat Dia	Band Length	Band Dia	Boom Length	Boom Dia	
154.74	594.74	920.90	543.20	4000.00	114.20	141.29	10.70	37.08	157.58	0.00	0.00	mm
1.000	3.843	5.951	3.510	25.8	0.738	0.913	0.069	0.240	1.018	0.000	0.000	Caliber

Mach	CX0	CX2	CX4	CNa	CNa3	CPN	CYpa	CXf	CXb	CNq
0.600	0.152	1.96	0.0	1.75	0.0	1.50	-0.85	0.039	0.113	2.3
0.700	0.152	2.16	0.0	1.77	0.0	1.54	-0.86	0.034	0.117	2.1
0.750	0.153	2.25	0.0	1.78	0.0	1.54	-0.87	0.033	0.119	2.1
0.800	0.155	2.34	0.0	1.81	0.0	1.56	-0.89	0.034	0.121	2.1
0.850	0.156	2.49	0.0	1.84	0.0	1.61	-0.91	0.032	0.124	2.2
0.875	0.163	2.60	0.0	1.88	0.0	1.66	-0.93	0.038	0.125	2.3
0.900	0.173	2.68	0.0	1.95	0.0	1.71	-0.95	0.048	0.126	2.8
0.925	0.184	2.89	0.0	2.05	0.0	1.78	-1.07	0.058	0.127	3.4
0.950	0.207	3.09	0.0	2.14	0.0	1.83	-1.21	0.079	0.128	4.4
0.975	0.237	3.30	0.0	2.19	0.0	1.88	-1.08	0.109	0.129	5.9
1.000	0.271	3.50	0.0	2.20	0.0	1.94	-1.00	0.107	0.164	6.7
1.025	0.301	3.70	0.0	2.23	0.0	1.95	-0.96	0.138	0.163	8.0
1.050	0.318	3.87	0.0	2.25	0.0	1.98	-0.92	0.157	0.162	8.7
1.100	0.324	4.34	0.0	2.31	0.0	2.04	-0.86	0.162	0.162	9.5
1.200	0.324	4.82	0.0	2.39	0.0	2.12	-0.78	0.165	0.159	10.0
1.350	0.315	4.32	0.0	2.43	0.0	2.12	-0.70	0.160	0.155	10.0
1.500	0.299	3.85	0.0	2.48	0.0	2.15	-0.68	0.150	0.149	10.0
1.750	0.276	3.32	0.0	2.61	0.0	2.26	-0.65	0.136	0.140	8.2
2.000	0.251	2.78	0.0	2.71	0.0	2.38	-0.61	0.123	0.129	7.2
2.250	0.232	2.49	0.0	2.79	0.0	2.44	-0.60	0.115	0.117	6.1
2.500	0.219	2.20	0.0	2.83	0.0	2.45	-0.60	0.113	0.106	5.8
3.000	0.196	1.77	0.0	2.87	0.0	2.47	-0.60	0.110	0.087	5.7
3.500	0.181	1.59	0.0	2.84	0.0	2.47	-0.60	0.110	0.070	5.5

Moments at Baseline CG = 3.74 Calibers from the Nose

Mach	Cma	Cma3	Cma5	Cmq	Cmq2	Cnpa@1	Cnpa@3	Cnpa@5	Clp	Cld
0.600	4.113	0.00	0.0	-8.33	0.0	-0.65	0.42	1.53	-0.0267	0.0000
0.700	4.084	0.00	0.0	-9.34	0.0	-0.80	0.29	1.53	-0.0264	0.0000
0.750	4.099	0.00	0.0	-10.31	0.0	-0.98	0.15	1.37	-0.0260	0.0000
0.800	4.136	0.00	0.0	-11.33	0.0	-1.10	0.00	1.28	-0.0257	0.0000
0.850	4.097	0.00	0.0	-12.23	0.0	-0.82	0.07	1.13	-0.0254	0.0000
0.875	4.119	0.00	0.0	-12.93	0.0	-0.63	0.13	1.07	-0.0252	0.0000
0.900	4.169	0.00	0.0	-13.73	0.0	-0.61	0.16	0.99	-0.0250	0.0000
0.925	4.239	0.00	0.0	-14.61	0.0	-0.41	0.27	1.18	-0.0248	0.0000
0.950	4.307	0.00	0.0	-15.70	0.0	-0.12	0.45	1.25	-0.0245	0.0000
0.975	4.293	0.00	0.0	-17.05	0.0	0.13	0.54	1.08	-0.0243	0.0000
1.000	4.187	0.00	0.0	-18.67	0.0	0.32	0.66	1.09	-0.0241	0.0000
1.025	4.220	0.00	0.0	-20.64	0.0	0.59	0.82	1.04	-0.0245	0.0000
1.050	4.208	0.00	0.0	-22.06	0.0	0.67	0.84	1.02	-0.0245	0.0000
1.100	4.155	0.00	0.0	-23.35	0.0	0.63	0.75	0.85	-0.0245	0.0000
1.200	4.121	0.00	0.0	-24.62	0.0	0.53	0.62	0.65	-0.0248	0.0000
1.350	4.188	0.00	0.0	-26.16	0.0	0.57	0.65	0.69	-0.0250	0.0000
1.500	4.202	0.00	0.0	-27.86	0.0	0.53	0.53	0.54	-0.0239	0.0000
1.750	4.117	0.00	0.0	-29.47	0.0	0.52	0.52	0.53	-0.0231	0.0000
2.000	3.976	0.00	0.0	-30.93	0.0	0.52	0.51	0.51	-0.0228	0.0000
2.250	3.909	0.00	0.0	-31.49	0.0	0.51	0.50	0.51	-0.0222	0.0000
2.500	3.949	0.00	0.0	-30.57	0.0	0.50	0.49	0.51	-0.0211	0.0000
3.000	3.925	0.00	0.0	-29.21	0.0	0.50	0.49	0.51	-0.0196	0.0000
3.500	3.890	0.00	0.0	-27.22	0.0	0.50	0.49	0.51	-0.0187	0.0000

Moments at Burn Out CG = 3.84 Calibers from the Nose

Mach	Cma	Cma3	Cma5	Cmq	Cmq2	Cnpa@1	Cnpa@3	Cnpa@5	Clp	Cld
0.600	3.925	0.00	0.0	-8.58	0.0	-0.75	0.32	1.43	-0.0267	0.0000
0.700	3.895	0.00	0.0	-9.57	0.0	-0.89	0.19	1.44	-0.0264	0.0000
0.750	3.909	0.00	0.0	-10.53	0.0	-1.07	0.06	1.28	-0.0260	0.0000
0.800	3.942	0.00	0.0	-11.55	0.0	-1.19	-0.09	1.19	-0.0257	0.0000
0.850	3.901	0.00	0.0	-12.47	0.0	-0.92	-0.03	1.04	-0.0254	0.0000
0.875	3.918	0.00	0.0	-13.17	0.0	-0.73	0.03	0.97	-0.0252	0.0000
0.900	3.960	0.00	0.0	-14.03	0.0	-0.71	0.06	0.89	-0.0250	0.0000
0.925	4.020	0.00	0.0	-14.98	0.0	-0.52	0.15	1.06	-0.0248	0.0000
0.950	4.079	0.00	0.0	-16.17	0.0	-0.25	0.32	1.12	-0.0245	0.0000
0.975	4.059	0.00	0.0	-17.68	0.0	0.01	0.43	0.96	-0.0243	0.0000
1.000	3.951	0.00	0.0	-19.38	0.0	0.21	0.56	0.98	-0.0241	0.0000
1.025	3.981	0.00	0.0	-21.50	0.0	0.49	0.72	0.94	-0.0245	0.0000
1.050	3.967	0.00	0.0	-22.99	0.0	0.57	0.74	0.92	-0.0245	0.0000
1.100	3.908	0.00	0.0	-24.36	0.0	0.54	0.66	0.76	-0.0245	0.0000
1.200	3.866	0.00	0.0	-25.69	0.0	0.44	0.53	0.57	-0.0248	0.0000
1.350	3.928	0.00	0.0	-27.23	0.0	0.50	0.57	0.62	-0.0250	0.0000
1.500	3.937	0.00	0.0	-28.94	0.0	0.46	0.46	0.47	-0.0239	0.0000
1.750	3.838	0.00	0.0	-30.35	0.0	0.45	0.45	0.46	-0.0231	0.0000
2.000	3.686	0.00	0.0	-31.70	0.0	0.45	0.45	0.44	-0.0228	0.0000
2.250	3.611	0.00	0.0	-32.14	0.0	0.44	0.43	0.44	-0.0222	0.0000
2.500	3.646	0.00	0.0	-31.20	0.0	0.44	0.43	0.44	-0.0211	0.0000
3.000	3.619	0.00	0.0	-29.82	0.0	0.44	0.43	0.44	-0.0196	0.0000
3.500	3.587	0.00	0.0	-27.81	0.0	0.44	0.43	0.44	-0.0187	0.0000

Moments at Baseline CG = 3.74 Calibers from the Nose
Magnus Moment Derivative - Cnpa
Angle of Attack - Degrees

Mach	0	1	2	3	4	5	7.5	10	15	20
0.600	-0.812	-0.654	-0.213	0.416	1.070	1.525	2.021	1.976	1.949	1.922
0.700	-0.956	-0.799	-0.356	0.286	0.981	1.529	1.991	1.945	1.918	1.890
0.750	-1.144	-0.978	-0.513	0.153	0.856	1.370	1.952	1.906	1.879	1.851
0.800	-1.256	-1.097	-0.648	0.004	0.714	1.281	1.633	1.586	1.558	1.530
0.850	-0.948	-0.820	-0.458	0.070	0.653	1.133	1.552	1.504	1.475	1.446
0.875	-0.738	-0.629	-0.320	0.132	0.637	1.067	1.528	1.479	1.449	1.419
0.900	-0.721	-0.608	-0.291	0.163	0.640	0.987	1.306	1.256	1.226	1.195
0.925	-0.502	-0.407	-0.136	0.269	0.739	1.177	1.487	1.430	1.395	1.361
0.950	-0.202	-0.123	0.104	0.446	0.852	1.249	1.574	1.509	1.470	1.431
0.975	0.072	0.130	0.295	0.541	0.823	1.079	1.449	1.392	1.357	1.323
1.000	0.273	0.321	0.459	0.663	0.892	1.090	1.079	1.026	0.994	0.962
1.025	0.560	0.595	0.690	0.824	0.958	1.040	1.048	0.997	0.967	0.936
1.050	0.649	0.673	0.740	0.838	0.941	1.018	1.024	0.975	0.946	0.916
1.100	0.617	0.634	0.682	0.748	0.813	0.850	0.907	0.861	0.834	0.807
1.200	0.510	0.525	0.566	0.618	0.658	0.652	0.657	0.616	0.591	0.566
1.350	0.561	0.573	0.605	0.647	0.684	0.694	0.688	0.652	0.630	0.608
1.500	0.528	0.528	0.529	0.532	0.536	0.543	0.554	0.519	0.498	0.477
1.750	0.521	0.520	0.521	0.522	0.525	0.533	0.528	0.495	0.474	0.454
2.000	0.517	0.516	0.514	0.511	0.509	0.510	0.510	0.478	0.459	0.440
2.250	0.508	0.506	0.502	0.497	0.497	0.509	0.504	0.473	0.454	0.435
2.500	0.505	0.503	0.498	0.493	0.494	0.508	0.504	0.473	0.454	0.435
3.000	0.503	0.501	0.497	0.493	0.494	0.509	0.505	0.474	0.455	0.436
3.500	0.503	0.501	0.497	0.493	0.494	0.509	0.505	0.474	0.455	0.436

Magnus Moment Coefficient - Cnp
Angle of Attack - Degrees

Mach	0	1	2	3	4	5	7.5	10	15	20
0.600	0.0000	-0.0114	-0.0074	0.0218	0.0746	0.1329	0.2638	0.3431	0.5044	0.6573
0.700	0.0000	-0.0139	-0.0124	0.0149	0.0684	0.1333	0.2598	0.3377	0.4963	0.6465
0.750	0.0000	-0.0171	-0.0179	0.0080	0.0597	0.1194	0.2548	0.3310	0.4862	0.6331
0.800	0.0000	-0.0191	-0.0226	0.0002	0.0498	0.1117	0.2132	0.2754	0.4032	0.5233
0.850	0.0000	-0.0143	-0.0160	0.0037	0.0455	0.0987	0.2026	0.2611	0.3817	0.4944
0.875	0.0000	-0.0110	-0.0112	0.0069	0.0445	0.0930	0.1994	0.2567	0.3759	0.4854
0.900	0.0000	-0.0106	-0.0101	0.0085	0.0447	0.0860	0.1705	0.2181	0.3172	0.4088
0.925	0.0000	-0.0071	-0.0048	0.0141	0.0515	0.1026	0.1940	0.2482	0.3611	0.4655
0.950	0.0000	-0.0021	0.0036	0.0234	0.0595	0.1089	0.2055	0.2621	0.3805	0.4895
0.975	0.0000	0.0023	0.0103	0.0283	0.0574	0.0941	0.1892	0.2417	0.3513	0.4525
1.000	0.0000	0.0056	0.0160	0.0347	0.0622	0.0950	0.1408	0.1781	0.2573	0.3291
1.025	0.0000	0.0104	0.0241	0.0431	0.0668	0.0906	0.1368	0.1731	0.2502	0.3202
1.050	0.0000	0.0117	0.0258	0.0438	0.0656	0.0887	0.1336	0.1693	0.2448	0.3134
1.100	0.0000	0.0111	0.0238	0.0391	0.0567	0.0741	0.1183	0.1496	0.2159	0.2760
1.200	0.0000	0.0092	0.0198	0.0324	0.0459	0.0568	0.0857	0.1069	0.1530	0.1938
1.350	0.0000	0.0100	0.0211	0.0339	0.0477	0.0605	0.0898	0.1132	0.1630	0.2078
1.500	0.0000	0.0092	0.0185	0.0278	0.0374	0.0473	0.0724	0.0902	0.1289	0.1631
1.750	0.0000	0.0091	0.0182	0.0273	0.0366	0.0464	0.0690	0.0859	0.1228	0.1553
2.000	0.0000	0.0090	0.0179	0.0268	0.0355	0.0445	0.0665	0.0830	0.1188	0.1505
2.250	0.0000	0.0088	0.0175	0.0260	0.0347	0.0444	0.0657	0.0821	0.1174	0.1488
2.500	0.0000	0.0088	0.0174	0.0258	0.0344	0.0443	0.0658	0.0821	0.1175	0.1488
3.000	0.0000	0.0088	0.0173	0.0258	0.0345	0.0444	0.0659	0.0823	0.1178	0.1493
3.500	0.0000	0.0088	0.0173	0.0258	0.0345	0.0444	0.0659	0.0823	0.1178	0.1493

Expressed in CD and CL Convention (CX, CNa and Magnus Poly Coeffs given for information)

Mach	CDo	CD2	CLa	CLa3	CXo	CX2	CNa	CNa3	Cmpa0	Cmpa3	Cmpa5
0.600	0.152	3.72	1.60	-1.96	0.152	1.96	1.75	0.00	-0.81	528.2	-28991.
0.700	0.152	3.93	1.62	-2.16	0.152	2.16	1.77	0.00	-0.96	525.0	-26001.
0.750	0.153	4.04	1.63	-2.25	0.153	2.25	1.78	0.00	-1.14	554.6	-29390.
0.800	0.155	4.15	1.66	-2.34	0.155	2.34	1.81	0.00	-1.26	532.1	-26014.
0.850	0.156	4.32	1.68	-2.49	0.156	2.49	1.84	0.00	-0.95	427.5	-20166.
0.875	0.163	4.48	1.72	-2.60	0.163	2.60	1.88	0.00	-0.74	363.1	-16474.
0.900	0.173	4.63	1.78	-2.68	0.173	2.68	1.95	0.00	-0.72	378.1	-20143.
0.925	0.184	4.94	1.87	-2.89	0.184	2.89	2.05	0.00	-0.50	315.9	-12433.
0.950	0.207	5.22	1.93	-3.09	0.207	3.09	2.14	0.00	-0.20	262.6	-9378.
0.975	0.237	5.49	1.95	-3.30	0.237	3.30	2.19	0.00	0.07	193.1	-7934.
1.000	0.271	5.71	1.93	-3.50	0.271	3.50	2.20	0.00	0.27	162.3	-7173.
1.025	0.301	5.93	1.93	-3.70	0.301	3.70	2.23	0.00	0.56	115.1	-6837.
1.050	0.318	6.12	1.93	-3.87	0.318	3.87	2.25	0.00	0.65	80.6	-4207.
1.100	0.324	6.65	1.98	-4.34	0.324	4.34	2.31	0.00	0.62	57.6	-3532.
1.200	0.324	7.21	2.06	-4.82	0.324	4.82	2.39	0.00	0.51	51.2	-4282.
1.350	0.315	6.75	2.12	-4.32	0.315	4.32	2.43	0.00	0.56	39.1	-2848.
1.500	0.299	6.33	2.18	-3.85	0.299	3.85	2.48	0.00	0.53	1.3	87.
1.750	0.276	5.93	2.33	-3.32	0.276	3.32	2.61	0.00	0.52	-0.2	241.
2.000	0.251	5.49	2.46	-2.78	0.251	2.78	2.71	0.00	0.52	-2.7	241.
2.250	0.232	5.28	2.56	-2.49	0.232	2.49	2.79	0.00	0.51	-6.9	917.
2.500	0.219	5.02	2.61	-2.20	0.219	2.20	2.83	0.00	0.51	-7.2	995.
3.000	0.196	4.64	2.67	-1.77	0.196	1.77	2.87	0.00	0.50	-6.6	966.
3.500	0.181	4.43	2.66	-1.59	0.181	1.59	2.84	0.00	0.50	-6.6	966.

Comparison of User Baseline Drag, Spin2004 Prediction and McDrag Prediction

Mach	User CXo	Diff1	2004 CXo	Diff2	McDrag CXo	Head CXH	Skin CXSF	Band CXBND	Boat CXBT	Base CXB
0.600	0.152	0.000	0.152	0.012	0.164	0.000	0.051	0.000	0.000	0.113
0.700	0.152	0.000	0.152	0.016	0.167	0.000	0.050	0.000	0.000	0.117
0.750	0.153	0.000	0.153	0.016	0.169	0.000	0.049	0.001	0.000	0.119
0.800	0.155	0.000	0.155	0.016	0.171	0.000	0.048	0.001	0.000	0.121
0.850	0.156	0.000	0.156	0.017	0.173	0.000	0.047	0.002	0.000	0.124
0.875	0.163	0.000	0.163	0.013	0.176	0.000	0.047	0.003	0.001	0.125
0.900	0.173	0.000	0.173	0.005	0.178	0.000	0.047	0.005	0.001	0.126
0.925	0.184	0.000	0.184	0.002	0.186	0.004	0.047	0.007	0.002	0.127
0.950	0.207	0.000	0.207	-0.005	0.202	0.015	0.046	0.010	0.003	0.128
0.975	0.237	0.000	0.237	-0.019	0.218	0.025	0.046	0.009	0.009	0.129
1.000	0.271	0.000	0.271	0.001	0.272	0.035	0.046	0.009	0.019	0.164
1.025	0.301	0.000	0.301	0.037	0.338	0.104	0.045	0.009	0.017	0.163
1.050	0.318	0.000	0.318	-0.005	0.314	0.087	0.044	0.008	0.012	0.162
1.100	0.324	0.000	0.324	-0.012	0.313	0.087	0.044	0.008	0.012	0.162
1.200	0.324	0.000	0.324	-0.016	0.308	0.078	0.043	0.007	0.020	0.159
1.350	0.315	0.000	0.315	-0.022	0.293	0.072	0.042	0.007	0.018	0.155
1.500	0.299	0.000	0.299	-0.020	0.280	0.068	0.040	0.006	0.016	0.149
1.750	0.276	0.000	0.276	-0.016	0.260	0.063	0.038	0.006	0.014	0.140
2.000	0.251	0.000	0.251	-0.010	0.241	0.060	0.036	0.005	0.012	0.129
2.250	0.232	0.000	0.232	-0.008	0.224	0.057	0.034	0.005	0.011	0.117
2.500	0.219	0.000	0.219	-0.011	0.208	0.055	0.032	0.005	0.010	0.106
3.000	0.196	0.000	0.196	-0.016	0.180	0.052	0.029	0.004	0.008	0.087
3.500	0.181	0.000	0.181	-0.023	0.158	0.049	0.027	0.004	0.007	0.070

Table A-2 Stability Analysis Output for projectile with muzzle velocity of 821m/s – 39 caliber gun, Std. atmospheric conditions:

```
Initial conditions:
Muzzle Velocity         821.0 m/sec
Aircraft Velocity       0.0 m/sec
Air Density             1.22500 kg/m^3
Air Temperature         15.0 C
Muzzle Spin Rate        264. CPS
Muzzle Exit Twist       20.1 cal/rev
CP from Nose            378.40 mm
CP from Nose            2.45 Calibers
CG from Nose            594.74 mm
CG from Nose            3.84 Calibers
Mach Number             2.41
Gyro Stab Factor        2.06
Ballistic Coeff.        7.181
Cd at Muzzle            0.225
Deceleration            42.66 m/s/1000m
Muzzle Jump Factor   0.198 mils/rad/sec
```

Projectile Data at the Muzzle

Projectile Dia.	154.740	mm
Weight	49.776	kg
Axial Inertia	0.171057	kg-m^2
Trans Inertia	2.07184	kg-m^2
CG (from nose)	594.74	mm

Met Data Utilised for Computations

Launch Altitude above SL	0.0	m			
Pressure	1013.2	millibars	Density	1.2250	kg/m^3
Temperature	15.0	C	Speed of Sound	340.3	m/sec

Muzzle Exit Aeroballistic Parameters

Total Velocity	821.0	m/sec			
Gun Twist	20.1	cal/rev			
Mach Number	2.41				
Muzzle Spin Rate	115.8	deg/m	1659.0	rad/sec	264.0 cyc/sec
Fast Mode Rate	8.2	deg/m	117.6	rad/sec	18.7 cyc/sec
Slow Mode Rate	1.4	deg/m	19.4	rad/sec	3.1 cyc/sec
Fast Mode Damping	-0.00177	1/m			
Slow Mode Damping	-0.00094	1/m			
Yaw Period	52.5	m			
Muzzle to Max Yaw	26.3	m			
Muzzle to Half Yaw	512.2	m			
Gyroscopic Factor	2.06				
Deceleration	42.66	m/s/1000m			
Drag Coefficient	0.225				
Muzzle Jump Factor	0.198	mils/rad/sec			
Ballistic Coefficient (based on Ingalls DF)	7.181				

Mach Number	Gyroscopic Stabilty Factor	Fast Arm Damping Rate at Angles of Attack					Slow Arm Damping Rate at Angles of Attack				
		1 1/m	2 1/m	5 1/m	7.5 1/m	10 1/m	1 1/m	2 1/m	5 1/m	7.5 1/m	10 1/m
0.600	1.97	-0.00134	-0.00083	0.00117	0.00174	0.00169	0.00038	-0.00013	-0.00213	-0.00270	-0.00265
0.700	1.98	-0.00158	-0.00107	0.00109	0.00161	0.00156	0.00055	0.00004	-0.00212	-0.00265	-0.00259
0.750	1.97	-0.00187	-0.00133	0.00083	0.00150	0.00144	0.00077	0.00023	-0.00193	-0.00260	-0.00254
0.800	1.96	-0.00209	-0.00157	0.00065	0.00106	0.00100	0.00092	0.00040	-0.00183	-0.00223	-0.00218
0.850	1.97	-0.00184	-0.00142	0.00040	0.00088	0.00083	0.00060	0.00018	-0.00164	-0.00212	-0.00207
0.875	1.96	-0.00168	-0.00132	0.00028	0.00081	0.00075	0.00038	0.00002	-0.00157	-0.00210	-0.00205
0.900	1.94	-0.00172	-0.00135	0.00013	0.00050	0.00044	0.00035	-0.00001	-0.00149	-0.00186	-0.00180
0.925	1.91	-0.00156	-0.00124	0.00029	0.00065	0.00059	0.00011	-0.00020	-0.00174	-0.00210	-0.00203
0.950	1.88	-0.00132	-0.00105	0.00030	0.00068	0.00061	-0.00022	-0.00049	-0.00184	-0.00222	-0.00215
0.975	1.88	-0.00113	-0.00093	-0.00001	0.00043	0.00036	-0.00051	-0.00071	-0.00163	-0.00207	-0.00200
1.000	1.93	-0.00103	-0.00087	-0.00014	-0.00015	-0.00021	-0.00072	-0.00088	-0.00161	-0.00160	-0.00154
1.025	1.92	-0.00087	-0.00076	-0.00035	-0.00034	-0.00040	-0.00102	-0.00113	-0.00154	-0.00155	-0.00149
1.050	1.92	-0.00090	-0.00082	-0.00049	-0.00049	-0.00054	-0.00109	-0.00117	-0.00150	-0.00150	-0.00145
1.100	1.95	-0.00104	-0.00099	-0.00079	-0.00073	-0.00078	-0.00105	-0.00110	-0.00130	-0.00136	-0.00131
1.200	1.96	-0.00127	-0.00122	-0.00112	-0.00112	-0.00116	-0.00092	-0.00097	-0.00107	-0.00108	-0.00103
1.350	1.93	-0.00134	-0.00130	-0.00119	-0.00120	-0.00124	-0.00097	-0.00101	-0.00111	-0.00110	-0.00106
1.500	1.93	-0.00152	-0.00152	-0.00151	-0.00149	-0.00153	-0.00090	-0.00091	-0.00092	-0.00093	-0.00089
1.750	1.97	-0.00165	-0.00165	-0.00164	-0.00164	-0.00168	-0.00091	-0.00091	-0.00093	-0.00092	-0.00088
2.000	2.03	-0.00176	-0.00176	-0.00177	-0.00177	-0.00181	-0.00092	-0.00092	-0.00092	-0.00092	-0.00088
2.250	2.07	-0.00181	-0.00182	-0.00181	-0.00181	-0.00185	-0.00093	-0.00092	-0.00093	-0.00093	-0.00089
2.500	2.05	-0.00174	-0.00175	-0.00174	-0.00174	-0.00178	-0.00095	-0.00094	-0.00095	-0.00095	-0.00091
3.000	2.06	-0.00163	-0.00164	-0.00162	-0.00163	-0.00166	-0.00097	-0.00097	-0.00098	-0.00098	-0.00094
3.500	2.08	-0.00147	-0.00148	-0.00146	-0.00147	-0.00150	-0.00099	-0.00099	-0.00100	-0.00100	-0.00096

Mach Number	Gyroscopic Stabilty Factor	Dynamic Stabilty Factor at Angles of Attack					Recipical Dynamic Factor at Angles of Attack				
		1	2	5	7.5	10	1	2	5	7.5	10
0.600	1.97	-0.35	0.45	3.60	4.49	4.41	-1.21	1.44	-0.17	-0.09	-0.09
0.700	1.98	-0.56	0.18	3.34	4.12	4.04	-0.70	3.01	-0.22	-0.11	-0.12
0.750	1.97	-0.80	-0.07	2.88	3.80	3.72	-0.45	-6.80	-0.39	-0.15	-0.16
0.800	1.96	-0.91	-0.25	2.57	3.09	3.02	-0.38	-1.77	-0.68	-0.30	-0.33
0.850	1.97	-0.47	0.03	2.23	2.81	2.74	-0.87	15.11	-1.93	-0.44	-0.49
0.875	1.96	-0.18	0.23	2.06	2.67	2.61	-2.56	2.47	-7.85	-0.56	-0.63
0.900	1.94	-0.12	0.27	1.88	2.28	2.22	-3.83	2.11	4.37	-1.57	-2.09
0.925	1.91	0.15	0.47	2.03	2.39	2.33	3.54	1.38	-17.43	-1.06	-1.32
0.950	1.88	0.48	0.73	2.01	2.38	2.30	1.37	1.08	-35.41	-1.11	-1.42
0.975	1.88	0.73	0.90	1.73	2.12	2.06	1.08	1.01	2.11	-4.08	-8.80
1.000	1.93	0.87	1.01	1.63	1.62	1.57	1.02	1.00	1.66	1.62	1.47
1.025	1.92	1.06	1.15	1.47	1.48	1.43	1.00	1.02	1.28	1.29	1.23
1.050	1.92	1.07	1.13	1.38	1.38	1.34	1.01	1.02	1.17	1.17	1.13
1.100	1.95	1.00	1.04	1.18	1.23	1.19	1.00	1.00	1.03	1.05	1.04
1.200	1.96	0.88	0.91	0.98	0.99	0.95	1.01	1.01	1.00	1.00	1.00
1.350	1.93	0.88	0.91	0.97	0.97	0.94	1.01	1.01	1.00	1.00	1.00
1.500	1.93	0.81	0.81	0.82	0.83	0.81	1.04	1.04	1.03	1.03	1.04
1.750	1.97	0.79	0.79	0.80	0.79	0.77	1.05	1.05	1.04	1.05	1.06
2.000	2.03	0.77	0.77	0.76	0.76	0.74	1.06	1.06	1.06	1.06	1.07
2.250	2.07	0.76	0.76	0.76	0.76	0.74	1.06	1.06	1.06	1.06	1.07
2.500	2.05	0.78	0.78	0.78	0.78	0.76	1.05	1.05	1.05	1.05	1.06
3.000	2.06	0.81	0.81	0.82	0.81	0.79	1.04	1.04	1.03	1.04	1.04
3.500	2.08	0.86	0.85	0.86	0.86	0.84	1.02	1.02	1.02	1.02	1.03

Mach Number	Gyroscopic Stabilty Factor	Fast Arm Rate deg/m	Slow Arm Rate deg/m	Slow Arm Limit deg	Fast Arm Unstable From deg	deg	Cnpa Limit Slow	Cnpa Limit Fast
0.600	1.97	8.13	1.43	1.6	3.1	15.0	-0.33	0.51
0.700	1.98	8.14	1.42	2.0	3.4	15.0	-0.32	0.58
0.750	1.97	8.14	1.42	2.3	3.7	15.0	-0.31	0.65
0.800	1.96	8.12	1.44	2.4	4.0	15.0	-0.30	0.72
0.850	1.97	8.14	1.42	2.3	4.2	15.0	-0.30	0.78
0.875	1.96	8.13	1.43	2.0	4.4	15.0	-0.30	0.83
0.900	1.94	8.11	1.45	1.9	4.6	15.0	-0.30	0.88
0.925	1.91	8.08	1.48	1.3	4.4	15.0	-0.31	0.93
0.950	1.88	8.05	1.51	0.0	4.3	15.0	-0.31	0.99
0.975	1.88	8.05	1.51	0.0	5.0	15.0	-0.31	1.09
1.000	1.93	8.10	1.46	0.0	0.0	0.0	-0.30	1.21
1.025	1.92	8.09	1.47	0.0	0.0	0.0	-0.28	1.34
1.050	1.92	8.09	1.47	0.0	0.0	0.0	-0.27	1.44
1.100	1.95	8.11	1.45	0.0	0.0	0.0	-0.27	1.54
1.200	1.96	8.13	1.43	0.0	0.0	0.0	-0.28	1.63
1.350	1.93	8.10	1.46	0.0	0.0	0.0	-0.26	1.72
1.500	1.93	8.09	1.47	0.0	0.0	0.0	-0.25	1.84
1.750	1.97	8.13	1.43	0.0	0.0	0.0	-0.27	1.96
2.000	2.03	8.19	1.37	0.0	0.0	0.0	-0.30	2.08
2.250	2.07	8.22	1.34	0.0	0.0	0.0	-0.32	2.12
2.500	2.05	8.20	1.36	0.0	0.0	0.0	-0.34	2.05
3.000	2.06	8.21	1.35	0.0	0.0	0.0	-0.37	1.95
3.500	2.08	8.22	1.34	0.0	0.0	0.0	-0.39	1.82

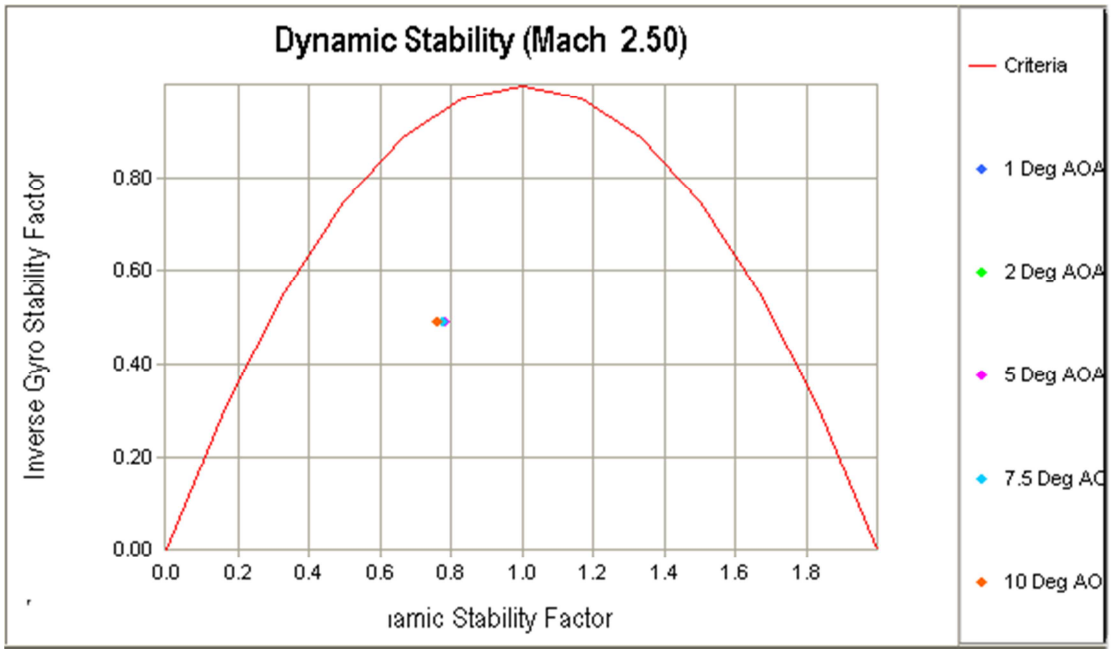

Figure A-1 Diagram of stability (stability coefficients) for 39 caliber gun and standard atmospheric conditions for Mach 2.50

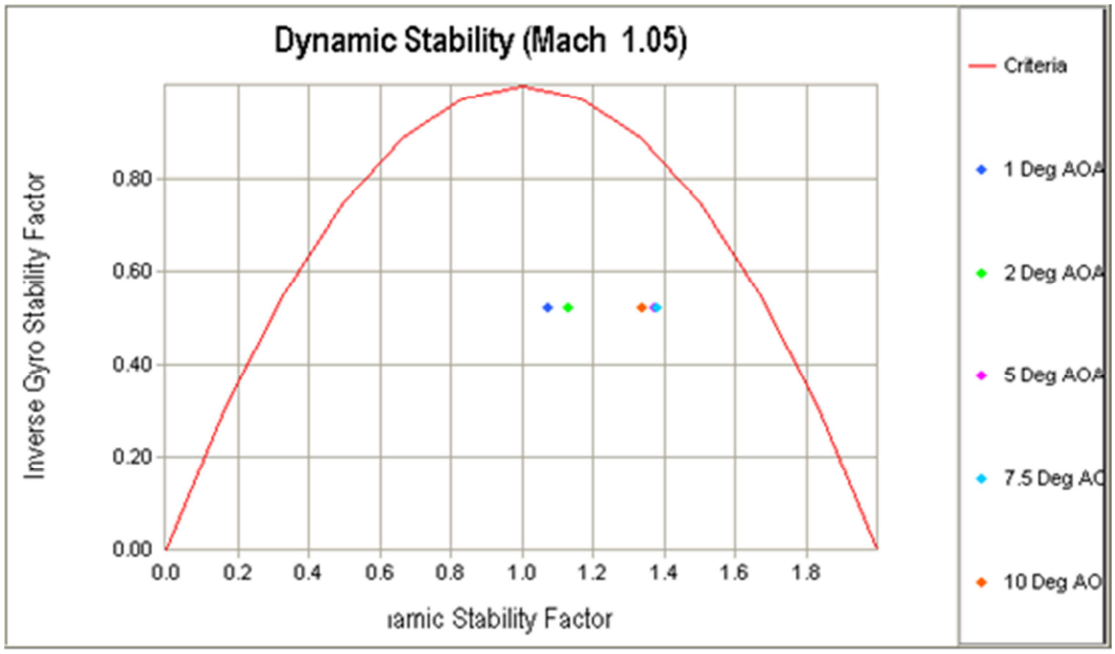

Figure A-2 Diagram of stability (stability coefficients) for 39 caliber gun and standard atmospheric conditions for Mach 1.05

Tables A-3 Stability Analysis Output for projectile with muzzle velocity of 930m/s – 52 caliber gun, Std. atmospheric conditions:

```
Intial conditions:
Muzzle Velocity          930.0 m/sec
Aircraft Velocity        0.0 m/sec
Air Density              1.22500 kg/m^3
Air Temperature          15.0 C
Muzzle Spin Rate         250. CPS
Muzzle Exit Twist        24.0 cal/rev
CP from Nose             380.52 mm
CP from Nose             2.46 Calibers
CG from Nose             594.74 mm
CG from Nose             3.84 Calibers
Mach Number              2.73
Gyro Stab Factor         1.43
Ballistic Coeff.         7.387
Cd at Muzzle             0.209
Deceleration             45.02 m/s/1000m
Muzzle Jump Factor       0.178 mils/rad/sec

Projectile Data at the Muzzle
-----------------------------------------------
       Projectile Dia.          154.740  mm
       Weight                    49.776  kg
       Axial Inertia           0.171057  kg-m^2
       Trans Inertia            2.07184  kg-m^2
       CG  (from nose)           594.74  mm
```

Met Data Utilised for Computations

Launch Altitude above SL	0.0	m			
Pressure	1013.2	millibars	Density	1.2250	kg/m^3
Temperature	15.0	C	Speed of Sound	340.3	m/sec

Muzzle Exit Aeroballistic Parameters

Total Velocity	930.0	m/sec		
Gun Twist	24.0	cal/rev		
Mach Number	2.73			
Muzzle Spin Rate	96.7	deg/m	1569.6 rad/sec	249.8 cyc/sec
Fast Mode Rate	6.2	deg/m	100.4 rad/sec	16.0 cyc/sec
Slow Mode Rate	1.8	deg/m	29.2 rad/sec	4.6 cyc/sec
Fast Mode Damping	-0.00180	1/m		
Slow Mode Damping	-0.00085	1/m		
Yaw Period	82.0	m		
Muzzle to Max Yaw	41.0	m		
Muzzle to Half Yaw	523.0	m		
Gyroscopic Factor	1.43			
Deceleration	45.02	m/s/1000m		
Drag Coefficient	0.209			
Muzzle Jump Factor	0.178	mils/rad/sec		
Ballistic Coefficient (based on Ingalls DF)	7.387			

Mach Number	Gyroscopic Stabilty Factor	Fast Arm Damping Rate at Angles of Attack					Slow Arm Damping Rate at Angles of Attack				
		1	2	5	7.5	10	1	2	5	7.5	10
		1/m	1/m	1/m	1/m	1/m	1/m	1/m	1/m	1/m	1/m
0.600	1.37	-0.00164	-0.00095	0.00174	0.00251	0.00244	0.00068	-0.00001	-0.00270	-0.00347	-0.00340
0.700	1.38	-0.00194	-0.00126	0.00163	0.00234	0.00227	0.00091	0.00023	-0.00266	-0.00337	-0.00330
0.750	1.38	-0.00232	-0.00160	0.00130	0.00220	0.00213	0.00122	0.00050	-0.00240	-0.00330	-0.00323
0.800	1.36	-0.00262	-0.00192	0.00109	0.00164	0.00156	0.00145	0.00075	-0.00226	-0.00281	-0.00274
0.850	1.38	-0.00225	-0.00170	0.00075	0.00140	0.00133	0.00102	0.00046	-0.00199	-0.00264	-0.00256
0.875	1.37	-0.00203	-0.00155	0.00060	0.00131	0.00124	0.00074	0.00026	-0.00190	-0.00261	-0.00253
0.900	1.35	-0.00209	-0.00159	0.00042	0.00093	0.00085	0.00073	0.00023	-0.00179	-0.00229	-0.00221
0.925	1.33	-0.00188	-0.00144	0.00068	0.00118	0.00109	0.00043	0.00000	-0.00213	-0.00263	-0.00254
0.950	1.31	-0.00154	-0.00116	0.00073	0.00127	0.00117	0.00000	-0.00038	-0.00227	-0.00281	-0.00271
0.975	1.31	-0.00125	-0.00098	0.00032	0.00093	0.00083	-0.00039	-0.00066	-0.00196	-0.00257	-0.00247
1.000	1.35	-0.00109	-0.00087	0.00013	0.00012	0.00003	-0.00067	-0.00088	-0.00189	-0.00187	-0.00178
1.025	1.34	-0.00084	-0.00069	-0.00013	-0.00012	-0.00020	-0.00105	-0.00120	-0.00176	-0.00177	-0.00169
1.050	1.34	-0.00086	-0.00075	-0.00031	-0.00030	-0.00038	-0.00113	-0.00124	-0.00168	-0.00169	-0.00161
1.100	1.36	-0.00104	-0.00097	-0.00070	-0.00061	-0.00069	-0.00105	-0.00112	-0.00139	-0.00147	-0.00140
1.200	1.37	-0.00133	-0.00126	-0.00113	-0.00112	-0.00119	-0.00086	-0.00093	-0.00106	-0.00107	-0.00100
1.350	1.35	-0.00140	-0.00135	-0.00121	-0.00122	-0.00128	-0.00090	-0.00095	-0.00109	-0.00108	-0.00103
1.500	1.34	-0.00164	-0.00164	-0.00162	-0.00160	-0.00165	-0.00079	-0.00079	-0.00081	-0.00083	-0.00077
1.750	1.37	-0.00178	-0.00178	-0.00176	-0.00177	-0.00182	-0.00078	-0.00078	-0.00080	-0.00080	-0.00074
2.000	1.42	-0.00189	-0.00190	-0.00190	-0.00190	-0.00195	-0.00079	-0.00079	-0.00078	-0.00078	-0.00073
2.250	1.44	-0.00194	-0.00195	-0.00194	-0.00195	-0.00199	-0.00080	-0.00079	-0.00080	-0.00079	-0.00075
2.500	1.43	-0.00186	-0.00187	-0.00186	-0.00186	-0.00191	-0.00082	-0.00082	-0.00083	-0.00083	-0.00078
3.000	1.44	-0.00173	-0.00174	-0.00172	-0.00173	-0.00177	-0.00088	-0.00087	-0.00089	-0.00088	-0.00083
3.500	1.45	-0.00154	-0.00155	-0.00153	-0.00154	-0.00158	-0.00092	-0.00092	-0.00093	-0.00093	-0.00088

Mach Number	Gyroscopic Stabilty Factor	Dynamic Stabilty Factor at Angles of Attack					Recipical Dynamic Factor at Angles of Attack				
		1	2	5	7.5	10	1	2	5	7.5	10
0.600	1.37	-0.35	0.45	3.60	4.50	4.41	-1.21	1.44	-0.17	-0.09	-0.09
0.700	1.38	-0.56	0.18	3.34	4.12	4.04	-0.70	3.02	-0.22	-0.11	-0.12
0.750	1.38	-0.80	-0.07	2.88	3.80	3.73	-0.45	-6.77	-0.39	-0.15	-0.16
0.800	1.36	-0.91	-0.25	2.57	3.09	3.02	-0.38	-1.77	-0.68	-0.30	-0.33
0.850	1.38	-0.47	0.03	2.23	2.81	2.75	-0.87	15.20	-1.93	-0.44	-0.49
0.875	1.37	-0.18	0.23	2.06	2.67	2.61	-2.56	2.47	-7.80	-0.56	-0.63
0.900	1.35	-0.12	0.27	1.88	2.28	2.22	-3.82	2.11	4.37	-1.57	-2.09
0.925	1.33	0.15	0.47	2.03	2.39	2.33	3.54	1.38	-17.31	-1.06	-1.31
0.950	1.31	0.48	0.73	2.01	2.38	2.30	1.37	1.08	-35.16	-1.11	-1.42
0.975	1.31	0.73	0.90	1.73	2.12	2.06	1.08	1.01	2.11	-4.08	-8.79
1.000	1.35	0.87	1.01	1.63	1.62	1.57	1.02	1.00	1.66	1.62	1.47
1.025	1.34	1.06	1.15	1.47	1.48	1.43	1.00	1.02	1.28	1.29	1.22
1.050	1.34	1.07	1.13	1.38	1.38	1.34	1.01	1.02	1.17	1.17	1.13
1.100	1.36	1.00	1.04	1.18	1.23	1.19	1.00	1.00	1.03	1.05	1.04
1.200	1.37	0.88	0.91	0.98	0.99	0.95	1.01	1.01	1.00	1.00	1.00
1.350	1.35	0.88	0.91	0.97	0.97	0.94	1.01	1.01	1.00	1.00	1.00
1.500	1.34	0.81	0.81	0.82	0.83	0.81	1.04	1.04	1.03	1.03	1.04
1.750	1.37	0.79	0.79	0.79	0.79	0.77	1.05	1.05	1.04	1.05	1.06
2.000	1.42	0.77	0.77	0.76	0.76	0.74	1.06	1.06	1.06	1.06	1.07
2.250	1.44	0.76	0.76	0.76	0.76	0.74	1.06	1.06	1.06	1.06	1.07
2.500	1.43	0.78	0.78	0.78	0.78	0.76	1.05	1.05	1.05	1.05	1.06
3.000	1.44	0.81	0.81	0.82	0.81	0.79	1.04	1.04	1.03	1.04	1.04
3.500	1.45	0.85	0.85	0.86	0.86	0.84	1.02	1.02	1.02	1.02	1.03

Mach Number	Gyroscopic Stabilty Factor	Fast Arm Rate deg/m	Slow Arm Rate deg/m	Slow Arm Limit deg	Fast Arm Unstable From deg		Cnpa Limit Slow	Cnpa Limit Fast
0.600	1.37	6.07	1.91	2.0	3.0	15.0	-0.22	0.40
0.700	1.38	6.09	1.89	2.2	3.2	15.0	-0.20	0.47
0.750	1.38	6.08	1.90	2.4	3.5	15.0	-0.19	0.53
0.800	1.36	6.05	1.93	2.7	3.8	15.0	-0.17	0.58
0.850	1.38	6.08	1.90	2.5	4.0	15.0	-0.16	0.64
0.875	1.37	6.07	1.92	2.3	4.1	15.0	-0.15	0.68
0.900	1.35	6.03	1.95	2.3	4.2	15.0	-0.15	0.72
0.925	1.33	5.98	2.00	2.0	4.0	15.0	-0.14	0.76
0.950	1.31	5.93	2.05	0.0	3.9	15.0	-0.12	0.81
0.975	1.31	5.94	2.04	0.0	4.2	15.0	-0.11	0.89
1.000	1.35	6.02	1.96	0.0	4.5	12.4	-0.10	1.01
1.025	1.34	6.00	1.99	0.0	0.0	0.0	-0.06	1.12
1.050	1.34	6.00	1.98	0.0	0.0	0.0	-0.03	1.21
1.100	1.36	6.04	1.94	0.0	0.0	0.0	-0.03	1.30
1.200	1.37	6.06	1.92	0.0	0.0	0.0	-0.03	1.38
1.350	1.35	6.02	1.97	0.0	0.0	0.0	0.01	1.46
1.500	1.34	6.01	1.98	0.0	0.0	0.0	0.03	1.56
1.750	1.37	6.07	1.92	0.0	0.0	0.0	0.02	1.67
2.000	1.42	6.16	1.82	0.0	0.0	0.0	-0.02	1.79
2.250	1.44	6.20	1.78	0.0	0.0	0.0	-0.04	1.84
2.500	1.43	6.18	1.80	0.0	0.0	0.0	-0.06	1.77
3.000	1.44	6.19	1.79	0.0	0.0	0.0	-0.10	1.69
3.500	1.45	6.22	1.77	0.0	0.0	0.0	-0.14	1.57

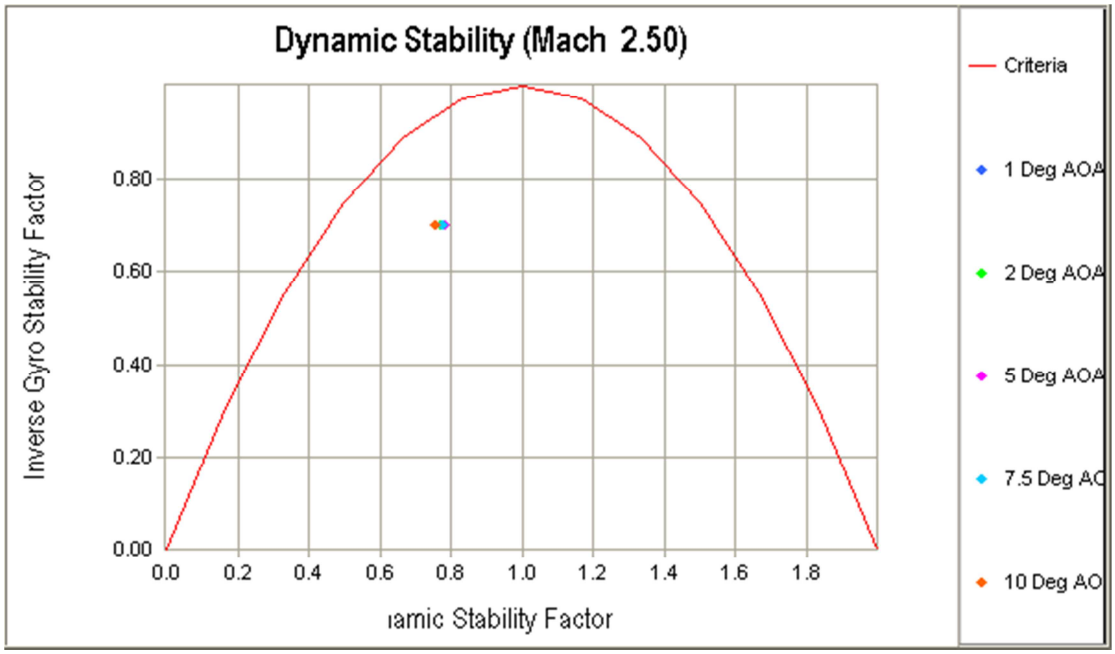

Figure A-3 Diagram of stability (stability coefficients) for 52 caliber gun and standard atmospheric conditions for Mach 2.50

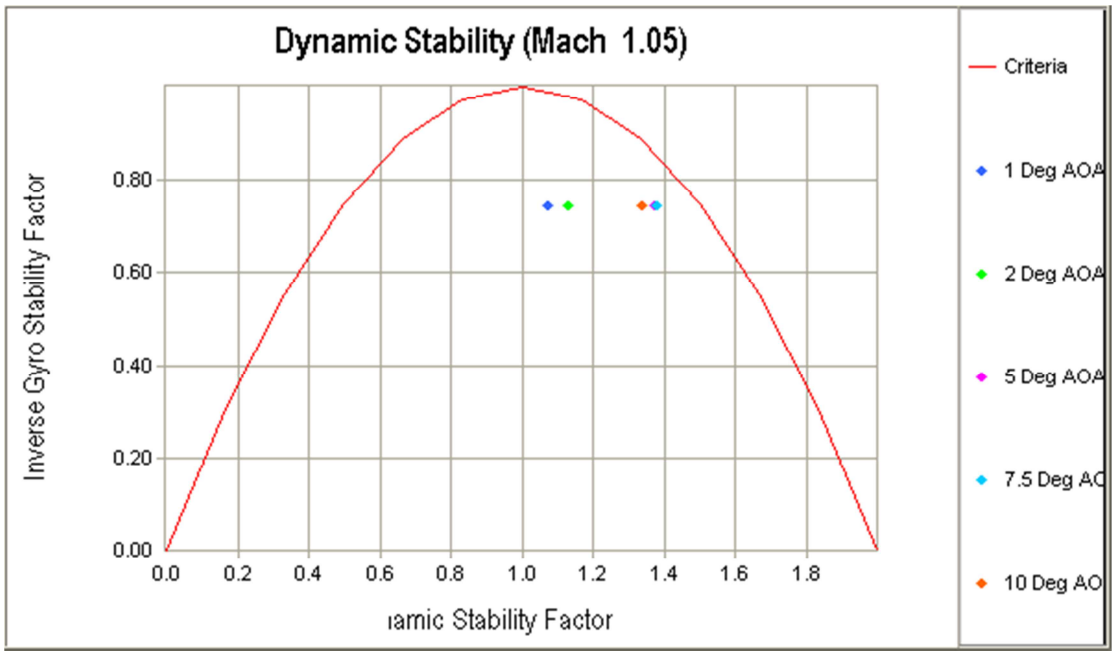

Figure A-4 Diagram of stability (stability coefficients) for 52 caliber gun and standard atmospheric conditions for Mach 1.05

Table A-4 Stability Analysis Output for projectile with muzzle velocity of 930m/s – 52 caliber gun, “Cold” atmospheric conditions:

```
Muzzle Velocity          930.0 m/sec
Aircraft Velocity        0.0 m/sec
Air Density              1.58966 kg/m^3
Air Temperature         -51.1 C
Muzzle Spin Rate         250. CPS
Muzzle Exit Twist        24.0 cal/rev
CP from Nose             382.69 mm
CP from Nose             2.47 Calibers
CG from Nose             594.74 mm
CG from Nose             3.84 Calibers
Mach Number              3.11
Gyro Stab Factor         1.11
Ballistic Coeff.         7.387
Cd at Muzzle             0.193
Deceleration             54.02 m/s/1000m
Muzzle Jump Factor       0.181 mils/rad/sec


Projectile Data at the Muzzle

      ---------------------------------------------
      Projectile Dia.          154.740  mm
      Weight                    49.776  kg
      Axial Inertia           0.171057  kg-m^2
      Trans Inertia             2.07184 kg-m^2
      CG  (from nose)           594.74  mm

       Met Data Utilised for Computations
   ---------------------------------------------   ---------------------------------------------
      Launch Altitude above SL      0.0 m
      Pressure                   1013.2 millibars    Density                    1.5897 kg/m^3
      Temperature                 -51.1 C            Speed of Sound              298.7 m/sec
       Muzzle Exit Aeroballistic Parameters
   ---------------------------------------------   ---------------------------------------------
      Total Velocity             930.0 m/sec
      Gun Twist                   24.0 cal/rev
      Mach Number                  3.11

      Muzzle Spin Rate            96.7 deg/m       1569.6 rad/sec    249.8 cyc/sec
      Fast Mode Rate               5.2 deg/m         85.2 rad/sec     13.6 cyc/sec
      Slow Mode Rate               2.7 deg/m         44.4 rad/sec      7.1 cyc/sec

      Fast Mode Damping        -0.00259 1/m
      Slow Mode Damping        -0.00076 1/m
      Yaw Period                 143.3  m
      Muzzle to Max Yaw           71.6  m
      Muzzle to Half Yaw         414.8  m

      Gyroscopic Factor            1.11
      Deceleration                54.02 m/s/1000m
      Drag Coefficient             0.193
      Muzzle Jump Factor           0.181 mils/rad/sec
      Ballistic Coefficient        7.387
        (based on Ingalls DF)
```

Mach Number	Gyroscopic Stabilty Factor	Fast Arm Damping Rate at Angles of Attack					Slow Arm Damping Rate at Angles of Attack				
		1 1/m	2 1/m	5 1/m	7.5 1/m	10 1/m	1 1/m	2 1/m	5 1/m	7.5 1/m	10 1/m
0.600	1.06	-0.00398	-0.00199	0.00583	0.00806	0.00786	0.00274	0.00075	-0.00707	-0.00931	-0.00910
0.700	1.06	-0.00462	-0.00274	0.00527	0.00723	0.00704	0.00328	0.00140	-0.00661	-0.00857	-0.00837
0.750	1.06	-0.00573	-0.00370	0.00454	0.00709	0.00688	0.00431	0.00227	-0.00596	-0.00851	-0.00831
0.800	1.05	-0.00695	-0.00482	0.00433	0.00600	0.00578	0.00542	0.00329	-0.00585	-0.00752	-0.00730
0.850	1.06	-0.00543	-0.00385	0.00308	0.00491	0.00469	0.00382	0.00224	-0.00469	-0.00651	-0.00630
0.875	1.06	-0.00491	-0.00350	0.00282	0.00492	0.00470	0.00323	0.00182	-0.00451	-0.00661	-0.00638
0.900	1.04	-0.00550	-0.00386	0.00272	0.00437	0.00411	0.00372	0.00209	-0.00449	-0.00614	-0.00588
0.925	1.03	-0.00568	-0.00388	0.00481	0.00686	0.00648	0.00380	0.00200	-0.00669	-0.00874	-0.00836
0.950	1.01	-0.00602	-0.00357	0.00883	0.01235	0.01164	0.00403	0.00157	-0.01082	-0.01435	-0.01364
0.975	1.01	-0.00348	-0.00195	0.00532	0.00875	0.00822	0.00135	-0.00018	-0.00745	-0.01088	-0.01035
1.000	1.04	-0.00186	-0.00111	0.00232	0.00226	0.00197	-0.00042	-0.00117	-0.00459	-0.00453	-0.00424
1.025	1.03	-0.00084	-0.00026	0.00186	0.00191	0.00160	-0.00161	-0.00219	-0.00432	-0.00437	-0.00406
1.050	1.03	-0.00079	-0.00040	0.00122	0.00125	0.00097	-0.00179	-0.00218	-0.00380	-0.00384	-0.00355
1.100	1.05	-0.00135	-0.00111	-0.00027	0.00001	-0.00022	-0.00136	-0.00160	-0.00244	-0.00272	-0.00249
1.200	1.06	-0.00210	-0.00192	-0.00152	-0.00150	-0.00169	-0.00074	-0.00093	-0.00132	-0.00134	-0.00115
1.350	1.04	-0.00236	-0.00218	-0.00170	-0.00173	-0.00193	-0.00063	-0.00080	-0.00129	-0.00126	-0.00106
1.500	1.03	-0.00310	-0.00309	-0.00302	-0.00295	-0.00315	-0.00005	-0.00006	-0.00014	-0.00020	0.00000
1.750	1.06	-0.00313	-0.00313	-0.00307	-0.00309	-0.00324	-0.00020	-0.00020	-0.00026	-0.00024	-0.00009
2.000	1.09	-0.00307	-0.00308	-0.00309	-0.00310	-0.00321	-0.00041	-0.00041	-0.00039	-0.00039	-0.00028
2.250	1.11	-0.00307	-0.00309	-0.00307	-0.00308	-0.00319	-0.00048	-0.00047	-0.00049	-0.00048	-0.00037
2.500	1.10	-0.00296	-0.00298	-0.00295	-0.00296	-0.00307	-0.00052	-0.00051	-0.00054	-0.00053	-0.00042
3.000	1.11	-0.00267	-0.00269	-0.00265	-0.00266	-0.00277	-0.00071	-0.00069	-0.00073	-0.00072	-0.00062
3.500	1.12	-0.00229	-0.00231	-0.00227	-0.00228	-0.00238	-0.00091	-0.00089	-0.00093	-0.00092	-0.00082

Mach Number	Gyroscopic Stabilty Factor	Dynamic Stabilty Factor at Angles of Attack					Recipical Dynamic Factor at Angles of Attack				
		1	2	5	7.5	10	1	2	5	7.5	10
0.600	1.06	-0.35	0.45	3.60	4.50	4.41	-1.21	1.44	-0.17	-0.09	-0.09
0.700	1.06	-0.56	0.18	3.34	4.12	4.04	-0.70	3.02	-0.22	-0.11	-0.12
0.750	1.06	-0.80	-0.07	2.88	3.80	3.73	-0.45	-6.77	-0.39	-0.15	-0.16
0.800	1.05	-0.91	-0.25	2.57	3.09	3.02	-0.38	-1.77	-0.68	-0.30	-0.33
0.850	1.06	-0.47	0.03	2.23	2.81	2.75	-0.87	15.20	-1.93	-0.44	-0.49
0.875	1.06	-0.18	0.23	2.06	2.67	2.61	-2.56	2.47	-7.80	-0.56	-0.63
0.900	1.04	-0.12	0.27	1.88	2.28	2.22	-3.82	2.11	4.37	-1.57	-2.09
0.925	1.03	0.15	0.47	2.03	2.39	2.33	3.54	1.38	-17.31	-1.06	-1.31
0.950	1.01	0.48	0.73	2.01	2.38	2.30	1.37	1.08	-35.16	-1.11	-1.42
0.975	1.01	0.73	0.90	1.73	2.12	2.06	1.08	1.01	2.11	-4.08	-8.79
1.000	1.04	0.87	1.01	1.63	1.62	1.57	1.02	1.00	1.66	1.62	1.47
1.025	1.03	1.06	1.15	1.47	1.48	1.43	1.00	1.02	1.28	1.29	1.22
1.050	1.03	1.07	1.13	1.38	1.38	1.34	1.01	1.02	1.17	1.17	1.13
1.100	1.05	1.00	1.04	1.18	1.23	1.19	1.00	1.00	1.03	1.05	1.04
1.200	1.06	0.88	0.91	0.98	0.99	0.95	1.01	1.01	1.00	1.00	1.00
1.350	1.04	0.88	0.91	0.97	0.97	0.94	1.01	1.01	1.00	1.00	1.00
1.500	1.03	0.81	0.81	0.82	0.83	0.81	1.04	1.04	1.03	1.03	1.04
1.750	1.06	0.79	0.79	0.79	0.79	0.77	1.05	1.05	1.04	1.05	1.06
2.000	1.09	0.77	0.77	0.76	0.76	0.74	1.06	1.06	1.06	1.06	1.07
2.250	1.11	0.76	0.76	0.76	0.76	0.74	1.06	1.06	1.06	1.06	1.07
2.500	1.10	0.78	0.78	0.78	0.78	0.76	1.05	1.05	1.05	1.05	1.06
3.000	1.11	0.81	0.81	0.82	0.81	0.79	1.04	1.04	1.03	1.04	1.04
3.500	1.12	0.85	0.85	0.86	0.86	0.84	1.02	1.02	1.02	1.02	1.03

Mach Number	Gyroscopic Stabilty Factor	Fast Arm Rate deg/m	Slow Arm Rate deg/m	Slow Arm Limit deg	Fast Arm Unstable From deg	deg	Cnpa Limit Slow	Cnpa Limit Fast
0.600	1.06	4.92	3.06	2.2	2.6	15.0	-0.05	0.23
0.700	1.06	4.97	3.01	2.4	3.0	15.0	-0.03	0.29
0.750	1.06	4.95	3.04	2.7	3.2	15.0	0.01	0.33
0.800	1.05	4.87	3.11	3.1	3.4	15.0	0.05	0.37
0.850	1.06	4.95	3.03	3.0	3.5	15.0	0.06	0.43
0.875	1.06	4.91	3.08	2.9	3.6	15.0	0.08	0.45
0.900	1.04	4.80	3.18	2.9	3.6	15.0	0.12	0.46
0.925	1.03	4.62	3.36	2.7	3.3	15.0	0.17	0.45
0.950	1.01	4.38	3.61	2.4	3.0	15.0	0.25	0.43
0.975	1.01	4.44	3.54	1.8	2.8	15.0	0.28	0.50
1.000	1.04	4.76	3.22	0.0	3.0	15.0	0.24	0.66
1.025	1.03	4.68	3.31	0.0	2.3	15.0	0.33	0.73
1.050	1.03	4.71	3.28	0.0	2.6	15.0	0.37	0.81
1.100	1.05	4.83	3.15	0.0	7.4	7.6	0.36	0.91
1.200	1.06	4.90	3.08	0.0	0.0	0.0	0.36	0.98
1.350	1.04	4.76	3.23	0.0	0.0	0.0	0.46	1.01
1.500	1.03	4.72	3.26	10.0	0.0	0.0	0.52	1.07
1.750	1.06	4.91	3.07	14.4	0.0	0.0	0.48	1.21
2.000	1.09	5.16	2.82	0.0	0.0	0.0	0.40	1.37
2.250	1.11	5.26	2.72	0.0	0.0	0.0	0.36	1.44
2.500	1.10	5.20	2.78	0.0	0.0	0.0	0.35	1.36
3.000	1.11	5.24	2.75	0.0	0.0	0.0	0.29	1.30
3.500	1.12	5.29	2.70	0.0	0.0	0.0	0.22	1.21

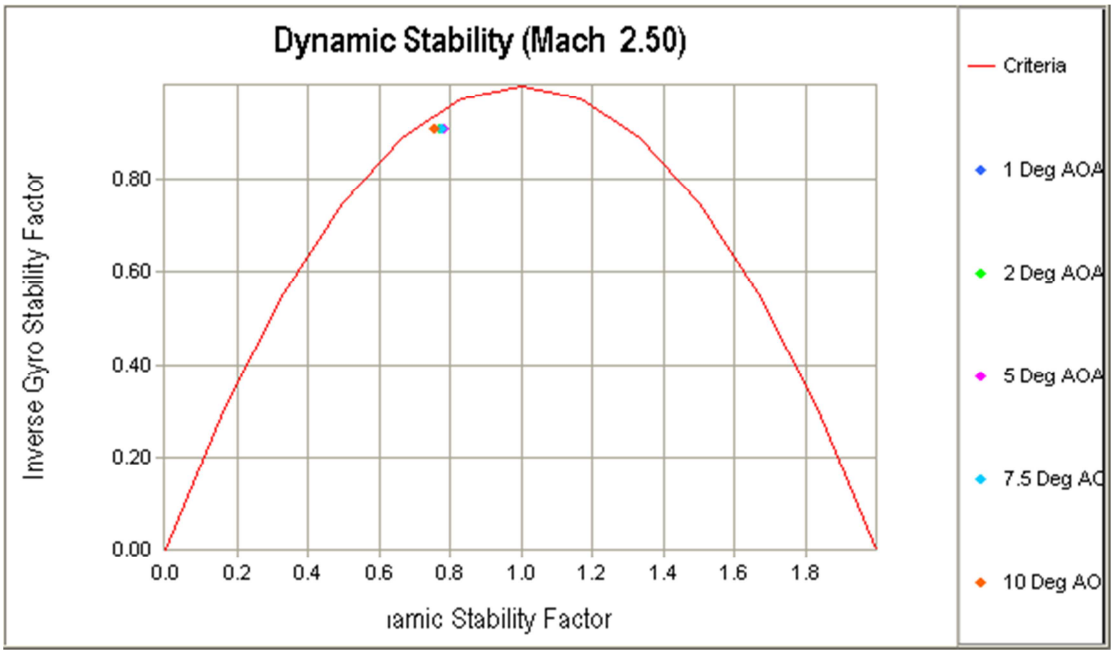

Figure A-5 Diagram of stability (stability coefficients) for 52 caliber gun and "cold" atmospheric conditions for Mach 2.5

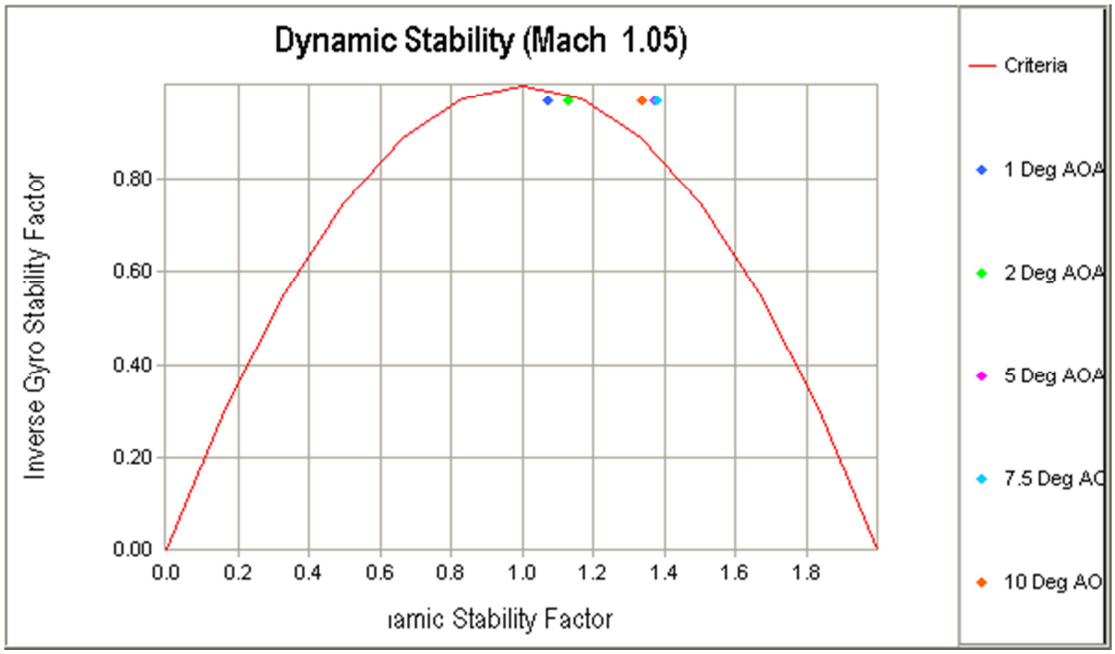

Figure A-6 Diagram of stability (stability coefficients) for 52 caliber gun and "cold" atmospheric conditions for Mach 1.05

Results for 6DOF trajectory calculations for the optimal angle of firing (max. ranges) for given cases:

- 39 calibre gun, muzzle velocity 821m/s, standard atmosphere conditions, H=0m - sea level,
- 52 calibre gun, muzzle velocity 930 m/s, standard atmosphere conditions, H=0m - sea level and
- 52 calibre gun, muzzle velocity 930 m/s, cold atmosphere conditions, H=0m - sea level,

are presented in next tables and diagrams. For the 6DOF fixed plain trajectory calculations PRODAS is used, with input for Base Bleed effect (base drag reduction) made in separate FORTRAN program, that calculates base drag reduction on the trajectory for given Base Bleed and SRM configuration.

Table A-5 Summary of 6 DOF Trajectory, 39 caliber gun Std. atmosphere

Parameter	Initial	Final	
Velocity	821.0	400.9	m/sec
Trajectory Angle	54.0	-66.3	deg
Time	0.0	120.1	sec
Range	0.0	40748.3	m
Deflection	0.00	-1833.27	m
Altitude (re sl)	0.00	0.00	m
Slant Range	0.0	40789.5	m
Mach Number	2.41	1.18	
Angle of Attack	0.00	0.09	deg

Pitch	[THETA]	(rad):	-0.9425	+ Nose Down
Pitch Rate	[Q]	(rad/sec):	0.0000	+ Nose moving down
Yaw	[PSI]	(rad):	0.0000	+ Nose Left
Yaw Rate	[R]	(rad/sec):	0.0000	+ Nose Moving Left
Travel	[X]	(m):	0.0000	+ Downrange
Velocity-Missile	[U]	(m/sec):	821.0000	+ Forward along axis
Horizontal Motion	[Y]	(m):	0.0000	+ to the left
Hor. Rate-Missile	[V]	(m/sec):	0.0000	+ to the left
Vertical Motion	[Z]	(m):	0.0000	+ up
Vertical Rate-Msle	[W]	(m/sec):	0.0000	+ up
Roll	[PHI]	(rad):	0.0000	+ clockwise
Roll Rate	[P]	(rad/sec):	1659.0000	+ clockwise
X-DOT	[Vx]	(m/s):	482.5715	+ Downrange
Y-DOT	[Vy]	(m/s):	0.0000	+ to the left
Z-DOT	[Vz]	(m/s):	664.2031	+ up

***** 6DOF Fixed Plane Trajectory (Auxiliary Outputs) ******

CDTOT=CXo+(CXa2+CNa)*Sin(A-bar)**2

Time	Slant	A-bar	CDTOT	Vrad	Gamma	Delta	Spin	Lambda_F	Lambda_S
0.0000	0.0	0.000	0.2238	821.00	54.00	0.00	1659.0	-0.0018	-0.0009
10.0000	6927.5	0.109	0.1748	593.84	48.93	-0.27	1506.6	-0.0009	-0.0006
20.0000	12278.6	0.227	0.1677	549.43	41.61	-0.70	1437.8	-0.0006	-0.0004
30.0000	17535.9	0.552	0.1755	478.67	33.29	-1.12	1393.5	-0.0004	-0.0003
40.0000	21911.0	1.262	0.2140	399.08	22.47	-1.62	1368.2	-0.0003	-0.0002
50.0000	25554.0	2.241	0.3293	331.01	9.09	-2.21	1350.7	-0.0002	-0.0002
60.0000	28578.9	2.700	0.3385	276.36	-6.02	-2.89	1336.2	-0.0002	-0.0002
70.0000	31128.1	2.094	0.3308	235.85	-20.99	-3.59	1321.3	-0.0002	-0.0002
80.0000	33341.7	1.128	0.3189	209.04	-34.09	-4.24	1302.2	-0.0003	-0.0002
90.0000	35349.0	0.507	0.3094	194.07	-44.74	-4.79	1274.1	-0.0005	-0.0003
100.0000	37247.2	0.247	0.3084	186.18	-53.25	-5.27	1231.5	-0.0007	-0.0005
110.0000	39069.7	0.135	0.3157	177.44	-60.23	-5.71	1168.9	-0.0010	-0.0007
120.0000	40770.0	0.089	0.3240	161.16	-66.22	-6.16	1085.7	-0.0013	-0.0010
120.1213	40789.5	0.089	0.3240	160.92	-66.29	-6.16	1084.6	-0.0013	-0.0011

No of High Res = 187 Time = 0.497

No of 3d points = 1 Time = 0.000

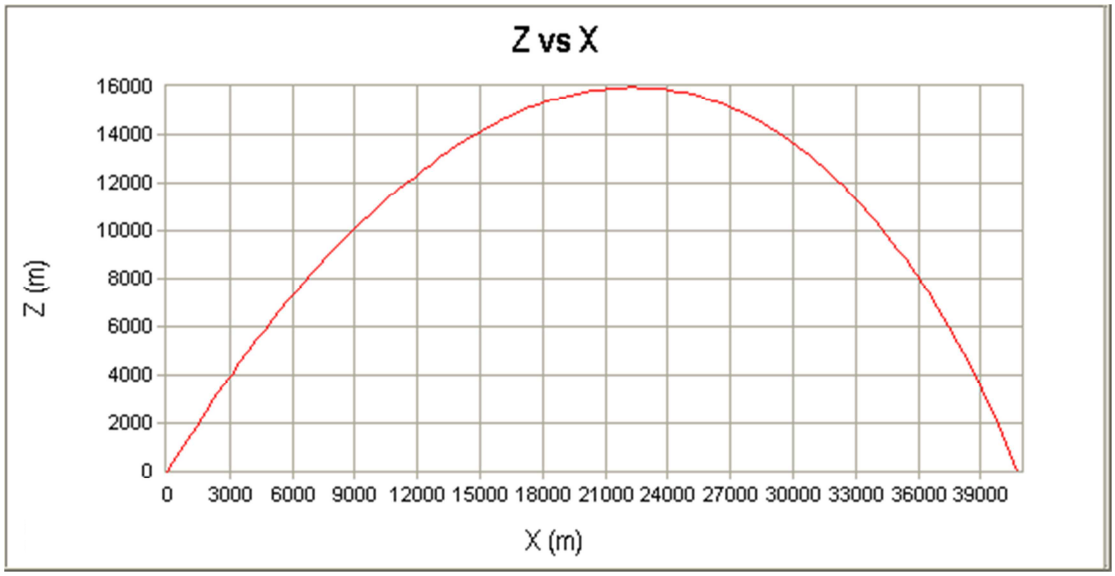

Figure A-7 Range vs. Altitude, 39 calibre gun, max. range

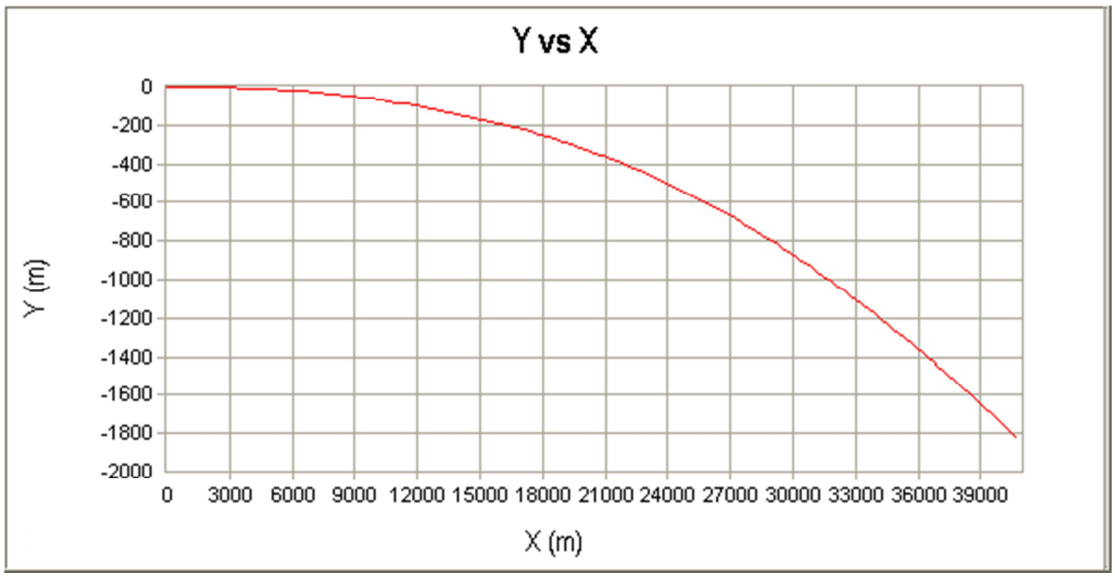

Figure A-8 Range vs. Drift (Deflection), 39 calibre gun, max. range

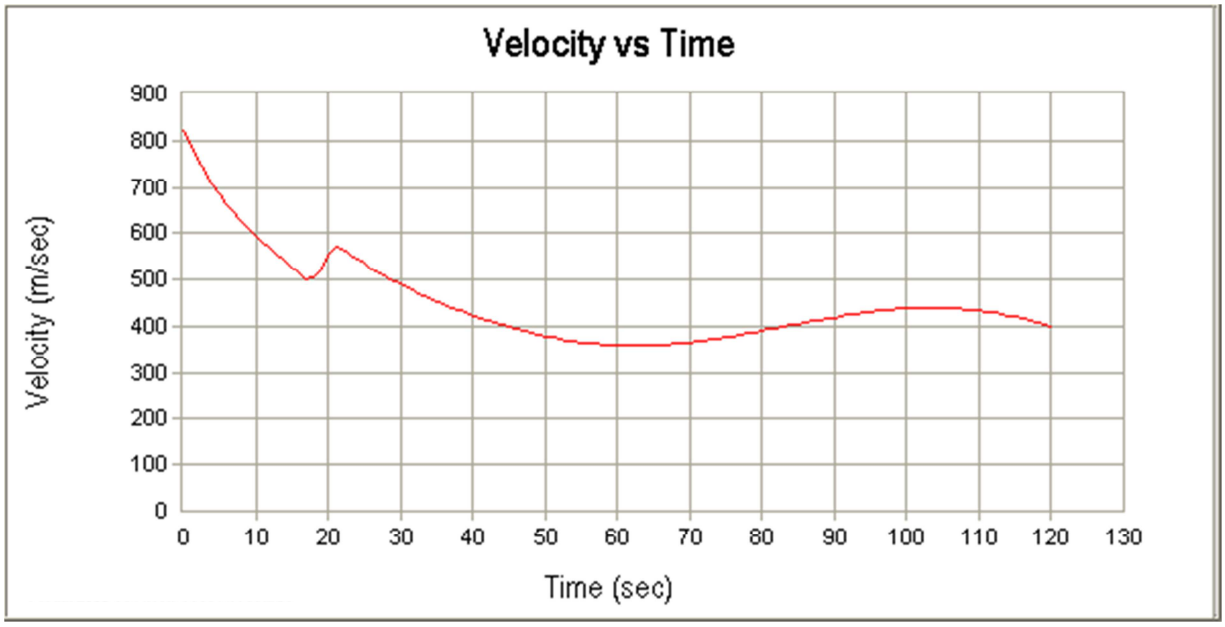

Figure A-9 Velocity vs. time, 39 calibre gun, max. range

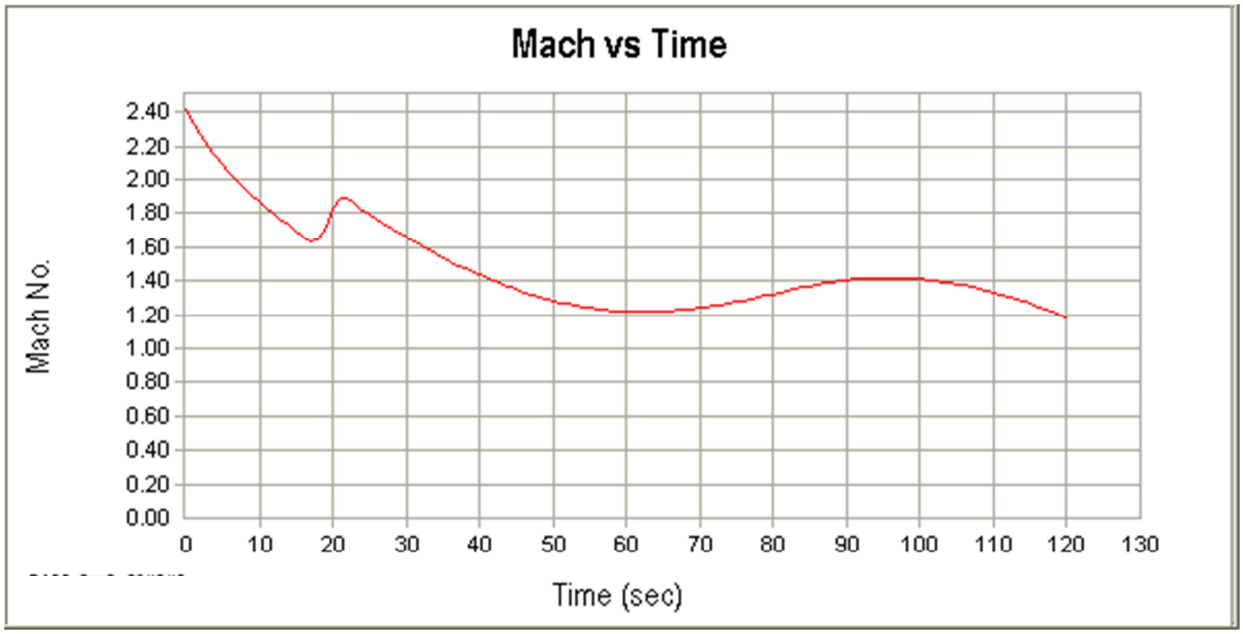

Figure A-10 Mach vs. time, 39 calibre gun, max. range

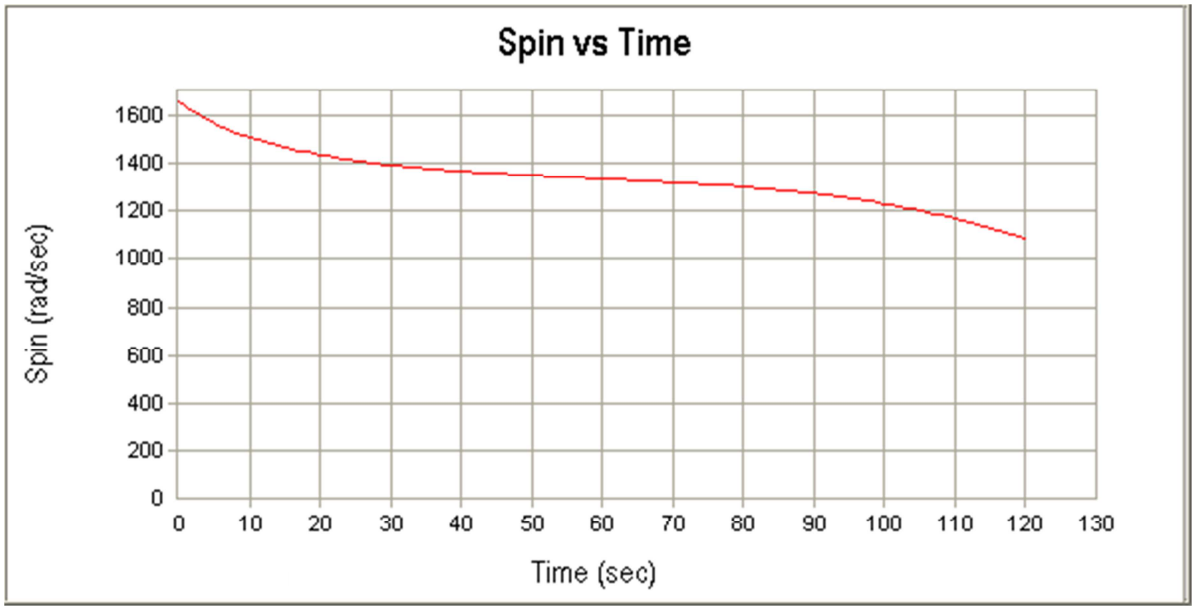

Figure A-11 Spin history, 39 calibre gun, max. range

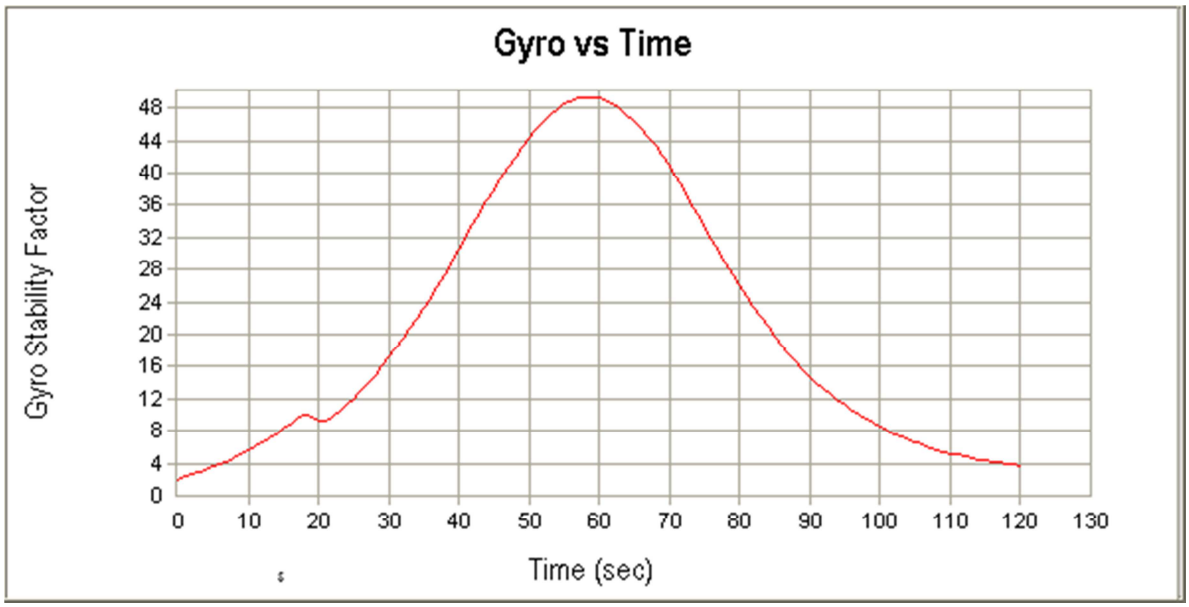

Figure A-12 Gyro stability factor history, 39 calibre gun, max. range

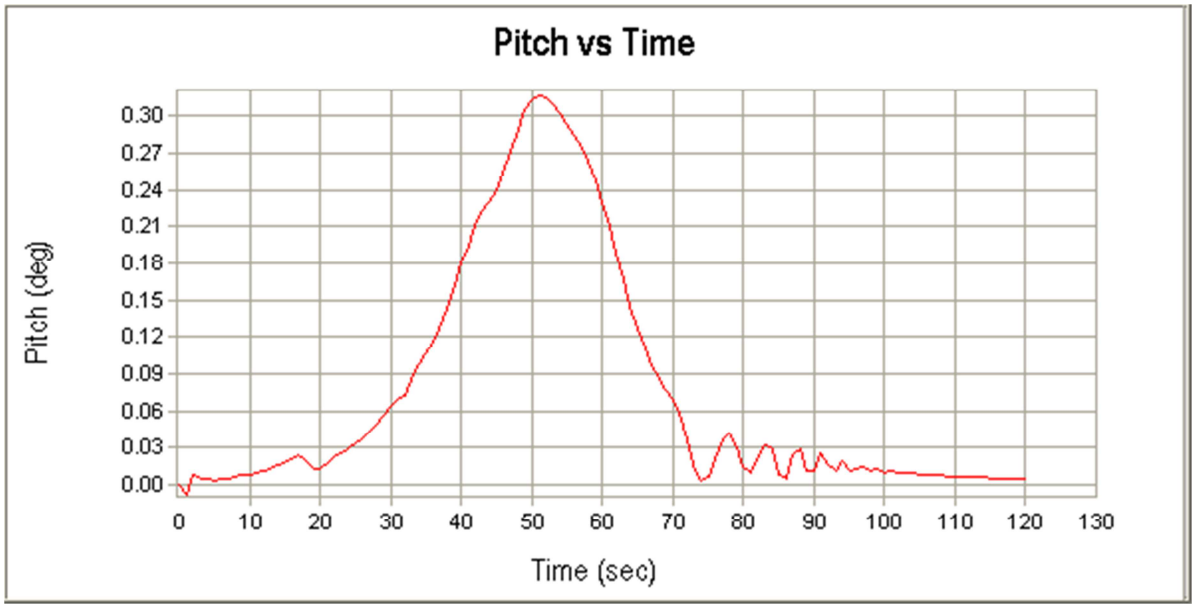

Figure A-13 Pitch angle history, 39 calibre gun, max. range

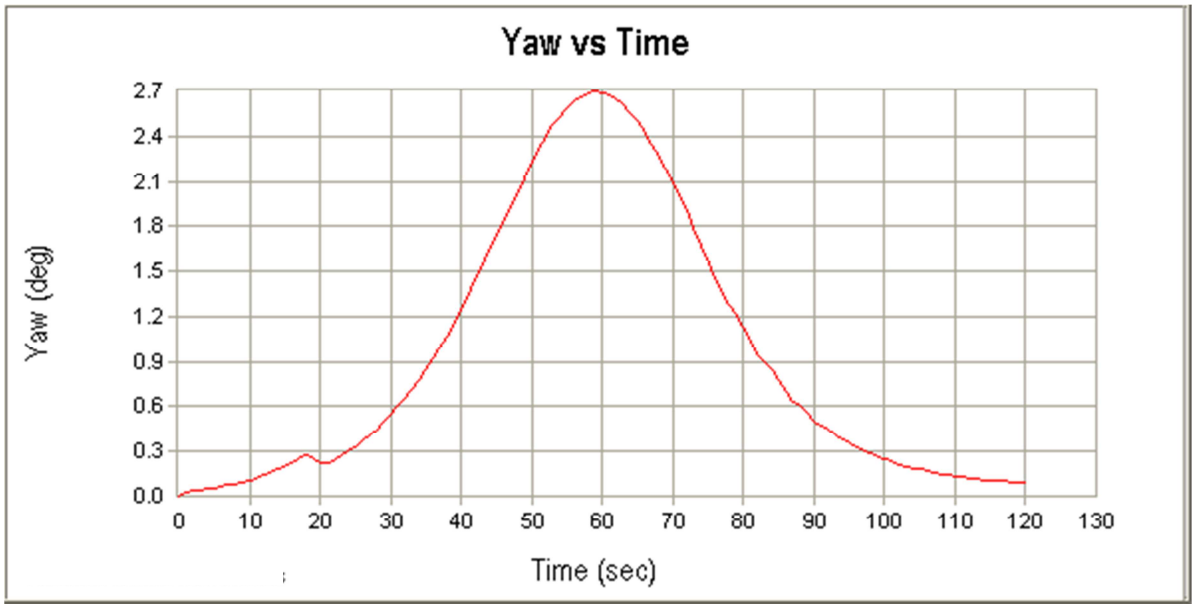

Figure A-14 Yaw angle history, 39 calibre gun, max. range

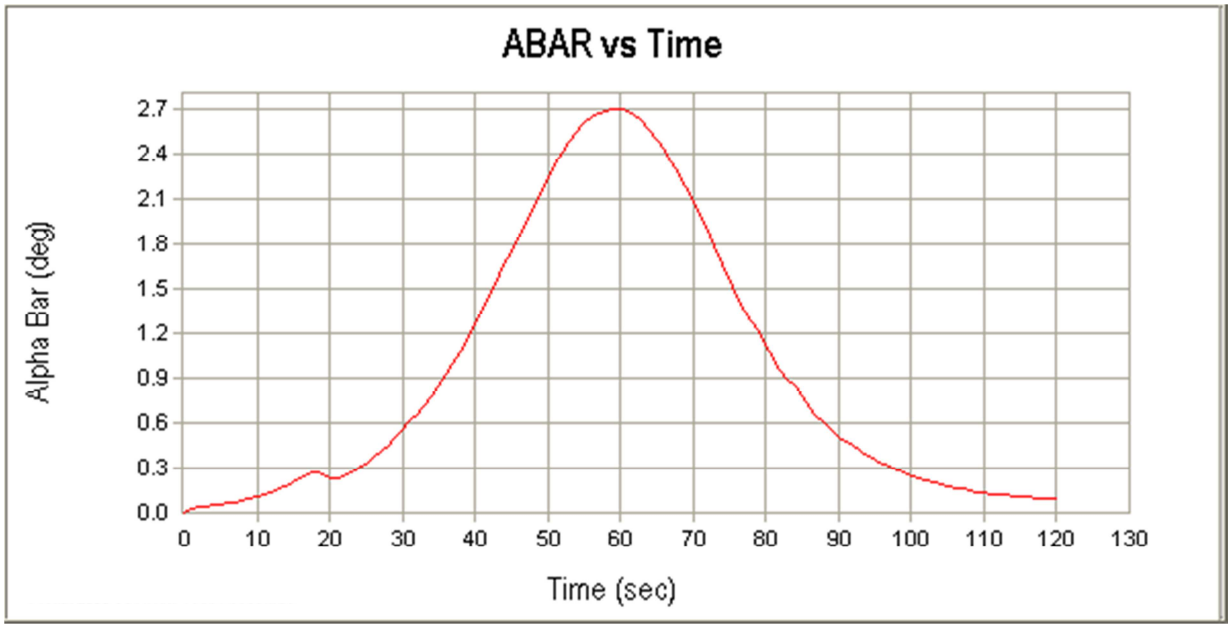

Figure A-15 "Total" angle of attack history, 39 calibre gun, max. range

Tables A-6 Summary of 6 DOF Trajectory, 52 calibre gun Std. atmosphere

Parameter	Initial	Final	
Velocity	930.0	438.1	m/sec
Trajectory Angle	54.0	-64.7	deg
Time	0.0	132.8	sec
Range	0.0	51540.8	m
Deflection	0.00	-2046.81	m
Altitude (re sl)	0.00	0.00	m
Slant Range	0.0	51581.4	m
Mach Number	2.73	1.29	
Angle of Attack	0.00	0.07	deg

Pitch	[THETA]	(rad):	-0.9425	+ Nose Down
Pitch Rate	[Q]	(rad/sec):	0.0000	+ Nose moving down
Yaw	[PSI]	(rad):	0.0000	+ Nose Left
Yaw Rate	[R]	(rad/sec):	0.0000	+ Nose Moving Left
Travel	[X]	(m):	0.0000	+ Downrange
Velocity-Missile	[U]	(m/sec):	930.0000	+ Forward along axis
Horizontal Motion	[Y]	(m):	0.0000	+ to the left
Hor. Rate-Missile	[V]	(m/sec):	0.0000	+ to the left
Vertical Motion	[Z]	(m):	0.0000	+ up
Vertical Rate-Msle	[W]	(m/sec):	0.0000	+ up
Roll	[PHI]	(rad):	0.0000	+ clockwise
Roll Rate	[P]	(rad/sec):	1569.5800	+ clockwise
X-DOT	[Vx]	(m/s):	546.6401	+ Downrange
Y-DOT	[Vy]	(m/s):	0.0000	+ to the left
Z-DOT	[Vz]	(m/s):	752.3859	+ up

***** 6DOF Fixed Plane Trajectory (Auxiliary Outputs) ******

CDTOT=CXo+(CXa2+CNa)*Sin(A-bar)**2

Time	Slant	A-bar	CDTOT	Vrad	Gamma	Delta	Spin	Lambda_F	Lambda_S
0.0000	0.0	0.000	0.2086	930.00	54.00	0.00	1569.6	-0.0018	-0.0008
10.0000	7823.4	0.078	0.1648	673.16	49.53	-0.21	1419.5	-0.0009	-0.0005
20.0000	13935.4	0.176	0.1564	623.62	43.23	-0.54	1354.9	-0.0006	-0.0003
30.0000	19934.3	0.464	0.1631	553.00	36.14	-0.88	1318.1	-0.0003	-0.0002
40.0000	25053.2	1.118	0.1916	473.40	27.11	-1.26	1299.2	-0.0002	-0.0001
50.0000	29438.4	2.113	0.3075	404.74	16.03	-1.69	1287.5	-0.0001	-0.0001
60.0000	33187.5	3.080	0.3276	347.16	3.21	-2.18	1278.5	-0.0001	-0.0001
70.0000	36422.1	3.018	0.3286	301.79	-10.32	-2.72	1270.1	-0.0001	-0.0001
80.0000	39265.0	2.026	0.3129	268.90	-23.16	-3.23	1260.6	-0.0001	-0.0001
90.0000	41842.8	1.025	0.2967	248.69	-34.29	-3.70	1247.9	-0.0002	-0.0001
100.0000	44274.8	0.463	0.2845	239.08	-43.48	-4.11	1227.9	-0.0004	-0.0002
110.0000	46638.9	0.206	0.2813	233.60	-51.03	-4.49	1193.8	-0.0006	-0.0004
120.0000	48927.7	0.108	0.2924	222.30	-57.44	-4.83	1138.9	-0.0010	-0.0006
130.0000	51035.6	0.073	0.3135	196.61	-63.18	-5.17	1059.4	-0.0013	-0.0010
132.8468	51581.4	0.068	0.3184	186.68	-64.74	-5.27	1032.6	-0.0014	-0.0011

No of High Res = 160 Time = 0.497
No of 3d points = 1 Time = 0.000

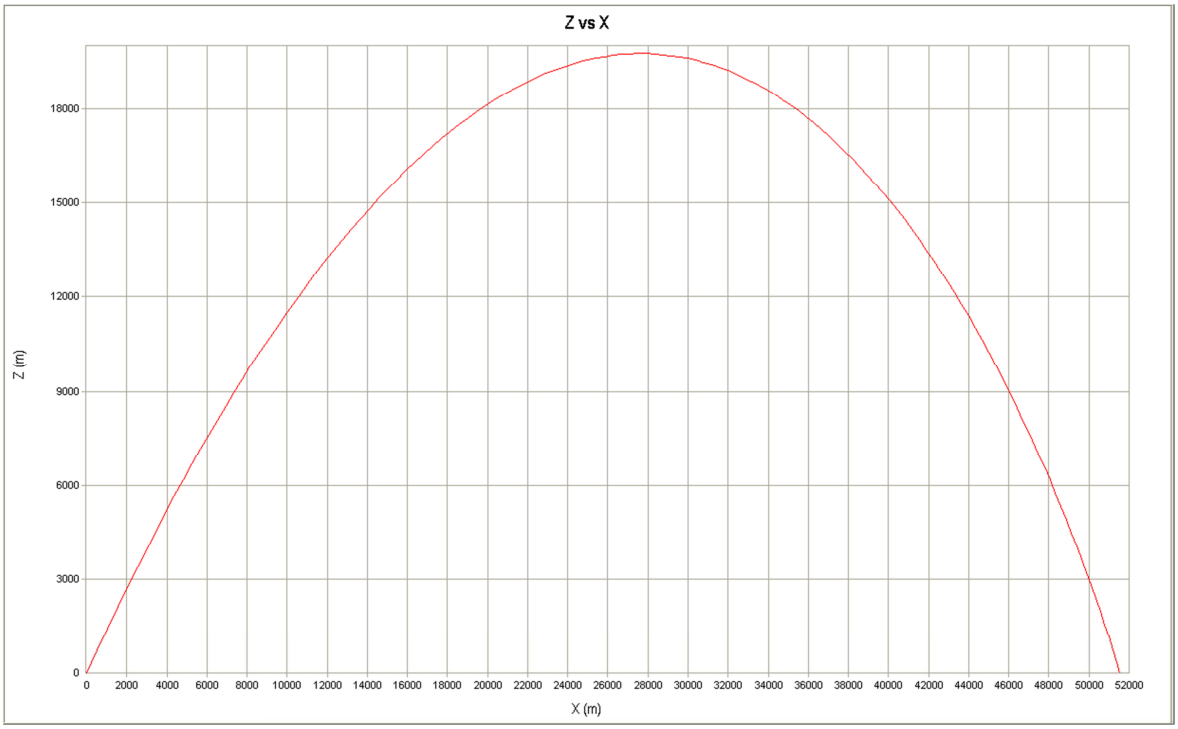

Figure A-16 Range vs. Altitude, 52 calibre gun, max. range, std. atmos.

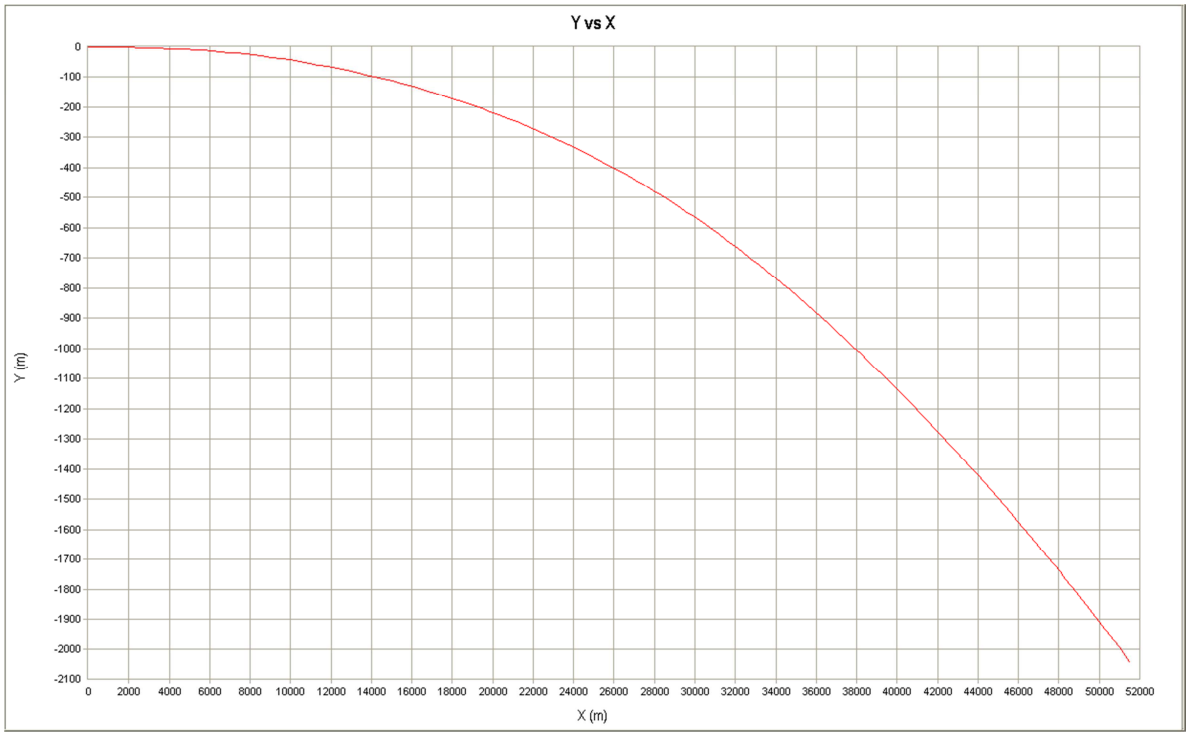

Figure A-17 Range vs. Drift(Deflection), 52 calibre gun, max. range, std. atmos.

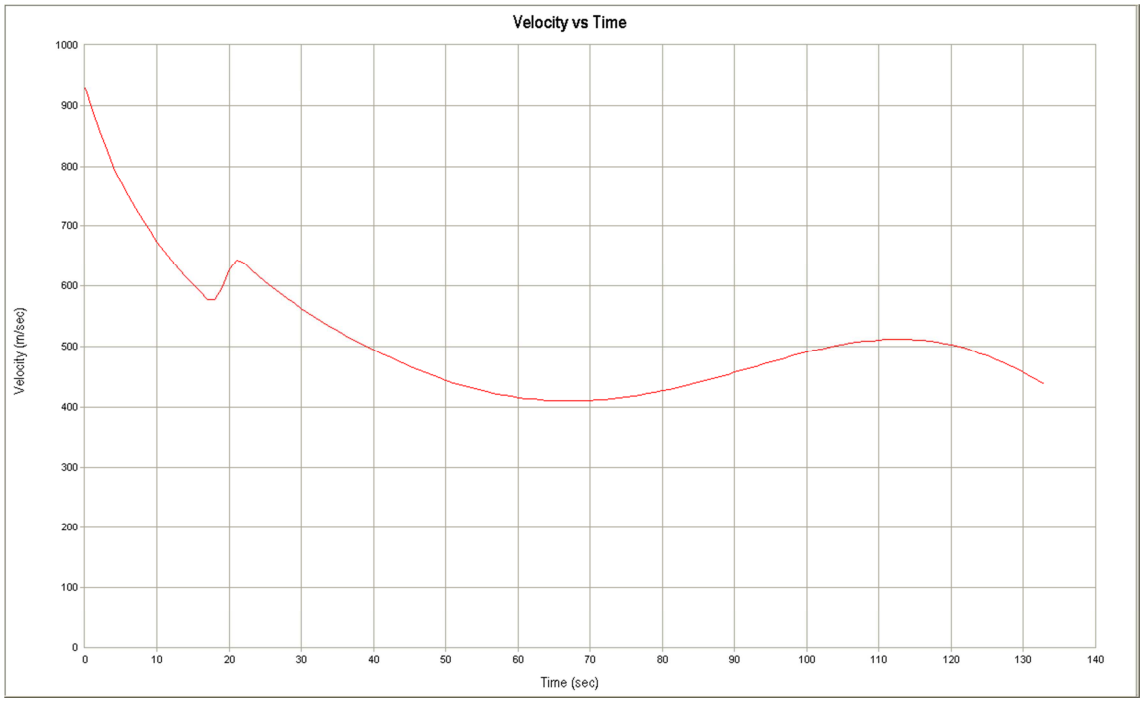

Figure A-18 Velocity vs. Time, 52 calibre gun, max. range, std. atmos.

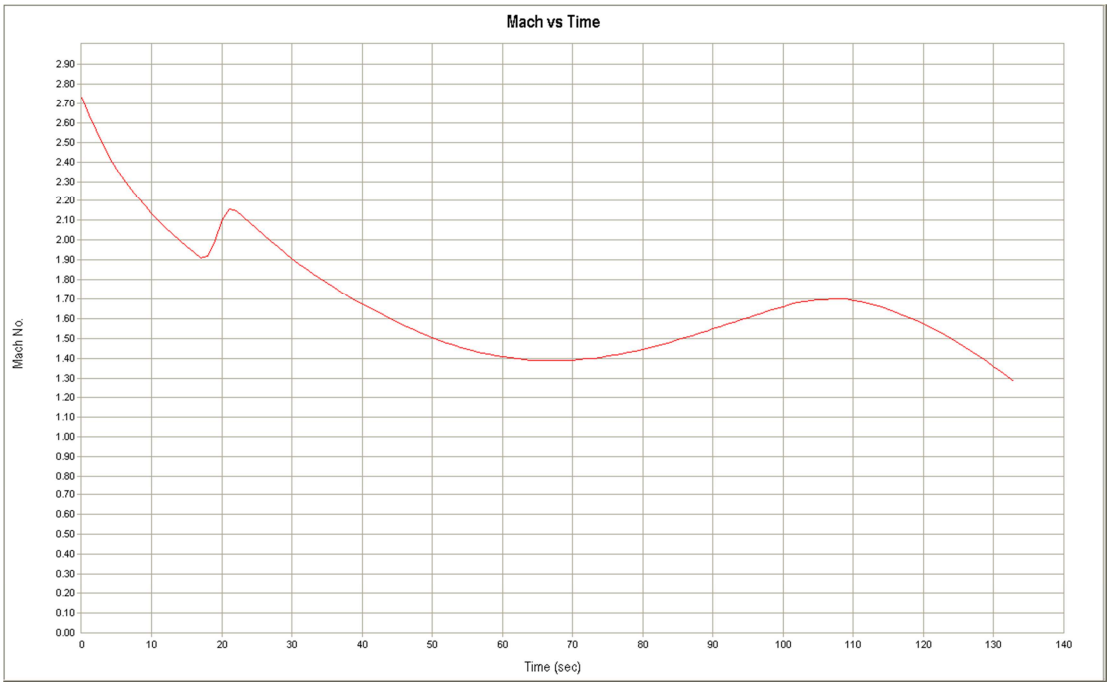

Figure A-19 Mach vs. Time, 52 calibre gun, max. range, std. atmos.

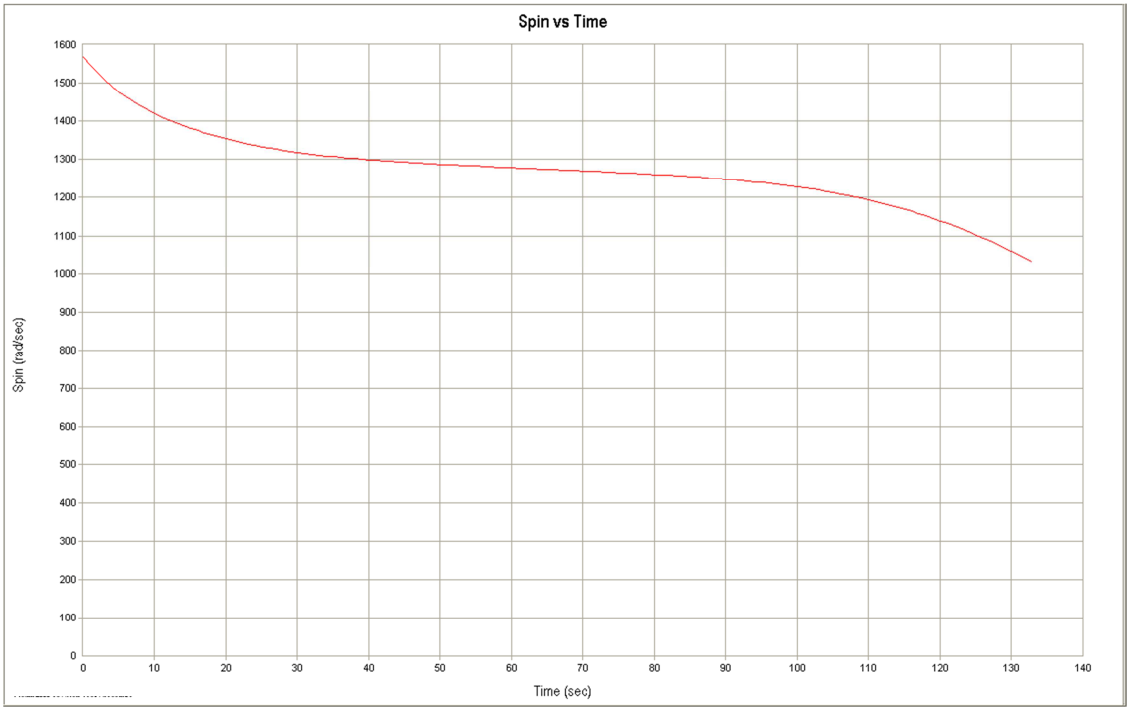

Figure A-20 Spin hystori, 52 calibre gun, max. range, std. atmos.

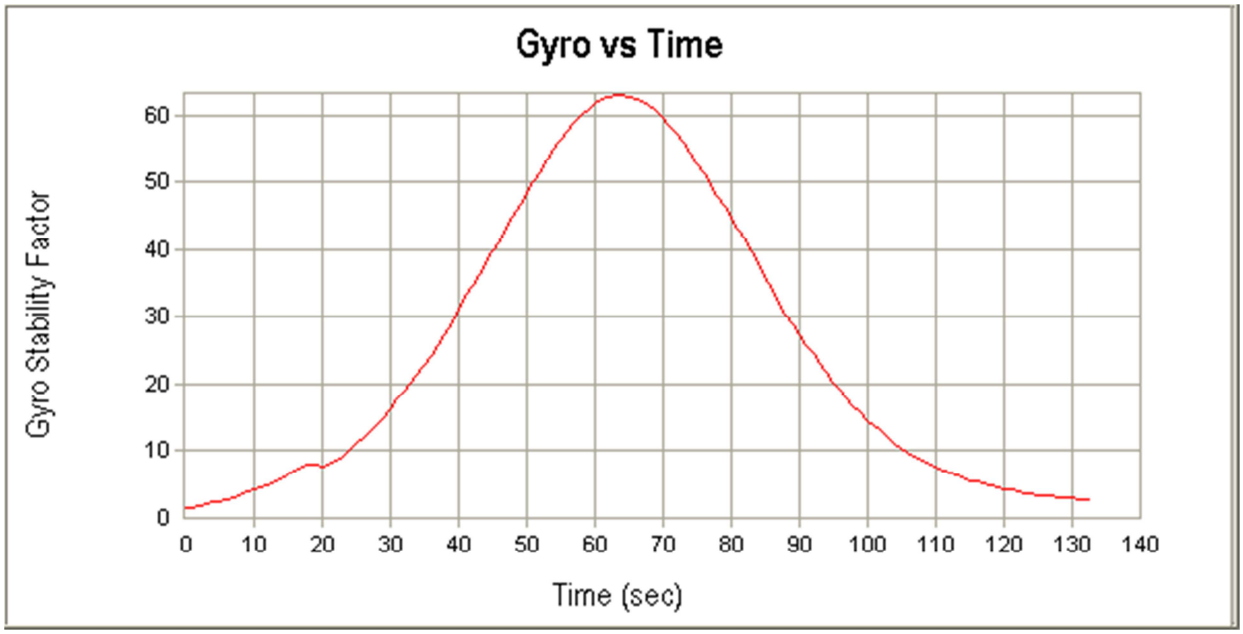

Figure A-21 Gyro stability factor history, 52 calibre gun, max. range, std. atmos.

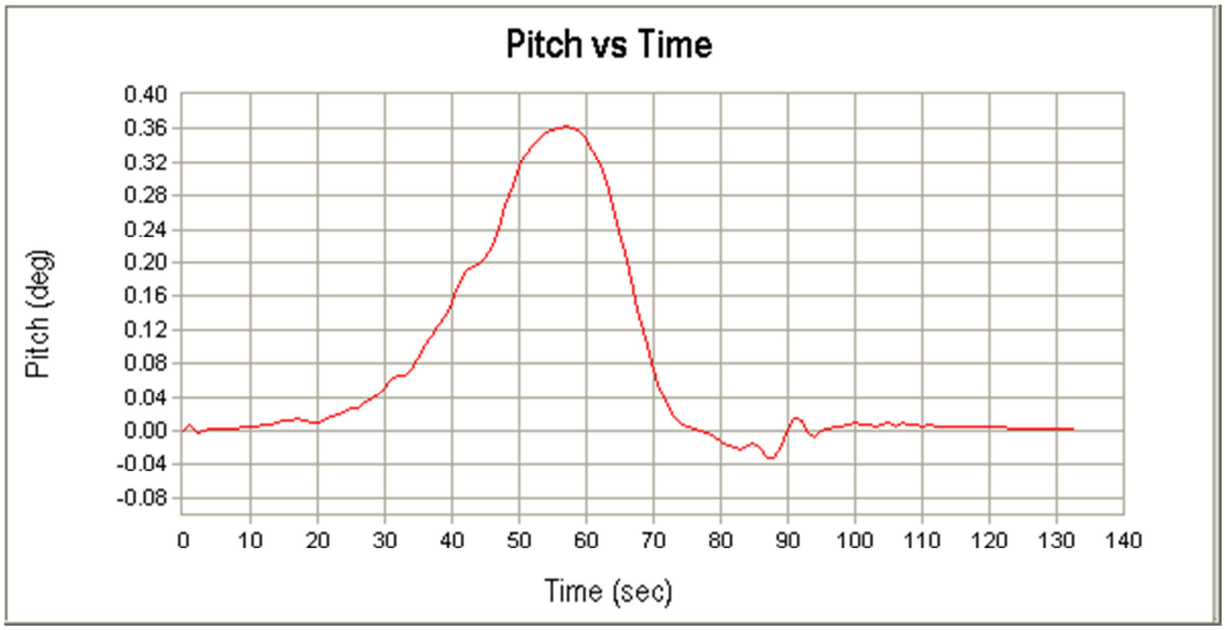

Figure A-22 Pitch angle history, 52 calibre gun, max. range, std. atmos.

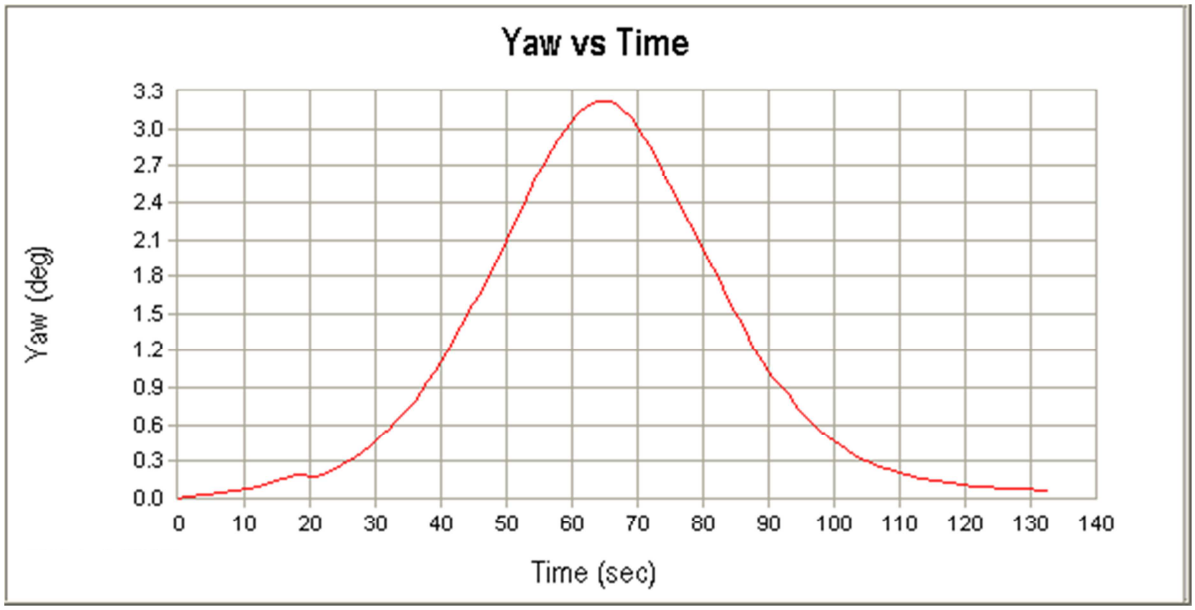

Figure A-23 Yaw angle history, 52 calibre gun, max. range, std. atmos.

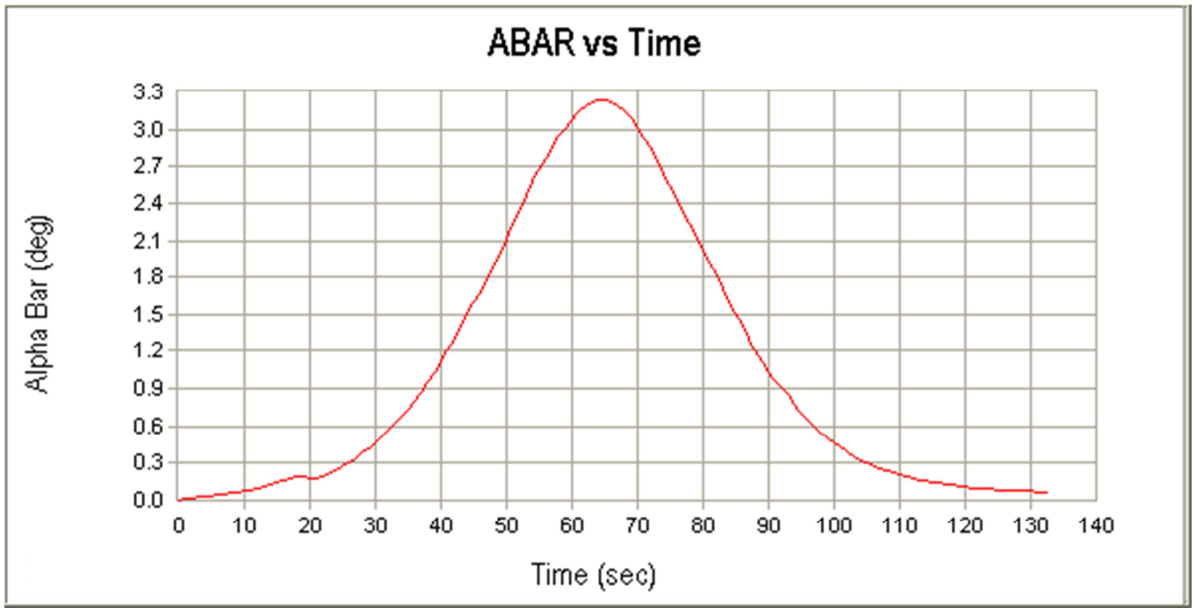

Figure A-24 "Total" angle of attack, 52 calibre gun, max. range, std. atmos

Tables A-7 Summary of 6 DOF Trajectory, 52 caliber gun "Cold" atmosphere

Parameter	Initial	Final	
Velocity	930.0	412.2	m/sec
Trajectory Angle	54.0	-65.9	deg
Time	0.0	131.0	sec
Range	0.0	48969.8	m
Deflection	0.00	-1987.75	m
Altitude (re sl)	0.00	0.00	m
Slant Range	0.0	49010.2	m
Mach Number	3.11	1.38	
Angle of Attack	0.00	0.06	deg

Pitch	[THETA]	(rad):	-0.9425	+ Nose Down
Pitch Rate	[Q]	(rad/sec):	0.0000	+ Nose moving down
Yaw	[PSI]	(rad):	0.0000	+ Nose Left
Yaw Rate	[R]	(rad/sec):	0.0000	+ Nose Moving Left
Travel	[X]	(m):	0.0000	+ Downrange
Velocity-Missile	[U]	(m/sec):	930.0000	+ Forward along axis
Horizontal Motion	[Y]	(m):	0.0000	+ to the left
Hor. Rate-Missile	[V]	(m/sec):	0.0000	+ to the left
Vertical Motion	[Z]	(m):	0.0000	+ up
Vertical Rate-Msle	[W]	(m/sec):	0.0000	+ up
Roll	[PHI]	(rad):	0.0000	+ clockwise
Roll Rate	[P]	(rad/sec):	1569.5800	+ clockwise
X-DOT	[Vx]	(m/s):	546.6401	+ Downrange
Y-DOT	[Vy]	(m/s):	0.0000	+ to the left
Z-DOT	[Vz]	(m/s):	752.3859	+ up

***** 6DOF Fixed Plane Trajectory (Auxiliary Outputs) ******

CDTOT=CXo+(CXa2+CNa)*Sin(A-bar)**2

Time	Slant	A-bar	CDTOT	Vrad	Gamma	Delta	Spin	Lambda_F	Lambda_S
0.0000	0.0	0.000	0.1929	930.00	54.00	0.00	1569.6	-0.0026	-0.0008
10.0000	7737.8	0.075	0.1614	661.60	49.48	-0.21	1406.6	-0.0010	-0.0006
20.0000	13723.0	0.170	0.1549	610.09	43.03	-0.55	1338.2	-0.0006	-0.0004
30.0000	19580.3	0.429	0.1580	538.26	35.73	-0.91	1299.1	-0.0004	-0.0002
40.0000	24545.3	0.988	0.1841	457.43	26.38	-1.32	1277.5	-0.0002	-0.0002
50.0000	28765.4	1.876	0.3009	387.68	14.85	-1.79	1263.7	-0.0002	-0.0001
60.0000	32340.2	2.637	0.3183	329.45	1.50	-2.31	1253.1	-0.0001	-0.0001
70.0000	35396.6	2.456	0.3173	283.92	-12.47	-2.88	1243.1	-0.0002	-0.0001
80.0000	38061.0	1.590	0.3026	251.14	-25.53	-3.42	1231.5	-0.0002	-0.0001
90.0000	40460.8	0.810	0.2898	230.78	-36.69	-3.91	1215.5	-0.0003	-0.0002
100.0000	42711.5	0.390	0.2860	220.80	-45.82	-4.34	1191.5	-0.0004	-0.0003
110.0000	44887.2	0.174	0.2834	213.93	-53.29	-4.72	1152.0	-0.0007	-0.0005
120.0000	46967.2	0.096	0.2970	200.18	-59.65	-5.08	1090.6	-0.0011	-0.0007
130.0000	48842.9	0.061	0.3116	171.93	-65.38	-5.45	1003.5	-0.0018	-0.0013
130.9842	49010.2	0.058	0.3115	167.89	-65.92	-5.49	992.8	-0.0019	-0.0014

No of High Res = 135 Time = 0.494
No of 3d points = 1 Time = 0.000

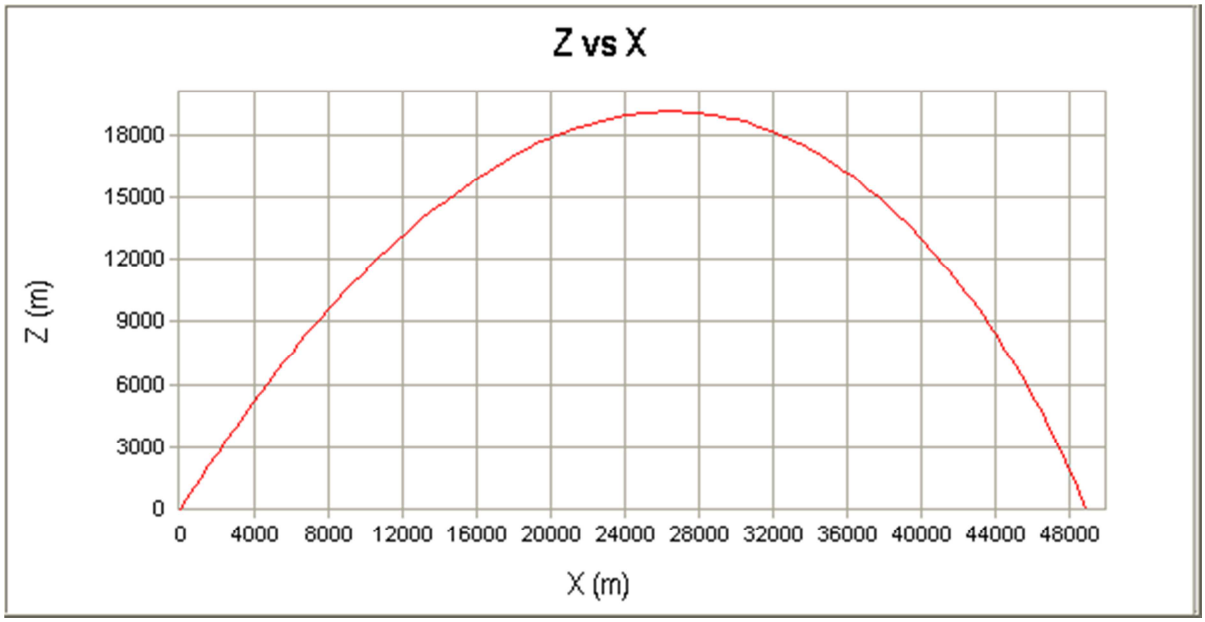

Figure A-25 Range vs. Altitude, 52 calibre gun, max. range, "cold" atmos.

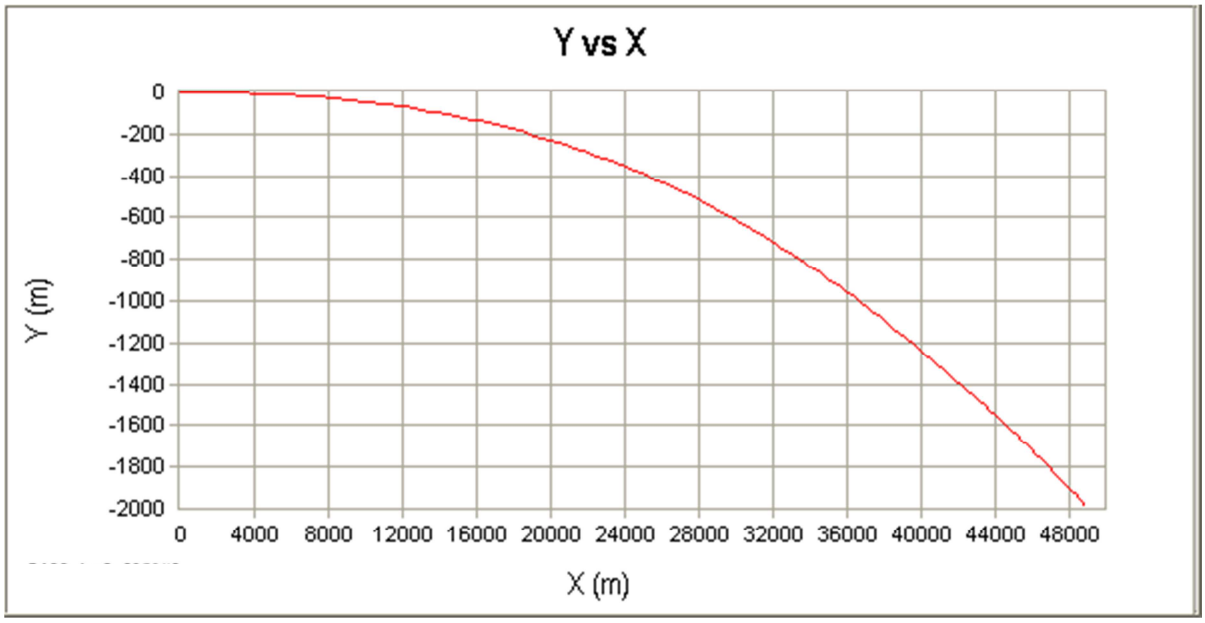

Figure A-26 Range vs. Drift (Deflection), 52 calibre gun, max. range, "cold" atmos.

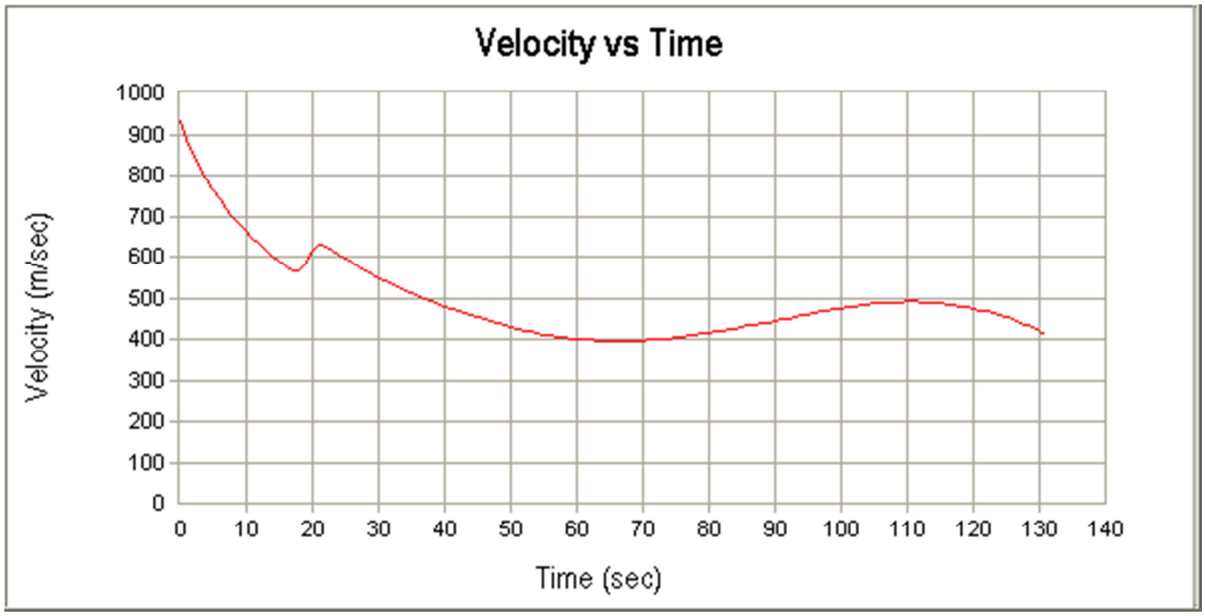

Figure A-27 Velocity vs. Time, 52 calibre gun, max. range, "cold" atmos.

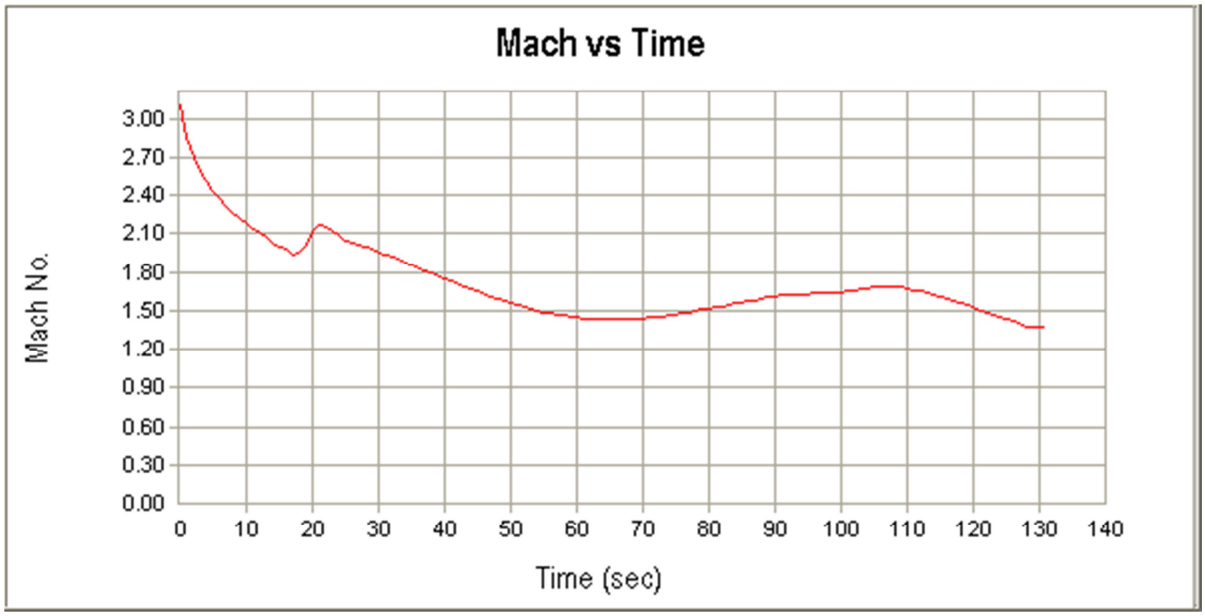

Figure A-28 Mach vs. Time, 52 calibre gun, max. range, "cold" atmos.

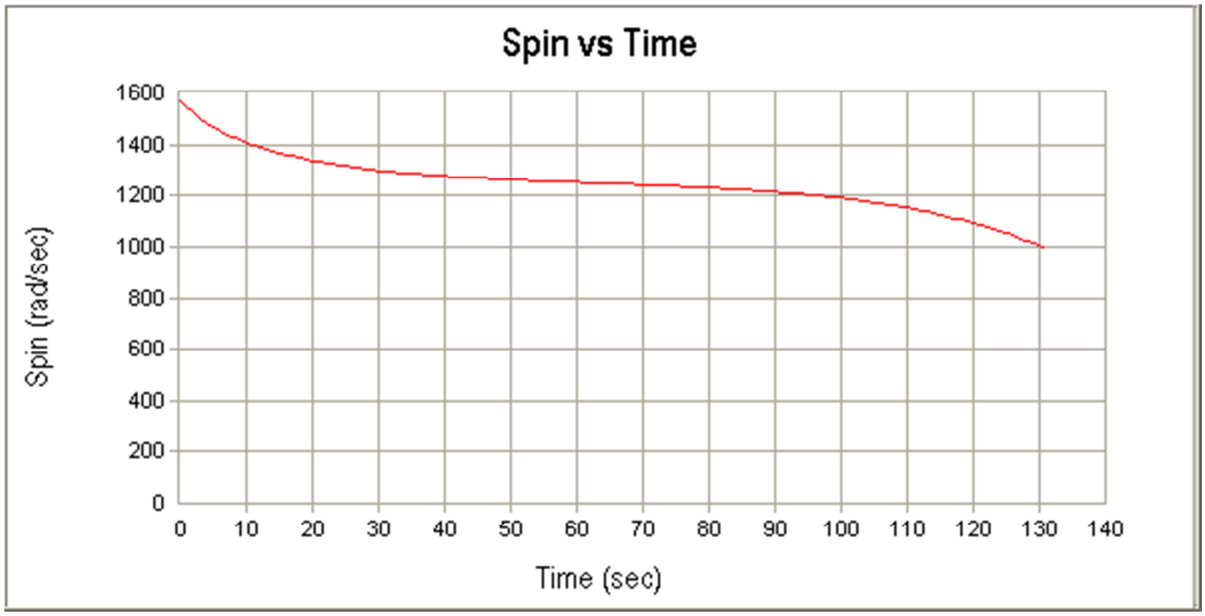

Figure A-29 Spin history, 52 calibre gun, max. range, "cold" atmos.

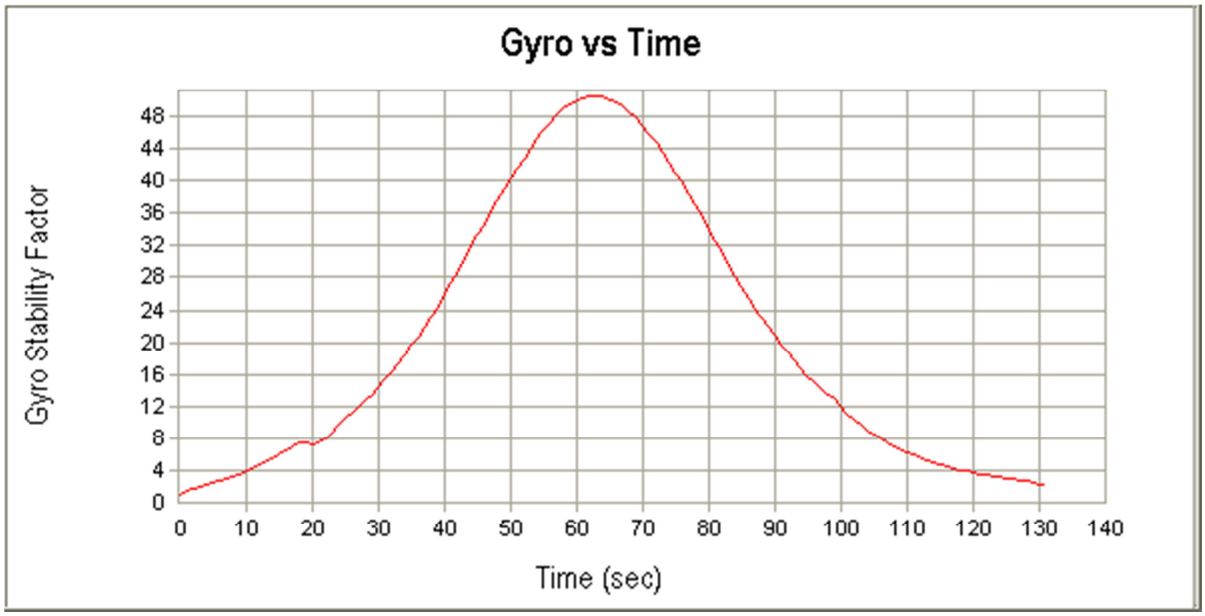

Figure A-30 Gyro stability factor history, 52 calibre gun, max. range, "cold" atmos.

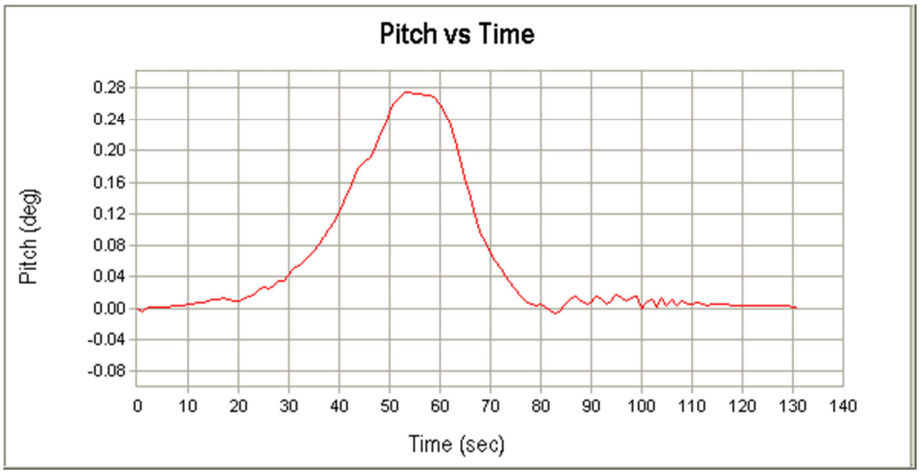

Figure A-31 Pitch angle history, 52 calibre gun, max. range, "cold" atmos.

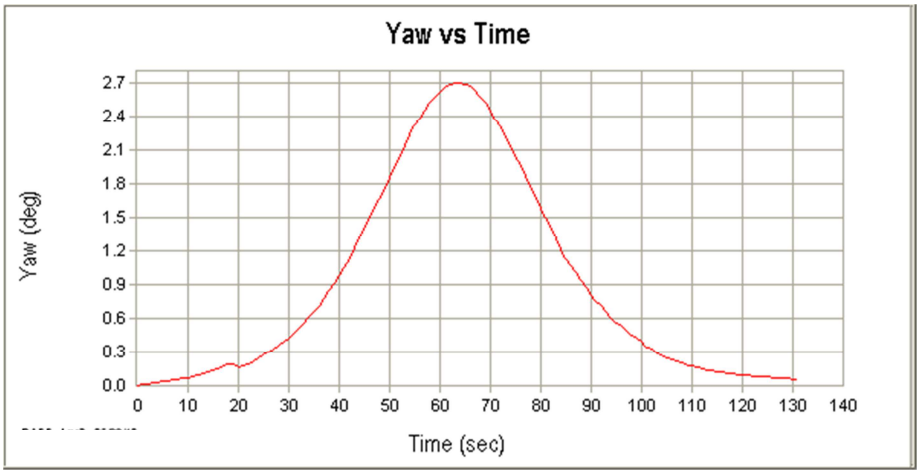

Figure A-32 Yaw angle history, 52 calibre gun, max. range, "cold" atmos.

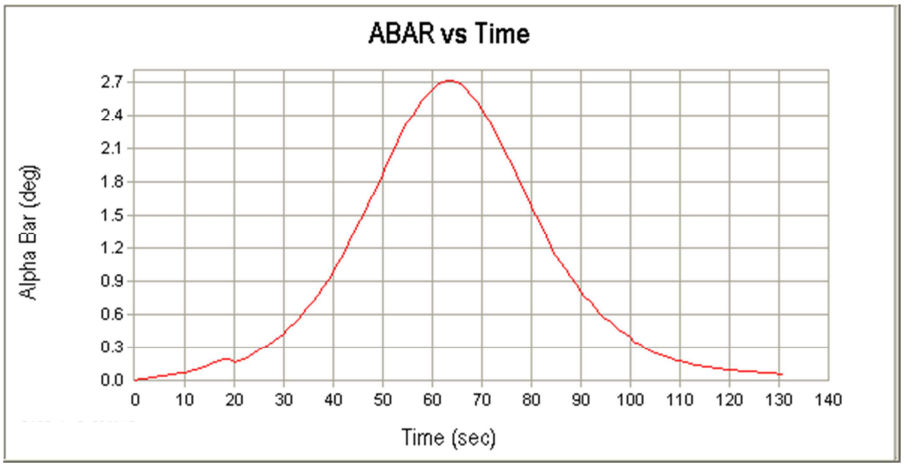

Figure A-33 "Total" angle history, 52 calibre gun, max. range, "cold" atmos.

For the calculation of 6 DOF fixed plain trajectory next model is used by PRODAS:

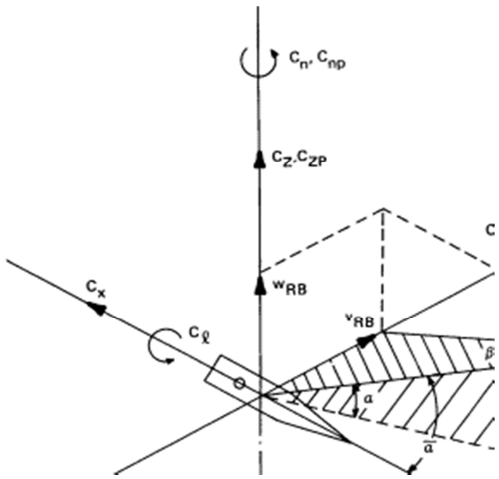

Figure A-34 Fixed plane trajectory model

Appendix B Programming in PTC Creo/Pro Enginer CAD package – propellant grain burning surface development

```
VERSION 2.0
REVNUM 24697
LISTING FOR M-REP PROPELLANT GRAIN BURNING SURFACE DEVELOPMENT
INPUT
 E NUMBER
END INPUT
RELATIONS
END RELATIONS

 ADD FEATURE (initial number 1)
 INTERNAL FEATURE ID  1

 DATUM PLANE
  NO.     ELEMENT NAME    INFO
  ---     -------------   -------------
   1      Feature Name    Defined
   2      Constraints     Defined
   2.1    Constraint #1   Defined
   2.1.1  Constr Type     X Axis
   3      Flip Datum Dir  Defined
   4      Fit             Defined
   4.1    Fit Type        Default
 NAME = RIGHT
    FEATURE IS IN LAYER(S) :
     01___PRT_ALL_DTM_PLN - OPERATION = SHOWN
     01___PRT_DEF_DTM_PLN - OPERATION = SHOWN
 END ADD

 ADD FEATURE (initial number 2)
 INTERNAL FEATURE ID  3

 DATUM PLANE
  NO.     ELEMENT NAME    INFO
  ---     -------------   -------------
   1      Feature Name    Defined
   2      Constraints     Defined
   2.1    Constraint #1   Defined
   2.1.1  Constr Type     Y Axis
   3      Flip Datum Dir  Defined
   4      Fit             Defined
   4.1    Fit Type        Default
 NAME = TOP
    FEATURE IS IN LAYER(S) :
     01___PRT_ALL_DTM_PLN - OPERATION = SHOWN
     01___PRT_DEF_DTM_PLN - OPERATION = SHOWN
 END ADD

 ADD FEATURE (initial number 3)
 INTERNAL FEATURE ID  5
```

```
DATUM PLANE
 NO.     ELEMENT NAME    INFO
 ---     -------------   -------------
  1      Feature Name    Defined
  2      Constraints     Defined
  2.1    Constraint #1   Defined
  2.1.1  Constr Type     Z Axis
  3      Flip Datum Dir  Defined
  4      Fit             Defined
  4.1    Fit Type        Default
NAME = FRONT
   FEATURE IS IN LAYER(S) :
    01___PRT_ALL_DTM_PLN - OPERATION = SHOWN
    01___PRT_DEF_DTM_PLN - OPERATION = SHOWN
END ADD

ADD FEATURE (initial number 4)
INTERNAL FEATURE ID  7
TYPE = COORDINATE SYSTEM
NAME = PRT_CSYS_DEF

   FEATURE IS IN LAYER(S) :
    05___PRT_ALL_DTM_CSYS - OPERATION = SHOWN
    05___PRT_DEF_DTM_CSYS - OPERATION = SHOWN
END ADD

ADD FEATURE (initial number 5)
INTERNAL FEATURE ID  39
PARENTS = 1(#1) 3(#2) 5(#3)

PROTRUSION: Revolve
 NO.     ELEMENT NAME        INFO
 ---     -------------       -------------
  1      Feature Name        Defined
  2      Extrude Feat type   Solid
  3      Material            Add
  4      Section             Defined
  4.1    Setup Plane         Defined
  4.1.1  Sketching Plane     FRONT:F3(DATUM PLANE)
  4.1.2  View Direction      Side 1
  4.1.3  Orientation         Right
  4.1.4  Reference           RIGHT:F1(DATUM PLANE)
  4.2    Sketch              Defined
  5      Feature Form        Solid
  6      Revolve Axis        Defined
  7      Revolve Axis Option  Internal Centerline
  8      Direction           Side 2
  9      Angle               Defined
  9.1    Side One            Defined
  9.1.1  Side One Angle      None
  9.2    Side Two            Defined
  9.2.1  Side Two Angle      Variable
  9.2.2  Value               360.00
SECTION NAME = Section 1
   FEATURE IS IN LAYER(S) :
    02___PRT_ALL_AXES - OPERATION = SHOWN
FEATURE'S DIMENSIONS:
d0 = (Displayed:) 360
```

```
    (   Stored:) 360.0 ( 0.01, -0.01 )
d2 = (Displayed:) 0.5R
    (   Stored:) 0.5 ( 0.01, -0.01 )
d3 = (Displayed:) 118.4 Dia
    (   Stored:) 118.4 ( 0.01, -0.01 )
d133 = (Displayed:) 214.3
      (   Stored:) 214.3 ( 0.01, -0.01 )
END ADD

ADD FEATURE (initial number 6)
INTERNAL FEATURE ID  90
PARENTS = 1(#1) 3(#2) 5(#3)

CUT: Revolve
 NO.      ELEMENT NAME         INFO
 ---      -------------        -------------
  1       Feature Name         Defined
  2       Extrude Feat type    Solid
  3       Material             Remove
  4       Section              Defined
  4.1     Setup Plane          Defined
  4.1.1   Sketching Plane      FRONT:F3(DATUM PLANE)
  4.1.2   View Direction       Side 1
  4.1.3   Orientation          Right
  4.1.4   Reference            RIGHT:F1(DATUM PLANE)
  4.2     Sketch               Defined
  5       Feature Form         Solid
  6       Material Side        Side Two
  7       Revolve Axis         Defined
  8       Revolve Axis Option  Internal Centerline
  9       Direction            Side 2
  10      Angle                Defined
  10.1    Side One             Defined
  10.1.1  Side One Angle       None
  10.2    Side Two             Defined
  10.2.1  Side Two Angle       Variable
  10.2.2  Value                360.00
NAME = INICIJALNI_KONUS
SECTION NAME = Section 1

FEATURE'S DIMENSIONS:
d5 = (Displayed:) 360
    (   Stored:) 360.0 ( 0.01, -0.01 )
d107 = (Displayed:) 0.11R
      (   Stored:) 0.11 ( 0.01, -0.01 )
d108 = (Displayed:) 30
      (   Stored:) 30.0 ( 0.5, -0.5 )
d154 = (Displayed:) 4.99
      (   Stored:) 4.99 ( 0.01, -0.01 )
END ADD
IF E<6.16
   ADD FEATURE (initial number 7)
   INTERNAL FEATURE ID  7099
   PARENTS = 1(#1) 3(#2) 5(#3)

CUT: Revolve
 NO.      ELEMENT NAME         INFO
 ---      -------------        -------------
```

```
  1       Feature Name         Defined
  2       Extrude Feat type    Solid
  3       Material             Remove
  4       Section              Defined
  4.1     Setup Plane          Defined
  4.1.1   Sketching Plane      FRONT:F3(DATUM PLANE)
  4.1.2   View Direction       Side 1
  4.1.3   Orientation          Right
  4.1.4   Reference            RIGHT:F1(DATUM PLANE)
  4.2     Sketch               Defined
  5       Feature Form         Solid
  6       Material Side        Side Two
  7       Revolve Axis         Defined
  8       Revolve Axis Option  Internal Centerline
  9       Direction            Side 1
  10      Angle                Defined
  10.1    Side One             Defined
  10.1.1  Side One Angle       None
  10.2    Side Two             Defined
  10.2.1  Side Two Angle       Variable
  10.2.2  Value                360.0
    NAME = ZAREZ1
    SECTION NAME = Section 1

    FEATURE'S DIMENSIONS:
    d141 = (Displayed:) 360
          (   Stored:) 360.0 ( 0.01, -0.01 )
    d142 = (Displayed:) 60
          (   Stored:) 60.0 ( 0.5, -0.5 )
    d143 = (Displayed:) 4.99
          (   Stored:) 4.99 ( 0.01, -0.01 )
    d144 = (Displayed:) 0.11R
          (   Stored:) 0.11 ( 0.01, -0.01 )
    d145 = (Displayed:) 10
          (   Stored:) 10.0 ( 0.01, -0.01 )
    END ADD
END IF

ADD FEATURE (initial number 8)
INTERNAL FEATURE ID  29798
PARENTS = 1(#1)

DATUM PLANE
 NO.     ELEMENT NAME       INFO
 ---     -------------      -------------
  1      Feature Name       Defined
  2      Constraints        Defined
  2.1    Constraint #1      Defined
  2.1.1  Constr Type        Offset
  2.1.2  Constr References  Surface RIGHT of feat #1 (DATUM PLANE)
  2.1.3  Constr Ref Offset  Value = -214.3000
  3      Flip Datum Dir     Defined
  4      Fit                Defined
  4.1    Fit Type           Default
NAME = DTM6
   FEATURE IS IN LAYER(S) :
     01___PRT_ALL_DTM_PLN - OPERATION = SHOWN
FEATURE'S DIMENSIONS:
```

```
d382 = (Displayed:) 214.3
      (   Stored:) -214.3 ( 0.01, -0.01 )
END ADD

ADD FEATURE (initial number 9)
INTERNAL FEATURE ID  29800
PARENTS = 3(#2) 29798(#8) 1(#1) 5(#3)

CUT: Revolve
 NO.      ELEMENT NAME         INFO
 ---      -------------        -------------
  1       Feature Name         Defined
  2       Extrude Feat type    Solid
  3       Material             Remove
  4       Section              Defined
  4.1     Setup Plane          Defined
  4.1.1   Sketching Plane      FRONT:F3(DATUM PLANE)
  4.1.2   View Direction       Side 1
  4.1.3   Orientation          Top
  4.1.4   Reference            RIGHT:F1(DATUM PLANE)
  4.2     Sketch               Defined
  5       Feature Form         Solid
  6       Material Side        Side Two
  7       Revolve Axis         Defined
  8       Revolve Axis Option  Internal Centerline
  9       Direction            Side 2
  10      Angle                Defined
  10.1    Side One             Defined
  10.1.1  Side One Angle       None
  10.2    Side Two             Defined
  10.2.1  Side Two Angle       Variable
  10.2.2  Value                360.0
SECTION NAME = Section 1

FEATURE'S DIMENSIONS:
d383 = (Displayed:) 360
      (   Stored:) 360.0 ( 0.5, -0.5 )
d384 = (Displayed:) 12
      (   Stored:) 12.0 ( 0.01, -0.01 )
d385 = (Displayed:) 58.5
      (   Stored:) 58.5 ( 0.01, -0.01 )
d386 = (Displayed:) 0.7
      (   Stored:) 0.7 ( 0.01, -0.01 )
d387 = (Displayed:) 5
      (   Stored:) 5.0 ( 0.01, -0.01 )
d388 = (Displayed:) 7.5
      (   Stored:) 7.5 ( 0.01, -0.01 )
d389 = (Displayed:) 100
      (   Stored:) 100.0 ( 0.01, -0.01 )
d390 = (Displayed:) 5
      (   Stored:) 5.0 ( 0.01, -0.01 )
d391 = (Displayed:) 5
      (   Stored:) 5.0 ( 0.01, -0.01 )
d392 = (Displayed:) 5
      (   Stored:) 5.0 ( 0.01, -0.01 )
d393 = (Displayed:) 7.5
      (   Stored:) 7.5 ( 0.01, -0.01 )
d394 = (Displayed:) 5
```

```
      (   Stored:) 5.0 ( 0.01, -0.01 )
d395 = (Displayed:) 63.5
      (   Stored:) 63.5 ( 0.01, -0.01 )
END ADD
IF E<14.82
   ADD FEATURE (initial number 10)
   INTERNAL FEATURE ID  7507
   PARENTS = 1(#1) 3(#2) 5(#3)

CUT: Revolve
 NO.      ELEMENT NAME        INFO
 ---      -------------       -------------
  1       Feature Name        Defined
  2       Extrude Feat type   Solid
  3       Material            Remove
  4       Section             Defined
  4.1     Setup Plane         Defined
  4.1.1   Sketching Plane     FRONT:F3(DATUM PLANE)
  4.1.2   View Direction      Side 1
  4.1.3   Orientation         Right
  4.1.4   Reference           RIGHT:F1(DATUM PLANE)
  4.2     Sketch              Defined
  5       Feature Form        Solid
  6       Material Side       Side Two
  7       Revolve Axis        Defined
  8       Revolve Axis Option  Internal Centerline
  9       Direction           Side 1
  10      Angle               Defined
  10.1    Side One            Defined
  10.1.1  Side One Angle      None
  10.2    Side Two            Defined
  10.2.1  Side Two Angle      Variable
  10.2.2  Value               360.0
   NAME = ZAREZ2
   SECTION NAME = Section 1

   FEATURE'S DIMENSIONS:
   d173 = (Displayed:) 360
         (   Stored:) 360.0 ( 0.01, -0.01 )
   d174 = (Displayed:) 60
         (   Stored:) 60.0 ( 0.5, -0.5 )
   d175 = (Displayed:) 4.99
         (   Stored:) 4.99 ( 0.01, -0.01 )
   d176 = (Displayed:) 0.11R
         (   Stored:) 0.11 ( 0.01, -0.01 )
   d177 = (Displayed:) 20
         (   Stored:) 20.0 ( 0.01, -0.01 )
   END ADD
END IF
IF E<23.48
   ADD FEATURE (initial number 11)
   INTERNAL FEATURE ID  7654
   PARENTS = 1(#1) 3(#2) 5(#3)

CUT: Revolve
 NO.      ELEMENT NAME        INFO
 ---      -------------       -------------
  1       Feature Name        Defined
```

```
  2       Extrude Feat type    Solid
  3       Material             Remove
  4       Section              Defined
  4.1     Setup Plane          Defined
  4.1.1   Sketching Plane      FRONT:F3(DATUM PLANE)
  4.1.2   View Direction       Side 1
  4.1.3   Orientation          Right
  4.1.4   Reference            RIGHT:F1(DATUM PLANE)
  4.2     Sketch               Defined
  5       Feature Form         Solid
  6       Material Side        Side Two
  7       Revolve Axis         Defined
  8       Revolve Axis Option  Internal Centerline
  9       Direction            Side 1
  10      Angle                Defined
  10.1    Side One             Defined
  10.1.1  Side One Angle       None
  10.2    Side Two             Defined
  10.2.1  Side Two Angle       Variable
  10.2.2  Value                360.0
    NAME = ZAREZ3
    SECTION NAME = Section 1

    FEATURE'S DIMENSIONS:
    d183 = (Displayed:) 360
          (   Stored:) 360.0 ( 0.01, -0.01 )
    d184 = (Displayed:) 60
          (   Stored:) 60.0 ( 0.5, -0.5 )
    d185 = (Displayed:) 4.99
          (   Stored:) 4.99 ( 0.01, -0.01 )
    d186 = (Displayed:) 0.11R
          (   Stored:) 0.11 ( 0.01, -0.01 )
    d187 = (Displayed:) 30
          (   Stored:) 30.0 ( 0.01, -0.01 )
    END ADD
END IF

ADD FEATURE (initial number 12)
INTERNAL FEATURE ID  6645
PARENTS = 1(#1) 3(#2) 5(#3)

CUT: Revolve
 NO.      ELEMENT NAME         INFO
 ---      -------------        -------------
  1       Feature Name         Defined
  2       Extrude Feat type    Solid
  3       Material             Remove
  4       Section              Defined
  4.1     Setup Plane          Defined
  4.1.1   Sketching Plane      FRONT:F3(DATUM PLANE)
  4.1.2   View Direction       Side 1
  4.1.3   Orientation          Right
  4.1.4   Reference            RIGHT:F1(DATUM PLANE)
  4.2     Sketch               Defined
  5       Feature Form         Solid
  6       Material Side        Side Two
  7       Revolve Axis         Defined
  8       Revolve Axis Option  Internal Centerline
```

```
  9       Direction           Side 2
  10      Angle               Defined
  10.1    Side One            Defined
  10.1.1  Side One Angle      None
  10.2    Side Two            Defined
  10.2.1  Side Two Angle      Variable
  10.2.2  Value               360.00
NAME = CELO_GORI
SECTION NAME = Section 1
   FEATURE IS IN LAYER(S) :
     02___PRT_ALL_AXES - OPERATION = SHOWN
FEATURE'S DIMENSIONS:
d114 = (Displayed:) 360
       (   Stored:) 360.0 ( 0.01, -0.01 )
d115 = (Displayed:) 70
       (   Stored:) 70.0 ( 0.01, -0.01 )
d116 = (Displayed:) 2.5
       (   Stored:) 2.5 ( 0.01, -0.01 )
d117 = (Displayed:) 0.101
       (   Stored:) 0.101 ( 0.01, -0.01 )
END ADD

ADD FEATURE (initial number 13)
INTERNAL FEATURE ID  159
PARENTS = 1(#1)

DATUM PLANE
 NO.     ELEMENT NAME       INFO
 ---     -------------      -------------
  1      Feature Name       Defined
  2      Constraints        Defined
  2.1    Constraint #1      Defined
  2.1.1  Constr Type        Offset
  2.1.2  Constr References  Surface RIGHT of feat #1 (DATUM PLANE)
  2.1.3  Constr Ref Offset  Value = -5.0000
  3      Flip Datum Dir     Defined
  4      Fit                Defined
  4.1    Fit Type           Default
NAME = DTM1
   FEATURE IS IN LAYER(S) :
     01___PRT_ALL_DTM_PLN - OPERATION = SHOWN
FEATURE'S DIMENSIONS:
d11 = (Displayed:) 5
      (   Stored:) -5.0 ( 0.001, -0.001 )
END ADD

ADD FEATURE (initial number 14)
INTERNAL FEATURE ID  21130
PARENTS = 1(#1)

DATUM PLANE
 NO.     ELEMENT NAME       INFO
 ---     -------------      -------------
  1      Feature Name       Defined
  2      Constraints        Defined
  2.1    Constraint #1      Defined
  2.1.1  Constr Type        Offset
  2.1.2  Constr References  Surface RIGHT of feat #1 (DATUM PLANE)
```

```
  2.1.3  Constr Ref Offset  Value = -17.3970
  3      Flip Datum Dir     Defined
  4      Fit                Defined
  4.1    Fit Type           Default
NAME = DTM2
   FEATURE IS IN LAYER(S) :
    01___PRT_ALL_DTM_PLN - OPERATION = SHOWN
FEATURE'S DIMENSIONS:
d334 = (Displayed:) 17.397
      (   Stored:) -17.397 ( 0.0001, -0.0001 )
END ADD

ADD FEATURE (initial number 15)
INTERNAL FEATURE ID  8514
NO. ELEMENT NAME    INFO                                  STATUS
--- ------------ -----------                            ------
 1  Type         Dimension                                   Defined
 2  Regen Method General                                     Defined
 3  1st Dir Dime                                          Defined
 4  1st Dir Inst 6,                                       Defined
 5  2nd Dir Dime                                            Optional
 6  Dimension-Va                                            Defined
 7  2nd Dir Inst                                          Optional
LEADER OF A (6 X 1) DIM GENERAL PATTERN

MAIN PATTERN DIMENSIONS:
d190 = (Displayed:) 15
      (   Stored:) 15.0 ( 0.5, -0.5 )
d191 = (Displayed:) 0.1
      (   Stored:) 0.103527618041 ( 0.01, -0.01 )
d195 = (Displayed:) 90
      (   Stored:) -90.0 ( 0.01, -0.01 )
d196 = (Displayed:) 20 Dia
      (   Stored:) 20.0 ( 0.01, -0.01 )
d225 = (Displayed:) 60
      (   Stored:) -60.0 ( 0.01, -0.01 )
END ADD

ADD FEATURE (initial number 16)
INTERNAL FEATURE ID  7726
PARENTS = 159(#13) 5(#3) 39(#5)

HOLE
 NO.   ELEMENT NAME       INFO
 ---   -------------      -------------
  1    Hole               Defined
  1.1  Hole Type          Sketched
  1.2  Sketcher           Defined
  1.3  Flip               Side 2
  2    Placement          Defined
  2.1  Primary Reference  DTM1:F13(DATUM PLANE)
  2.2  Placement Type     Diameter
  2.3  Axial Reference    A_2(AXIS):F5(REVOLVE_1)
  2.4  Diameter           20.00
  2.5  Angular Reference  FRONT:F3(DATUM PLANE)
  2.6  Angle              90.00
  3    Feature Name       Defined
SECTION NAME = S2D0016
```

```
PLACEMENT = RADIAL
MEMBER (1, 1) IN A (6 X 1) DIM GENERAL PATTERN
   FEATURE IS IN LAYER(S) :
    02___PRT_ALL_AXES - OPERATION = SHOWN
MAIN PATTERN DIMENSIONS:
d190 = (Displayed:) 15
      (   Stored:) 15.0 ( 0.5, -0.5 )
d191 = (Displayed:) 0.1
      (   Stored:) 0.103527618041 ( 0.01, -0.01 )
d195 = (Displayed:) 90
      (   Stored:) -90.0 ( 0.01, -0.01 )
d196 = (Displayed:) 20 Dia
      (   Stored:) 20.0 ( 0.01, -0.01 )
d225 = (Displayed:) 60
      (   Stored:) -60.0 ( 0.01, -0.01 )
END ADD

ADD FEATURE (initial number 17)
INTERNAL FEATURE ID  8515
PARENTS = 159(#13) 7726(#16) 5(#3) 39(#5)

HOLE
 NO.   ELEMENT NAME       INFO
 ---   -------------      -------------
  1    Hole               Defined
  1.1  Hole Type          Sketched
  1.2  Sketcher           Defined
  1.3  Flip               Side 2
  2    Placement          Defined
  2.1  Primary Reference  DTM1:F13(DATUM PLANE)
  2.2  Placement Type     Diameter
  2.3  Axial Reference    A_2(AXIS):F5(REVOLVE_1)
  2.4  Diameter           20.00
  2.5  Angular Reference  FRONT:F3(DATUM PLANE)
  2.6  Angle              90.00
  3    Feature Name       Defined
SECTION NAME = S2D0016
PLACEMENT = RADIAL
MEMBER (2, 1) IN A (6 X 1) DIM GENERAL PATTERN
   FEATURE IS IN LAYER(S) :
    02___PRT_ALL_AXES - OPERATION = SHOWN
MAIN PATTERN DIMENSIONS:
d190 = (Displayed:) 15
      (   Stored:) 15.0 ( 0.5, -0.5 )
d191 = (Displayed:) 0.1
      (   Stored:) 0.103527618041 ( 0.01, -0.01 )
d195 = (Displayed:) 90
      (   Stored:) -90.0 ( 0.01, -0.01 )
d196 = (Displayed:) 20 Dia
      (   Stored:) 20.0 ( 0.01, -0.01 )
d225 = (Displayed:) 60
      (   Stored:) -60.0 ( 0.01, -0.01 )
END ADD

ADD FEATURE (initial number 18)
INTERNAL FEATURE ID  8566
PARENTS = 159(#13) 7726(#16) 5(#3) 39(#5)
```

```
HOLE
 NO.   ELEMENT NAME       INFO
 ---   -------------      -------------
  1    Hole               Defined
  1.1  Hole Type          Sketched
  1.2  Sketcher           Defined
  1.3  Flip               Side 2
  2    Placement          Defined
  2.1  Primary Reference  DTM1:F13(DATUM PLANE)
  2.2  Placement Type     Diameter
  2.3  Axial Reference    A_2(AXIS):F5(REVOLVE_1)
  2.4  Diameter           20.00
  2.5  Angular Reference  FRONT:F3(DATUM PLANE)
  2.6  Angle              90.00
  3    Feature Name       Defined
SECTION NAME = S2D0016
PLACEMENT = RADIAL
MEMBER (3, 1) IN A (6 X 1) DIM GENERAL PATTERN
   FEATURE IS IN LAYER(S) :
    02___PRT_ALL_AXES - OPERATION = SHOWN
MAIN PATTERN DIMENSIONS:
d190 = (Displayed:) 15
      (   Stored:) 15.0 ( 0.5, -0.5 )
d191 = (Displayed:) 0.1
      (   Stored:) 0.103527618041 ( 0.01, -0.01 )
d195 = (Displayed:) 90
      (   Stored:) -90.0 ( 0.01, -0.01 )
d196 = (Displayed:) 20 Dia
      (   Stored:) 20.0 ( 0.01, -0.01 )
d225 = (Displayed:) 60
      (   Stored:) -60.0 ( 0.01, -0.01 )
END ADD

ADD FEATURE (initial number 19)
INTERNAL FEATURE ID  8567
PARENTS = 159(#13) 7726(#16) 5(#3) 39(#5)

HOLE
 NO.   ELEMENT NAME       INFO
 ---   -------------      -------------
  1    Hole               Defined
  1.1  Hole Type          Sketched
  1.2  Sketcher           Defined
  1.3  Flip               Side 2
  2    Placement          Defined
  2.1  Primary Reference  DTM1:F13(DATUM PLANE)
  2.2  Placement Type     Diameter
  2.3  Axial Reference    A_2(AXIS):F5(REVOLVE_1)
  2.4  Diameter           20.00
  2.5  Angular Reference  FRONT:F3(DATUM PLANE)
  2.6  Angle              90.00
  3    Feature Name       Defined
SECTION NAME = S2D0016
PLACEMENT = RADIAL
MEMBER (4, 1) IN A (6 X 1) DIM GENERAL PATTERN
   FEATURE IS IN LAYER(S) :
    02___PRT_ALL_AXES - OPERATION = SHOWN
MAIN PATTERN DIMENSIONS:
```

```
d190 = (Displayed:) 15
      (   Stored:) 15.0 ( 0.5, -0.5 )
d191 = (Displayed:) 0.1
      (   Stored:) 0.103527618041 ( 0.01, -0.01 )
d195 = (Displayed:) 90
      (   Stored:) -90.0 ( 0.01, -0.01 )
d196 = (Displayed:) 20 Dia
      (   Stored:) 20.0 ( 0.01, -0.01 )
d225 = (Displayed:) 60
      (   Stored:) -60.0 ( 0.01, -0.01 )
END ADD

ADD FEATURE (initial number 20)
INTERNAL FEATURE ID  8568
PARENTS = 159(#13) 7726(#16) 5(#3) 39(#5)

HOLE
 NO.   ELEMENT NAME       INFO
 ---   -------------      -------------
  1    Hole               Defined
  1.1  Hole Type          Sketched
  1.2  Sketcher           Defined
  1.3  Flip               Side 2
  2    Placement          Defined
  2.1  Primary Reference  DTM1:F13(DATUM PLANE)
  2.2  Placement Type     Diameter
  2.3  Axial Reference    A_2(AXIS):F5(REVOLVE_1)
  2.4  Diameter           20.00
  2.5  Angular Reference  FRONT:F3(DATUM PLANE)
  2.6  Angle              90.00
  3    Feature Name       Defined
SECTION NAME = S2D0016
PLACEMENT = RADIAL
MEMBER (5, 1) IN A (6 X 1) DIM GENERAL PATTERN
   FEATURE IS IN LAYER(S) :
    02___PRT_ALL_AXES - OPERATION = SHOWN
MAIN PATTERN DIMENSIONS:
d190 = (Displayed:) 15
      (   Stored:) 15.0 ( 0.5, -0.5 )
d191 = (Displayed:) 0.1
      (   Stored:) 0.103527618041 ( 0.01, -0.01 )
d195 = (Displayed:) 90
      (   Stored:) -90.0 ( 0.01, -0.01 )
d196 = (Displayed:) 20 Dia
      (   Stored:) 20.0 ( 0.01, -0.01 )
d225 = (Displayed:) 60
      (   Stored:) -60.0 ( 0.01, -0.01 )
END ADD

ADD FEATURE (initial number 21)
INTERNAL FEATURE ID  8569
PARENTS = 159(#13) 7726(#16) 5(#3) 39(#5)

HOLE
 NO.   ELEMENT NAME       INFO
 ---   -------------      -------------
  1    Hole               Defined
  1.1  Hole Type          Sketched
```

```
  1.2  Sketcher          Defined
  1.3  Flip              Side 2
  2    Placement         Defined
  2.1  Primary Reference  DTM1:F13(DATUM PLANE)
  2.2  Placement Type     Diameter
  2.3  Axial Reference    A_2(AXIS):F5(REVOLVE_1)
  2.4  Diameter           20.00
  2.5  Angular Reference  FRONT:F3(DATUM PLANE)
  2.6  Angle              90.00
  3    Feature Name       Defined
SECTION NAME = S2D0016
PLACEMENT = RADIAL
MEMBER (6, 1) IN A (6 X 1) DIM GENERAL PATTERN
   FEATURE IS IN LAYER(S) :
    02___PRT_ALL_AXES - OPERATION = SHOWN
MAIN PATTERN DIMENSIONS:
d190 = (Displayed:) 15
      (   Stored:) 15.0 ( 0.5, -0.5 )
d191 = (Displayed:) 0.1
      (   Stored:) 0.103527618041 ( 0.01, -0.01 )
d195 = (Displayed:) 90
      (   Stored:) -90.0 ( 0.01, -0.01 )
d196 = (Displayed:) 20 Dia
      (   Stored:) 20.0 ( 0.01, -0.01 )
d225 = (Displayed:) 60
      (   Stored:) -60.0 ( 0.01, -0.01 )
END ADD

ADD FEATURE (initial number 22)
INTERNAL FEATURE ID  8931
NO. ELEMENT NAME    INFO                                STATUS
--- ------------ -----------                          ------
 1  Type         Dimension                              Defined
 2  Regen Method General                                  Defined
 3  1st Dir Dime                                       Defined
 4  1st Dir Inst 6,                                    Defined
 5  2nd Dir Dime                                       Optional
 6  Dimension-Va                                       Defined
 7  2nd Dir Inst                                       Optional
LEADER OF A (6 X 1) DIM GENERAL PATTERN

MAIN PATTERN DIMENSIONS:
d236 = (Displayed:) 15
      (   Stored:) 15.0 ( 0.5, -0.5 )
d237 = (Displayed:) 0.1
      (   Stored:) 0.103527618041 ( 0.01, -0.01 )
d240 = (Displayed:) 40 Dia
      (   Stored:) 40.0 ( 0.01, -0.01 )
d241 = (Displayed:) 60
      (   Stored:) -60.0 ( 0.01, -0.01 )
d242 = (Displayed:) 60
      (   Stored:) -60.0 ( 0.01, -0.01 )
END ADD

ADD FEATURE (initial number 23)
INTERNAL FEATURE ID  8881
PARENTS = 159(#13) 5(#3) 39(#5)
```

```
HOLE
 NO.   ELEMENT NAME       INFO
 ---   -------------      -------------
  1    Hole               Defined
  1.1  Hole Type          Sketched
  1.2  Sketcher           Defined
  1.3  Flip               Side 2
  2    Placement          Defined
  2.1  Primary Reference  DTM1:F13(DATUM PLANE)
  2.2  Placement Type     Diameter
  2.3  Axial Reference    A_2(AXIS):F5(REVOLVE_1)
  2.4  Diameter           40.00
  2.5  Angular Reference  FRONT:F3(DATUM PLANE)
  2.6  Angle              60.00
  3    Feature Name       Defined
SECTION NAME = S2D0017
PLACEMENT = RADIAL
MEMBER (1, 1) IN A (6 X 1) DIM GENERAL PATTERN
   FEATURE IS IN LAYER(S) :
    02___PRT_ALL_AXES - OPERATION = SHOWN
MAIN PATTERN DIMENSIONS:
d236 = (Displayed:) 15
      (   Stored:) 15.0 ( 0.5, -0.5 )
d237 = (Displayed:) 0.1
      (   Stored:) 0.103527618041 ( 0.01, -0.01 )
d240 = (Displayed:) 40 Dia
      (   Stored:) 40.0 ( 0.01, -0.01 )
d241 = (Displayed:) 60
      (   Stored:) -60.0 ( 0.01, -0.01 )
d242 = (Displayed:) 60
      (   Stored:) -60.0 ( 0.01, -0.01 )
END ADD

ADD FEATURE (initial number 24)
INTERNAL FEATURE ID  8932
PARENTS = 159(#13) 8881(#23) 5(#3) 39(#5)

HOLE
 NO.   ELEMENT NAME       INFO
 ---   -------------      -------------
  1    Hole               Defined
  1.1  Hole Type          Sketched
  1.2  Sketcher           Defined
  1.3  Flip               Side 2
  2    Placement          Defined
  2.1  Primary Reference  DTM1:F13(DATUM PLANE)
  2.2  Placement Type     Diameter
  2.3  Axial Reference    A_2(AXIS):F5(REVOLVE_1)
  2.4  Diameter           40.00
  2.5  Angular Reference  FRONT:F3(DATUM PLANE)
  2.6  Angle              60.00
  3    Feature Name       Defined
SECTION NAME = S2D0017
PLACEMENT = RADIAL
MEMBER (2, 1) IN A (6 X 1) DIM GENERAL PATTERN
   FEATURE IS IN LAYER(S) :
    02___PRT_ALL_AXES - OPERATION = SHOWN
MAIN PATTERN DIMENSIONS:
```

```
d236 = (Displayed:) 15
      (   Stored:) 15.0 ( 0.5, -0.5 )
d237 = (Displayed:) 0.1
      (   Stored:) 0.103527618041 ( 0.01, -0.01 )
d240 = (Displayed:) 40 Dia
      (   Stored:) 40.0 ( 0.01, -0.01 )
d241 = (Displayed:) 60
      (   Stored:) -60.0 ( 0.01, -0.01 )
d242 = (Displayed:) 60
      (   Stored:) -60.0 ( 0.01, -0.01 )
END ADD

ADD FEATURE (initial number 25)
INTERNAL FEATURE ID  8933
PARENTS = 159(#13) 8881(#23) 5(#3) 39(#5)

HOLE
 NO.   ELEMENT NAME       INFO
 ---   -------------      -------------
  1    Hole               Defined
  1.1  Hole Type          Sketched
  1.2  Sketcher           Defined
  1.3  Flip               Side 2
  2    Placement          Defined
  2.1  Primary Reference  DTM1:F13(DATUM PLANE)
  2.2  Placement Type     Diameter
  2.3  Axial Reference    A_2(AXIS):F5(REVOLVE_1)
  2.4  Diameter           40.00
  2.5  Angular Reference  FRONT:F3(DATUM PLANE)
  2.6  Angle              60.00
  3    Feature Name       Defined
SECTION NAME = S2D0017
PLACEMENT = RADIAL
MEMBER (3, 1) IN A (6 X 1) DIM GENERAL PATTERN
   FEATURE IS IN LAYER(S) :
    02___PRT_ALL_AXES - OPERATION = SHOWN
MAIN PATTERN DIMENSIONS:
d236 = (Displayed:) 15
      (   Stored:) 15.0 ( 0.5, -0.5 )
d237 = (Displayed:) 0.1
      (   Stored:) 0.103527618041 ( 0.01, -0.01 )
d240 = (Displayed:) 40 Dia
      (   Stored:) 40.0 ( 0.01, -0.01 )
d241 = (Displayed:) 60
      (   Stored:) -60.0 ( 0.01, -0.01 )
d242 = (Displayed:) 60
      (   Stored:) -60.0 ( 0.01, -0.01 )
END ADD

ADD FEATURE (initial number 26)
INTERNAL FEATURE ID  8934
PARENTS = 159(#13) 8881(#23) 5(#3) 39(#5)

HOLE
 NO.   ELEMENT NAME       INFO
 ---   -------------      -------------
  1    Hole               Defined
  1.1  Hole Type          Sketched
```

```
  1.2  Sketcher          Defined
  1.3  Flip              Side 2
  2    Placement         Defined
  2.1  Primary Reference  DTM1:F13(DATUM PLANE)
  2.2  Placement Type     Diameter
  2.3  Axial Reference    A_2(AXIS):F5(REVOLVE_1)
  2.4  Diameter           40.00
  2.5  Angular Reference  FRONT:F3(DATUM PLANE)
  2.6  Angle              60.00
  3    Feature Name       Defined
SECTION NAME = S2D0017
PLACEMENT = RADIAL
MEMBER (4, 1) IN A (6 X 1) DIM GENERAL PATTERN
   FEATURE IS IN LAYER(S) :
    02___PRT_ALL_AXES - OPERATION = SHOWN
MAIN PATTERN DIMENSIONS:
d236 = (Displayed:) 15
      (   Stored:) 15.0 ( 0.5, -0.5 )
d237 = (Displayed:) 0.1
      (   Stored:) 0.103527618041 ( 0.01, -0.01 )
d240 = (Displayed:) 40 Dia
      (   Stored:) 40.0 ( 0.01, -0.01 )
d241 = (Displayed:) 60
      (   Stored:) -60.0 ( 0.01, -0.01 )
d242 = (Displayed:) 60
      (   Stored:) -60.0 ( 0.01, -0.01 )
END ADD

ADD FEATURE (initial number 27)
INTERNAL FEATURE ID  8935
PARENTS = 159(#13) 8881(#23) 5(#3) 39(#5)

HOLE
 NO.   ELEMENT NAME       INFO
 ---   -------------      -------------
  1    Hole               Defined
  1.1  Hole Type          Sketched
  1.2  Sketcher           Defined
  1.3  Flip               Side 2
  2    Placement          Defined
  2.1  Primary Reference  DTM1:F13(DATUM PLANE)
  2.2  Placement Type     Diameter
  2.3  Axial Reference    A_2(AXIS):F5(REVOLVE_1)
  2.4  Diameter           40.00
  2.5  Angular Reference  FRONT:F3(DATUM PLANE)
  2.6  Angle              60.00
  3    Feature Name       Defined
SECTION NAME = S2D0017
PLACEMENT = RADIAL
MEMBER (5, 1) IN A (6 X 1) DIM GENERAL PATTERN
   FEATURE IS IN LAYER(S) :
    02___PRT_ALL_AXES - OPERATION = SHOWN
MAIN PATTERN DIMENSIONS:
d236 = (Displayed:) 15
      (   Stored:) 15.0 ( 0.5, -0.5 )
d237 = (Displayed:) 0.1
      (   Stored:) 0.103527618041 ( 0.01, -0.01 )
d240 = (Displayed:) 40 Dia
```

```
      (   Stored:) 40.0 ( 0.01, -0.01 )
d241 = (Displayed:) 60
      (   Stored:) -60.0 ( 0.01, -0.01 )
d242 = (Displayed:) 60
      (   Stored:) -60.0 ( 0.01, -0.01 )
END ADD

ADD FEATURE (initial number 28)
INTERNAL FEATURE ID  8936
PARENTS = 159(#13) 8881(#23) 5(#3) 39(#5)

HOLE
 NO.   ELEMENT NAME       INFO
 ---   -------------      -------------
  1    Hole               Defined
  1.1  Hole Type          Sketched
  1.2  Sketcher           Defined
  1.3  Flip               Side 2
  2    Placement          Defined
  2.1  Primary Reference  DTM1:F13(DATUM PLANE)
  2.2  Placement Type     Diameter
  2.3  Axial Reference    A_2(AXIS):F5(REVOLVE_1)
  2.4  Diameter           40.00
  2.5  Angular Reference  FRONT:F3(DATUM PLANE)
  2.6  Angle              60.00
  3    Feature Name       Defined
SECTION NAME = S2D0017
PLACEMENT = RADIAL
MEMBER (6, 1) IN A (6 X 1) DIM GENERAL PATTERN
   FEATURE IS IN LAYER(S) :
    02___PRT_ALL_AXES - OPERATION = SHOWN
MAIN PATTERN DIMENSIONS:
d236 = (Displayed:) 15
      (   Stored:) 15.0 ( 0.5, -0.5 )
d237 = (Displayed:) 0.1
      (   Stored:) 0.103527618041 ( 0.01, -0.01 )
d240 = (Displayed:) 40 Dia
      (   Stored:) 40.0 ( 0.01, -0.01 )
d241 = (Displayed:) 60
      (   Stored:) -60.0 ( 0.01, -0.01 )
d242 = (Displayed:) 60
      (   Stored:) -60.0 ( 0.01, -0.01 )
END ADD

ADD FEATURE (initial number 29)
INTERNAL FEATURE ID  10050
NO. ELEMENT NAME    INFO                                STATUS
--- ------------ -----------                          ------
 1  Type         Dimension                                 Defined
 2  Regen Method General                                      Defined
 3  1st Dir Dime                                           Defined
 4  1st Dir Inst 12,                                       Defined
 5  2nd Dir Dime                                            Optional
 6  Dimension-Va                                             Defined
 7  2nd Dir Inst                                           Optional
LEADER OF A (12 X 1) DIM GENERAL PATTERN

MAIN PATTERN DIMENSIONS:
```

```
d261 = (Displayed:) 15
      (   Stored:) 15.0 ( 0.5, -0.5 )
d262 = (Displayed:) 0.1
      (   Stored:) 0.103527618041 ( 0.01, -0.01 )
d266 = (Displayed:) 15
      (   Stored:) -15.0 ( 0.01, -0.01 )
d267 = (Displayed:) 60 Dia
      (   Stored:) 60.0 ( 0.01, -0.01 )
d268 = (Displayed:) 30
      (   Stored:) -30.0 ( 0.01, -0.01 )
END ADD

ADD FEATURE (initial number 30)
INTERNAL FEATURE ID  9999
PARENTS = 159(#13) 5(#3) 39(#5)

HOLE
 NO.   ELEMENT NAME       INFO
 ---   -------------      -------------
  1    Hole               Defined
  1.1  Hole Type          Sketched
  1.2  Sketcher           Defined
  1.3  Flip               Side 2
  2    Placement          Defined
  2.1  Primary Reference  DTM1:F13(DATUM PLANE)
  2.2  Placement Type     Diameter
  2.3  Axial Reference    A_2(AXIS):F5(REVOLVE_1)
  2.4  Diameter           60.00
  2.5  Angular Reference  FRONT:F3(DATUM PLANE)
  2.6  Angle              15.00
  3    Feature Name       Defined
SECTION NAME = S2D0018
PLACEMENT = RADIAL
MEMBER (1, 1) IN A (12 X 1) DIM GENERAL PATTERN
   FEATURE IS IN LAYER(S) :
    02___PRT_ALL_AXES - OPERATION = SHOWN
MAIN PATTERN DIMENSIONS:
d261 = (Displayed:) 15
      (   Stored:) 15.0 ( 0.5, -0.5 )
d262 = (Displayed:) 0.1
      (   Stored:) 0.103527618041 ( 0.01, -0.01 )
d266 = (Displayed:) 15
      (   Stored:) -15.0 ( 0.01, -0.01 )
d267 = (Displayed:) 60 Dia
      (   Stored:) 60.0 ( 0.01, -0.01 )
d268 = (Displayed:) 30
      (   Stored:) -30.0 ( 0.01, -0.01 )
END ADD

ADD FEATURE (initial number 31)
INTERNAL FEATURE ID  10051
PARENTS = 159(#13) 9999(#30) 5(#3) 39(#5)

HOLE
 NO.   ELEMENT NAME       INFO
 ---   -------------      -------------
  1    Hole               Defined
  1.1  Hole Type          Sketched
```

```
  1.2  Sketcher          Defined
  1.3  Flip              Side 2
  2    Placement         Defined
  2.1  Primary Reference  DTM1:F13(DATUM PLANE)
  2.2  Placement Type     Diameter
  2.3  Axial Reference    A_2(AXIS):F5(REVOLVE_1)
  2.4  Diameter           60.00
  2.5  Angular Reference  FRONT:F3(DATUM PLANE)
  2.6  Angle              15.00
  3    Feature Name       Defined
SECTION NAME = S2D0018
PLACEMENT = RADIAL
MEMBER (2, 1) IN A (12 X 1) DIM GENERAL PATTERN
   FEATURE IS IN LAYER(S) :
    02___PRT_ALL_AXES - OPERATION = SHOWN
MAIN PATTERN DIMENSIONS:
d261 = (Displayed:) 15
      (   Stored:) 15.0 ( 0.5, -0.5 )
d262 = (Displayed:) 0.1
      (   Stored:) 0.103527618041 ( 0.01, -0.01 )
d266 = (Displayed:) 15
      (   Stored:) -15.0 ( 0.01, -0.01 )
d267 = (Displayed:) 60 Dia
      (   Stored:) 60.0 ( 0.01, -0.01 )
d268 = (Displayed:) 30
      (   Stored:) -30.0 ( 0.01, -0.01 )
END ADD

ADD FEATURE (initial number 32)
INTERNAL FEATURE ID  10052
PARENTS = 159(#13) 9999(#30) 5(#3) 39(#5)

HOLE
 NO.   ELEMENT NAME       INFO
 ---   -------------      -------------
  1    Hole               Defined
  1.1  Hole Type          Sketched
  1.2  Sketcher           Defined
  1.3  Flip               Side 2
  2    Placement          Defined
  2.1  Primary Reference  DTM1:F13(DATUM PLANE)
  2.2  Placement Type     Diameter
  2.3  Axial Reference    A_2(AXIS):F5(REVOLVE_1)
  2.4  Diameter           60.00
  2.5  Angular Reference  FRONT:F3(DATUM PLANE)
  2.6  Angle              15.00
  3    Feature Name       Defined
SECTION NAME = S2D0018
PLACEMENT = RADIAL
MEMBER (3, 1) IN A (12 X 1) DIM GENERAL PATTERN
   FEATURE IS IN LAYER(S) :
    02___PRT_ALL_AXES - OPERATION = SHOWN
MAIN PATTERN DIMENSIONS:
d261 = (Displayed:) 15
      (   Stored:) 15.0 ( 0.5, -0.5 )
d262 = (Displayed:) 0.1
      (   Stored:) 0.103527618041 ( 0.01, -0.01 )
d266 = (Displayed:) 15
```

```
      (   Stored:) -15.0 ( 0.01, -0.01 )
d267 = (Displayed:) 60 Dia
      (   Stored:) 60.0 ( 0.01, -0.01 )
d268 = (Displayed:) 30
      (   Stored:) -30.0 ( 0.01, -0.01 )
END ADD

ADD FEATURE (initial number 33)
INTERNAL FEATURE ID  10053
PARENTS = 159(#13) 9999(#30) 5(#3) 39(#5)

HOLE
 NO.   ELEMENT NAME       INFO
 ---   -------------      -------------
  1    Hole               Defined
  1.1  Hole Type          Sketched
  1.2  Sketcher           Defined
  1.3  Flip               Side 2
  2    Placement          Defined
  2.1  Primary Reference  DTM1:F13(DATUM PLANE)
  2.2  Placement Type     Diameter
  2.3  Axial Reference    A_2(AXIS):F5(REVOLVE_1)
  2.4  Diameter           60.00
  2.5  Angular Reference  FRONT:F3(DATUM PLANE)
  2.6  Angle              15.00
  3    Feature Name       Defined
SECTION NAME = S2D0018
PLACEMENT = RADIAL
MEMBER (4, 1) IN A (12 X 1) DIM GENERAL PATTERN
   FEATURE IS IN LAYER(S) :
    02___PRT_ALL_AXES - OPERATION = SHOWN
MAIN PATTERN DIMENSIONS:
d261 = (Displayed:) 15
      (   Stored:) 15.0 ( 0.5, -0.5 )
d262 = (Displayed:) 0.1
      (   Stored:) 0.103527618041 ( 0.01, -0.01 )
d266 = (Displayed:) 15
      (   Stored:) -15.0 ( 0.01, -0.01 )
d267 = (Displayed:) 60 Dia
      (   Stored:) 60.0 ( 0.01, -0.01 )
d268 = (Displayed:) 30
      (   Stored:) -30.0 ( 0.01, -0.01 )
END ADD

ADD FEATURE (initial number 34)
INTERNAL FEATURE ID  10054
PARENTS = 159(#13) 9999(#30) 5(#3) 39(#5)

HOLE
 NO.   ELEMENT NAME       INFO
 ---   -------------      -------------
  1    Hole               Defined
  1.1  Hole Type          Sketched
  1.2  Sketcher           Defined
  1.3  Flip               Side 2
  2    Placement          Defined
  2.1  Primary Reference  DTM1:F13(DATUM PLANE)
  2.2  Placement Type     Diameter
```

```
  2.3  Axial Reference    A_2(AXIS):F5(REVOLVE_1)
  2.4  Diameter           60.00
  2.5  Angular Reference  FRONT:F3(DATUM PLANE)
  2.6  Angle              15.00
  3    Feature Name       Defined
SECTION NAME = S2D0018
PLACEMENT = RADIAL
MEMBER (5, 1) IN A (12 X 1) DIM GENERAL PATTERN
   FEATURE IS IN LAYER(S) :
     02___PRT_ALL_AXES - OPERATION = SHOWN
MAIN PATTERN DIMENSIONS:
d261 = (Displayed:) 15
       (   Stored:) 15.0 ( 0.5, -0.5 )
d262 = (Displayed:) 0.1
       (   Stored:) 0.103527618041 ( 0.01, -0.01 )
d266 = (Displayed:) 15
       (   Stored:) -15.0 ( 0.01, -0.01 )
d267 = (Displayed:) 60 Dia
       (   Stored:) 60.0 ( 0.01, -0.01 )
d268 = (Displayed:) 30
       (   Stored:) -30.0 ( 0.01, -0.01 )
END ADD

ADD FEATURE (initial number 35)
INTERNAL FEATURE ID  10055
PARENTS = 159(#13) 9999(#30) 5(#3) 39(#5)

HOLE
 NO.   ELEMENT NAME       INFO
 ---   -------------      -------------
  1    Hole               Defined
  1.1  Hole Type          Sketched
  1.2  Sketcher           Defined
  1.3  Flip               Side 2
  2    Placement          Defined
  2.1  Primary Reference  DTM1:F13(DATUM PLANE)
  2.2  Placement Type     Diameter
  2.3  Axial Reference    A_2(AXIS):F5(REVOLVE_1)
  2.4  Diameter           60.00
  2.5  Angular Reference  FRONT:F3(DATUM PLANE)
  2.6  Angle              15.00
  3    Feature Name       Defined
SECTION NAME = S2D0018
PLACEMENT = RADIAL
MEMBER (6, 1) IN A (12 X 1) DIM GENERAL PATTERN
   FEATURE IS IN LAYER(S) :
     02___PRT_ALL_AXES - OPERATION = SHOWN
MAIN PATTERN DIMENSIONS:
d261 = (Displayed:) 15
       (   Stored:) 15.0 ( 0.5, -0.5 )
d262 = (Displayed:) 0.1
       (   Stored:) 0.103527618041 ( 0.01, -0.01 )
d266 = (Displayed:) 15
       (   Stored:) -15.0 ( 0.01, -0.01 )
d267 = (Displayed:) 60 Dia
       (   Stored:) 60.0 ( 0.01, -0.01 )
d268 = (Displayed:) 30
       (   Stored:) -30.0 ( 0.01, -0.01 )
```

```
END ADD

ADD FEATURE (initial number 36)
INTERNAL FEATURE ID  10056
PARENTS = 159(#13) 9999(#30) 5(#3) 39(#5)

HOLE
 NO.   ELEMENT NAME       INFO
 ---   -------------      -------------
  1    Hole               Defined
  1.1  Hole Type          Sketched
  1.2  Sketcher           Defined
  1.3  Flip               Side 2
  2    Placement          Defined
  2.1  Primary Reference  DTM1:F13(DATUM PLANE)
  2.2  Placement Type     Diameter
  2.3  Axial Reference    A_2(AXIS):F5(REVOLVE_1)
  2.4  Diameter           60.00
  2.5  Angular Reference  FRONT:F3(DATUM PLANE)
  2.6  Angle              15.00
  3    Feature Name       Defined
SECTION NAME = S2D0018
PLACEMENT = RADIAL
MEMBER (7, 1) IN A (12 X 1) DIM GENERAL PATTERN
   FEATURE IS IN LAYER(S) :
    02___PRT_ALL_AXES - OPERATION = SHOWN
MAIN PATTERN DIMENSIONS:
d261 = (Displayed:) 15
      (   Stored:) 15.0 ( 0.5, -0.5 )
d262 = (Displayed:) 0.1
      (   Stored:) 0.103527618041 ( 0.01, -0.01 )
d266 = (Displayed:) 15
      (   Stored:) -15.0 ( 0.01, -0.01 )
d267 = (Displayed:) 60 Dia
      (   Stored:) 60.0 ( 0.01, -0.01 )
d268 = (Displayed:) 30
      (   Stored:) -30.0 ( 0.01, -0.01 )
END ADD

ADD FEATURE (initial number 37)
INTERNAL FEATURE ID  10057
PARENTS = 159(#13) 9999(#30) 5(#3) 39(#5)

HOLE
 NO.   ELEMENT NAME       INFO
 ---   -------------      -------------
  1    Hole               Defined
  1.1  Hole Type          Sketched
  1.2  Sketcher           Defined
  1.3  Flip               Side 2
  2    Placement          Defined
  2.1  Primary Reference  DTM1:F13(DATUM PLANE)
  2.2  Placement Type     Diameter
  2.3  Axial Reference    A_2(AXIS):F5(REVOLVE_1)
  2.4  Diameter           60.00
  2.5  Angular Reference  FRONT:F3(DATUM PLANE)
  2.6  Angle              15.00
  3    Feature Name       Defined
```

```
SECTION NAME = S2D0018
PLACEMENT = RADIAL
MEMBER (8, 1) IN A (12 X 1) DIM GENERAL PATTERN
  FEATURE IS IN LAYER(S) :
    02___PRT_ALL_AXES - OPERATION = SHOWN
MAIN PATTERN DIMENSIONS:
d261 = (Displayed:) 15
      (   Stored:) 15.0 ( 0.5, -0.5 )
d262 = (Displayed:) 0.1
      (   Stored:) 0.103527618041 ( 0.01, -0.01 )
d266 = (Displayed:) 15
      (   Stored:) -15.0 ( 0.01, -0.01 )
d267 = (Displayed:) 60 Dia
      (   Stored:) 60.0 ( 0.01, -0.01 )
d268 = (Displayed:) 30
      (   Stored:) -30.0 ( 0.01, -0.01 )
END ADD

ADD FEATURE (initial number 38)
INTERNAL FEATURE ID  10058
PARENTS = 159(#13) 9999(#30) 5(#3) 39(#5)

HOLE
 NO.   ELEMENT NAME       INFO
 ---   -------------      -------------
  1    Hole               Defined
  1.1  Hole Type          Sketched
  1.2  Sketcher           Defined
  1.3  Flip               Side 2
  2    Placement          Defined
  2.1  Primary Reference  DTM1:F13(DATUM PLANE)
  2.2  Placement Type     Diameter
  2.3  Axial Reference    A_2(AXIS):F5(REVOLVE_1)
  2.4  Diameter           60.00
  2.5  Angular Reference  FRONT:F3(DATUM PLANE)
  2.6  Angle              15.00
  3    Feature Name       Defined
SECTION NAME = S2D0018
PLACEMENT = RADIAL
MEMBER (9, 1) IN A (12 X 1) DIM GENERAL PATTERN
  FEATURE IS IN LAYER(S) :
    02___PRT_ALL_AXES - OPERATION = SHOWN
MAIN PATTERN DIMENSIONS:
d261 = (Displayed:) 15
      (   Stored:) 15.0 ( 0.5, -0.5 )
d262 = (Displayed:) 0.1
      (   Stored:) 0.103527618041 ( 0.01, -0.01 )
d266 = (Displayed:) 15
      (   Stored:) -15.0 ( 0.01, -0.01 )
d267 = (Displayed:) 60 Dia
      (   Stored:) 60.0 ( 0.01, -0.01 )
d268 = (Displayed:) 30
      (   Stored:) -30.0 ( 0.01, -0.01 )
END ADD

ADD FEATURE (initial number 39)
INTERNAL FEATURE ID  10059
PARENTS = 159(#13) 9999(#30) 5(#3) 39(#5)
```

```
HOLE
 NO.   ELEMENT NAME       INFO
 ---   -------------      -------------
  1    Hole               Defined
  1.1  Hole Type          Sketched
  1.2  Sketcher           Defined
  1.3  Flip               Side 2
  2    Placement          Defined
  2.1  Primary Reference  DTM1:F13(DATUM PLANE)
  2.2  Placement Type     Diameter
  2.3  Axial Reference    A_2(AXIS):F5(REVOLVE_1)
  2.4  Diameter           60.00
  2.5  Angular Reference  FRONT:F3(DATUM PLANE)
  2.6  Angle              15.00
  3    Feature Name       Defined
SECTION NAME = S2D0018
PLACEMENT = RADIAL
MEMBER (10, 1) IN A (12 X 1) DIM GENERAL PATTERN
   FEATURE IS IN LAYER(S) :
     02___PRT_ALL_AXES - OPERATION = SHOWN
MAIN PATTERN DIMENSIONS:
d261 = (Displayed:) 15
       (   Stored:) 15.0 ( 0.5, -0.5 )
d262 = (Displayed:) 0.1
       (   Stored:) 0.103527618041 ( 0.01, -0.01 )
d266 = (Displayed:) 15
       (   Stored:) -15.0 ( 0.01, -0.01 )
d267 = (Displayed:) 60 Dia
       (   Stored:) 60.0 ( 0.01, -0.01 )
d268 = (Displayed:) 30
       (   Stored:) -30.0 ( 0.01, -0.01 )
END ADD

ADD FEATURE (initial number 40)
INTERNAL FEATURE ID  10060
PARENTS = 159(#13) 9999(#30) 5(#3) 39(#5)

HOLE
 NO.   ELEMENT NAME       INFO
 ---   -------------      -------------
  1    Hole               Defined
  1.1  Hole Type          Sketched
  1.2  Sketcher           Defined
  1.3  Flip               Side 2
  2    Placement          Defined
  2.1  Primary Reference  DTM1:F13(DATUM PLANE)
  2.2  Placement Type     Diameter
  2.3  Axial Reference    A_2(AXIS):F5(REVOLVE_1)
  2.4  Diameter           60.00
  2.5  Angular Reference  FRONT:F3(DATUM PLANE)
  2.6  Angle              15.00
  3    Feature Name       Defined
SECTION NAME = S2D0018
PLACEMENT = RADIAL
MEMBER (11, 1) IN A (12 X 1) DIM GENERAL PATTERN
   FEATURE IS IN LAYER(S) :
     02___PRT_ALL_AXES - OPERATION = SHOWN
```

```
MAIN PATTERN DIMENSIONS:
d261 = (Displayed:) 15
      (   Stored:) 15.0 ( 0.5, -0.5 )
d262 = (Displayed:) 0.1
      (   Stored:) 0.103527618041 ( 0.01, -0.01 )
d266 = (Displayed:) 15
      (   Stored:) -15.0 ( 0.01, -0.01 )
d267 = (Displayed:) 60 Dia
      (   Stored:) 60.0 ( 0.01, -0.01 )
d268 = (Displayed:) 30
      (   Stored:) -30.0 ( 0.01, -0.01 )
END ADD

ADD FEATURE (initial number 41)
INTERNAL FEATURE ID  10061
PARENTS = 159(#13) 9999(#30) 5(#3) 39(#5)

HOLE
 NO.   ELEMENT NAME       INFO
 ---   -------------      -------------
  1    Hole               Defined
  1.1  Hole Type          Sketched
  1.2  Sketcher           Defined
  1.3  Flip               Side 2
  2    Placement          Defined
  2.1  Primary Reference  DTM1:F13(DATUM PLANE)
  2.2  Placement Type     Diameter
  2.3  Axial Reference    A_2(AXIS):F5(REVOLVE_1)
  2.4  Diameter           60.00
  2.5  Angular Reference  FRONT:F3(DATUM PLANE)
  2.6  Angle              15.00
  3    Feature Name       Defined
SECTION NAME = S2D0018
PLACEMENT = RADIAL
MEMBER (12, 1) IN A (12 X 1) DIM GENERAL PATTERN
   FEATURE IS IN LAYER(S) :
    02___PRT_ALL_AXES - OPERATION = SHOWN
MAIN PATTERN DIMENSIONS:
d261 = (Displayed:) 15
      (   Stored:) 15.0 ( 0.5, -0.5 )
d262 = (Displayed:) 0.1
      (   Stored:) 0.103527618041 ( 0.01, -0.01 )
d266 = (Displayed:) 15
      (   Stored:) -15.0 ( 0.01, -0.01 )
d267 = (Displayed:) 60 Dia
      (   Stored:) 60.0 ( 0.01, -0.01 )
d268 = (Displayed:) 30
      (   Stored:) -30.0 ( 0.01, -0.01 )
END ADD

ADD FEATURE (initial number 42)
INTERNAL FEATURE ID  11716
PARENTS = 39(#5) 159(#13)

HOLE
 NO.   ELEMENT NAME       INFO
 ---   -------------      -------------
  1    Hole               Defined
```

```
  1.1  Hole Type         Sketched
  1.2  Sketcher          Defined
  1.3  Flip              Side 2
  2    Placement         Defined
  2.1  Primary Reference  DTM1:F13(DATUM PLANE)
  2.2  Placement Type     Coaxial
  2.3  CoAxial Reference  A_2(AXIS):F5(REVOLVE_1)
  3    Feature Name       Defined
SECTION NAME = S2D0019
PLACEMENT = COAXIAL

FEATURE'S DIMENSIONS:
d303 = (Displayed:) 15
      (   Stored:) 15.0 ( 0.5, -0.5 )
d304 = (Displayed:) 0.1
      (   Stored:) 0.103527618041 ( 0.01, -0.01 )
END ADD

ADD FEATURE (initial number 43)
INTERNAL FEATURE ID  17613
NO. ELEMENT NAME    INFO                                STATUS
--- ------------ -----------                          ------
 1  Type         Dimension                              Defined
 2  Regen Method General                                  Defined
 3  1st Dir Dime                                       Defined
 4  1st Dir Inst 12,                                   Defined
 5  2nd Dir Dime                                        Optional
 6  Dimension-Va                                       Defined
 7  2nd Dir Inst                                       Optional
LEADER OF A (12 X 1) DIM GENERAL PATTERN

MAIN PATTERN DIMENSIONS:
d315 = (Displayed:) 15
      (   Stored:) 15.0 ( 0.5, -0.5 )
d316 = (Displayed:) 0.1
      (   Stored:) 0.103527618041 ( 0.01, -0.01 )
d319 = (Displayed:) 90 Dia
      (   Stored:) 90.0 ( 0.01, -0.01 )
d320 = (Displayed:) 30
      (   Stored:) -30.0 ( 0.01, -0.01 )
d321 = (Displayed:) 30
      (   Stored:) -30.0 ( 0.01, -0.01 )
END ADD

ADD FEATURE (initial number 44)
INTERNAL FEATURE ID  17465
PARENTS = 5(#3) 39(#5) 21130(#14)

HOLE
 NO.   ELEMENT NAME       INFO
 ---   -------------      -------------
  1    Hole               Defined
  1.1  Hole Type          Sketched
  1.2  Sketcher           Defined
  1.3  Flip               Side 1
  2    Placement          Defined
  2.1  Primary Reference  DTM2:F14(DATUM PLANE)
  2.2  Placement Type     Diameter
```

```
  2.3  Axial Reference    A_2(AXIS):F5(REVOLVE_1)
  2.4  Diameter           90.00
  2.5  Angular Reference  FRONT:F3(DATUM PLANE)
  2.6  Angle              30.00
  3    Feature Name       Defined
SECTION NAME = S2D0021
PLACEMENT = RADIAL
MEMBER (1, 1) IN A (12 X 1) DIM GENERAL PATTERN
   FEATURE IS IN LAYER(S) :
     02___PRT_ALL_AXES - OPERATION = SHOWN
MAIN PATTERN DIMENSIONS:
d315 = (Displayed:) 15
       (   Stored:) 15.0 ( 0.5, -0.5 )
d316 = (Displayed:) 0.1
       (   Stored:) 0.103527618041 ( 0.01, -0.01 )
d319 = (Displayed:) 90 Dia
       (   Stored:) 90.0 ( 0.01, -0.01 )
d320 = (Displayed:) 30
       (   Stored:) -30.0 ( 0.01, -0.01 )
d321 = (Displayed:) 30
       (   Stored:) -30.0 ( 0.01, -0.01 )
END ADD

ADD FEATURE (initial number 45)
INTERNAL FEATURE ID  17614
PARENTS = 17465(#44) 5(#3) 39(#5) 21130(#14)

HOLE
 NO.   ELEMENT NAME       INFO
 ---   -------------      -------------
  1    Hole               Defined
  1.1  Hole Type          Sketched
  1.2  Sketcher           Defined
  1.3  Flip               Side 1
  2    Placement          Defined
  2.1  Primary Reference  DTM2:F14(DATUM PLANE)
  2.2  Placement Type     Diameter
  2.3  Axial Reference    A_2(AXIS):F5(REVOLVE_1)
  2.4  Diameter           90.00
  2.5  Angular Reference  FRONT:F3(DATUM PLANE)
  2.6  Angle              30.00
  3    Feature Name       Defined
SECTION NAME = S2D0021
PLACEMENT = RADIAL
MEMBER (2, 1) IN A (12 X 1) DIM GENERAL PATTERN
   FEATURE IS IN LAYER(S) :
     02___PRT_ALL_AXES - OPERATION = SHOWN
MAIN PATTERN DIMENSIONS:
d315 = (Displayed:) 15
       (   Stored:) 15.0 ( 0.5, -0.5 )
d316 = (Displayed:) 0.1
       (   Stored:) 0.103527618041 ( 0.01, -0.01 )
d319 = (Displayed:) 90 Dia
       (   Stored:) 90.0 ( 0.01, -0.01 )
d320 = (Displayed:) 30
       (   Stored:) -30.0 ( 0.01, -0.01 )
d321 = (Displayed:) 30
       (   Stored:) -30.0 ( 0.01, -0.01 )
```

```
END ADD

ADD FEATURE (initial number 46)
INTERNAL FEATURE ID  17615
PARENTS = 17465(#44) 5(#3) 39(#5) 21130(#14)

HOLE
 NO.   ELEMENT NAME       INFO
 ---   -------------      -------------
  1    Hole               Defined
  1.1  Hole Type          Sketched
  1.2  Sketcher           Defined
  1.3  Flip               Side 1
  2    Placement          Defined
  2.1  Primary Reference  DTM2:F14(DATUM PLANE)
  2.2  Placement Type     Diameter
  2.3  Axial Reference    A_2(AXIS):F5(REVOLVE_1)
  2.4  Diameter           90.00
  2.5  Angular Reference  FRONT:F3(DATUM PLANE)
  2.6  Angle              30.00
  3    Feature Name       Defined
SECTION NAME = S2D0021
PLACEMENT = RADIAL
MEMBER (3, 1) IN A (12 X 1) DIM GENERAL PATTERN
   FEATURE IS IN LAYER(S) :
    02___PRT_ALL_AXES - OPERATION = SHOWN
MAIN PATTERN DIMENSIONS:
d315 = (Displayed:) 15
      (   Stored:) 15.0 ( 0.5, -0.5 )
d316 = (Displayed:) 0.1
      (   Stored:) 0.103527618041 ( 0.01, -0.01 )
d319 = (Displayed:) 90 Dia
      (   Stored:) 90.0 ( 0.01, -0.01 )
d320 = (Displayed:) 30
      (   Stored:) -30.0 ( 0.01, -0.01 )
d321 = (Displayed:) 30
      (   Stored:) -30.0 ( 0.01, -0.01 )
END ADD

ADD FEATURE (initial number 47)
INTERNAL FEATURE ID  17616
PARENTS = 17465(#44) 5(#3) 39(#5) 21130(#14)

HOLE
 NO.   ELEMENT NAME       INFO
 ---   -------------      -------------
  1    Hole               Defined
  1.1  Hole Type          Sketched
  1.2  Sketcher           Defined
  1.3  Flip               Side 1
  2    Placement          Defined
  2.1  Primary Reference  DTM2:F14(DATUM PLANE)
  2.2  Placement Type     Diameter
  2.3  Axial Reference    A_2(AXIS):F5(REVOLVE_1)
  2.4  Diameter           90.00
  2.5  Angular Reference  FRONT:F3(DATUM PLANE)
  2.6  Angle              30.00
  3    Feature Name       Defined
```

```
SECTION NAME = S2D0021
PLACEMENT = RADIAL
MEMBER (4, 1) IN A (12 X 1) DIM GENERAL PATTERN
  FEATURE IS IN LAYER(S) :
    02___PRT_ALL_AXES - OPERATION = SHOWN
MAIN PATTERN DIMENSIONS:
d315 = (Displayed:) 15
      (   Stored:) 15.0 ( 0.5, -0.5 )
d316 = (Displayed:) 0.1
      (   Stored:) 0.103527618041 ( 0.01, -0.01 )
d319 = (Displayed:) 90 Dia
      (   Stored:) 90.0 ( 0.01, -0.01 )
d320 = (Displayed:) 30
      (   Stored:) -30.0 ( 0.01, -0.01 )
d321 = (Displayed:) 30
      (   Stored:) -30.0 ( 0.01, -0.01 )
END ADD

ADD FEATURE (initial number 48)
INTERNAL FEATURE ID  17617
PARENTS = 17465(#44) 5(#3) 39(#5) 21130(#14)

HOLE
 NO.   ELEMENT NAME       INFO
 ---   -------------      -------------
  1    Hole               Defined
  1.1  Hole Type          Sketched
  1.2  Sketcher           Defined
  1.3  Flip               Side 1
  2    Placement          Defined
  2.1  Primary Reference  DTM2:F14(DATUM PLANE)
  2.2  Placement Type     Diameter
  2.3  Axial Reference    A_2(AXIS):F5(REVOLVE_1)
  2.4  Diameter           90.00
  2.5  Angular Reference  FRONT:F3(DATUM PLANE)
  2.6  Angle              30.00
  3    Feature Name       Defined
SECTION NAME = S2D0021
PLACEMENT = RADIAL
MEMBER (5, 1) IN A (12 X 1) DIM GENERAL PATTERN
  FEATURE IS IN LAYER(S) :
    02___PRT_ALL_AXES - OPERATION = SHOWN
MAIN PATTERN DIMENSIONS:
d315 = (Displayed:) 15
      (   Stored:) 15.0 ( 0.5, -0.5 )
d316 = (Displayed:) 0.1
      (   Stored:) 0.103527618041 ( 0.01, -0.01 )
d319 = (Displayed:) 90 Dia
      (   Stored:) 90.0 ( 0.01, -0.01 )
d320 = (Displayed:) 30
      (   Stored:) -30.0 ( 0.01, -0.01 )
d321 = (Displayed:) 30
      (   Stored:) -30.0 ( 0.01, -0.01 )
END ADD

ADD FEATURE (initial number 49)
INTERNAL FEATURE ID  17618
PARENTS = 17465(#44) 5(#3) 39(#5) 21130(#14)
```

```
HOLE
 NO.   ELEMENT NAME       INFO
 ---   -------------      -------------
  1    Hole               Defined
  1.1  Hole Type          Sketched
  1.2  Sketcher           Defined
  1.3  Flip               Side 1
  2    Placement          Defined
  2.1  Primary Reference  DTM2:F14(DATUM PLANE)
  2.2  Placement Type     Diameter
  2.3  Axial Reference    A_2(AXIS):F5(REVOLVE_1)
  2.4  Diameter           90.00
  2.5  Angular Reference  FRONT:F3(DATUM PLANE)
  2.6  Angle              30.00
  3    Feature Name       Defined
SECTION NAME = S2D0021
PLACEMENT = RADIAL
MEMBER (6, 1) IN A (12 X 1) DIM GENERAL PATTERN
   FEATURE IS IN LAYER(S) :
     02___PRT_ALL_AXES - OPERATION = SHOWN
MAIN PATTERN DIMENSIONS:
d315 = (Displayed:) 15
       (   Stored:) 15.0 ( 0.5, -0.5 )
d316 = (Displayed:) 0.1
       (   Stored:) 0.103527618041 ( 0.01, -0.01 )
d319 = (Displayed:) 90 Dia
       (   Stored:) 90.0 ( 0.01, -0.01 )
d320 = (Displayed:) 30
       (   Stored:) -30.0 ( 0.01, -0.01 )
d321 = (Displayed:) 30
       (   Stored:) -30.0 ( 0.01, -0.01 )
END ADD

ADD FEATURE (initial number 50)
INTERNAL FEATURE ID  17619
PARENTS = 17465(#44) 5(#3) 39(#5) 21130(#14)

HOLE
 NO.   ELEMENT NAME       INFO
 ---   -------------      -------------
  1    Hole               Defined
  1.1  Hole Type          Sketched
  1.2  Sketcher           Defined
  1.3  Flip               Side 1
  2    Placement          Defined
  2.1  Primary Reference  DTM2:F14(DATUM PLANE)
  2.2  Placement Type     Diameter
  2.3  Axial Reference    A_2(AXIS):F5(REVOLVE_1)
  2.4  Diameter           90.00
  2.5  Angular Reference  FRONT:F3(DATUM PLANE)
  2.6  Angle              30.00
  3    Feature Name       Defined
SECTION NAME = S2D0021
PLACEMENT = RADIAL
MEMBER (7, 1) IN A (12 X 1) DIM GENERAL PATTERN
   FEATURE IS IN LAYER(S) :
     02___PRT_ALL_AXES - OPERATION = SHOWN
```

```
MAIN PATTERN DIMENSIONS:
d315 = (Displayed:) 15
      (   Stored:) 15.0 ( 0.5, -0.5 )
d316 = (Displayed:) 0.1
      (   Stored:) 0.103527618041 ( 0.01, -0.01 )
d319 = (Displayed:) 90 Dia
      (   Stored:) 90.0 ( 0.01, -0.01 )
d320 = (Displayed:) 30
      (   Stored:) -30.0 ( 0.01, -0.01 )
d321 = (Displayed:) 30
      (   Stored:) -30.0 ( 0.01, -0.01 )
END ADD

ADD FEATURE (initial number 51)
INTERNAL FEATURE ID  17620
PARENTS = 17465(#44) 5(#3) 39(#5) 21130(#14)

HOLE
 NO.   ELEMENT NAME       INFO
 ---   -------------      -------------
  1    Hole               Defined
  1.1  Hole Type          Sketched
  1.2  Sketcher           Defined
  1.3  Flip               Side 1
  2    Placement          Defined
  2.1  Primary Reference  DTM2:F14(DATUM PLANE)
  2.2  Placement Type     Diameter
  2.3  Axial Reference    A_2(AXIS):F5(REVOLVE_1)
  2.4  Diameter           90.00
  2.5  Angular Reference  FRONT:F3(DATUM PLANE)
  2.6  Angle              30.00
  3    Feature Name       Defined
SECTION NAME = S2D0021
PLACEMENT = RADIAL
MEMBER (8, 1) IN A (12 X 1) DIM GENERAL PATTERN
   FEATURE IS IN LAYER(S) :
    02___PRT_ALL_AXES - OPERATION = SHOWN
MAIN PATTERN DIMENSIONS:
d315 = (Displayed:) 15
      (   Stored:) 15.0 ( 0.5, -0.5 )
d316 = (Displayed:) 0.1
      (   Stored:) 0.103527618041 ( 0.01, -0.01 )
d319 = (Displayed:) 90 Dia
      (   Stored:) 90.0 ( 0.01, -0.01 )
d320 = (Displayed:) 30
      (   Stored:) -30.0 ( 0.01, -0.01 )
d321 = (Displayed:) 30
      (   Stored:) -30.0 ( 0.01, -0.01 )
END ADD

ADD FEATURE (initial number 52)
INTERNAL FEATURE ID  17621
PARENTS = 17465(#44) 5(#3) 39(#5) 21130(#14)

HOLE
 NO.   ELEMENT NAME       INFO
 ---   -------------      -------------
  1    Hole               Defined
```

```
  1.1  Hole Type          Sketched
  1.2  Sketcher           Defined
  1.3  Flip               Side 1
  2    Placement          Defined
  2.1  Primary Reference  DTM2:F14(DATUM PLANE)
  2.2  Placement Type     Diameter
  2.3  Axial Reference    A_2(AXIS):F5(REVOLVE_1)
  2.4  Diameter           90.00
  2.5  Angular Reference  FRONT:F3(DATUM PLANE)
  2.6  Angle              30.00
  3    Feature Name       Defined
SECTION NAME = S2D0021
PLACEMENT = RADIAL
MEMBER (9, 1) IN A (12 X 1) DIM GENERAL PATTERN
   FEATURE IS IN LAYER(S) :
     02___PRT_ALL_AXES - OPERATION = SHOWN
MAIN PATTERN DIMENSIONS:
d315 = (Displayed:) 15
       (   Stored:) 15.0 ( 0.5, -0.5 )
d316 = (Displayed:) 0.1
       (   Stored:) 0.103527618041 ( 0.01, -0.01 )
d319 = (Displayed:) 90 Dia
       (   Stored:) 90.0 ( 0.01, -0.01 )
d320 = (Displayed:) 30
       (   Stored:) -30.0 ( 0.01, -0.01 )
d321 = (Displayed:) 30
       (   Stored:) -30.0 ( 0.01, -0.01 )
END ADD

ADD FEATURE (initial number 53)
INTERNAL FEATURE ID  17622
PARENTS = 17465(#44) 5(#3) 39(#5) 21130(#14)

HOLE
 NO.   ELEMENT NAME       INFO
 ---   -------------      -------------
  1    Hole               Defined
  1.1  Hole Type          Sketched
  1.2  Sketcher           Defined
  1.3  Flip               Side 1
  2    Placement          Defined
  2.1  Primary Reference  DTM2:F14(DATUM PLANE)
  2.2  Placement Type     Diameter
  2.3  Axial Reference    A_2(AXIS):F5(REVOLVE_1)
  2.4  Diameter           90.00
  2.5  Angular Reference  FRONT:F3(DATUM PLANE)
  2.6  Angle              30.00
  3    Feature Name       Defined
SECTION NAME = S2D0021
PLACEMENT = RADIAL
MEMBER (10, 1) IN A (12 X 1) DIM GENERAL PATTERN
   FEATURE IS IN LAYER(S) :
     02___PRT_ALL_AXES - OPERATION = SHOWN
MAIN PATTERN DIMENSIONS:
d315 = (Displayed:) 15
       (   Stored:) 15.0 ( 0.5, -0.5 )
d316 = (Displayed:) 0.1
       (   Stored:) 0.103527618041 ( 0.01, -0.01 )
```

```
d319 = (Displayed:) 90 Dia
      (   Stored:) 90.0 ( 0.01, -0.01 )
d320 = (Displayed:) 30
      (   Stored:) -30.0 ( 0.01, -0.01 )
d321 = (Displayed:) 30
      (   Stored:) -30.0 ( 0.01, -0.01 )
END ADD

ADD FEATURE (initial number 54)
INTERNAL FEATURE ID  17623
PARENTS = 17465(#44) 5(#3) 39(#5) 21130(#14)

HOLE
 NO.   ELEMENT NAME       INFO
 ---   -------------      -------------
  1    Hole               Defined
  1.1  Hole Type          Sketched
  1.2  Sketcher           Defined
  1.3  Flip               Side 1
  2    Placement          Defined
  2.1  Primary Reference  DTM2:F14(DATUM PLANE)
  2.2  Placement Type     Diameter
  2.3  Axial Reference    A_2(AXIS):F5(REVOLVE_1)
  2.4  Diameter           90.00
  2.5  Angular Reference  FRONT:F3(DATUM PLANE)
  2.6  Angle              30.00
  3    Feature Name       Defined
SECTION NAME = S2D0021
PLACEMENT = RADIAL
MEMBER (11, 1) IN A (12 X 1) DIM GENERAL PATTERN
   FEATURE IS IN LAYER(S) :
    02___PRT_ALL_AXES - OPERATION = SHOWN
MAIN PATTERN DIMENSIONS:
d315 = (Displayed:) 15
      (   Stored:) 15.0 ( 0.5, -0.5 )
d316 = (Displayed:) 0.1
      (   Stored:) 0.103527618041 ( 0.01, -0.01 )
d319 = (Displayed:) 90 Dia
      (   Stored:) 90.0 ( 0.01, -0.01 )
d320 = (Displayed:) 30
      (   Stored:) -30.0 ( 0.01, -0.01 )
d321 = (Displayed:) 30
      (   Stored:) -30.0 ( 0.01, -0.01 )
END ADD

ADD FEATURE (initial number 55)
INTERNAL FEATURE ID  17624
PARENTS = 17465(#44) 5(#3) 39(#5) 21130(#14)

HOLE
 NO.   ELEMENT NAME       INFO
 ---   -------------      -------------
  1    Hole               Defined
  1.1  Hole Type          Sketched
  1.2  Sketcher           Defined
  1.3  Flip               Side 1
  2    Placement          Defined
  2.1  Primary Reference  DTM2:F14(DATUM PLANE)
```

```
  2.2  Placement Type     Diameter
  2.3  Axial Reference    A_2(AXIS):F5(REVOLVE_1)
  2.4  Diameter           90.00
  2.5  Angular Reference  FRONT:F3(DATUM PLANE)
  2.6  Angle              30.00
  3    Feature Name       Defined
SECTION NAME = S2D0021
PLACEMENT = RADIAL
MEMBER (12, 1) IN A (12 X 1) DIM GENERAL PATTERN
   FEATURE IS IN LAYER(S) :
    02___PRT_ALL_AXES - OPERATION = SHOWN
MAIN PATTERN DIMENSIONS:
d315 = (Displayed:) 15
      (   Stored:) 15.0 ( 0.5, -0.5 )
d316 = (Displayed:) 0.1
      (   Stored:) 0.103527618041 ( 0.01, -0.01 )
d319 = (Displayed:) 90 Dia
      (   Stored:) 90.0 ( 0.01, -0.01 )
d320 = (Displayed:) 30
      (   Stored:) -30.0 ( 0.01, -0.01 )
d321 = (Displayed:) 30
      (   Stored:) -30.0 ( 0.01, -0.01 )
END ADD

ADD FEATURE (initial number 56)
INTERNAL FEATURE ID  22581
PARENTS = 1(#1)

DATUM PLANE
 NO.     ELEMENT NAME       INFO
 ---     -------------      -------------
  1      Feature Name       Defined
  2      Constraints        Defined
  2.1    Constraint #1      Defined
  2.1.1  Constr Type        Offset
  2.1.2  Constr References  Surface RIGHT of feat #1 (DATUM PLANE)
  2.1.3  Constr Ref Offset  Value = -51.2700
  3      Flip Datum Dir     Defined
  4      Fit                Defined
  4.1    Fit Type           Default
NAME = DTM3
   FEATURE IS IN LAYER(S) :
    01___PRT_ALL_DTM_PLN - OPERATION = SHOWN
FEATURE'S DIMENSIONS:
d335 = (Displayed:) 51.27
      (   Stored:) -51.27 ( 0.01, -0.01 )
END ADD

ADD FEATURE (initial number 57)
INTERNAL FEATURE ID  25289
NO. ELEMENT NAME    INFO                                STATUS
--- ------------ -----------                          ------
 1  Type         Dimension                              Defined
 2  Regen Method General                                  Defined
 3  1st Dir Dime                                       Defined
 4  1st Dir Inst 12,                                   Defined
 5  2nd Dir Dime                                        Optional
 6  Dimension-Va                                         Defined
```

```
 7  2nd Dir Inst                                    Optional
LEADER OF A (12 X 1) DIM GENERAL PATTERN

MAIN PATTERN DIMENSIONS:
d340 = (Displayed:) 15
      (   Stored:) 15.0 ( 0.5, -0.5 )
d341 = (Displayed:) 0.1
      (   Stored:) 0.103527618041 ( 0.01, -0.01 )
d342 = (Displayed:) 104.4 Dia
      (   Stored:) 104.4 ( 0.01, -0.01 )
d343 = (Displayed:) 45
      (   Stored:) 45.0 ( 0.01, -0.01 )
d369 = (Displayed:) 30
      (   Stored:) 30.0 ( 0.01, -0.01 )
END ADD

ADD FEATURE (initial number 58)
INTERNAL FEATURE ID  22583
PARENTS = 22581(#56) 5(#3) 39(#5)

HOLE
 NO.   ELEMENT NAME       INFO
 ---   -------------      -------------
  1    Hole               Defined
  1.1  Hole Type          Sketched
  1.2  Sketcher           Defined
  1.3  Flip               Side 1
  2    Placement          Defined
  2.1  Primary Reference  DTM3:F56(DATUM PLANE)
  2.2  Placement Type     Diameter
  2.3  Axial Reference    A_2(AXIS):F5(REVOLVE_1)
  2.4  Diameter           104.40
  2.5  Angular Reference  FRONT:F3(DATUM PLANE)
  2.6  Angle              45.00
  3    Feature Name       Defined
SECTION NAME = S2D0017
PLACEMENT = RADIAL
MEMBER (1, 1) IN A (12 X 1) DIM GENERAL PATTERN
   FEATURE IS IN LAYER(S) :
    02___PRT_ALL_AXES - OPERATION = SHOWN
MAIN PATTERN DIMENSIONS:
d340 = (Displayed:) 15
      (   Stored:) 15.0 ( 0.5, -0.5 )
d341 = (Displayed:) 0.1
      (   Stored:) 0.103527618041 ( 0.01, -0.01 )
d342 = (Displayed:) 104.4 Dia
      (   Stored:) 104.4 ( 0.01, -0.01 )
d343 = (Displayed:) 45
      (   Stored:) 45.0 ( 0.01, -0.01 )
d369 = (Displayed:) 30
      (   Stored:) 30.0 ( 0.01, -0.01 )
END ADD

ADD FEATURE (initial number 59)
INTERNAL FEATURE ID  25290
PARENTS = 22581(#56) 22583(#58) 5(#3) 39(#5)

HOLE
```

```
 NO.   ELEMENT NAME       INFO
 ---   -------------      -------------
  1    Hole               Defined
  1.1  Hole Type          Sketched
  1.2  Sketcher           Defined
  1.3  Flip               Side 1
  2    Placement          Defined
  2.1  Primary Reference  DTM3:F56(DATUM PLANE)
  2.2  Placement Type     Diameter
  2.3  Axial Reference    A_2(AXIS):F5(REVOLVE_1)
  2.4  Diameter           104.40
  2.5  Angular Reference  FRONT:F3(DATUM PLANE)
  2.6  Angle              45.00
  3    Feature Name       Defined
SECTION NAME = S2D0017
PLACEMENT = RADIAL
MEMBER (2, 1) IN A (12 X 1) DIM GENERAL PATTERN
   FEATURE IS IN LAYER(S) :
     02___PRT_ALL_AXES - OPERATION = SHOWN
MAIN PATTERN DIMENSIONS:
d340 = (Displayed:) 15
       (   Stored:) 15.0 ( 0.5, -0.5 )
d341 = (Displayed:) 0.1
       (   Stored:) 0.103527618041 ( 0.01, -0.01 )
d342 = (Displayed:) 104.4 Dia
       (   Stored:) 104.4 ( 0.01, -0.01 )
d343 = (Displayed:) 45
       (   Stored:) 45.0 ( 0.01, -0.01 )
d369 = (Displayed:) 30
       (   Stored:) 30.0 ( 0.01, -0.01 )
END ADD

ADD FEATURE (initial number 60)
INTERNAL FEATURE ID  25291
PARENTS = 22581(#56) 22583(#58) 5(#3) 39(#5)

HOLE
 NO.   ELEMENT NAME       INFO
 ---   -------------      -------------
  1    Hole               Defined
  1.1  Hole Type          Sketched
  1.2  Sketcher           Defined
  1.3  Flip               Side 1
  2    Placement          Defined
  2.1  Primary Reference  DTM3:F56(DATUM PLANE)
  2.2  Placement Type     Diameter
  2.3  Axial Reference    A_2(AXIS):F5(REVOLVE_1)
  2.4  Diameter           104.40
  2.5  Angular Reference  FRONT:F3(DATUM PLANE)
  2.6  Angle              45.00
  3    Feature Name       Defined
SECTION NAME = S2D0017
PLACEMENT = RADIAL
MEMBER (3, 1) IN A (12 X 1) DIM GENERAL PATTERN
   FEATURE IS IN LAYER(S) :
     02___PRT_ALL_AXES - OPERATION = SHOWN
MAIN PATTERN DIMENSIONS:
d340 = (Displayed:) 15
```

```
      (   Stored:) 15.0 ( 0.5, -0.5 )
d341 = (Displayed:) 0.1
      (   Stored:) 0.103527618041 ( 0.01, -0.01 )
d342 = (Displayed:) 104.4 Dia
      (   Stored:) 104.4 ( 0.01, -0.01 )
d343 = (Displayed:) 45
      (   Stored:) 45.0 ( 0.01, -0.01 )
d369 = (Displayed:) 30
      (   Stored:) 30.0 ( 0.01, -0.01 )
END ADD

ADD FEATURE (initial number 61)
INTERNAL FEATURE ID  25292
PARENTS = 22581(#56) 22583(#58) 5(#3) 39(#5)

HOLE
 NO.   ELEMENT NAME       INFO
 ---   -------------      -------------
  1    Hole               Defined
  1.1  Hole Type          Sketched
  1.2  Sketcher           Defined
  1.3  Flip               Side 1
  2    Placement          Defined
  2.1  Primary Reference  DTM3:F56(DATUM PLANE)
  2.2  Placement Type     Diameter
  2.3  Axial Reference    A_2(AXIS):F5(REVOLVE_1)
  2.4  Diameter           104.40
  2.5  Angular Reference  FRONT:F3(DATUM PLANE)
  2.6  Angle              45.00
  3    Feature Name       Defined
SECTION NAME = S2D0017
PLACEMENT = RADIAL
MEMBER (4, 1) IN A (12 X 1) DIM GENERAL PATTERN
   FEATURE IS IN LAYER(S) :
    02___PRT_ALL_AXES - OPERATION = SHOWN
MAIN PATTERN DIMENSIONS:
d340 = (Displayed:) 15
      (   Stored:) 15.0 ( 0.5, -0.5 )
d341 = (Displayed:) 0.1
      (   Stored:) 0.103527618041 ( 0.01, -0.01 )
d342 = (Displayed:) 104.4 Dia
      (   Stored:) 104.4 ( 0.01, -0.01 )
d343 = (Displayed:) 45
      (   Stored:) 45.0 ( 0.01, -0.01 )
d369 = (Displayed:) 30
      (   Stored:) 30.0 ( 0.01, -0.01 )
END ADD

ADD FEATURE (initial number 62)
INTERNAL FEATURE ID  25293
PARENTS = 22581(#56) 22583(#58) 5(#3) 39(#5)

HOLE
 NO.   ELEMENT NAME       INFO
 ---   -------------      -------------
  1    Hole               Defined
  1.1  Hole Type          Sketched
  1.2  Sketcher           Defined
```

```
  1.3  Flip              Side 1
  2    Placement         Defined
  2.1  Primary Reference  DTM3:F56(DATUM PLANE)
  2.2  Placement Type     Diameter
  2.3  Axial Reference    A_2(AXIS):F5(REVOLVE_1)
  2.4  Diameter           104.40
  2.5  Angular Reference  FRONT:F3(DATUM PLANE)
  2.6  Angle              45.00
  3    Feature Name       Defined
SECTION NAME = S2D0017
PLACEMENT = RADIAL
MEMBER (5, 1) IN A (12 X 1) DIM GENERAL PATTERN
   FEATURE IS IN LAYER(S) :
    02___PRT_ALL_AXES - OPERATION = SHOWN
MAIN PATTERN DIMENSIONS:
d340 = (Displayed:) 15
      (   Stored:) 15.0 ( 0.5, -0.5 )
d341 = (Displayed:) 0.1
      (   Stored:) 0.103527618041 ( 0.01, -0.01 )
d342 = (Displayed:) 104.4 Dia
      (   Stored:) 104.4 ( 0.01, -0.01 )
d343 = (Displayed:) 45
      (   Stored:) 45.0 ( 0.01, -0.01 )
d369 = (Displayed:) 30
      (   Stored:) 30.0 ( 0.01, -0.01 )
END ADD

ADD FEATURE (initial number 63)
INTERNAL FEATURE ID  25294
PARENTS = 22581(#56) 22583(#58) 5(#3) 39(#5)

HOLE
 NO.   ELEMENT NAME       INFO
 ---   -------------      -------------
  1    Hole               Defined
  1.1  Hole Type          Sketched
  1.2  Sketcher           Defined
  1.3  Flip               Side 1
  2    Placement          Defined
  2.1  Primary Reference  DTM3:F56(DATUM PLANE)
  2.2  Placement Type     Diameter
  2.3  Axial Reference    A_2(AXIS):F5(REVOLVE_1)
  2.4  Diameter           104.40
  2.5  Angular Reference  FRONT:F3(DATUM PLANE)
  2.6  Angle              45.00
  3    Feature Name       Defined
SECTION NAME = S2D0017
PLACEMENT = RADIAL
MEMBER (6, 1) IN A (12 X 1) DIM GENERAL PATTERN
   FEATURE IS IN LAYER(S) :
    02___PRT_ALL_AXES - OPERATION = SHOWN
MAIN PATTERN DIMENSIONS:
d340 = (Displayed:) 15
      (   Stored:) 15.0 ( 0.5, -0.5 )
d341 = (Displayed:) 0.1
      (   Stored:) 0.103527618041 ( 0.01, -0.01 )
d342 = (Displayed:) 104.4 Dia
      (   Stored:) 104.4 ( 0.01, -0.01 )
```

```
d343 = (Displayed:) 45
      (   Stored:) 45.0 ( 0.01, -0.01 )
d369 = (Displayed:) 30
      (   Stored:) 30.0 ( 0.01, -0.01 )
END ADD

ADD FEATURE (initial number 64)
INTERNAL FEATURE ID  25295
PARENTS = 22581(#56) 22583(#58) 5(#3) 39(#5)

HOLE
 NO.   ELEMENT NAME       INFO
 ---   -------------      -------------
  1    Hole               Defined
  1.1  Hole Type          Sketched
  1.2  Sketcher           Defined
  1.3  Flip               Side 1
  2    Placement          Defined
  2.1  Primary Reference  DTM3:F56(DATUM PLANE)
  2.2  Placement Type     Diameter
  2.3  Axial Reference    A_2(AXIS):F5(REVOLVE_1)
  2.4  Diameter           104.40
  2.5  Angular Reference  FRONT:F3(DATUM PLANE)
  2.6  Angle              45.00
  3    Feature Name       Defined
SECTION NAME = S2D0017
PLACEMENT = RADIAL
MEMBER (7, 1) IN A (12 X 1) DIM GENERAL PATTERN
   FEATURE IS IN LAYER(S) :
    02___PRT_ALL_AXES - OPERATION = SHOWN
MAIN PATTERN DIMENSIONS:
d340 = (Displayed:) 15
      (   Stored:) 15.0 ( 0.5, -0.5 )
d341 = (Displayed:) 0.1
      (   Stored:) 0.103527618041 ( 0.01, -0.01 )
d342 = (Displayed:) 104.4 Dia
      (   Stored:) 104.4 ( 0.01, -0.01 )
d343 = (Displayed:) 45
      (   Stored:) 45.0 ( 0.01, -0.01 )
d369 = (Displayed:) 30
      (   Stored:) 30.0 ( 0.01, -0.01 )
END ADD

ADD FEATURE (initial number 65)
INTERNAL FEATURE ID  25296
PARENTS = 22581(#56) 22583(#58) 5(#3) 39(#5)

HOLE
 NO.   ELEMENT NAME       INFO
 ---   -------------      -------------
  1    Hole               Defined
  1.1  Hole Type          Sketched
  1.2  Sketcher           Defined
  1.3  Flip               Side 1
  2    Placement          Defined
  2.1  Primary Reference  DTM3:F56(DATUM PLANE)
  2.2  Placement Type     Diameter
  2.3  Axial Reference    A_2(AXIS):F5(REVOLVE_1)
```

```
  2.4  Diameter          104.40
  2.5  Angular Reference  FRONT:F3(DATUM PLANE)
  2.6  Angle             45.00
  3    Feature Name      Defined
SECTION NAME = S2D0017
PLACEMENT = RADIAL
MEMBER (8, 1) IN A (12 X 1) DIM GENERAL PATTERN
   FEATURE IS IN LAYER(S) :
    02___PRT_ALL_AXES - OPERATION = SHOWN
MAIN PATTERN DIMENSIONS:
d340 = (Displayed:) 15
      (   Stored:) 15.0 ( 0.5, -0.5 )
d341 = (Displayed:) 0.1
      (   Stored:) 0.103527618041 ( 0.01, -0.01 )
d342 = (Displayed:) 104.4 Dia
      (   Stored:) 104.4 ( 0.01, -0.01 )
d343 = (Displayed:) 45
      (   Stored:) 45.0 ( 0.01, -0.01 )
d369 = (Displayed:) 30
      (   Stored:) 30.0 ( 0.01, -0.01 )
END ADD

ADD FEATURE (initial number 66)
INTERNAL FEATURE ID  25297
PARENTS = 22581(#56) 22583(#58) 5(#3) 39(#5)

HOLE
 NO.   ELEMENT NAME      INFO
 ---   -------------     -------------
  1    Hole              Defined
  1.1  Hole Type         Sketched
  1.2  Sketcher          Defined
  1.3  Flip              Side 1
  2    Placement         Defined
  2.1  Primary Reference  DTM3:F56(DATUM PLANE)
  2.2  Placement Type     Diameter
  2.3  Axial Reference    A_2(AXIS):F5(REVOLVE_1)
  2.4  Diameter          104.40
  2.5  Angular Reference  FRONT:F3(DATUM PLANE)
  2.6  Angle             45.00
  3    Feature Name      Defined
SECTION NAME = S2D0017
PLACEMENT = RADIAL
MEMBER (9, 1) IN A (12 X 1) DIM GENERAL PATTERN
   FEATURE IS IN LAYER(S) :
    02___PRT_ALL_AXES - OPERATION = SHOWN
MAIN PATTERN DIMENSIONS:
d340 = (Displayed:) 15
      (   Stored:) 15.0 ( 0.5, -0.5 )
d341 = (Displayed:) 0.1
      (   Stored:) 0.103527618041 ( 0.01, -0.01 )
d342 = (Displayed:) 104.4 Dia
      (   Stored:) 104.4 ( 0.01, -0.01 )
d343 = (Displayed:) 45
      (   Stored:) 45.0 ( 0.01, -0.01 )
d369 = (Displayed:) 30
      (   Stored:) 30.0 ( 0.01, -0.01 )
END ADD
```

```
ADD FEATURE (initial number 67)
INTERNAL FEATURE ID  25298
PARENTS = 22581(#56) 22583(#58) 5(#3) 39(#5)

HOLE
 NO.   ELEMENT NAME       INFO
 ---   -------------      -------------
  1    Hole               Defined
  1.1  Hole Type          Sketched
  1.2  Sketcher           Defined
  1.3  Flip               Side 1
  2    Placement          Defined
  2.1  Primary Reference  DTM3:F56(DATUM PLANE)
  2.2  Placement Type     Diameter
  2.3  Axial Reference    A_2(AXIS):F5(REVOLVE_1)
  2.4  Diameter           104.40
  2.5  Angular Reference  FRONT:F3(DATUM PLANE)
  2.6  Angle              45.00
  3    Feature Name       Defined
SECTION NAME = S2D0017
PLACEMENT = RADIAL
MEMBER (10, 1) IN A (12 X 1) DIM GENERAL PATTERN
   FEATURE IS IN LAYER(S) :
    02___PRT_ALL_AXES - OPERATION = SHOWN
MAIN PATTERN DIMENSIONS:
d340 = (Displayed:) 15
      (   Stored:) 15.0 ( 0.5, -0.5 )
d341 = (Displayed:) 0.1
      (   Stored:) 0.103527618041 ( 0.01, -0.01 )
d342 = (Displayed:) 104.4 Dia
      (   Stored:) 104.4 ( 0.01, -0.01 )
d343 = (Displayed:) 45
      (   Stored:) 45.0 ( 0.01, -0.01 )
d369 = (Displayed:) 30
      (   Stored:) 30.0 ( 0.01, -0.01 )
END ADD

ADD FEATURE (initial number 68)
INTERNAL FEATURE ID  25299
PARENTS = 22581(#56) 22583(#58) 5(#3) 39(#5)

HOLE
 NO.   ELEMENT NAME       INFO
 ---   -------------      -------------
  1    Hole               Defined
  1.1  Hole Type          Sketched
  1.2  Sketcher           Defined
  1.3  Flip               Side 1
  2    Placement          Defined
  2.1  Primary Reference  DTM3:F56(DATUM PLANE)
  2.2  Placement Type     Diameter
  2.3  Axial Reference    A_2(AXIS):F5(REVOLVE_1)
  2.4  Diameter           104.40
  2.5  Angular Reference  FRONT:F3(DATUM PLANE)
  2.6  Angle              45.00
  3    Feature Name       Defined
SECTION NAME = S2D0017
```

```
PLACEMENT = RADIAL
MEMBER (11, 1) IN A (12 X 1) DIM GENERAL PATTERN
   FEATURE IS IN LAYER(S) :
     02___PRT_ALL_AXES - OPERATION = SHOWN
MAIN PATTERN DIMENSIONS:
d340 = (Displayed:) 15
       (   Stored:) 15.0 ( 0.5, -0.5 )
d341 = (Displayed:) 0.1
       (   Stored:) 0.103527618041 ( 0.01, -0.01 )
d342 = (Displayed:) 104.4 Dia
       (   Stored:) 104.4 ( 0.01, -0.01 )
d343 = (Displayed:) 45
       (   Stored:) 45.0 ( 0.01, -0.01 )
d369 = (Displayed:) 30
       (   Stored:) 30.0 ( 0.01, -0.01 )
END ADD

ADD FEATURE (initial number 69)
INTERNAL FEATURE ID  25300
PARENTS = 22581(#56) 22583(#58) 5(#3) 39(#5)

HOLE
 NO.   ELEMENT NAME       INFO
 ---   -------------      -------------
  1    Hole               Defined
  1.1  Hole Type          Sketched
  1.2  Sketcher           Defined
  1.3  Flip               Side 1
  2    Placement          Defined
  2.1  Primary Reference  DTM3:F56(DATUM PLANE)
  2.2  Placement Type     Diameter
  2.3  Axial Reference    A_2(AXIS):F5(REVOLVE_1)
  2.4  Diameter           104.40
  2.5  Angular Reference  FRONT:F3(DATUM PLANE)
  2.6  Angle              45.00
  3    Feature Name       Defined
SECTION NAME = S2D0017
PLACEMENT = RADIAL
MEMBER (12, 1) IN A (12 X 1) DIM GENERAL PATTERN
   FEATURE IS IN LAYER(S) :
     02___PRT_ALL_AXES - OPERATION = SHOWN
MAIN PATTERN DIMENSIONS:
d340 = (Displayed:) 15
       (   Stored:) 15.0 ( 0.5, -0.5 )
d341 = (Displayed:) 0.1
       (   Stored:) 0.103527618041 ( 0.01, -0.01 )
d342 = (Displayed:) 104.4 Dia
       (   Stored:) 104.4 ( 0.01, -0.01 )
d343 = (Displayed:) 45
       (   Stored:) 45.0 ( 0.01, -0.01 )
d369 = (Displayed:) 30
       (   Stored:) 30.0 ( 0.01, -0.01 )
END ADD
IF E < 40.6745
    ADD FEATURE (initial number 70)
    INTERNAL FEATURE ID  6586
    PARENTS = 1(#1) 3(#2) 39(#5) 5(#3)
```

```
CUT: Revolve
 NO.      ELEMENT NAME         INFO
 ---      -------------        -------------
  1       Feature Name         Defined
  2       Extrude Feat type    Solid
  3       Material             Remove
  4       Section              Defined
  4.1     Setup Plane          Defined
  4.1.1   Sketching Plane      FRONT:F3(DATUM PLANE)
  4.1.2   View Direction       Side 1
  4.1.3   Orientation          Right
  4.1.4   Reference            RIGHT:F1(DATUM PLANE)
  4.2     Sketch               Defined
  5       Feature Form         Solid
  6       Material Side        Side Two
  7       Revolve Axis         Defined
  8       Revolve Axis Option  Internal Centerline
  9       Direction            Side 1
  10      Angle                Defined
  10.1    Side One             Defined
  10.1.1  Side One Angle       None
  10.2    Side Two             Defined
  10.2.1  Side Two Angle       Variable
  10.2.2  Value                360.00
    NAME = SPOLNJI_KON_DO40_39
    SECTION NAME = Section 1

    FEATURE'S DIMENSIONS:
    d109 = (Displayed:) 360
          (   Stored:) 360.0 ( 0.01, -0.01 )
    d135 = (Displayed:) 5
          (   Stored:) 5.0 ( 0.01, -0.01 )
    d136 = (Displayed:) 12
          (   Stored:) 12.0 ( 0.5, -0.5 )
    d138 = (Displayed:) 104.4 Dia
          (   Stored:) 104.4 ( 0.01, -0.01 )
    d139 = (Displayed:) 0.11R
          (   Stored:) 0.11 ( 0.01, -0.01 )
    d140 = (Displayed:) 51.26
          (   Stored:) 51.26 ( 0.01, -0.01 )
    END ADD
END IF
IF E >= 40.5
    ADD SUPPRESSED FEATURE
    INTERNAL FEATURE ID  14175
    PARENTS = 1(#1) 3(#2) 5(#3)

CUT: Revolve
 NO.      ELEMENT NAME         INFO
 ---      -------------        -------------
  1       Feature Name         Defined
  2       Extrude Feat type    Solid
  3       Material             Remove
  4       Section              Defined
  4.1     Setup Plane          Defined
  4.1.1   Sketching Plane      FRONT:F3(DATUM PLANE)
  4.1.2   View Direction       Side 1
  4.1.3   Orientation          Right
```

```
  4.1.4   Reference          RIGHT:F1(DATUM PLANE)
  4.2     Sketch             Defined
  5       Feature Form       Solid
  6       Material Side      Side Two
  7       Revolve Axis       Defined
  8       Revolve Axis Option  Internal Centerline
  9       Direction          Side 1
  10      Angle              Defined
  10.1    Side One           Defined
  10.1.1  Side One Angle     None
  10.2    Side Two           Defined
  10.2.1  Side Two Angle     Variable
  10.2.2  Value              360.00
    NAME = SPOLJNI_KONUS_OD_40_5
    SECTION NAME = Section 1

    FEATURE'S DIMENSIONS:
    d307 = (Displayed:) 360
          (   Stored:) 360.0 ( 0.01, -0.01 )
    d308 = (Displayed:) 55
          (   Stored:) 55.0 ( 0.01, -0.01 )
    d309 = (Displayed:) 40.5R
          (   Stored:) 40.5 ( 0.01, -0.01 )
    d310 = (Displayed:) 70
          (   Stored:) 70.0 ( 0.01, -0.01 )
    d311 = (Displayed:) 51
          (   Stored:) 51.0 ( 0.01, -0.01 )
    d312 = (Displayed:) 20
          (   Stored:) 20.0 ( 0.01, -0.01 )
    END ADD
END IF

ADD FEATURE (initial number 71)
INTERNAL FEATURE ID  7034

ANALYSIS
 NO.     ELEMENT NAME     INFO
 ---     -------------    -------------
  1      Name             CEO
  2      Type             Measure
  3      RegenRequest     Always
  4      Definition       Defined
  5      Result params    Defined
  5.1    AREA             Defined
  5.1.1  Create           YES
  5.1.2  Param name       AREA
NAME = CEO

Analysis class                  Analysis type
----------------                ----------------------
Measure                         Area
END ADD

ADD FEATURE (initial number 72)
INTERNAL FEATURE ID  27701
PARENTS = 39(#5)

ANALYSIS
```

```
 NO.     ELEMENT NAME     INFO
 ---     -------------    -------------
  1      Name             CILINDAR
  2      Type             Measure
  3      RegenRequest     Always
  4      Definition       Defined
  5      Result params    Defined
  5.1    AREA             Defined
  5.1.1  Create           YES
  5.1.2  Param name       AREA
NAME = CILINDAR

Analysis class                  Analysis type
----------------                ----------------------
Measure                         Area
END ADD

ADD FEATURE (initial number 73)
INTERNAL FEATURE ID  7036
PARENTS = 39(#5)

ANALYSIS
 NO.     ELEMENT NAME     INFO
 ---     -------------    -------------
  1      Name             KALOTA
  2      Type             Measure
  3      RegenRequest     Always
  4      Definition       Defined
  5      Result params    Defined
  5.1    AREA             Defined
  5.1.1  Create           YES
  5.1.2  Param name       AREA
NAME = KALOTA

Analysis class                  Analysis type
----------------                ----------------------
Measure                         Area
END ADD

ADD FEATURE (initial number 74)
INTERNAL FEATURE ID  7037
PARENTS = 39(#5)

ANALYSIS
 NO.     ELEMENT NAME     INFO
 ---     -------------    -------------
  1      Name             CELO
  2      Type             Measure
  3      RegenRequest     Always
  4      Definition       Defined
  5      Result params    Defined
  5.1    AREA             Defined
  5.1.1  Create           YES
  5.1.2  Param name       AREA
NAME = CELO

Analysis class                  Analysis type
----------------                ----------------------
```

```
Measure                         Area
END ADD

ADD FEATURE (initial number 75)
INTERNAL FEATURE ID  7038

ANALYSIS
 NO.   ELEMENT NAME     INFO
 ---   -------------    -------------
  1    Name             SAGOR
  2    Type             Relation
  3    RegenRequest     Always
  4    Definition       Defined
NAME = SAGOR

Analysis class                  Analysis type
---------------                 ----------------------
Relation
END ADD

ADD FEATURE (initial number 76)
INTERNAL FEATURE ID  22580

ANALYSIS
 NO.   ELEMENT NAME     INFO
 ---   -------------    -------------
  1    Name             POVRSINA_S
  2    Type             Relation
  3    RegenRequest     Always
  4    Definition       Defined
NAME = POVRSINA_S

Analysis class                  Analysis type
---------------                 ----------------------
Relation
END ADD
MASSPROP
END MASSPROP
```